



HAL
open science

Investigating herbicide targets in the very long-chain fatty acid biosynthesis pathway

Claire Le Ruyet

► **To cite this version:**

Claire Le Ruyet. Investigating herbicide targets in the very long-chain fatty acid biosynthesis pathway. Agricultural sciences. Université de Bordeaux, 2024. English. NNT : 2024BORD0125 . tel-04725994

HAL Id: tel-04725994

<https://theses.hal.science/tel-04725994v1>

Submitted on 8 Oct 2024

HAL is a multi-disciplinary open access archive for the deposit and dissemination of scientific research documents, whether they are published or not. The documents may come from teaching and research institutions in France or abroad, or from public or private research centers.

L'archive ouverte pluridisciplinaire **HAL**, est destinée au dépôt et à la diffusion de documents scientifiques de niveau recherche, publiés ou non, émanant des établissements d'enseignement et de recherche français ou étrangers, des laboratoires publics ou privés.

THÈSE PRÉSENTÉE POUR OBTENIR LE GRADE DE

**DOCTEUR DE
L'UNIVERSITÉ DE BORDEAUX**

ÉCOLE DOCTORALE SCIENCES DE LA VIE ET DE LA SANTÉ

SPÉCIALITÉ SCIENCES AGRONOMIQUES

Par Claire LE RUYET

**ÉTUDE DES CIBLES DES HERBICIDES DANS LA VOIE DE
BIOSYNTHESE DES ACIDES GRAS À TRÈS LONGUE CHAÎNE**

**INVESTIGATING HERBICIDE TARGETS IN THE VERY LONG-CHAIN
FATTY ACID BIOSYNTHESIS PATHWAY**

Sous la direction de : Jérôme JOUBES

Soutenue le 02 juillet 2024

Membres du jury :

M. JOUBES, Jérôme	Professeur, Université de Bordeaux	Directeur de thèse
M. BLANCHARD, Alain	Professeur, Université de Bordeaux	Président
Mme. JOUHET, Juliette	Directrice de recherche, CNRS Grenoble	Rapporteuse
M. BEAUDOIN, Frédéric	Directeur de recherche, Rothamsted research	Rapporteur
Mme. VENEGAS-CALERÓN, Mónica	Directrice de recherche, Instituto de la Grasa	Examinatrice
M. DOMERGUE, Frédéric	Chargé de recherche, CNRS Bordeaux	Invité
M. LUEMMEN, Peter	Docteur, BAYER SA Francfort	Invité

Titre : ETUDE DES CIBLES DES HERBICIDES DANS LA VOIE DE BIOSYNTHESE DES ACIDES GRAS A TRES LONGUE CHAINE

Résumé : Les acides gras à très longue chaîne (AGTLC) sont des molécules essentielles avec des fonctions physiologiques et structurales importantes chez les plantes. Ces acides gras, qui ont des chaînes acyles de 20 carbones ou plus, peuvent être modifiés en composants de lipides clés tels que les phospholipides et les sphingolipides des membranes, les triacylglycérols (TAG) dans les graines, les cires cuticulaires dans l'épiderme et la subérine dans les racines.

L'élongation des AGTLC est réalisée par le complexe d'élongation des acides gras (FAE complex). Ce complexe comprend quatre enzymes distinctes ancrées à la membrane du réticulum endoplasmique (RE) : KCS, KCR, HCD et ECR. Le complexe FAE réalise un cycle de réaction en quatre étapes qui ajoute deux carbones à la chaîne pour allonger la chaîne acyle. L'enzyme KCS est responsable de la première réaction, qui implique une condensation entre un malonyl-CoA et un acyl-CoA. Les enzymes KCS sont connues pour leur grande diversité génétique chez les plantes, et la caractérisation fonctionnelle de plusieurs gènes AtKCS a révélé différentes spécificités de substrat. Cela suggère que la sélectivité de la longueur de chaîne des complexes FAE est déterminée par la sous-unité KCS du complexe.

Les herbicides qui inhibent la synthèse des AGTLC (groupe HRAC 15), tels que le flufenacet, le pyroxasulfone ou les chloroacétamides, jouent un rôle crucial dans les stratégies de gestion des mauvaises herbes. Le mode d'action de ces composés a été initialement identifié sur la base du phénotype caractéristique observé chez les plantes traitées, suggérant une inhibition de la synthèse des VLCFA. Dans ce processus d'inhibition, plusieurs herbicides ciblent la sous-unité KCS des complexes FAE. Des essais enzymatiques *in vitro* ont démontré l'inhibition de la KCS par divers herbicides, cependant, plusieurs autres herbicides, qui induisent un phénotype similaire chez les plantes, ne semblent pas inhiber l'enzyme KCS et leurs cibles moléculaires restent inconnues. La plupart des herbicides disponibles dans le commerce présentent une activité plus forte contre les plantes herbacées (monocotylédones) que contre les plantes à feuilles larges (dicotylédones), bien que les raisons de cette sélectivité ne soient pas bien comprises.

L'objectif de ce projet de doctorat était d'explorer davantage l'inhibition de la synthèse des AGTLC. Pour ce faire, une analyse phylogénétique et une analyse fonctionnelle comparative des KCS provenant de diverses espèces végétales ont été réalisées en utilisant un système hétérologue de levure reconstituant le complexe FAE complet de la plante. De plus, des études *in vivo* utilisant la levure exprimant des KCS actives, traitées avec plusieurs herbicides, ont été menées pour étudier leur mode d'action et leur sélectivité. Enfin, un essai *in vitro* sans radioactivité a été développé pour évaluer l'activité de la KCS et l'inhibition par les herbicides du groupe HRAC 15.

Mots clés : AGTLC – plant – herbicides – FAE – spectrométrie de masse – KCS

Title: INVESTIGATING HERBICIDE TARGETS IN THE VERY LONG-CHAIN FATTY ACID BIOSYNTHESIS PATHWAY

Abstract: Very-long-chain fatty acids (VLCFA) are essential molecules with significant physiological and structural functions in plants. These fatty acids, which have acyl chains of 20 or more carbons, can be modified into components of key lipids such as phospholipids and sphingolipids of membranes, triacylglycerols (TAGs) in seeds, cuticular waxes in the epidermis, and suberin in roots.

The elongation of VLCFA is carried out by the Fatty Acid Elongase complex (FAE complex). This complex comprises four distinct enzymes anchored to the endoplasmic reticulum (ER) membrane: KCS, KCR, HCD, and ECR. The FAE complex performs a four-step reaction cycle that adds two carbons to elongate the fatty acyl chain. The KCS enzyme is responsible for the first reaction, which involves a condensation between a malonyl-CoA and an acyl-CoA. KCS enzymes are known for their high genetic diversity in plants, and functional characterization of several AtKCS genes has revealed different substrate specificities. This suggests that the chain length selectivity of FAE complexes is determined by the KCS subunit of the complex.

Herbicides that inhibit VLCFA synthesis (HRAC group 15), such as flufenacet, pyroxasulfone, or chloroacetamides, play a crucial role in weed management strategies. The mode of action of these compounds was initially identified based on the characteristic phenotype observed in treated plants, suggesting inhibition of VLCFA synthesis. In this inhibition process, several herbicides target the KCS subunit of the FAE complexes. *In vitro* enzymatic assays have demonstrated inhibition of KCS by various herbicides, however, several other herbicides, that induce similar phenotype in plants, do not appear to inhibit the KCS enzyme and their molecular targets remain unknown. Most commercially available herbicides exhibit stronger activity against grass plants (monocotyledonous) than broadleaf plants (dicotyledonous), though the reasons for this selectivity are not well understood.

The objective of this PhD project was to further explore the inhibition of VLCFA synthesis. To do so, a phylogenetic analysis and a comparative functional analysis of KCS from various plant species were performed using a yeast heterologous system reconstituting the complete plant FAE complex. In addition, *in vivo* studies using yeast expressing active KCSs treated with several herbicides, were conducted to investigate their mode of action and selectivity. Finally, a non-radiolabeled *in vitro* assay was developed to evaluate KCS activity and inhibition by HRAC 15 group herbicides.

Keywords : VLCFA – plant – herbicide – FAE – mass spectrometry – KCS

Unité de recherche Laboratoire de biogenèse membranaire, UMR 5200, CNRS, Université de Bordeaux, Campus INRAE Bordeaux Aquitaine



Remerciements

Je remercie tout d'abord **Alain Blanchard, Frédéric Beaudoin, Juliette Jouhet** et **Monica Vegenas-Caleròn** d'avoir accepté de discuter et d'évaluer mon travail de thèse.

Avant tout, je tiens à adresser ma gratitude à **Jérôme** pour son encadrement toujours bienveillant, et sa confiance depuis le début de ma thèse, même si j'attends toujours mes « éclairs de génie » ! Et comme Tic n'est jamais sans Tac, je voudrais aussi remercier ici **FredDo**, qui m'a officiellement encadré durant ces 3 ans. Par-dessus tout, je voulais vous remercier pour votre soutien, pour l'autonomie que vous m'avez laissée et surtout pour votre bonne humeur, vos partages de vie et vos blagues ... Votre duo infernal va beaucoup me manquer.

Je souhaite également adresser un remerciement particulier envers le reste de la WAX team. Stéphanie, merci pour ton énergie toujours positive, ton aide et ton altruisme. Erwan, merci pour ta personnalité rayonnante et tes mots toujours gentils et justes, je suis admirative de la quantité de travail que tu fournis au quotidien avec toutes les personnes que tu manages. Merci **Didier** et **François** pour votre bonne humeur et vos questions pertinentes de prof !!

Ensuite je voudrai adresser ma reconnaissance aux membres de la plateforme lipidomique, **Pierre** et **Laëtitia**, qui m'ont initié à la chimie analytique, pour le meilleur et pour le pire... Merci infiniment pour votre confiance et votre soutien. Votre duo fonctionne très bien, j'ai beaucoup apprécié apprendre à vos côtés et discuter avec vous chimie analytique et autres

À celui qui fait presque parti des murs du LBM, **Jean-Jacques/JJB**, je voulais te remercier pour ton implication, tes conseils, tes explications (parfois trop longues), même tes humeurs (bonnes ou mauvaises), et certaines de tes blagues... pas toutes.

Jorg, Peter, and Gilbert, your collaboration and advices were extremely valuable. Thanks to **Peter** for welcoming me to the laboratory in Frankfurt and for the lessons on LC. **Simona, Suzanna**, and specially **Gerlinda**, thank you for your good mood, your jokes and your help which brightened up my days in Frankfurt. I really enjoyed my experience in Frankfurt, I learnt a lot, both scientifically and personally.

A tous les membres du LBM, merci. Travailler à vos côtés a été une super expérience pour moi, le LBM ne serait pas ce qu'il est sans vous. Merci à **Sebastien, Denis, Franziska, Claire, Amélie, Valérie, Marina, Elia, Jennifer, Terezinha, Yohan, Magali, Rémi, Karim, Camille, Pathy, Emeline, Marija, Hortense, Jonathan**.

Je vais évidemment remercier celles avec qui j'ai partagé cette aventure depuis le début, mes collègues de bureau et amies, **Julie** et **Louise**. Merci du fond du cœur. Ces années n'auraient pas été aussi merveilleuses sans votre soutien sans faille, nos discussions (parfois tard), nos éclats de rires, et nos montages photos évidemment ! Merci, merci pour tout, je suis très heureuse d'avoir partagé votre quotidien pendant 3 ans. Ce quotidien avec vous va profondément me manquer.

Je voulais aussi remercier les grandes sœurs, celles qui sont déjà docteurs et dont les réussites m'ont inspirée et motivée, **MD, Marguerite** et **Delphine**, merci pour les conseils, les rigolades et tout le reste ! Merci à celles qui sont arrivées récemment, **Léna** et **Inès**, merci pour votre joie de vivre et vos rires. Vous avez aussi été de vrais soutiens pendant la fin de cette thèse, merci. À mes « strong friends », **Clément** et **Matthieu**, merci pour ces moments d'escalade entrecoupés de bavardages (un peu) et de rigolades (beaucoup). Merci pour tout, nos blessures en témoigneront toujours... Merci également à **Victor, Matheus, Josselin, Jessi, Rodrigo, Tatiana, Bastien & Youcef** pour tous les moments partagés.

Je souhaitais aussi remercier mes amis, qui malgré la distance, je retrouve toujours comme si nous ne nous étions jamais quittés, **Laurie et Ben, Léa, Laurianne, Audrey, Sarah, Elodie.**

Merci à ma **belle-famille Rochelaise/Oléronaise/Gapençaise**, pour leur amour et leur bienveillance. Je note ici que j'étais avec vous la veille du dépôt de ce manuscrit. Corriger les derniers détails avec 4 enfants dans la pièce + un Hugo qui me fait la discussion : challenge accepted.

J'en viens évidemment à remercier ma famille, sans qui je ne serais pas là où j'en suis aujourd'hui. À **mes parents**, et à **ma sœur** et **mon frère**, merci d'avoir contribué à forger la personne que je suis aujourd'hui, et de m'avoir soutenue à chaque étape de ma vie. Je remercie profondément ma **maman** qui me fait grandir de son amour et de sa générosité chaque jour.

Et enfin, merci infiniment à mon **Jules**, celui qui a été le pilier de ma vie depuis quelques années, et donc de ce travail. Merci de prendre soin de moi au quotidien, sans toi j'aurais sans doute fini par m'alimenter exclusivement d'avocado toast et d'œufs. Merci d'avoir été là pour m'épauler dans les moments difficiles, merci de me faire rire tous les jours, merci pour ton soutien, sans toi j'aurais peut-être fini par « péter un câble ». Merci pour ton amour.

Merci à chacun et chacune d'entre vous pour avoir rendu ces trois années si exceptionnelles, grâce à votre soutien, votre énergie positive et nos rires. Cette expérience m'a permis de grandir et d'apprendre, tant sur le plan professionnel que personnel.

To my beloved father

"Le problème c'est le temps" Erwan

"Si c'était facile, ça aurait déjà été fait" Jérôme

"Les plus grandes douleurs sont muettes" JJB

"Tu es patiente mais pressée d'être indépendante" Pierre

"Il court il court le furet" FredDo

TABLE OF CONTENTS

Introduction	10
1. Fatty acid structure.....	10
2. Physiological role of VLCFA.....	11
3. VLCFA biosynthesis.....	15
3.1 FAS : Fatty Acids Synthase	15
3.2. FAE : Fatty Acid Elongase complex	16
3.3. KCS : 3-ketoacyl-CoA synthase.....	17
3.3.1. Description and mechanism.....	17
3.3.2. Recent novel findings about Arabidopsis KCSs.....	21
3.3.3. Homology modeling	22
3.3.4. Molecular basis of substrate specificity	25
3.3.5. Protein-protein interactions.....	27
3.4. Acyl-CoA.....	30
3.4.1. Acyl-CoA structure.....	30
3.4.2. Methods for Acyl-CoA analyses.....	31
a. Sample preparation and extraction.....	31
b. Chromatographic conditions for acyl-CoA separation	32
c. Mechanisms of mass spectrometry to detect acyl-CoA	34
4. Herbicides targeting the biosynthesis of VLCFAs	36
4.1. Phenotype in plants.....	38
4.2. Target protein	41
4.3. Inhibitor reaction with the target protein	41
5. Methods for studying KCS	44
Objectives	46
Chapter 1 - Functional characterization of plant KCS family in a yeast system	49
1. Evolution of KCS gene family in plants	49
1.1. Phylogenetic tree.....	52
2. Characterization of plant KCS family in a yeast system.....	55
2.1. KCS candidates for enzyme activities through plant species	55
2.2. Heterologous expression of KCS in yeast.....	58
2.3. Comparative analysis of KCS activity across diverse plant species	59
2.3.1. Comparative analysis of clade γ KCS activity	61
2.3.2. Comparative analysis of clade α KCS activity.....	63
2.3.3. Comparative analysis of clade ζ / ι KCS activity	68
2.4. Identification of putative specificity-determining residues through multisequence alignments of KCS4-,9-,17-like	71

3. Conclusion	75
Chapter 2 - Mechanistic understanding of herbicide molecular target and plants selectivity	
<i>in vivo</i>	78
1. Studies on the mechanism of action of group 15 herbicides	80
1.1. Influence of K3 herbicides on endogenous VLCFA biosynthesis and yeast growth	80
1.2. Influence of HRAC group 15 herbicides on elongases expressed in yeast	82
1.2.1. KCSs from <i>Arabidopsis thaliana</i>	82
1.2.2. KCSs from several plant species	84
1.2.3. Concentration dependence of inhibition	87
2. Studies on the mechanism of action new herbicides developed by Bayer SA	88
2.1. Influence of herbicides on elongases expressed in yeast	88
2.2. Concentration dependence of inhibition	89
3. Conclusion	90
Chapter 3 - Development of a non-radiolabeled <i>in vitro</i> assay for evaluating KCS activity and inhibition	
and inhibition	92
1. Validation of yeast microsomes preparation	93
2. Elongase activity assay	97
2.1. GC-FID detection strategy: odd acyl-CoA as substrate	98
2.2. HPLC-MS/MS : acyl-CoA detection	101
2.2.1. HPLC method – HPLC-MS/MS	101
a. MS Detection of Methylated Acyl-CoAs	102
b. Chromatographic Improvement after derivatization	104
c. Yeast matrix effect on Acyl-CoA	105
d. Sample preparation before derivatization step	106
2.2.2. HPLC method – HPLC-UV-MS/MS	108
2.2.2.1. Method validation	108
a. Linearity and range	108
b. Sensitivity	109
c. Stability	109
2.2.2.2. Enzyme activity	110
a. Substrate specificity	112
b. Dose response-curve	115
3. Conclusion	117
Discussion and perspectives	119
Materials and Methods	126
References	134

INTRODUCTION & OBJECTIVES

Introduction

1. Fatty acid structure

Fatty acids (FAs) constitute a large class of molecules characterized by a carboxylic acid moiety attached to an aliphatic tail. FAs are classified based on their hydrocarbon chain length, ranging from short-chain FAs (SCFAs; C4-C8), medium-chain FAs (MCFAs; C10-C14), long-chain FAs (LCFAs; C16-18), to very-long-chain FAs (VLCFAs; C20-C38) (Figure 1). The diversity of FAs arises from variations in the acyl chain length and the presence of double bonds or hydroxyl groups. The physical and structural properties of FAs, such as melting point and water solubility, are influenced by factors like the degree of unsaturation and chain length, which subsequently affect their biological functions.

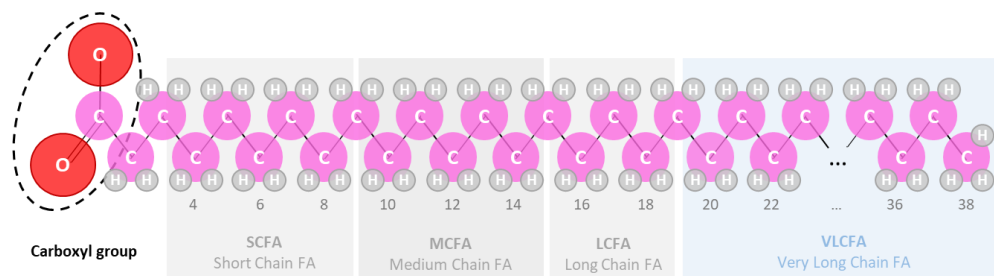


Figure 1. Fatty acid structure

In the context of plant physiology and development, lipid molecules play a crucial role in enabling adaptation to environmental changes. Among these lipids, VLCFAs are essential participants in numerous biological processes that cannot proceed via C14–18 aliphatic chains alone. VLCFAs are then components of the polar lipids in biomembranes, contribute to the formation of surface barriers on leaves, stems, and roots, and are also part of the storage lipids in the seeds of some plant species.

2. Physiological role of VLCFA

VLCFAs are found in five major lipid pools in Arabidopsis: sphingolipids, phospholipids, triacylglycerols, suberin, and cuticular waxes (Figure 2). The presence of VLCFAs in these lipid pools highlights their vital role in a wide variety of functions in Arabidopsis (Figure 3). Two comprehensive reviews on VLCFA biosynthesis in plant tissues were recently published by Batsale et al. (2021) and Zhukov and Popov (2022).

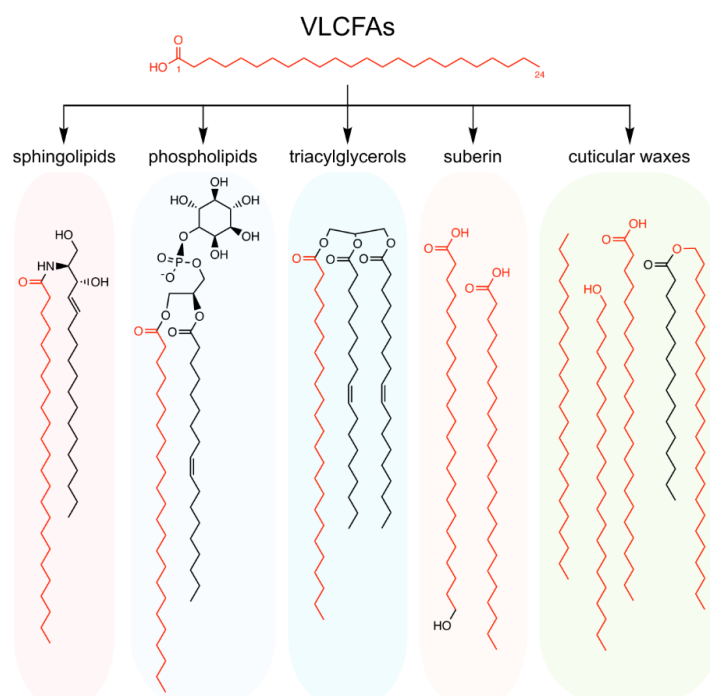


Figure 2. Structure of VLCFAs and their derivatives from Chen manuscript 2022. VLCFAs are incorporated into a variety of different lipids.

Phospholipids constitute a vital structural component of cellular membranes, and their composition significantly influences membrane properties and functions. Phosphatidylcholine (PC), phosphatidylethanolamine (PE), and phosphatidylserine (PS) are major phospholipid species in cell membranes. These phospholipids exhibit a preference for incorporating saturated very-long-chain fatty acids (VLCFAs), with carbon chain lengths ranging from C20 to C24 (Devaiah et al. 2006). These VLCFAs are essential for maintaining membrane integrity and fluidity, as well as facilitating various biological processes. The ester, ether or amide bonds connecting VLCFAs to the polar heads of phospholipid molecules contribute to membrane stability and functionality.

Sphingolipids are components of plasma membranes, important signaling molecules, and form membrane microdomains (lipid rafts). They also play a role in programmed cell death. Sphingolipids are predominantly located in the outer leaflet of the plasma membrane. These lipids, enriched in α -hydroxylated saturated and monounsaturated VLCFAs with chain lengths of C24 and C26, play crucial roles in membrane lipid asymmetry, charge balance, and curvature (Markham et al., 2006; 2013). The unique properties of sphingolipids contribute to the dynamic nature of the cellular membranes and facilitate essential cellular functions.

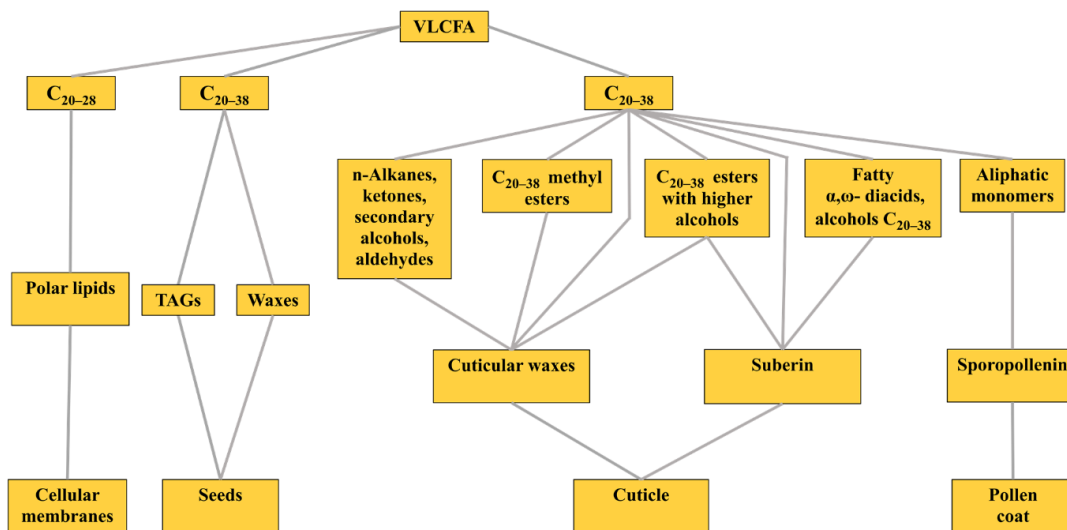


Figure 3. The distribution of very-long-chain fatty acids (VLCFA) in plant cells and tissues from Zhukov and Popov review (2022). C20–28 VLCFA are the components of polar lipids (PL) of cell membranes. C20–38 VLCFA are found in developing seeds as a part of reserve triacylglycerols and can be derived in several molecules found in lipid barriers such as cuticular waxes, suberin and pollen coat.

The cuticle serves as a protective barrier against various biotic and abiotic stress in terrestrial plants. This continuous layer, consisting of lipophilic materials, covers the surfaces of all the epidermal cells in terrestrial plants. The cuticle is composed of cuticular waxes and cutin, with cuticular waxes being either epicuticular or intracuticular and embedded within the cutin layer that adheres to the primary cell wall (Zhukov and Popov, 2022).

Cuticular waxes, crucial components of the plant cuticle, contain a diverse array of aliphatic compounds, predominantly derived from very-long-chain fatty acids (VLCFAs). In dicotyledonous plants, although most intracellular VLCFAs contain twenty-six or fewer carbon atoms ($\leq C26$), plant cuticular VLCFAs and their derivatives typically contain approximately 30 carbon atoms, which are mostly saturated. These compounds comprise a wide variety of chain lengths and chemical structures, including aldehydes, secondary alcohols, n-alkanes, and ketones, each of which has a chain length of C21–35, as well as fatty alcohols with C22–34. Additionally, free VLCFAs, along with C16–18 fatty acids, are present in cuticular waxes and are often linked by ester bonds with alcohols to form wax esters.

Notably, in cuticular waxes and the pollen coat, the total length of the VLCFA chain in conjunction with higher alcohols can extend from C38 to C60 (Razeq et al., 2014). These newly formed VLCFAs, along with C16–18 fatty acids, serve as substrates for enzymes involved in the synthesis of primary aliphatic components of cuticular waxes, suberin, and pollen coats (Hegebarth et al., 2017; Haslam and Kunst, 2013; Lü et al., 2009). The hydrophobic “film” formed by cuticular waxes on plant aerial surfaces serves as a protective barrier against environmental stress such as desiccation, infection, and herbivory (Todd et al., 1999; Serrano et al., 2014; Xue et al., 2017).

Suberins distributed on the inner surfaces of primary cell walls in various plant parts, including the peridermal tissues of shoots and roots as well as the root endoderm. Suberin is known to contain significant amounts of VLCFA-derived components, and VLCFA are specifically hydroxylated VLCFA. Comprising a polyester of glycerin, phenols, and fatty acid derivatives, the aliphatic portion of suberin includes hydroxy-fatty acids, and small amounts of free VLCFA. Suberin is known to contain significant amounts of VLCFA-derived α -, ω -dicarboxylic acids, alcohols, and diols (Franke et al., 2005; Pollard et al., 2008; Domergue et al., 2010). Suberin has important functions including controlling the movement of water and solutes, providing strength to the cell wall, and acting as a barrier against pathogen infection.

Finally, VLCFA are also present in developing seeds, where they constitute a significant portion of the total amount of fatty acids. In seeds, VLCFA may be incorporated into triacylglycerols (TAG) to serve as a reserve of energy for germinating seeds. For example, in *Arabidopsis* seeds, storage lipids VLCFA represent approximately 27% of the total acyl chains, and if C20 and C22 monounsaturated VLCFA dominate (Batsale et al., 2021), polyunsaturated VLCFA with up to three double bonds are also present in minor amounts (Millar and Kunst, 1997).

Each modification of the acyl chain has a direct effect on the chemical and physical properties of the resulting fatty acids and derivatives (Figure 4), allowing for a wide diversity of lipid functional specializations.

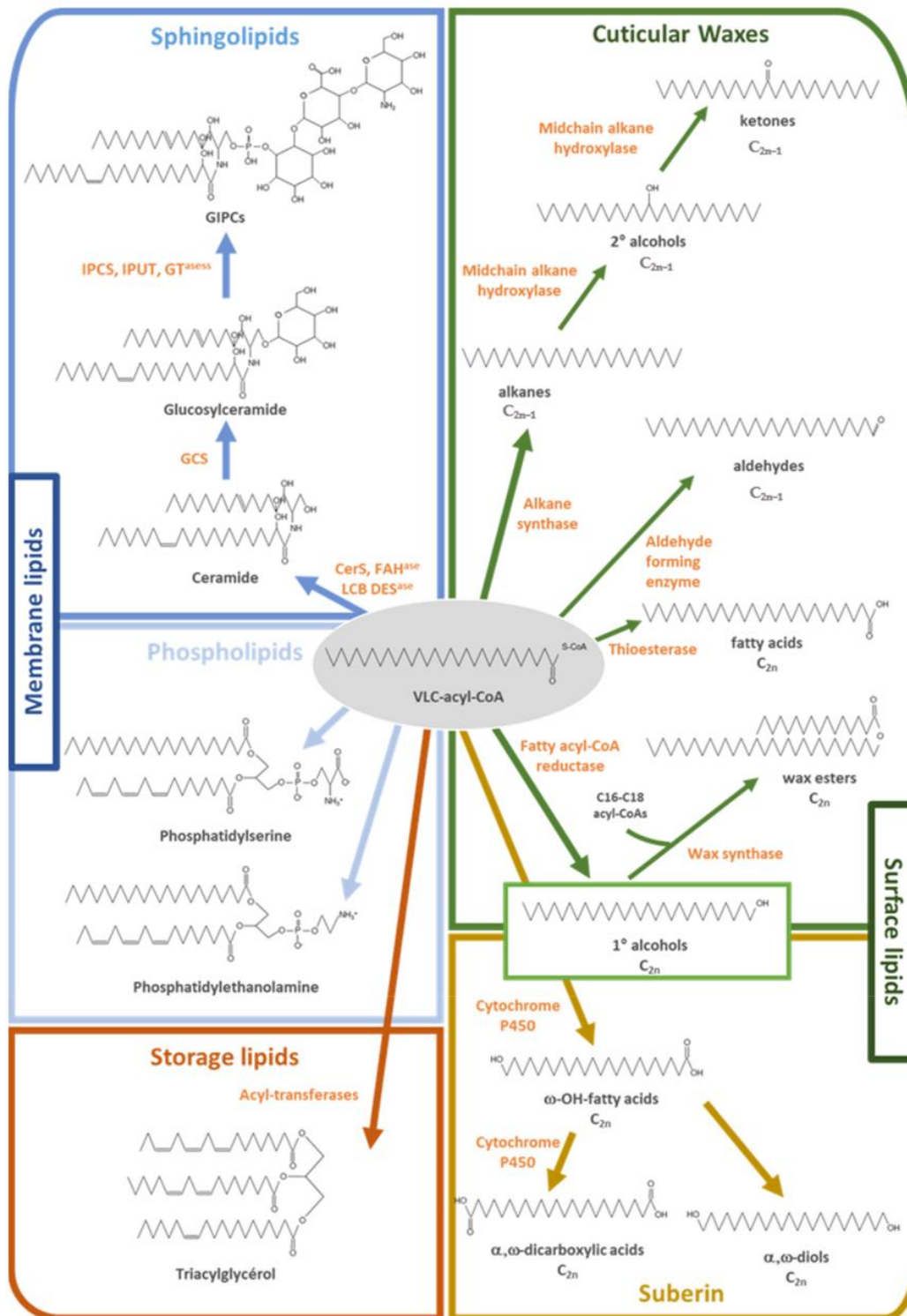


Figure 4. Metabolic fates of very long-chain acyl-CoAs from Batsale et al. (2021). VLC-acyl-CoA produced by fatty acid elongation complexes can be converted into aliphatic derivatives incorporated into the cuticle as cuticular waxes or serve as building blocks for the suberin biopolyester biosynthesis. VLC-acyl-CoA can be incorporated into storage lipids as triacylglycerols or in membrane lipids such as phospholipids (phosphatidylserine and phosphatidylethanolamine) or sphingolipids (ceramide, glucosylceramide and GIPCs). Abbreviations: CerS, ceramide synthase; FAHase, fatty acid hydroxylase; GCS, glucosylceramide synthase; GIPCs, glycosyl-inositolphosphoryl-ceramides; GTases, glycosyl-transferases; IPCS, inositolphosphoryl-ceramide synthase; IPUT, inositolphosphoryl-ceramide glucuronosyl-transferase; LCB DESase, LCB desaturase; VLC-acyl-CoA, very-long-chain acyl-CoA.

3. VLCFA biosynthesis

VLCFA production requires two enzyme systems: de novo fatty acid synthase (FAS) and fatty acid elongase (FAE). In plants and yeast, FAS produces fatty acids with chain lengths of 16 or 18 carbon atoms. FAE is a distinct enzyme system localized in the ER that extends these long-chain fatty acids through a series of iterative reactions until C38 (Figure 5).

3.1 FAS : Fatty Acids Synthase

The carbon for fatty acid synthesis is provided by photosynthesis. The first enzyme in FA biosynthesis is acetyl-CoA carboxylase (ACCase). This enzyme catalyzes the ATP-dependent carboxylation of acetyl-CoA to produce malonyl-CoA, needed to generate malonyl-ACP. The transfer of an acyl group to ACP by transacylase is necessary for the production of malonyl-ACP from malonyl CoA.

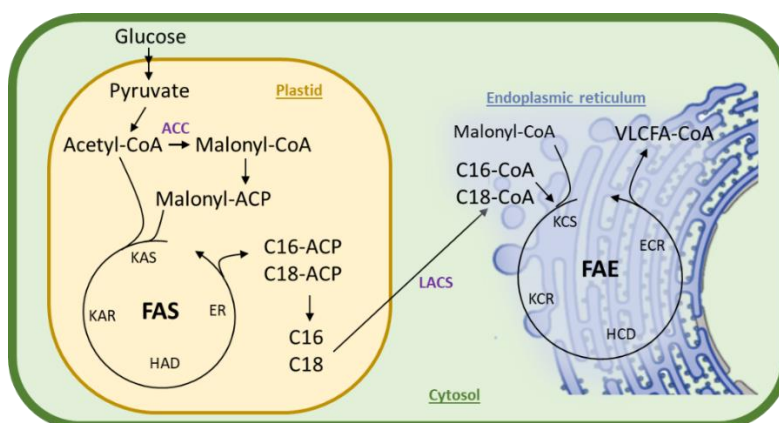


Figure 5. Biosynthesis and selective involvement of VLC acyl-CoAs in the different lipid biosynthesis pathways in plant cell.

The next step of FA biosynthesis involves fatty acid synthase (FAS), a multiprotein complex. The following reactions are catalysed by this complex in plants : an acyl transfer reaction, four reactions involved in a 2 carbon addition. Until is a 16-18 carbon chain length. This process start with a condensation reaction that is catalyzed by one of three 3-ketoacyl-ACP synthase (KAS) enzymes, depending on the length of the substrate chain. KAS III catalyzes the first reaction between acetyl-CoA and malonyl-ACP producing a 4-carbon product (Ohlrogge and Browse, 1995; Harwood, 1996). KAS I extends the chain from 4 to 16 carbons, and KAS II catalyzes the final condensation reaction to create 18-carbon chains. The second step in the 2-carbon addition is a reduction reaction, catalyzed by 3-ketoacyl-ACP reductase (KAR). The third reaction is a dehydration reaction, catalyzed by 3-hydroxyacyl-ACP dehydratase (HAD). The fourth reaction is a reduction reaction, catalyzed by enoyl-ACP

reductase (ER). This process is terminated by the release of fatty acyl-ACP as free fatty acids by acyl-ACP thioesterases.

VLCFA biosynthesis is accomplished by the elongation of LCFAs in the endoplasmic reticulum (ER). Since plants synthesize LCFAs in the plastid, an extra step is needed to export FAs to the ER. This is accomplished by long-chain acyl-CoA synthetases 9 (LACS9), as recently reported in Zhao et al. (2021) review. These enzymes activate saturated and monounsaturated C16 and C18 fatty acids by the addition of Coenzyme A to transport them across the membrane into the cytosol (Pulsifer et al., 2012) and exported to the ER (Harwood, 1996). These long-chain acyl-CoAs are the immediate precursors of VLCFA as they are further elongated through FAE complexes localized in the endoplasmic reticulum membranes.

3.2. FAE : Fatty Acid Elongase complex

Several studies have suggested the existence of multiple fatty acid elongase complexes (FAE complexes) that perform sequential and/or parallel reactions to produce the broad range of VLCFA found in plants.

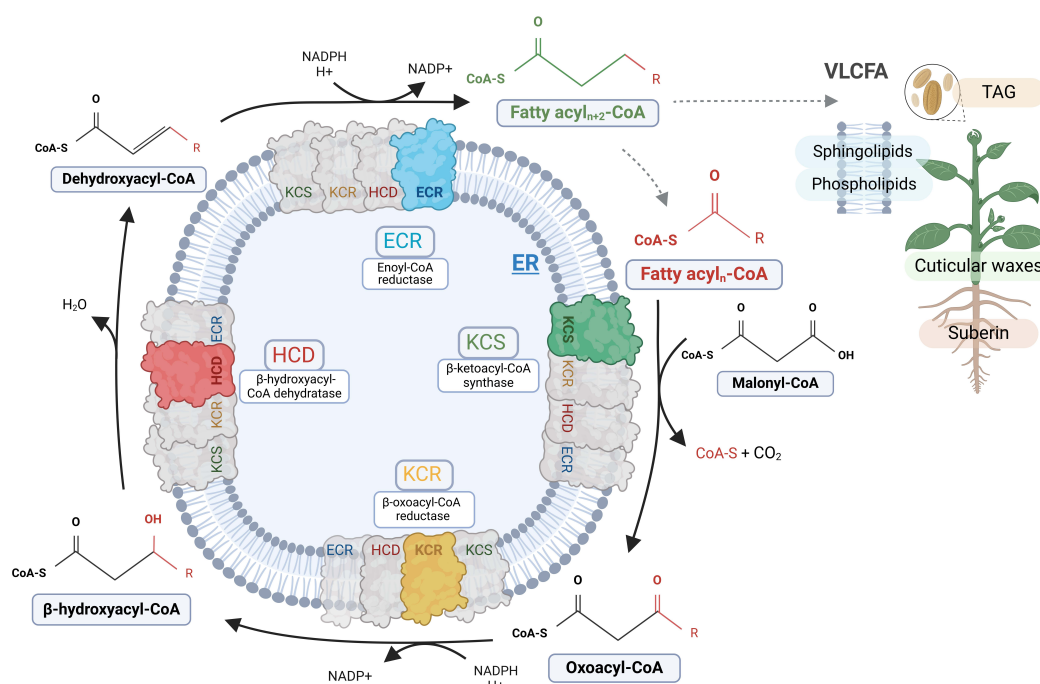


Figure 6. Biosynthesis of VLC acyl-CoAs. VLC acyl-CoAs are elongated from C16 and C18 long-chain fatty acids. Oxoacyl-CoA is also 3-keto-acyl-CoA

The four core enzymes of the FAE complex are involved in the sequential addition of a C2 unit from malonyl-CoA to the acyl chain acceptor (Figure 6). The first reaction involving the condensation of the acyl-CoA substrate (n) with malonyl-CoA, is catalyzed by β -keto-acyl-CoA synthase (KCS), and produces β -keto-acyl-CoA (n+2). A β -keto-acyl-CoA reductase (KCR) then reduces the β -keto group into an alcohol using NAD(P)H as reductant, yielding 3-hydroxyacyl-CoA. A 3-Hydroxyacyl-CoA Dehydratase (HCD) then converts this intermediate into enoyl-CoA, which is reduced by the Enoyl-CoA Reductase (ECR) to form a fatty acyl-CoA which is 2 carbon longer (n+2) than the initial acyl-CoA substrate. This reaction cycle is repeated to yield VLCFA with various chain lengths, ranging from C20 to C38 or more. The current understanding of the elongase complex structure is limited. The KCS, also known as condensing enzyme, plays the key role in catalyzing the rate-limiting step of the process and in determining the substrate and tissue specificities of fatty acid elongation. In contrast, the remaining three enzymes (KCR, ECD and ECR) have broad substrate specificities and are present in all tissues capable of synthesizing VLCFAs (Fehling and Mukherjee, 1991; Millar and Kunst, 1997; Roudier et al., 2010). Therefore, the various FAE complexes present in plant cells only differ by their KCS constituent.

3.3. KCS : 3-ketoacyl-CoA synthase

3.3.1. Description and mechanism

KCS catalyzes the first step in the microsomal FAE complex, which involves the condensation of a fatty acyl-CoA and malonyl-CoA through a decarboxylative Claisen condensation. The fatty acyl-CoA and malonyl-CoA substrates are delivered cytosolically (Blacklock and Jaworski 2002). KCSs anchored to the membrane of the ER through two predicted N-terminal helices, with the bulk of the protein being on the cytosolic face of the membrane. The 3-ketoacyl-CoA product is then expected to be released into back the cytosol where the rest of the FAE complex can catalyze the subsequent steps of VLCFA elongation.

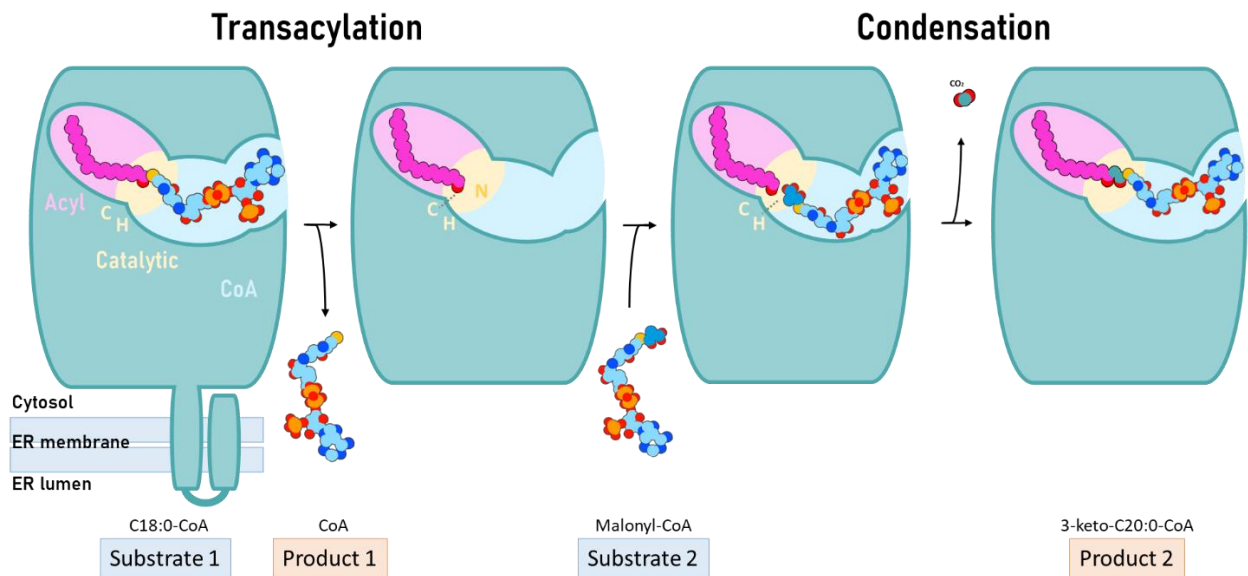


Figure 7. Suggested model of ketoacyl-CoA synthase (KCS) ping-pong catalytic mechanism modified from Haslam and Kunst (2013), and Nie et al. (2021). An acyl group is transferred from acyl-CoA on to a cysteine residue of the KCS. Decarboxylation of the malonyl-CoA driven by the catalytic histidine and asparagine residues, release of a molecule of CO₂, nucleophilic attack of the carbanion intermediate onto the C1 of the thio-acyl intermediate, led to release a β -ketoacyl product.

The first KCS enzyme to be identified in plants was fatty acid elongation 1 (KCS18/FAE1) (James et al., 1995). This reaction was suggested to be the rate limiting step in VLCFA synthesis and determines the product length of the elongase complex (Millar and Kunst, 1997). Three residues in the active site of KCS18/FAE1 were shown to be essential for its catalysis: Cys-233, His-391, and Asn-424 (Ghanevati and Jaworski, 2002). Supported by the mutagenesis of these key residues, KCS catalysis is thought to occur through a ping-pong (i.e., double displacement) mechanism (Ghanevati and Jaworski, 2001). In ping-pong reaction, the two substrates (fatty acyl-CoA and malonyl-CoA) do not bind to the enzyme at the same time. Instead, the first substrate (fatty acyl-CoA) binds to the enzyme, transferring the fatty acyl group to the catalytic cysteine residue and releasing the first product (CoA). This acyl-enzyme intermediate then binds to the second substrate (malonylCoA) and catalyzes its decarboxylation to a reactive acetyl enolate or carbanion. This results in the covalent transfer of the fatty acyl group from the enzyme to the carbanion, and the release of the second product (3-ketoacyl-CoA). This makes modeling by homology difficult with relevant enzyme with substrates template structure.

The discovery of FAE1 led to the discovery of other KCS enzymes which are known as FAE1- like genes, of which, 21 have been found in *Arabidopsis thaliana* (Costaglioli et al., 2005). KCS from Arabidopsis were classified based on the eight Arabidopsis KCS subclasses, labeled as clades α to θ (Joubès et al.,

2008) (Figure 8). Among these 21 isoforms, several have been characterized either through chemical analysis of lipids containing VLCFA in the corresponding *Arabidopsis kcs* mutants, or through heterologous expression in yeast (Figure 9).

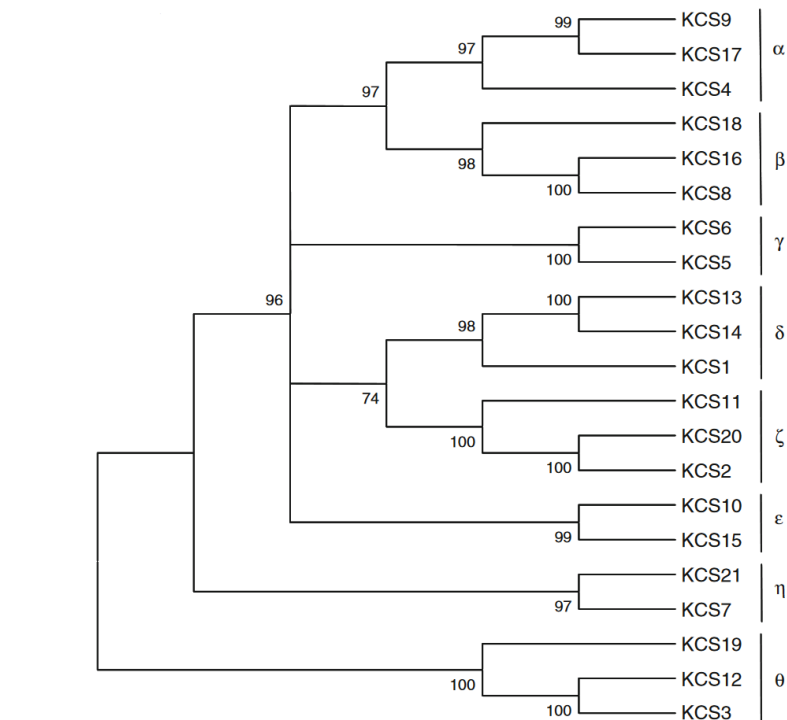


Figure 8. Phylogenetic analysis of the *Arabidopsis* KCS sequences from Joubès et al. (2008)

For example, KCS1 produces saturated and monounsaturated C20:0, C20:1, C22:0, C22:1 and C24:0 by using C16:1, C16:0, C18:1, C18:0 as precursors, but the disruption of *kcs1* in *Arabidopsis* caused no significant reduction in total wax load or in the levels of any individual wax component, suggesting functional redundancy between different KCSs (Todd et al., 1999; Trenkamp et al., 2004; Blacklock and Jaworski, 2006; Paul et al., 2006; Tresch et al., 2012). DAISY/KCS2 and KCS20 catalyze the synthesis of saturated C24, which are required for the production of cuticular waxes and root suberins (Trenkamp et al., 2004; Paul et al., 2006; Franke et al., 2009; Lee et al., 2009; Tresch et al., 2012; Batsale et al., 2023). KCS4 functions in root and pollen tube growth by synthesizing VLCFA longer than C24 (Blacklock and Jaworski, 2006). KCS5 and KCS6 can produce C24 to C28 VLCFA, while KCS6 co-expressed with CER2 or CER2-LIKEs further elongates VLCFA up to C34 to synthesize cuticular waxes (Millar et al., 1999; Fiebig et al., 2000; Tresch et al., 2012; Haslam et al., 2012; 2015). KCS9 produces C22 and mostly C24 VLCFA in yeast (Paul et al., 2006), and *Arabidopsis kcs9* mutant shows a general decrease of C24 acyl-chains, which are found in cuticular waxes, aliphatic suberins, sphingolipids, and phospholipids including phosphatidylserine and phosphatidylethanolamine (Kim et al., 2013). AtKCS11 shows a weak activity in yeast by using C18:0 (Blacklock and Jaworski, 2006) and KCS11 in *N. benthamia* C20-C22 are used.

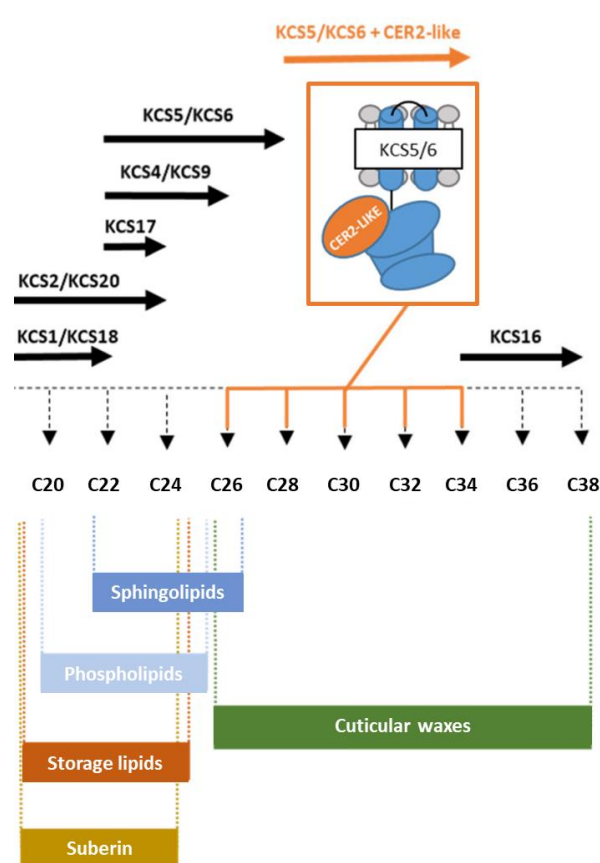


Figure 9. Involvement of VLC acyl-CoAs in the different lipid biosynthesis pathways in Arabidopsis from Batsale et al. (2021). The pool of acyl-CoAs synthesized by FAE complex is exploited towards the synthesis of different lipid categories such as membrane lipids (sphingolipids and phospholipids), surface lipids (cuticular waxes and suberin) and storage lipids (TAG).

The co-expression of Arabidopsis wax biosynthesis genes CER6 (KCS6) and CER26 in yeast resulted in the production of fatty acyl products up to C32 and C34, as reported in previous literature (Haslam et al. 2015). When co-expressed with CER6 (KCS6) and CER26, KCS16 elongates C34 VLCFAs to C38 which serve for wax production of leaf trichomes (Hegebarth et al., 2017). Additionally, AtKCS16 has the ability to produce C22 and C24 VLCFA during lateral root development (Lv et al., 2021). KCS17 mainly produces C24 VLCFA by using C20:0 and C22:0 as substrates (Blacklock and Jaworski, 2006; Tresch et al., 2012). KCS18/FAE1 elongates saturated and monounsaturated C16 and C18 into the corresponding C20 and C22 VLCFAs, which are necessary for synthesizing Arabidopsis seed storage lipids (Kunst et al., 1992; Millar and Kunst 1997; Beaudoin et al., 2002; Ghanevati et al., 2002; Blacklock and Jaworski 2002; 2006; Trenkamp et al., 2004; Paul et al., 2006). Additionally, the roles of certain KCS have been studied in plants during development or in response to environmental conditions. The loss of KCS10/FIDDLEHEAD (FDH) function resulted in the fusion of leaves and floral organs and accumulation of alkanes and aldehydes, suggesting that FDH is involved in epidermal cell development and cuticular waxes biosynthesis (Lolle et al., 1992; Yephremov et al., 1999; Pruitt et al., 2000, Voisin et al., 2009). KCS13 levels have been found to play a role in regulating stomatal development under elevated CO₂

levels (Gray et al., 2000). Thus, the investigation of multiple KCS has led to a more comprehensive understanding of their catalytic activity, their metabolic function in planta, and their ability to respond to environmental conditions in specific tissues.

3.3.2. Recent novel findings about Arabidopsis KCSs

To comprehensively describe Arabidopsis KCS (AtKCS), an analytical platform, which combines and compares the expression of KCS activities in yeast and in plants, has been developed (Batsale et al., 2023). To ensure optimal conditions for AtKCS activity in yeast, the entire Arabidopsis FAE complex was reconstructed and the endogenous yeast condensing enzyme named *ELO3* was deleted to avoid competition with yeast endogenous FAE activity. Within this optimized yeast system, the activity of nine functional AtKCS already described (AtKCS1, 2, 4, 5, 6, 9, 17, 18, and 20) was confirmed. In contrast to Tresch et al. (2012), who did not detect any modification of the yeast fatty acid profile when expressing AtKCS4, Batsale et al. (2023) showed in the TRIPLE $\Delta elo3$ yeast strain that AtKCS4 was able to extend C22 VLCFA up to C26 VLCFA. This discrepancy suggests that AtKCS4 preferentially interacts with the FAE Arabidopsis complex (containing Arabidopsis KCR, HCD and ECR) rather than with the yeast complex (containing YBR159, PHS1, and TSC13). Additionally, AtKCS were expressed in the epidermis of *N. Benthamiana* to provide plant co-factors and a plant cell/membrane environment. The ectopic expression of KCS10, KCS11, and KCS15 induced significant changes in the FAMES profiles of *N. benthamiana* leaves. This strategy allows the first description of the activity of KCS11, belonging to subclass ζ with KCS2 and KCS20. While Blacklock and Jaworski (2006) previously showed that AtKCS11 elongates C18:0 *in vitro*, Batsale et al. (2023) found that KCS11 enhances the accumulation of C22 and C24 in planta. In the subgroup ϵ , AtKCS10 and AtKCS15 promote the accumulation of C22-C24 and C22-C26 levels, respectively. These results suggest that KCS10, KCS11, and KCS15 may require obligatory plant-specific cofactors for their activities.

A recent functional characterization of KCS4 revealed that the enzyme isoform is predominantly expressed in mature pollen and root meristematic regions (Kim et al., 2021). Results from the analysis of total fatty acids in the roots of wildtype, *kcs4*, and *kcs4*-complemented lines indicated that KCS4 might play a role in the synthesis of VLCFAs longer than C24, which are necessary for optimal pollen tube and primary root development in Arabidopsis. Additionally, a metabolomic genome-wide association study has revealed that KCS4 helps control the levels of polyunsaturated triacylglycerols by sequestering saturated VLCFAs into cuticular waxes under carbon starvation conditions, such as heat, darkness, or extended darkness (Luzarowska et al., 2023).

Arabidopsis KCS17 has recently been shown to be involved in the two-carbon elongation of C22 to C24 VLCFA, which are used as precursors for synthesizing seed coat suberin, based on several arguments (Kim et al., 2023). They investigated the expression of KCS17 in developing Arabidopsis seed coat and showed that KCS17 was highly expressed in the outer integument of the seed coat. In *kcs17* mutants, all C24 suberin monomer levels decreased while all C22 suberin monomer levels increased compared to those in the wild type. These results indicate that KCS17 is involved in elongating C22 to C24 VLCFAs and support the specific role of KCS17 in synthesizing seed coat suberin. Additionally, since seed waxes were unaffected in *kcs17* mutants, this study suggests the presence of other KCS isoforms involved in the production of C28 VLCFA required for seed waxes synthesis. Finally, the inactivation of KCS17 was correlated to an increase of seed coat permeability to tetrazolium salts, as well as inhibition of seed germination and seedling establishment under salt and osmotic stresses.

3.3.3. Homology modeling

Structural models of KCS plant proteins and active site topology could help to understand the substrate preferences of this large enzyme family. However, to date, no crystal data have been reported for any plant KCS due to difficulties related to the purification and solubilization of membrane-bound proteins. Homology modeling can be used to predict the KCS structure. Indeed, several studies have modelled KCS structure and active site topology using closely related enzymes as templates, such as *Medicago sativa* chalcone synthase (1BI5), *E. coli* FabH and Type III polyketide synthases (PKS) (Joubès et al., 2008; González-Mellado et al., 2019; Chen et al., 2022; Kim et al., 2022).

These studies defined a triangular form, in which one of the arms is made up of two α -helices, corresponding to the transmembrane domains, that anchor the enzyme to the endoplasmic reticulum membrane. These two hydrophobic domains are present in the N-terminus of the sequence corresponding to residues 44–66 and 85–103 of AtKCS1 (Joubès et al., 2008), 85–467 and 104–485 of HaKCS1 and HaKCS2 (González-Mellado et al., 2019), 1–103 of KCS9 (Kim et al., 2022), and 1–106 in PtKCS1, 2, and 4 (Chen et al., 2022). However, AtKCS of subclasses θ (KCS12, 19, 3) and η (KCS21, KCS7), but also KCS18 and KCS15 from the β and ϵ subgroups, respectively, have no or only one putative hydrophobic domain with lower statistical significance, as amino-acid residues 20–43 of AtKCS21. This may impact the localization of these proteins and, like in the case of KCS18 that was shown to be associated with membranes (Ghanevati and Jaworski, 2001), could suggest an alternative mode of membrane anchoring (via interaction with an integral membrane protein, post-translational modifications ...) (Joubès et al., 2008). Generally, these transmembrane domains are not included in 3D modeling because of their low confidence and the absence of amino acid sequences matching with the templates.

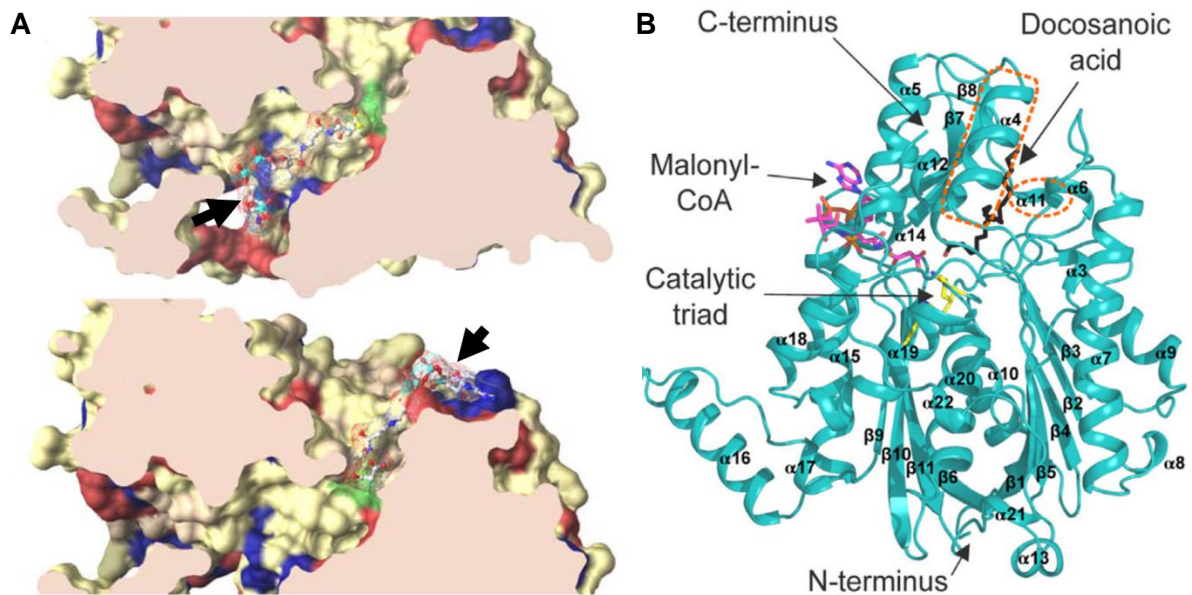


Figure 10. Structural analysis of proteins from the KCS family by homology modeling. (A) Two potential docking positions for malonylCoA (meshed surface) in the AtKCS1 (plain surface) binding pocket from Joubès et. (2008). Black arrows point to the CoA ring. The AtKCS1 residues are colored in bright yellow when hydrophobic and not charged, in red when positive, in blue when negative, in green for the active Cys258. The AtKCS1 surface was cut by a plane perpendicular to the line of sight to reveal the shape of the binding pocket. **(B)** Homology model of PtKCS1 from Chen et al. (2022). Homology model of the cytosolic portion of PtKCS1 docked with docosanoic acid (black) and malonyl-CoA (magenta), with the catalytic triad shown as yellow sticks. Alpha helix 4 and position 277 are highlighted by an orange dotted line.

The main bodies of the secondary structures have been described with two potential conformations. On one hand, an α - β - α - β - α structure with both coupled monomers displaying triangle forms, conserved between Type III PKSs, 3-keto-acyl-ACP synthases and thiolase proteins has been proposed (Mathieu et al., 1994). On the other hand, a monomer α - β - α - α structure was proposed in the secondary structure of AtKCS1 (Joubès et al., 2008). These structures encompassed the residues of the catalytic triad : Cys258, His425, Asn458 in *Arabidopsis thaliana* KCS1 (Joubès et al., 2008); Cys223, His390, and Asn423 in HaKCS1; Cys241, His408, and Asn441 in *Helianthus annuus* KCS2 (González-Mellado et al., 2019); Cys249, His416 and Asn449 in *Populus trichocarpa* KCS1 (Chen et al., 2022) and they were grouped close to each other to form a hydrophobic cavity within the protein, facilitating substrate entry (González-Mellado et al., 2019). Joubès et al. (2008) confirmed the presence of this putative catalytic triad in all AtKCS, except KCS10 in which the histidine residue is replaced by a leucine residue, suggesting that KCS10 is inactive. In HaKCS2, the three catalytic residues are accessible to the acyl moiety of the substrate, which accommodated into a cavity crossing the protein from one side to the other (González-Mellado et al., 2019). These configurations are analogous to that previously described for the catalytic activity of FabH proteins (Qiu et al., 1999; 2001), supporting a phylogenetic relationship between KCS and bacterial KASIII from a cyanobacterial ancestor.

Joubès et al. (2008) described two entry points for the binding pocket of AtKCS1 (Figure 10A), three for KCS3 and only one for KCS19. Indeed, the capping of the protein surface by parallel planes allows for different sizes and shapes of the predicted binding pockets. For example, these pockets are described as strikingly small for KCS18, KCS19, and KCS21, in which only one entry exists for the ligand to access the active cysteine. Chen et al. (2022) described the binding tunnel of PtKCS1 is kinked compared to PtKCS2 and 4, due to helice-4 position (Figure 10B). Therefore, two models of PtKCS1 docked with *cis*- ω 9 monounsaturated fatty acid have been proposed by Chen et al. (2022) (Figure 11). They indicate that four helices (4, 6, 7, 11) and an amino acid seems to influence the pocket binding size in PtKCS1.

While the CoA moiety is positioned close to helices 5 and 12, which contain only few substitutions between paralogs, showing that the malonyl-CoA occupies a constant position in the different KCS: close to the Sulphur atom from the active cysteine residue allowing this atom to conduct nucleophilic attack on the carbonyl of acetyl-CoA (Joubès et al., 2008).

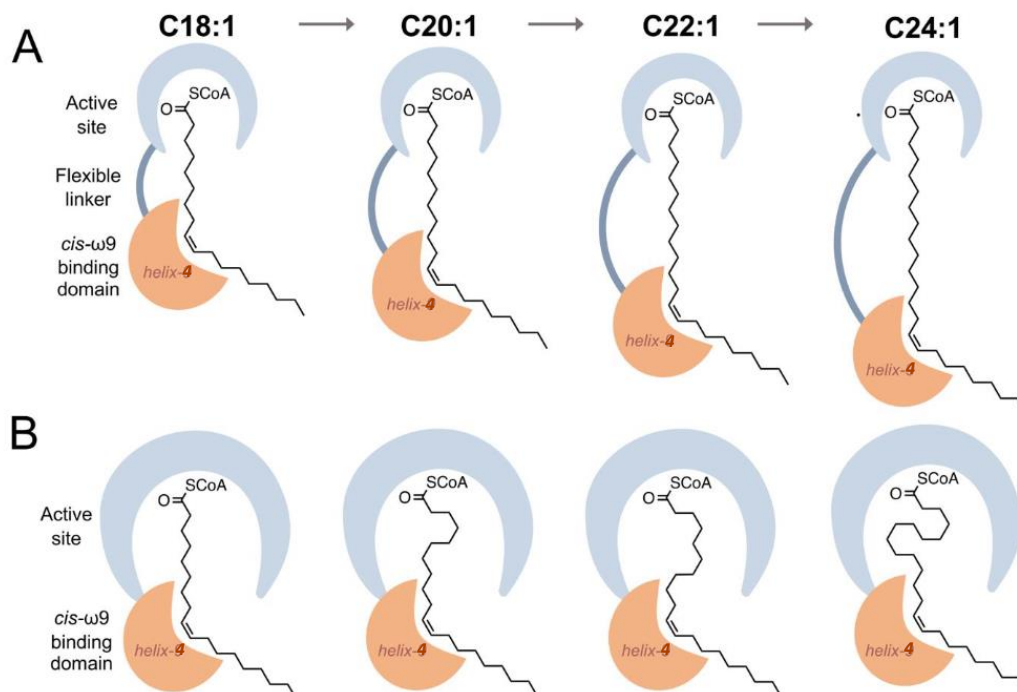


Figure 11. Proposed models of PtKCS1 elongation of *cis*- ω 9 monounsaturated fatty acids by Chen et al., (2022). Schematic representation of the acyl-CoA substrates in the PtKCS1 active site for the (A) flexible model and (B) fixed model. In the flexible model, a *cis*- ω 9 binding domain (containing helix-4) recognizes the unsaturated motif while a flexible binding tunnel accommodates for longer chain lengths. In the fixed model, the unsaturated motif binds to a fixed *cis*- ω 9 binding domain while the acyl end of the substrate conforms to fit inside the active site pocket, allowing for elongation of longer chain lengths.

Interestingly, in the homodimer model predicted by González-Mellado et al (2019), one residue from the other monomer, Thr196 in HaKCS1 and Thr214 in HaKCS2, protrudes into the active site, suggesting that it participates in interaction with the substrate or the enzymatic reaction. Similar observation has been found in type III ketoacyl-ACP synthases and polyketide synthases, where a single phenylalanine residue from each monomer protrudes into the active site of the other (Qiu et al., 2001), suggesting that dimer formation plays an important role in the enzymatic activity.

3.3.4. Molecular basis of substrate specificity

Understanding the molecular mechanisms can help to elucidate the variability of substrate specificities characterizing plant KCS, predict functional changes directly from sequences, and enable enzyme engineering. However, these studies are likely hindered by the lack of structural resources and insolubility of membrane proteins, limiting our understanding of these mechanisms.

Several critical domains and residues that play a role in determining the substrate specificity of *Brassicaceae* FAE1/KCS18 enzymes have been identified through various approaches. FAE1 orthologs from *A. thaliana* and *Brassica napus*, which share 86% amino acid identity, are involved in the elongation of a C18:1 substrate into C20:1 and C22:1 products. However, when expressed in yeast, they produced different ratios of C22:1/C20:1 products, with a value of 0.12 for AtFAE1 and 0.34 for BnFAE1. Using domain swap, the first 173 residues of N-terminal domain (excluding transmembrane helices) were able to convert the product ratio of C20:1 to C22:1 from one KCS to another (Blacklock and Jaworski, 2002). Moreover, directed mutagenesis revealed that the lysine 92 is involved in catalytic activity as well as substrate specificity. To identify candidate genes involved in seed VLCFA content variations between Bay-0 and Shahdara *Arabidopsis thaliana* ecotypes, quantitative trait loci (QTL) analyses were performed. The analyses determined a single nucleotide polymorphism (SNP) in position 407 the FAE1/KCS18 sequence (Jasinski et al., 2012). The L407V change leads to a 25% narrowing of the catalytic pocket in Shahdara KCS18 compared to the Bay0 enzyme. Sun et al (2013) utilized these results to investigate the correlation between KCS18/FAE1 genetic variations and seed erucic acid (C22:1) content in a comprehensive analysis of 60 *Brassicaceae* accessions.

In a second approach, Jasinski et al. (2012) performed quantitative trait loci (QTL) analyses. Consistent with this, only Bay-0 KCS18 leads to the accumulation of C20:1 products after expression in yeast, suggesting that conformational changes in Shahdara KCS18 alter its activity towards VLC-CoAs. The approach proposed by Jasinski et al. (2012), which combines genetic analyses with functional and structural characterization, presents a promising opportunity to elucidate the molecular mechanisms underlying KCS substrate specificity. KCS18/FAE1 enzyme is a strong candidate for this study due to its

high level of genetic diversity, the availability of its sequence data in multiple accessions, and measurable functional activity. However, these residues are not located in the domain and residues determinant for KCS18/FAE1 substrate specificity or functional activity, as identified by Blacklock and Jaworski (2002) and Jasinski et al. (2012). Additionally, the variability in seed erucic acid content between Brassicaceae accessions may not be directly related to KCS18/FAE1 genetic variability, despite the correlation established by Sun et al. (2013). Therefore, these residues may represent potential determinants of FAE1 orthologs functional activity, but further experiments are needed to establish a direct link between KCS18/FAE1 genetic variability and seed erucic acid content.

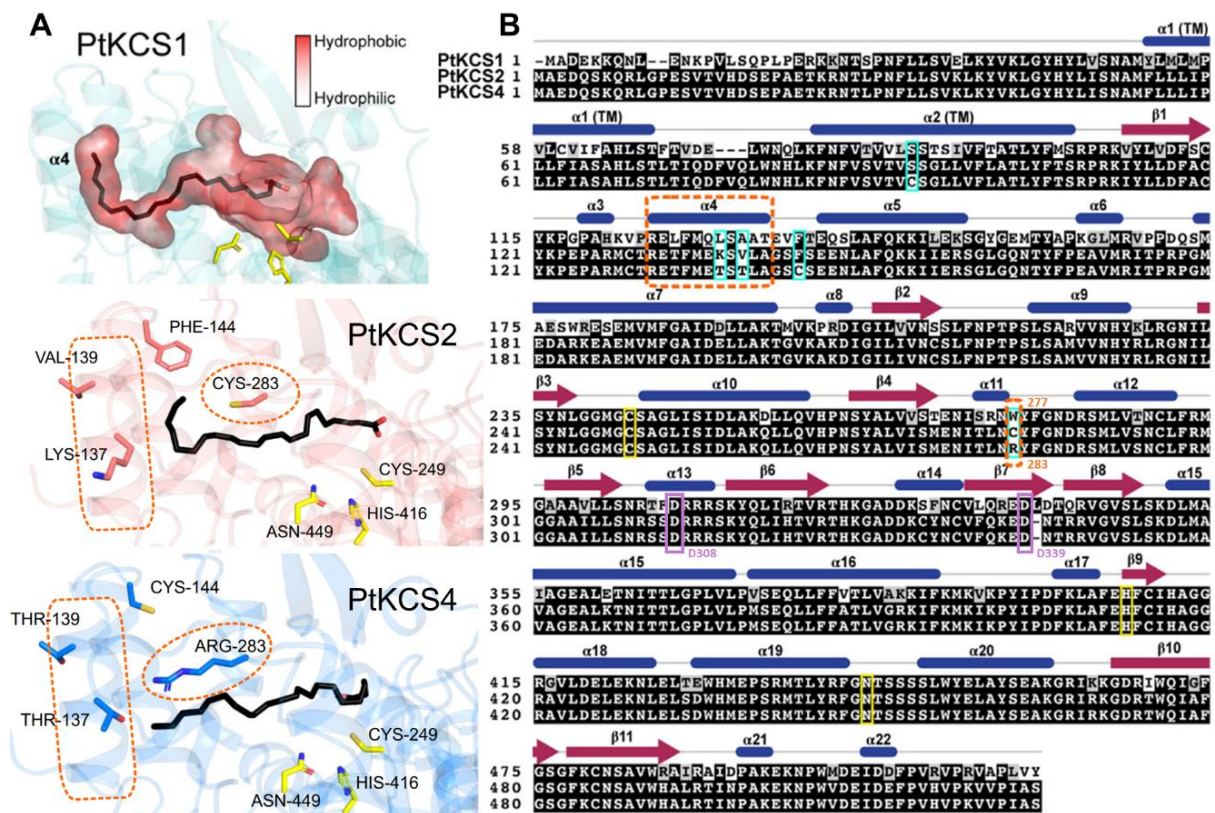


Figure 12. Structural and sequence comparisons of PtKCS1, 2, and 4 from Chen et al. (2022). **A** comparison of the binding tunnel in PtKCS1, 2, and 4 homology models, close-up view of the region in PtKCS2 and 4 where docosanoic acid (black) is docked. Amino acid differences between PtKCS2 and 4 are labeled and shown in stick representation. The residues of the catalytic triad are shown as yellow sticks. Alpha helix 4 and position 283 are highlighted by an orange dotted line. **B** sequence alignment of PtKCS1, 2, and 4 including predicted secondary structures from PtKCS1. The five amino acid differences between PtKCS2 and 4 are highlighted in turquoise, and the three catalytic residues are highlighted in yellow. Predicted transmembrane helices are labeled (TM). Key residues described in Kim et al., (2022) are framed in purple.

Chen et al. (2022) attempted to change substrate specificity of site-directed mutants between two KCS enzymes from *Populus trichocarpa* expressed in yeast. Despite sharing 99% identity, PtKCS2 and PtKCS4 display different elongation activities: PtKCS4 synthesizes short monounsaturated VLCFAs, while PtKCS2 elongates longer saturated VLCFAs. By introducing T137K and R283C mutations in PtKCS4 (Figure 12), the overall substrate preference of PtKCS4 was nearly completely converted to that of PtKCS2. Indeed, the authors observed that in PtKCS4 both the polar threonine (at position 137) and

arginine (at position 283) point into the binding tunnel effectively constricting and decreasing its hydrophobicity, which could explain why PtKCS4 is restricted to synthesizing shorter VLCFAs compared to PtKCS2 (Figure 12A). While PtKCS1 and PtKCS2 only share 74% identity, the authors demonstrated that the 277 residues of PtKCS1 are sufficient for converting the substrate specificity of PtKCS2 to that of PtKCS1, which accumulates shorter and monounsaturated VLCFA. Additionally, Chen et al. (2022) showed that helix-4 is close to the acyl-chain substrate (Figure 12A). Only nine substitutions around helix-4 (PtKCS2 129-143) were sufficient to increase the production of monounsaturated fatty acids (predominantly C20:1 and C22:1) and consequently decrease the production of C28 without affecting activity toward saturated VLCFAs. They investigated whether the product could be rationally modified to obtain longer VLCFAs by replacing the amino acid at this position 277 in PtKCS1 (position 283 in PtKCS2 and 4) with a smaller amino acids. Therefore, these results show that helix-4 and site 277 are key determinants of substrate specificity of PtKCS1 and PtKCS2, where small amino acid at this position lead to longer VLCFA products.

To investigate KCS9 amino acids involved in VLCFA synthesis, Kim et al. (2022) revealed that both D339 and D308 residues of KCS9 are involved in the synthesis of C24 VLCFAs from C22, with a greater contribution of D339 compared to D308. However, multiple alignments of amino acid sequences of 21 KCS isoforms showed that the aspartic acid of the D339 and D308 were well conserved. D308 aspartic acid was not present in KCS3, KCS12, and KCS19, which do not exhibit VLCFA elongation activity. These observations suggest that two Asp residues of KCS9 at positions 308 and 339 are required for VLCFA synthesis.

3.3.5. Protein-protein interactions

Previous studies have confirmed the substrate specificity of several KCS using yeast microsomes expressing Arabidopsis genes, but no detectable activity was observed for KCS3 (Blacklock and Jaworski, 2006). Recently, Huang et al. (2023a) reported that overexpression of Arabidopsis KCS3 leads to a glossy stem phenotype similar to the wax-deficient phenotypes observed in *kcs6* mutants (Huang et al., 2022). The authors showed a physical interaction between KCS3 and KCS6, which results in the suppression of KCS6 activities in yeast, possibly due to the disrupted interactions of KCS6 with other FAE members or KCS6. These results suggest that the KCS3–KCS6 regulatory module is required for sustaining cuticular wax homeostasis (Figure 13A). Since KCS3, KCS12, and KCS19 fall into the same subgroup, and KCS12 is a paralog of KCS3 (Joubès et al. 2008), Huang et al., (2023b) reported that KCS12 plays a similar role in wax production negative regulation by interacting with only KCS6 over the eight KCS tested in this study, although KCS12 has weaker interactions with KCS6 and inhibition activity than KCS3. Thus, KCS3 and KCS12 mutation led to increased levels of >C30 VLCFA wax derived

components, with *kcs3* mutant having higher levels than *kcs12* mutant. These results indicate that KCS12 and KCS3 play a similar negative role in wax synthesis, which is consistent with the finding that KCS12 acts as a suppressor of wax synthesis in *Medicago truncatula* (Chai et al., 2021). Furthermore, changes in KCS3 and KCS12 expression affected cutin accumulation in Arabidopsis. The simultaneous mutation of both genes resulted in additive effects on cutin and wax synthesis, suggesting that KCS3 and KCS12 play redundant roles in both biosynthetic pathways (Huang et al., 2023b). In contrast, KCS19 over expression in Arabidopsis and co-expression with KCS6 in yeast did not show any significant results, suggesting that KCS19 has a different function than the one of KCS12 and KCS3, which remains unknown (Huang et al., 2023a).

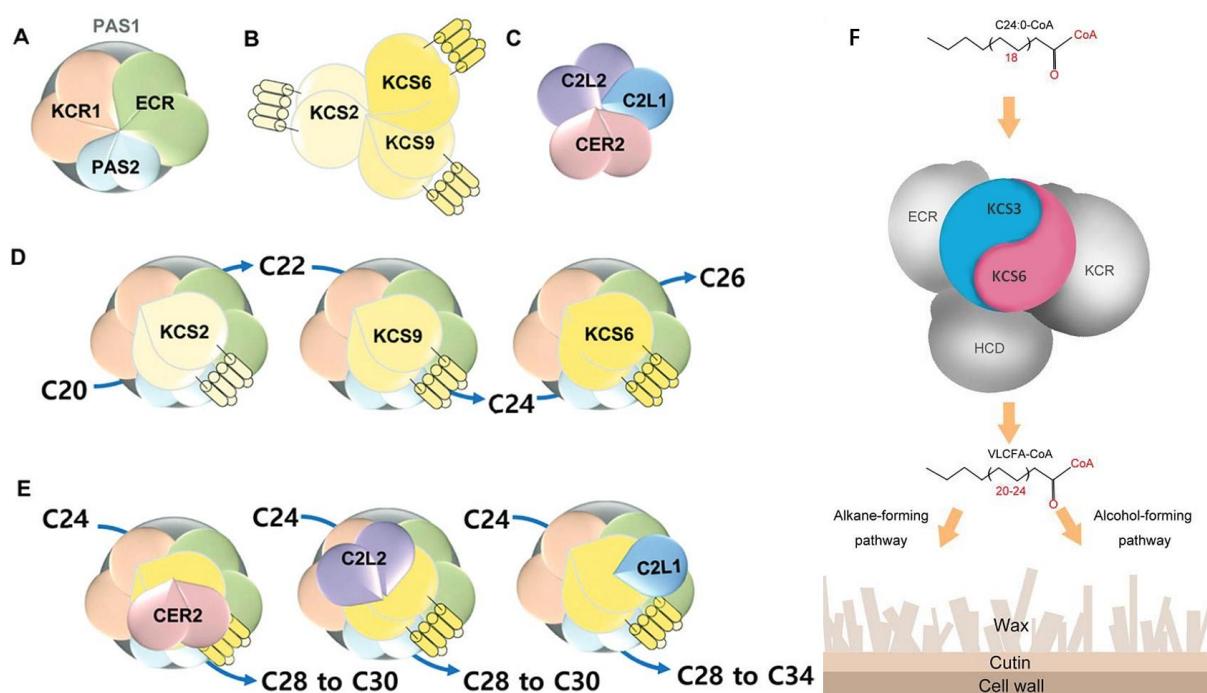


Figure 13. Proposed supramolecular FAE complex model from Huang et al. (2023a) and Kim et al. (2022). (A) FAE core complex comprising KCR1, PAS2, ECR, and PAS1. (B) Homo- and heterointeractions of KCSs. (C) Homo- and heterointeractions of CER2 and C2L2 and hetero-interactions of C2L1. (D) Multisubunit elongase complexes comprising the FAE core complex and KCS2, KCS9, or KCS6. C20 to C28 are VLCFAs. (E) Multisubunit elongase complexes comprising the FAE core complex, KCS6, and CER2, C2L2, or C2L1. C26 to C34 are VLCFAs (Haslam et al., 2015) (F) Proposed model illustrating the interactions between KCS3 and KCS6 during wax synthesis (note that wax is also deposited within the cutin layer). The Tai-Chi symbol is used to highlight the mechanism of the KCS3–KCS6 module in VLCFA elongation. The Tai-Chi symbol with KCS3 shown in blue and KCS6 shown in red indicates that KCS3 plays a negative role and KCS6 plays a positive role in balancing the elongation process of VLCFAs.

According to a previous study (Haslam et al., 2015), substrate specificities of KCS6 and KCS5 expressed in yeast are influenced by the co-expression of the CER2 enzyme family (CER2, CER2like). The authors reported that KCS5 or KCS6 co-expressed with CER2 in yeast produced more C28 and C30 VLCFA than KCS alone, revealing that CER2 enhances the catalytic capacity of KCS5 and KCS6 during the elongation process of C26 and C28 VLCFA. Additionally, CER26, which is a CER2-like1, could assist KCS5 and KCS6 in catalyzing the production of VLCFA longer than C30. When CER2 and CER26 are expressed together

with KCS5 or KCS6, the amounts of C32 and C34 VLCFA increase. BiFC assays confirmed that KCS5 physically interacts with KCS6, CER2 and CER26 (Huang et al., 2022). Moreover, studies have shown homo- and heterodimer interactions between KCS2, KCS6, KCS9 and the other FAE subunits (KCR1, HCD, ECR) (Kim et al., 2022) (Figure 13B, D). KCS6 also interacts more strongly with CER2 et CER2like than with KCS9 or KCS2 (Kim et al., 2022) (Figure 13E).

	AtKCS2	AtKCS3	AtKCS5	AtKCS6	AtKCS9	AtKCS12	AtKCS16	AtKCS18	AtKCS19	AtKCS20	PAS2	ECR	KCR1
AtKCS1		no									yes		
AtKCS2	yes	no		yes							yes	yes	yes
AtKCS3			yes	yes		yes	no	no		no			
AtKCS5											yes		
AtKCS6				yes	yes	yes			no		yes	yes	yes
AtKCS8											yes		
AtKCS9					yes						yes	yes	yes
AtKCS10											yes		
AtKCS17											yes	yes	yes
AtKCS18											yes		
AtKCS20											yes		
PAS1 (=scaffold)											yes	yes	yes
PAS2												yes	yes
ECR													yes

Table 1. Overview of protein-protein interactions described in the literature. References : Roudier et al., 2010; Morineau et al., 2016; Kim et al., 2022; Huang et al., 2022; Huang et al., 2023a; 2023b. Grey boxes represent homodimer.

Before engaging in bioactive lipid networks and cellular processes, fatty acids necessitate conjugation with coenzyme A (CoA) to form acyl-CoAs. Acyl-CoA contribute to multiple cellular activities including energy metabolism, the biosynthesis and recycling of complex lipids, posttranslational modifications of proteins and regulation of gene expression.

3.4. Acyl-CoA

3.4.1. Acyl-CoA structure

Acyl-CoAs, derivatives of fatty acid molecules, comprise a Coenzyme A moiety, fatty acid of specific length, and thioester bond. Coenzyme A is a coenzyme involved in numerous biochemical reactions in cells. It consists of a nucleotide adenine, ribose sugar, and phosphate group linked to a thiol group containing a reactive sulfur atom. The thiol group is crucial for the formation of thioester bonds with fatty acids to form acyl-CoA. Coenzyme A (CoASH or CoA) itself is a complex and highly polar molecule consisting of adenosine 3',5' diphosphate linked to 4-phosphopantetheine (Figure 14). The adenosine 3',5' diphosphate moiety functions as a recognition site, as many proteins have nucleotide-binding folds, and it increases the affinity for CoA binding to enzymes. The fatty acid moiety is attached to Coenzyme A via a thioester bond. This bond forms between the carboxyl group of the fatty acid and the thiol group of Coenzyme A resulting in the formation of acyl-CoA. A comprehensive review of acyl-CoA analysis has been published by Riverra and Bartlett (2018).

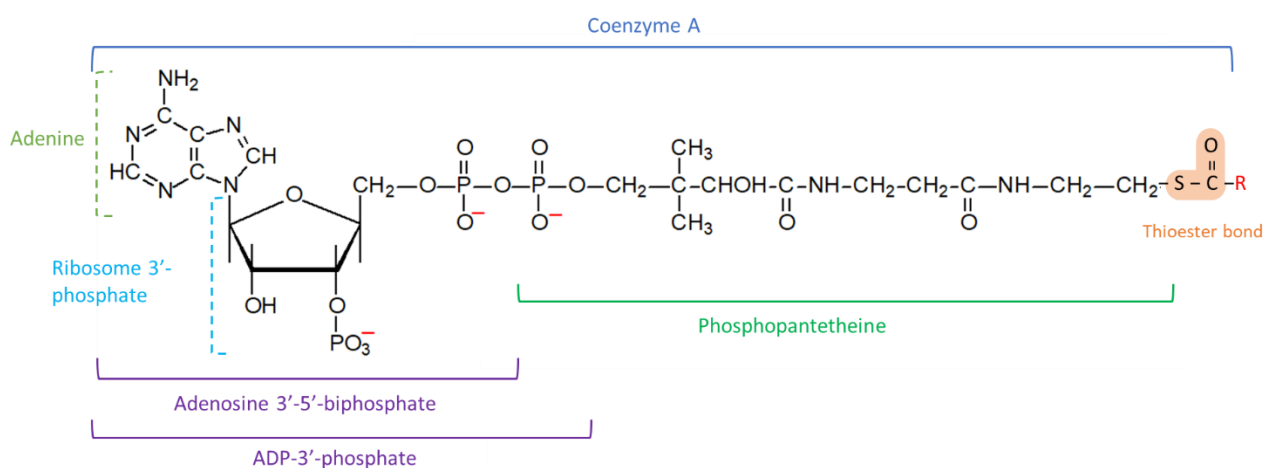


Figure 14. Structure acyl-CoA modified from Sun et al. (2006).

3.4.2. Methods for Acyl-CoA analyses

High performance liquid chromatography electrospray ionization tandem mass spectrometry (HPLC/ESI-MS/MS) combines the ability of mass spectrometry to measure specific compounds within a mixture by monitoring the specific fragmentation pattern of the compounds, with the ability of HPLC to separate compounds with different retention times. This provides double the resolving power and allows for accurate analyte quantification. It also reduces the number of interfering compounds and reduces contamination of the mass spectrometer by compounds in the extract that are non-volatile. The liquid chromatography separates compounds by retention time as each of the compounds bind to the column with a different affinity. The compounds are eluted by changing the properties of the mobile phase. The eluent from the HPLC is then passed onto the electrospray probe to be ionized, before passing into the MS.

Although HPLC-ESI-MS/MS has been commonly utilized, many existing methods can only detect short, medium, or long-chain acyl-CoAs separately. Despite the well-established detection capabilities of mass spectrometry, chromatography remains challenging because of the complex structures of these compounds. Despite the advancements in the latest LC-MS systems and their improved analytical capabilities, challenges persist, particularly in achieving enhanced sensitivity for analyzing small biological samples.

a. Sample preparation and extraction

Prior to HPLC and MS/MS analyses, acyl-CoAs have to be extracted from the biological samples. Many techniques have been developed for the measurement of acyl-CoA in mammalian cells and tissues. Acyl-CoA analyses of plant tissues and microalgae have proven to be more challenging because they are difficult to grind (fibrous or silica-based material), the quantities available may only be in the milligram range, and extracts are complicated by the presence of high concentrations of pigments and phenolic compounds, which may interfere with enzyme assays and chromatographic separations.

Several protocols have been developed for the extraction of fatty acyl-CoAs. Table 2 lists several Solid-Phase Extraction (SPE) phases that have been used to purify acyl-CoAs from yeast or cell cultures with different chain lengths. Globally, a reverse-phase SPE column is used for acyl-CoA, acidic methanol is used for conditioning, and elution proceeds with ammonium acetate or formate in methanol.

Alternatively, liquid-liquid extraction (LLE) is used to extract acyl-CoA and may prevent possible analyte loss resulting from adherence to the SPE column. The protocols for acyl-CoA extraction used for various tissues (mammalian, plant) were derived from the methodology developed by Mancha et al. (1975), used for the plant tissue samples. This LLE utilizes an isopropanol-water and chloroform–methanol mixture, which allows the separation of polar (containing acyl-CoA) and non-polar lipid species. Recently, another LLE method has been mostly used for short-to very-long-chain acyl-CoA analyses from plant and yeast samples (Tonon et al., 2005; Sayanova et al., 2007; Batsale et al., 2023). This extraction method was firstly developed by Larson and Graham (2001) then adapted by Haslam et al. (2021), in which acetic acid and extracted with hot petroleum ether saturated with aqueous isopropanol was added to the sample suspension to remove free fatty acids and less-polar lipids (Woldegiorgis et al., 1985). After addition of saturated ammonium sulfate to the washed aqueous phase from impurities, the acyl-CoA esters were extracted with chloroform-methanol (1:2).

SPE	Biological samples	Conditioning solvent	Wash	Elution solvent	Type acyl-CoA	Reference
Oasis HLB 1cc	Cell cultures <i>Methylobacterium extorquens</i> (bacteria)	methanol, TCA at 0,15 %	water	methanol, water	Short-chain acyl CoA	Yang et al., 2009
silica gel SPE tubes (Supelco)	Yeast cells	ACN/IPA/water/AA(9:3:4:4)	ACN/IPA/water/a cetic acid (9:3:4:4)	250 mM aqueous ammonium formate/methanol (1:4)	Short, medium, long chain acyl-CoA	Snyder et al., 2015
Oasis WAX	HeLa cells	methanol/eau/AA (3:1:1), 50% methanol (v/v)		isopropanol/methanol/ammoniac 3% (6:3:1)	Short, medium, long, very long chain acyl-CoA	Li et al., 2021
OASIS WAX	HepG2 cells	methanol, water	water	acetate ammonium 25mM in methanol	Short, medium, long, very long chain acyl-CoA	Jones et al., 2021
Oasis HLB 1cc	Cell culture, mammalian tissues	methanol, water	water	methanol with 25 mM ammonium acetate	Short-chain acyl CoA	Trefely et al., 2022
Oasis WAX	Plant tissues	Methanol, ACN/IPA/water/AA (9:3:4:4)	ACN/IPA/water/a cetic acid (9:3:4:4)	250 mM Ammonium Hydroxide in 80% methanol	Short-chain acyl CoA	Purves et al., 2015

Table 2. SPE cartridges and solvents used for the acyl-CoA extraction from various samples Abbreviations used: AA, acetic acid; ACN, acetonitrile; CoA, coenzyme A; csFBS, IPA, 2-propanol; SPE, solid phase extraction; TCA, trichloroacetic acid.

b. Chromatographic conditions for acyl-CoA separation

Acyl-CoA molecules possess a thioester group, which renders them relatively polar and, as a result, non-volatile. This polarity renders them difficult to separate effectively using gas chromatography (GC), whereas high-performance liquid chromatography coupled with tandem mass spectrometry (HPLC-MS/MS) is a more appropriate method for analyzing acyl-CoA. In HPLC, a sample is dissolved in a liquid solvent and separated based on its interactions with a stationary phase. However, acyl-CoA

variability in terms of fatty acyl chain length, saturation levels, and functional groups poses a significant challenge in developing comprehensive analytical techniques. Short-chain acyl-CoAs, due to the high polarity of the CoA residue, require acidic mobile phases for improved retention in reversed-phase liquid chromatography-tandem mass spectrometry (RPLC-MS/MS). Conversely, long-chain acyl-CoAs tend to exhibit peak tailing under such conditions because of higher apolarity and so excessive retention, necessitating the use of basic mobile phases to achieve better peak shapes. However, achieving adequate separation and optimal peak shapes for both short- and long-chain acyl-CoAs simultaneously using a single method remains elusive. Haslam and Larson (2021) utilized a comprehensive range of acyl-CoA standards across varying chain lengths to establish accurate quantification methods. Furthermore, owing to their negative charge, acyl-CoAs have a propensity to adhere to glassware and stainless-steel surfaces, leading to performance degradation after multiple injections. To neutralize the negatively charged phosphate groups of the CoA molecule, acidic eluents containing acetonitrile, water, formic acid, or phosphoric acid were used between injections. This acidic wash eliminates coeluting and interfering impurities from the chromatography system, especially long-chain acyl-CoA (Abrankó et al., 2018; Haslam et al., 2021). Table 3 lists several HPLC methods for acyl-CoA separation.

Solvent A	Solvent B	Solvent C	Column	Biological sample	Type acyl-coa	
Water 50 mmol.L-1 NH4OAc (Ammonium acetate) pH 6.9	Acetonitrile		Atlantis T3 guard	bacteria Megasphaera elsdenii	short chain acyl-coenzyme A	Neubauer et al., 2015
90% 10mM ammonium formate, pH 4.6, 10% methanol	10% 10mM ammonium formate, pH 4.6, 90% methanol		Ascentis TM C18	leaf and siliques arabidopsis thaliana	short chain acyl-coenzyme A	Perera et al., 2009
ammonium bicarbonate (10 mM), adjusted to pH 9.5	(B1) Acetonitrile	acidic wash - neutral wash	Waters Acquity BEH C18	mouse liver, human hepatic (HepG2) and skeletal muscle (LHCNM2) cells	medium to very long chain acyl-coenzyme A	Abrankó et al., 2018
water 10 mM ammonium acetate (pH _ 8.5, adjusted with ammonium hydroxide)	acetonitrile		Luna C18 Phenomenex	mouse liver	medium and long chain acyl-coenzyme A	Liu et al., 2015
5 mM ammonium acetate + 2.5 mM DMBA (pH 5.6)	95% acetonitrile, 5% H2O + 5 mM ammonium acetate		Phenomenex Kinetex C18	human hepatic (HepG2)	short chain acyl-coenzyme A	Jones et al., 2021
100% Acetonitrile, 15mM Ammonium hydroxide.	90% H2O, 10% acetonitrile, 15mM Ammonium hydroxide.	30% H2O, 70% acetonitrile, 0.1% Formic acid.	Agilent Eclipse XDB-C18	plant	short to very long chain acyl-coenzyme A	Haslam & Larson 2021
93% H2O, 5% acetonitrile, and 2% of 0.5 M ammonium acetate adjusted to pH 6 with glacial acetic acid	18% H2O, 80% acetonitrile, and 2% of 0.5 M ammonium acetate adjusted to pH 6 with glacial acetic acid			lonal isolate of Spodoptera frugiperda Sf21 cells	3-keto-C20:0-CoA	Nie et al., 2021
5 mM ammonium acetate in water	5 mM ammonium acetate in acetonitrile/water (95:5. v/v)	acetonitrile/water/ formic acid (80/20/0.1, v/v/v)	Luna C18 Phenomenex	Yeast cells	Short, medium, long chain acyl-CoA	Snyder et al., 2015

Table 3. HPLC methods used for acyl-CoA separation

To adapt for Electrospray ionization- Mass spectrometry (ESI-MS) detection, phosphate buffer used in earlier protocols employing LC separation by UV at slightly acidic pH (4.5–5.5) is substituted with a volatile buffer(s) such as ammonium-formate, acetate, bicarbonate or highly alkaline mobile phase conditions with pH adjusted. Abrankó et al. (2018) reported several LC condition for medium acyl-coa analyses. The results indicated that after multiple injections, omitting the acidic wash step, less analyte loss for long chain fatty acyl-CoA was observed after several injections with ammonium bicarbonate at pH 9.5.

c. Mechanisms of mass spectrometry to detect acyl-CoA

Electrospray ionization (ESI) produces gas-phase ions from the solvent flow of a liquid chromatography (LC) system. These ions then enter the high-vacuum system before reaching the various mass analyzers, to be analyzed by the mass spectrometry (MS) (Figure 15). Tandem mass spectrometer (MS/MS) comprises two quadrupole filters, Q1 and Q3, which are separated by a collision cell, known as Q2 (Figure 16). A gas is introduced into the collision cell for fragmentation. The process begins in Q1 where the ions were filtered according to their mass charge ratio. In Q2 the ions are fragmented, resulting in the creation of daughter ions that are then analyzed in Q3.

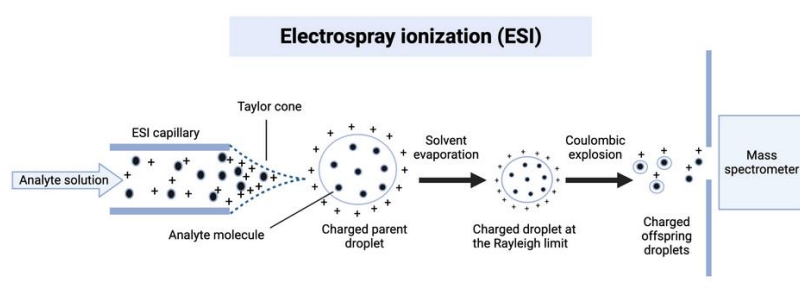


Figure 15. Schematic representation of the electrospray ionization process adapted from Banerjee and Mazumdar (2012)

ESI coupled with MS/MS has been employed for the determination of acyl-CoA in both positive and negative ion modes. Despite the capabilities of both ion modes, ESI in positive ion mode is more commonly used due to its higher sensitivity and its ability to utilize the loss of neutral 3'-phosphonucleoside diphosphate (507 Da) using multiple reaction monitoring (MRM). It monitored precursor and products ions, the MRM pairs, that were specific to a particular acyl-CoA molecule (Figure). As demonstrated in the Figure, the fragmentation of C16:0-CoA (m/z 1006) yielded two abundant fragments in ESI+, the fatty acyl pantetheine ion (m/z 499) and the 3'-phosphate-AMP product ion (m/z 428). The fatty acyl pantetheine ion (m/z 499.3) was the most abundant fragment ion resulting from a neutral loss of 507 Da, while the 3'-phosphate-AMP product ion (m/z 428) is a characteristic fragment of the acyl-CoA family (Figure 17).

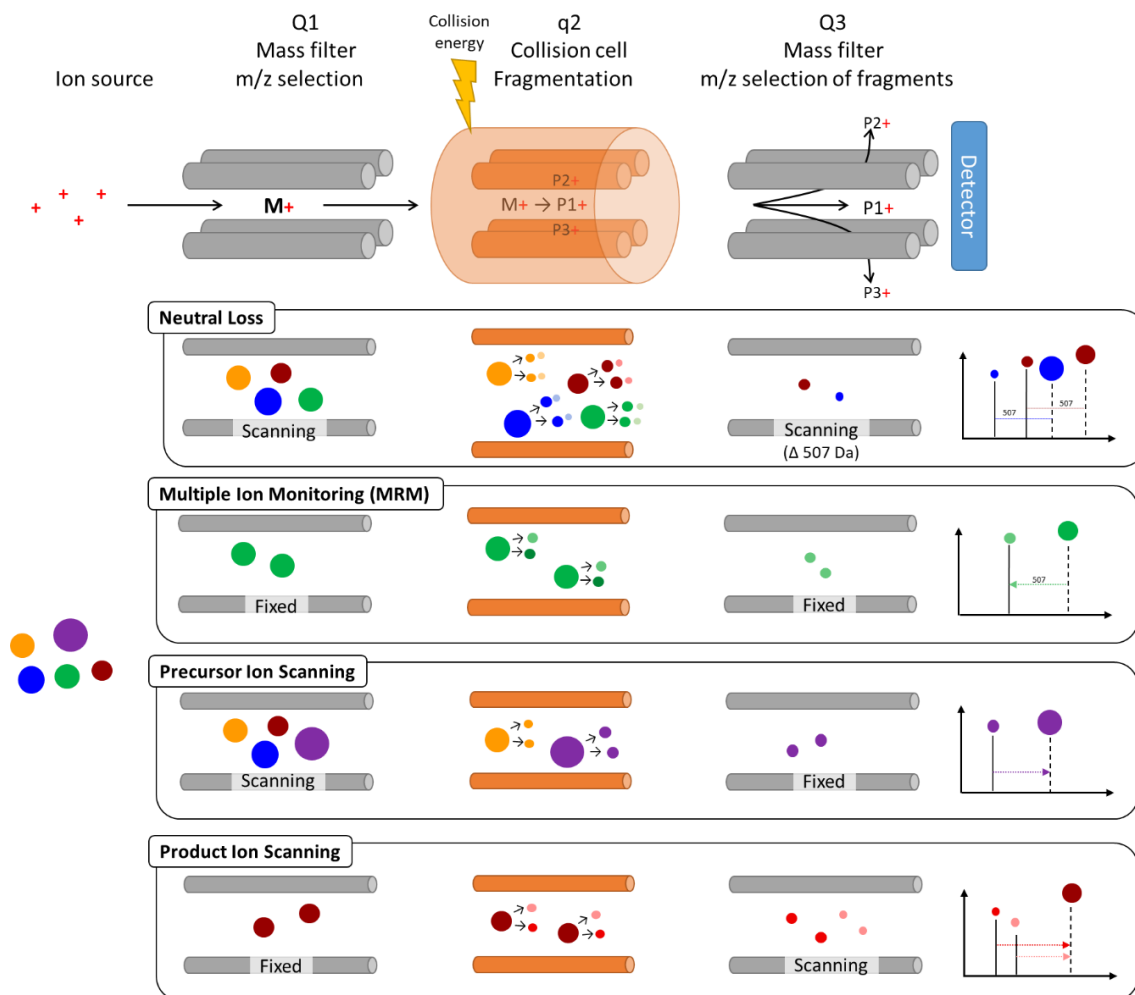


Figure 16. Scan modes of tandem mass spectrometry modified from Lin et al. (2014).

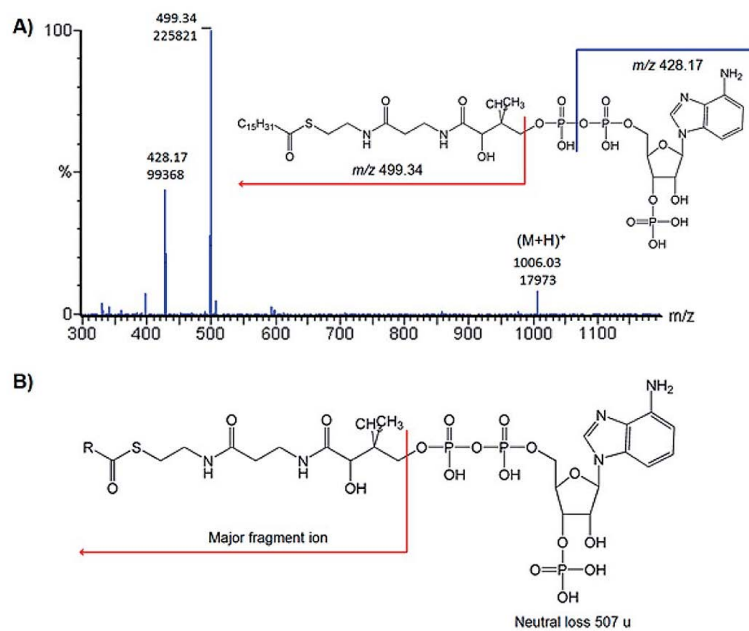


Figure 17. Fragment ions of acyl-CoA from Yang et al., 2017. (A) Fragment ions of C16:0-CoA (B) Major fragmentation mechanism for acyl-CoAs : a neutral loss of 507.

4. Herbicides targeting the biosynthesis of VLCFAs

The Herbicide Resistance Action Committee (HRAC, <https://hracglobal.com/>) categorizes herbicides based on their modes of action, target sites, induced symptoms, or chemical classes. Most commercially available herbicides have known target sites, but for HRAC classes K3 and N, the primary targets have not yet been clearly identified. First, these herbicides have been grouped based on the results of physiological and biochemical studies conducted with chloroacetamide herbicides. For several years, the K3 herbicides were described as "inhibitors of cell division" by HRAC, as observed in onion cells (*Allium cepa* L.), *Chlamydomonas* algae and *Avena sativa* (Dilhon and Anderson, 1972; Deal and Hess, 1980; Fedtke, 1991). Herbicides of group N, including thiocarbamate and benzofuran herbicides, were defined as inhibitors of lipid synthesis altering the production of leaf surface layers (waxes, cutin and suberin). It was assumed that this effect may be due to inhibition of the VLCFA synthesis (Lechelt-Kunze et al., 2003). Therefore, herbicides that inhibit VLCFA synthesis classified by the HRAC as groups K3 and N have been more recently gathered in the group 15 of the HRAC classification (Figure 18, Table 4).

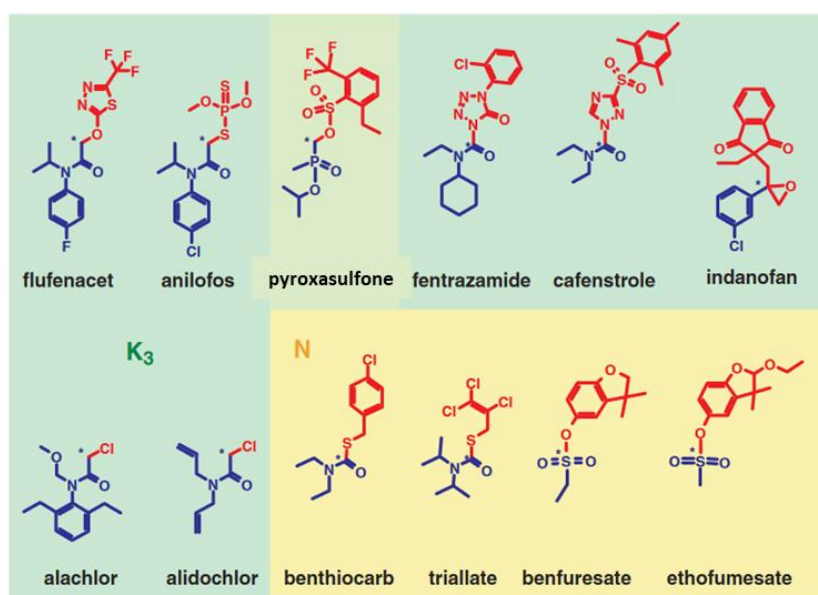


Figure 18. Chemical structures of flufenacet, benfuresate and other different herbicides with similar modes of action from Lechelt-Kunze et al. (2003). HRAC group K3 herbicides are underlain green, HRAC group N herbicides are underlain yellow. Blue asterisks indicate possible sites for nucleophilic attack, eg by an active site cysteine. The parts of the molecules drawn in blue would then remain covalently attached to the enzyme, whereas the leaving anions are drawn in red.

Mode of action	Chemical classification	Active molecule	HRAC	LEGACY GLOBAL HRAC
Inhibition of VLCFA Synthesis	α -Chloroacetamides	Acetochlor	15	K3
Inhibition of VLCFA Synthesis	α -Chloroacetamides	Alachlor	15	K3
Inhibition of VLCFA Synthesis	α -Chloroacetamides	Allidochlor=CDA	15	K3
Inhibition of VLCFA Synthesis	α -Thioacetamides	Anilofos	15	K3
Inhibition of VLCFA Synthesis	Benzofurans	Benfuresate	15	K3/N
Inhibition of VLCFA Synthesis	α -Chloroacetamides	Butachlor	15	K3
Inhibition of VLCFA Synthesis	α -Chloroacetamides	Butenachlor	15	K3
Inhibition of VLCFA Synthesis	Thiocarbamates	Butylate	15	K3/N
Inhibition of VLCFA Synthesis	Azolyl-carboxamides	Cafenstrole	15	K3
Inhibition of VLCFA Synthesis	Thiocarbamates	Cycloate	15	K3/N
Inhibition of VLCFA Synthesis	α -Chloroacetamides	Delachlor	15	K3
Inhibition of VLCFA Synthesis	α -Chloroacetamides	Diethyl-ethyl	15	K3
Inhibition of VLCFA Synthesis	Thiocarbamates	Dimepiperate	15	K3/N
Inhibition of VLCFA Synthesis	α -Chloroacetamides	Dimethachlor	15	K3
Inhibition of VLCFA Synthesis	α -Chloroacetamides	Dimethenamid	15	K3
Inhibition of VLCFA Synthesis	Thiocarbamates	EPTC	15	K3/N
Inhibition of VLCFA Synthesis	Thiocarbamates	Esprocarb	15	K3/N
Inhibition of VLCFA Synthesis	Benzofurans	Ethofumesate	15	K3/N
Inhibition of VLCFA Synthesis	Isoxazolines	Fenoxasulfone	15	K3
Inhibition of VLCFA Synthesis	Azolyl-carboxamides	Fentrazamide	15	K3
Inhibition of VLCFA Synthesis	α -Oxyacetamides	Flufenacet	15	K3
Inhibition of VLCFA Synthesis	Oxiranes	Indanofan	15	K3/Z
Inhibition of VLCFA Synthesis	Azolyl-carboxamides	Ipfencarbazone	15	K3
Inhibition of VLCFA Synthesis	α -Oxyacetamides	Mefenacet	15	K3
Inhibition of VLCFA Synthesis	α -Chloroacetamides	Metazachlor	15	K3
Inhibition of VLCFA Synthesis	α -Chloroacetamides	Metolachlor	15	K3
Inhibition of VLCFA Synthesis	Thiocarbamates	Molinate	15	K3/N
Inhibition of VLCFA Synthesis	Thiocarbamates	Orbencarb	15	K3/N
Inhibition of VLCFA Synthesis	Thiocarbamates	Pebulate	15	K3/N
Inhibition of VLCFA Synthesis	α -Chloroacetamides	Pethoxamid	15	K3
Inhibition of VLCFA Synthesis	α -Thioacetamides	Piperophos	15	K3
Inhibition of VLCFA Synthesis	α -Chloroacetamides	Pretilachlor	15	K3
Inhibition of VLCFA Synthesis	α -Chloroacetamides	Propachlor	15	K3
Inhibition of VLCFA Synthesis	α -Chloroacetamides	Propisochlor	15	K3
Inhibition of VLCFA Synthesis	Thiocarbamates	Prosulfocarb	15	K3/N
Inhibition of VLCFA Synthesis	α -Chloroacetamides	Prynachlor	15	K3
Inhibition of VLCFA Synthesis	Isoxazolines	Pyroxasulfone	15	K3
Inhibition of VLCFA Synthesis	α -Chloroacetamides	Thenylchlor	15	K3
Inhibition of VLCFA Synthesis	Thiocarbamates	Thiobencarb (=Benthocarb)	15	K3/N
Inhibition of VLCFA Synthesis	Thiocarbamates	Tiocarbazil	15	K3/N
Inhibition of VLCFA Synthesis	Thiocarbamates	Tri-allate	15	K3/N
Inhibition of VLCFA Synthesis	Oxiranes	Tridiphane	15	K3
Inhibition of VLCFA Synthesis	Thiocarbamates	Vernolate	15	K3/N
Unknown (inconclusive MoA data)	Trifluoromethanesulfonanilides	Mefluidide	0	Z
Unknown	Trifluoromethanesulfonanilides	Perfluidone	0	Z

Table 4. Very-long-chain fatty acid-inhibiting herbicide chemical families and active ingredients according to the Herbicide Resistance Action Committee classification list (<https://hracglobal.com/>). Potential VLCFA inhibitors are indicated in blue.

4.1. Phenotype in plants

Efforts toward identifying the molecular targets of K3 and N herbicides were initiated through a study that investigated the phenotype and gene expression of plants exposed to these herbicides. *Arabidopsis thaliana* plants treated with these molecules at low concentrations showed a phenotype similar to that of mutant *fiddlehead* (*fdh/kcs10*) (Figure 19), including fusion of the aerial organs (Lechelt-Kunze et al., 2003; Trenkamp et al., 2004). This phenotype is due to a modification of cuticular wax amount that derived from VLCFA (Voisin et al., 2009) leading to epidermal cell fusion (Lolle et al., 1992; Yephremov et al., 1999).

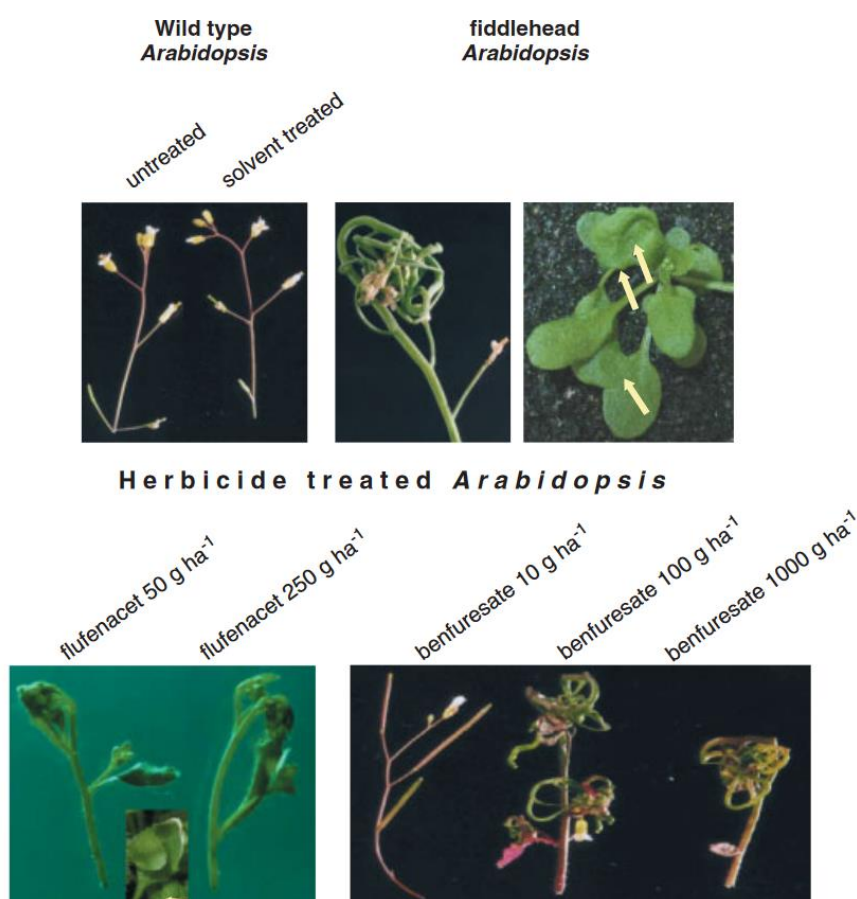


Figure 19. Flufenacet and benfuresate phenocopy fiddlehead from Lechelt-Kunze et al. (2003). Inflorescences and leaves of control, fiddlehead mutant, and herbicide-treated *Arabidopsis thaliana*. Pictures were taken 8 days after herbicide treatment of plants grown under long-day conditions.

Monocotyledonous plants also displayed a phenotype that resembled a *fiddlehead* phenotype when treated with group 15 herbicides. Indeed, tips of treated leaves of *Echinochloa crus*, *Setaria viridis*, *Zea mays* stick to their bases while continuing to grow, forming a fiddlehead-like bow in presence of flufenacet, ethofumesate, or cafenstrole (Lechelt-Kunze et al., 2003). This characteristic phenotypic symptom is therefore used to identify this herbicide family, even if it is not always verified (Trenkamp et al., 2004; Lechelt-Kunze et al., 2003). Furthermore *Chlamydomonas algae* cells treated with

oxyacetamid do not segregate after cell division (Lechelt-Kunze et al., 2003). The observed phenotype resulting from group 15 herbicides is attributable to deficiencies in surface lipid components, such as the cuticle and suberin. Tresch et al. (2013) reported that chloroacetamide metazachlor and non-VLCFA synthesis inhibitors, mefluidide and perfluidone, resulted in defects in cuticle function when shoots of cress seedlings (*L. sativum*) were treated. Additionally, Wilkinson and Hardcastle (1969) found that the cuticle thickness on the upper and lower leaf surfaces of sicklepods decreased as EPTC herbicide concentration increased. Wattlelet–Boyer et al. (2016) also showed that metazachlor slightly alters the acylcomposition of fatty alcohol compounds and omega-OH VLCFA, which are present in the suberin polymer. Acetochlor completely blocked cotton fiber elongation (Qin et al., 2007), but this inhibition was overcome by adding saturated C24 or C26 VLCFAs. In contrast, other VLCFAs, such as C20:0, C22:0, C28:0, and C30:0, only partially compensated, and LCFAs did not reverse the acetochlor-induced inhibition. These findings indicate that VLCFAs, particularly C24:0, play a crucial role in fiber elongation and emphasize the critical impact of herbicide exposure on plant development and surface lipid function.

It has been shown that these herbicides also inhibit plant growth and reduce VLCFA accumulation in both dicotyledonous and monocotyledonous plants. This reduction can be used to determine the potency of herbicides across different plant species and between different herbicides by testing them in planta. For example, based on plant growth measurements, Italian ryegrass, barnyard millet, and rice have been described as more sensitive to pyroxasulfone than maize or wheat (Tanaya thesis, 2013). Tanetani et al. (2011b) showed differences in the inhibitory potencies against VLCFA elongases between pyroxasulfone-susceptible plants (rice, Italian ryegrass, and barnyard millet) and tolerant plants (wheat, corn, and soybean), which exhibited 80% and 60% inhibition of C24:0 to C26:0 elongation, respectively (Figure 20).

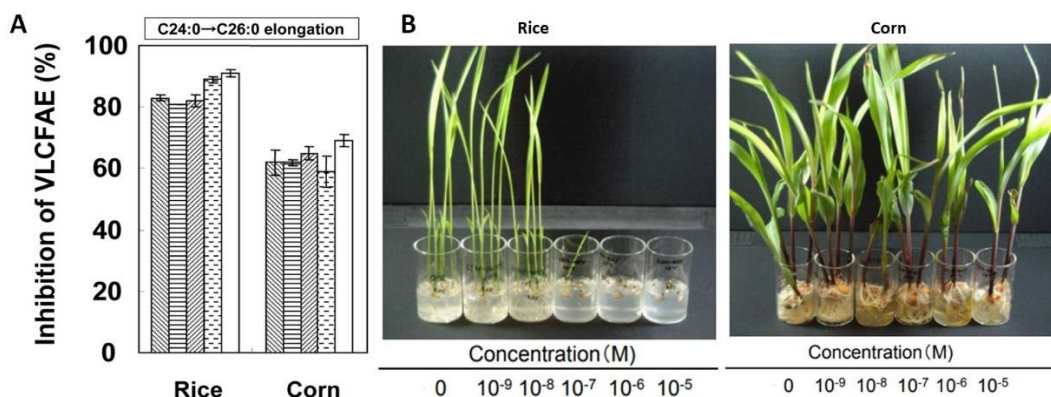


Figure 20. Effects of pyroxasulfone on seedling growth of rice and corn from and). (A) Effects of pre-incubation periods on inhibition of VLCFAE activities in plant seedlings from Tanetani et al. (2011b) (0 min; 5 min; 10 min; 20 min; 30min. (B) Effect of increasing concentration of pyroxasulfone on seedlings from Tanaya manuscript (2022).

This is considered one of the factors involved in the selectivity of pyroxasulfone between weeds and crops. Additionally, sorghum is more sensitive than maize to metazachlor treatment (Ekler and Stephenson, 1989). Kasahara et al. (2019) determined that late water grass is more sensitive to ipfencarbazono than rice, and ipfencarbazono had stronger inhibition potency than cafenstrole. These results show difference of sensitivity between species even ecotypes. Cafenstrole strongly inhibits fatty acid elongation from C20:0 to C22:0 and C24:0 in Arabidopsis seedlings, cucumber, and barley leaves (Nobuwasa and Umeda, 2012; Yang et al., 2010b). In Lemna tissues, mefenacet, mefluidide, and perfluidone strongly decreased the level of C24:0, accompanied by moderate reductions in C22:0; metazachlor also reduced the level of C20:0 (Tresch et al., 2012, Campe et al., 2018). VLCFA synthesis was inhibited in barley, cucumber, and maize leaves treated with metazachlor, with a reduction of C20:0, C22:0, and C24:0 (Matthes et al., 1998). Alachlor and metazachlor affect the plant growth and lipid production of the marine diatom *Fistulifera solaris* (Suhaimi et al., 2022).

As consequences of group 15 herbicides on plant, by Vercampt et al. (2016) hypothesized that the destabilization of lipid bilayers of cell membranes could be caused by metazachlor. Indeed, metazachlor induces a reduction of the incorporation of radiolabeled C20-C24 VLCFAs into intracellular membranes and into the plasma membrane, but did not impact C16 and C18 LCFA incorporation (Matthes and Böger, 2002). Since the plasma membrane of plant cells contains VLCFAs in the form of sphingolipids and phospholipids, metazachlor strongly decreased the incorporation of C24 fatty acids, especially hydroxy-VLCFA in sphingolipids (Wattelet-Boyer et al., 2016; Ito et al., 2021). However, this chloroacetamide herbicide did not alter the total quantity of fatty acids in glycerophospholipids, GlcCer, GIPCs pools, and triacylglycerols (TAG). Furthermore, metazachlor have an effect on cell polarity and localisation of auxin transpors, because it affects root gravitropism in Arabidopsis seedlings, that is, the ability of the root to reorient its growth direction following a gravistimulus (Wattelet-Boyer et al., 2016; Ito et al., 2021).

4.2. Target protein

Advances in our understanding of the mode of action of herbicides were achieved through cloning experiments with *A. thaliana* KCS genes. Both putative and known KCS genes from *A. thaliana* were cloned, heterologously expressed, and characterized in *Saccharomyces cerevisiae* using endogenous or externally supplied substrates. The transformed yeasts were used to assess the impact of various K3 and N herbicides on the spectrum of VLCFAs produced. The activities of the investigated AtKCS enzymes CER60 (KCS5), CER6 (KCS6), KCS1, KCS2, KCS20, and FAE1 (KCS18) were strongly inhibited by metazachlor, flufenacet, and cafenstrole at concentrations of 1 or 100 μM (Böger, 2003; Trenkamp et al., 2004; Tresch et al., 2012). Other herbicides (such as alachlor, anilofos, and fentrazamide) resulted in differential inhibition of the tested KCSs (Trenkamp et al., 2004). Recently, four K3 herbicides (alachlor, anilofos, fentrazamide, and flufenacet) were tested on KCS activity of *Populus trichocarpa* expressed in a yeast system (Chen et al., 2022). The effect of inhibition varied among the three paralogs PtKCS1, 2, and 4, which have different substrate preferences. Indeed, flufenacet and fentrazamide had the greatest effect on reducing VLCFA elongation activity of all three KCSs, whereas alachlor and anilofos slightly reduced their activity. PtKCS1 was the most sensitive to inhibition, although there were also minor differences between PtKCS2 and 4. Since PtKCS2 and 4 differ by only five amino acids, these results imply that at least one of these residues is involved in conferring sensitivity to alachlor and anilofos.

4.3. Inhibitor reaction with the target protein

Schmalfuß et al. (1998; 2000) first identified chloroacetamide compounds as inhibitors of VLCFA synthesis. *In vitro* assays were conducted to test acyl-CoA elongation in leek (*Allium porrum*) microsomes in relation to exogenous acyl-CoA concentrations of either 16:0, 18:0, 20:0, or 22:0 chain length and radioactive malonyl-CoA, and all elongation steps were strongly inhibited by metazachlor and S-metolachlor (Böger et al., 2000). They proposed a high sensitivity of the elongase target to its inhibitor, which consisted of (1) the inhibition of several elongation steps combined in series, (2) covalent binding of the inhibitor to the elongase target site, leading to irreversible inhibition of VLCFAE with pre-incubation between inhibitor and proteins, and (3) competition between acyl-CoA and inhibitor (Böger et al., 2000).

Moreover, the irreversible nature of the enzyme–inhibitor complex was tested using *in vitro* assay. That is, the pre-incubation time of herbicides with enzymes increased, and its inhibitory activity increased. Enzyme activity assays in yeast using radiolabeled substrates have shown that metazachlor and pyroxasulfone inhibit in time-dependant manner the activity of KCS18/FAE1 (Figure 21A, B) (Götz and Böger, 2003; Tanetani et al., 2011b). This result suggests an irreversible inhibition by covalent binding between metazachlor chloroacetamide and the active site cysteine residue in condensing enzymes. Conversely, pyroxasulfone inhibits a VLCFAE from rice (Q6F365, *Oryza sativa subsp. Japonica*), which catalyzes the elongation step from C18:0 to C20:0 in a time-independent manner (Tanetani et al., 2011b); the elongases were inhibited at 80% regardless of the pre-incubation time (Figure 21C), unlike FAE1. They supposed that the inhibition mechanism of Q6F365 by pyroxasulfone was reversible. A similar inhibition was observed for in etiolated barnyard millet seedlings treated with thiobencarb sulfoxide (Tanetani et al., 2013b), similar to fenoxasulfone (Tanetani et al., 2011a). It is assumed that this time-independent reversible inhibition of VLCFAE is applicable to isoxazoline-type herbicides such as pyroxasulfone, fenoxasulfone, and other thiocarbamate herbicides such as thiobencarb sulfoxide (Tanetani, 2012; Tanetani et al., 2013a). Therefore, these inhibitors might not react with the SH group of the cysteine residue in the active site of these enzymes, revealing a new inhibition mechanism of VLCFAE.

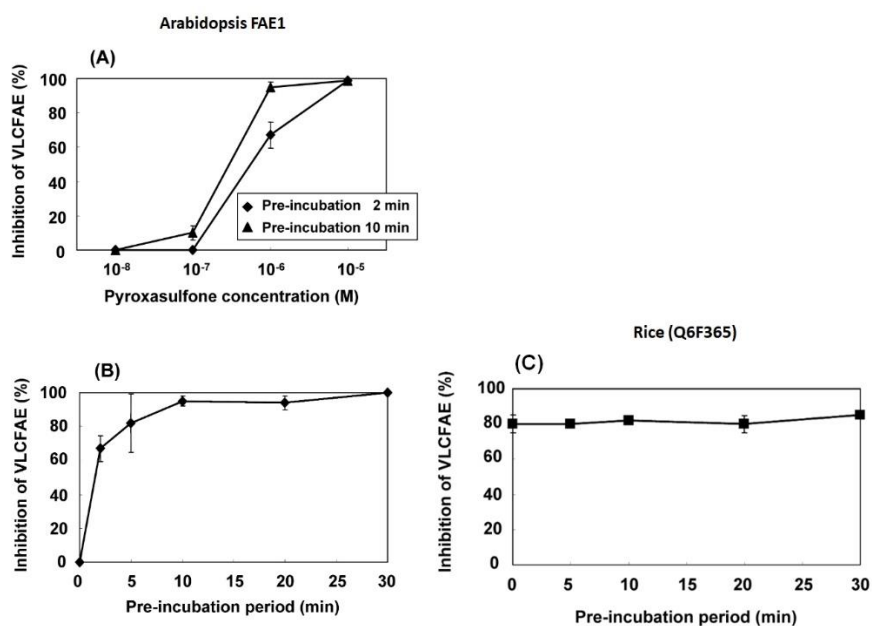


Figure 21. Inhibitory effects of pyroxasulfone on VLCFAE activity of Arabidopsis FAE1 and recombinant rice Q6F365. (A) Inhibitory potencies against VLCFAE activity of FAE1, which catalyzes the elongation step from C18:1 to C20:1, was 2.7 nmol/mg protein/90 min. (B) Inhibition of FAE1 by 10^{-6} molar concentration of pyroxasulfone. VLCFAE activity of recombinant FAE1, which catalyzes the elongation step from C18 : 1 to C20 : 1, was 2.7 nmol/mg protein/90 min. (C) Inhibition at different

pre-incubation periods using recombinant Q6F365 by 10^{-5} molar concentration of pyroxasulfone. VLCFAE activity of recombinant Q6F365, which catalyzes the elongation step from C18 : 0 to C20 : 0, was 79.4 pmol/mg protein/30 min.

Generally, VLCFAE-inhibiting compounds contain highly electrophilic carbon atom in their chemical structure. VLCFAE inhibition has been hypothesized to occur through a nucleophilic reaction between the SH group of the cysteine residue in the active center of the enzyme and the herbicide (Figure 22) (Böger et al., 2000). Thus, the compound irreversibly binds to KCS elongase-condensing enzymes via covalent binding at the conserved cysteine of the reactive site. This assertion is supported by peptide mapping analysis, demonstrating covalent binding between metazachlor chloroacetamide and the active site cysteine residue in condensing enzymes, such as chalcone synthase or stilbene synthase (Eckermann et al., 2003). Interestingly, some of the Type III PKSs tested (4-coumaroyltriacytic acid synthase and pyrone synthase) were not inhibited by K3 herbicides, likely due to differences in the structure or accessibility of the active site (Eckermann et al., 2003).

It hypothesized that the group 15 herbicides should have an electrophilic atom of carbon; in the chloro- or oxyacetamides, an active methylene may be formed by the leaving chloro moiety or the oxo-heterocycle. Tetrazolinones (e.g. fentrazamide) may bind with a target enzyme through a nucleophilic addition to the carbamoyl moiety, thus eliminating the tetrazolinone moiety (Figure 22) (Böger et al., 2000).

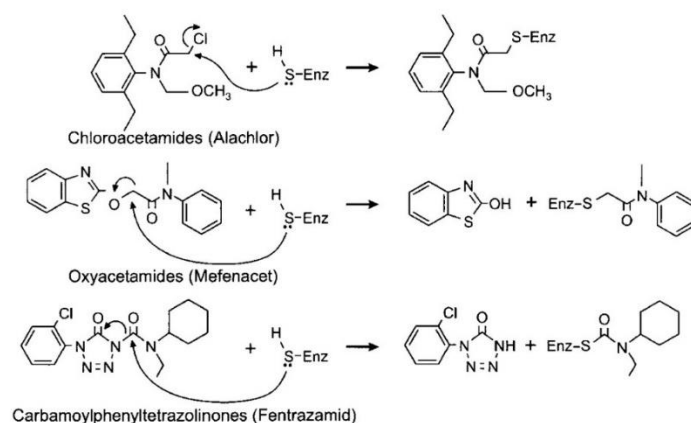


Figure 22. Assumed nucleophilic interaction of the elongase-condensing enzyme (= Enz) with structures showing chloroacetamide activity from Böger et al. (2000). The bowed arrows point to the electrophilic part of the structures which will react with the nucleophilic thiol-group of the cysteine residue of the condensing enzyme provided that a leaving group or an oxirane ring is present.

Böger et al. (2000) first speculated that there is competition between acyl-CoA and an VLCFAE-inhibitor at the active (substrate) site. This assumption is corroborated by using moderate concentrations of metazachlor or (S)indanofan and by varying the concentration of C18:0-CoA or C18:1-CoA (Götz and Böger 2003; Kato et al., 2005). Acyl-CoA substrates can protect the enzyme against inhibition in a concentration-dependent manner, whereas malonyl-CoA has no effect (Götz

and Böger 2003). This demonstrated that the acyl-CoA substrate and inhibitor competed for the same target domain, and that acyl-CoA is likely to bind first.

5. Methods for studying KCS

Studies of FAE are compromised by the redundancy of the activity, solubilization, and purification of the membrane-associated KCS enzymes. Indeed, studying KCS activity **in planta** is possible by performing transient transformation of *Nicotiana benthamiana* leaves with AtKCS (Batsale et al., 2023), to provide plant co-factors and a closed cell/membrane environment which seems necessary for AtKCS10, KCS11, and KCS15. Notably, because the Arabidopsis single KO mutant is not relevant to elongation activity due to KCS redundancy activities, except for KCS18/FAE1, a solution should be to produce double or triple mutants for KCS with the same activity as AtKCS2, 20 (Lee et al., 2009). Another approach is to generate transgenic plant lines overexpressing the KCS gene of interest and compare their wax profiles with those of the wild-type plants (Lee et al., 2009; Huang et al., 2023b), even if only few KCS contribute to wax biosynthesis. Additionally, protein-protein interactions between KCS enzymes and other members of the fatty acid elongase complex can be investigated using bimolecular fluorescence complementation (BiFC) or yeast two-hybrid assays (Y2H).

To overcome these difficulties, the activity and specificities of KCS are often assessed through **heterologous expression in yeast** (reviewed in Haslam and Kunst, 2013). The yeast core elongase complex is compatible with KCS and can catalyze three other reactions (reduction, dehydration, and reduction) to complete a cycle of VLCFA elongation. Even if some KCSs seem to have a preference for the Arabidopsis FAE complex, such as AtKCS4 described by Batsale et al. (2023), in which the coding sequences of Arabidopsis genes KCR, PAS2/HCD, and ECR were introduced into the *Saccharomyces cerevisiae* yeast genome to replace the yeast FAE complex (YBR159, PHS1, and Tsc13) using the CRISPRCas9 method. With heterologous expression of KCS in yeast, changes in the composition of VLCFAs or elongation products after substrate addition serve as an indicator of enzymatic activity. Since VLCFAs elongate by 2 carbons, substrate preference can easily be deduced (Tresch et al., 2012; Trenkamp et al., 2004; Chen et al., 2022). The abundance of VLCFAs in wild-type yeast was generally low, with the exception of C24:0 and C26:0, which makes it suitable for detecting KCS activity. ELO3, which is involved in the endogenous elongation of C22 to C24 and C26 VLCFA, can be deleted to inhibit the elongation of VLCFA beyond C22, which accumulates together with C20 (Batsale et al., 2023).

Unlike **in vivo assays**, *in vitro* assays provide valuable information about enzyme kinetics and inhibition. Isolating and assaying enzymes with a broad range of substrates is necessary for the precise characterization of known and putative membrane-bound KCSs. However, elucidating the mechanism

of their reactions is hindered by their membrane-bound nature. Therefore, very-long-chain fatty acids (VLCFAs) are synthesized as acyl-CoAs by the endoplasmic reticulum-localized elongase multiprotein complex. Few reports have conducted elongation assays using microsomal fraction isolated from yeast expressing AtKCSs or plants, or from tagged-KCSs isolated in detergent. Enzyme assays enable direct assay of fatty elongase complex or condensation activity with malonyl-CoA and a broad variety of acyl-CoA substrates, allowing examination of the substrate specificities of the KCSs (Millar and Kunst 1997; Ghanevati and Jaworski, 2001; 2002; Blacklock and Jaworski, 2006; Paul et al., 2006). Additionally, enzyme assays can be used to perform enzyme kinetics and inhibition studies. For instance, enzyme assays were used to investigate the properties of fenoxasulfone and pyroxasulfone as a VLCFAE-inhibiting herbicide in more detail (Tanetani et al., 2011a; 2011b), revealing different inhibition mechanisms by pyroxasulfone between KCS18/FAE1 and KCS from rice, and potential selectivity between plant species. Moreover, the potency of the inhibitor was determined by calculating the concentration required for 50% inhibition (IC₅₀), providing insight into the sensitivity of KCS to different VLCFAE-inhibitors. These assays require the use of a radioactive substrate, primarily malonyl-CoA, in order to quantify radiolabeled acyl-CoA product to determine enzyme activity. However, the use of radiolabeled substrates presents challenges, such as the need for dedicated equipment and waste, and the risk of radiation exposure to laboratory personnel. Therefore, it is important to improve the traditional *in vitro* KCS assay by minimizing or eliminating the use of radiolabeled substrates.

Objectives

Since the publication by Böger et al. (2003), which identified the enzymatic target of metazachlor, a molecule belonging to the herbicides targeting the VLCFA synthesis, only few studies have been conducted in this area. Notably, several herbicides in this group have been tested on *Arabidopsis* KCS expressed in a yeast system, and *in vitro* investigations have been carried out to examine the inhibition of AtKCS18/FAE1 activity by pyroxasulfone using radioactive substrates. Nevertheless, the biochemical pathway targeted by these herbicides remains a promising area for herbicide discovery and design due to the search for new Group 15 chemotypes and the low incidence of weeds resistant to VLCFA inhibitors, very recently reviewed by Jhala et al. (2023). Several factors may have contributed to the low incidence of VLCFA inhibitor-resistant weeds, including the low frequency of mutations in condensing enzymes in long-chain fatty acid synthesis (Tanetani et al., 2009; Trenkamp et al., 2004), and the genetic redundancy of fatty acid elongases. Understanding the mode of action and chemical properties of herbicides targeting the VLCFA synthesis can lead to the development of new molecules that are more effective, with improved selectivity and a reduced environmental impact.

My PhD project aims to investigate the herbicides targeting the VLCFA synthesis in plants and further understand their mechanism of action and potential selective inhibition.

As part of this CIFRE (Convention Industrielle de Formation et de Recherche - Industrial Training and Research Agreement) thesis project with BAYER SA, a phylogenetic and comparative functional analysis of KCS from various plants species was conducted using a yeast heterologous system that reconstitutes the complete plant FAE complex (1). Additionally, yeast expressing active KCSs were treated *in vivo* with various group 15 herbicides to investigate mode of action and selectivity (2). Finally, a non-radiolabeled *in vitro* assay have been developed to evaluate rapidly KCS activity and inhibition by HRAC group 15 herbicides (3).

1- Functional characterization of plant KCS family in a yeast system

Understanding the selectivity of herbicides targeting VLCFA synthesis necessitates a comprehensive exploration of KCS activity across diverse plant species. Although many studies have examined the KCS phylogeny, only few have focused on KCS activity in other species than *Arabidopsis thaliana* (Campbell et al., 2019; Chen et al., 2022).

To date, the most in-depth study investigating evolution events behind KCS great genetic diversity was conducted by Guo et al. (2016) with 28 species. This study included two algae, three early three plants and a variety of angiosperms, encompassing both monocots and dicots. We explored the evolution of KCS in order to better understand the KCS distribution within the classes annotated in *Arabidopsis thaliana* by Joubès et al. (2008) within the monocot-specific groups identified by Campbell et al. (2019). Subsequently, a yeast heterologous system reconstituting the complete plant FAE complex was used to assess substrate specificity across different clades and species, with a focus on the α and ζ KCS groups.

2- Mechanistic understanding of herbicide molecular target and plants selectivity *in vivo*

The Herbicide Resistance Action Committee (HRAC) categorizes herbicides into different groups based on their target sites, modes of action, similarities in induced symptoms, or chemical classes. HRAC group K3 and N herbicides were grouped together as HRAC group 15 based on their similar physiological, morphological symptoms. The most comprehensive study on herbicides of this group was reported by Trenkamp et al. (2004), which demonstrated the inhibition of AtKCS by several molecules.

However, the selectivity of herbicides towards target plants remains a critical challenge. By using a yeast expression system *in vivo*, we aim to investigate the plant KCS selectivity towards herbicides, particularly between monocotyledonous and dicotyledonous plants. Additionally, this work explores the inhibitory activity of newly developed herbicides by Bayer SA, providing insights into their mechanism of action and selectivity compared to known inhibitors.

3- Development of a non-radiolabeled *in vitro* assay for evaluating KCS activity and inhibition

In vitro assays provide valuable information about enzyme activity and inhibition. However, elucidating their reaction mechanism can be complicated by their membrane-bound nature. Enzyme assays enable direct measurement of fatty elongase complex or condensation activity with malonyl-CoA and a broad variety of acyl-CoA substrates, allowing examination of the substrate specificities of the KCSs (Millar and Kunst 1997; Ghanevati et al. 2001; 2002; Blacklock and Jaworski, 2002; 2006; Paul et al., 2006). Additionally, enzyme assays can be used to conduct inhibition studies. Such enzymatic assays have been used to investigate the properties of fenoxasulfone and pyroxasulfone, revealing different inhibition mechanisms by pyroxasulfone on *Arabidopsis* KCS18/FAE1 and rice KCS, as well as potential selectivity between plant species. However, traditional *in vitro* assays often use radioactive substrates, presenting challenges such as safety concerns and specialized equipment requirements.

This chapter describes the development of a high-throughput *in vitro* assay that does not use radioactive substrates for evaluating KCS activity and inhibition. HPLC-UV-MS/MS method was employed to quantify the direct product of KCS, the 3-ketoacyl-CoA intermediate.

CHAPTER 1 – FUNCTIONAL CHARACTERIZATION OF PLANT KCS FAMILY IN A YEAST SYSTEM

Chapter 1 - Functional characterization of plant KCS family in a yeast system

To comprehensively evaluate the specificity of herbicides targeting VLCFA synthesis, it is necessary to investigate KCS activity from various plant species. Although many studies have examined the KCS phylogeny, only few are focusing on the study of KCS activity from other species than *Arabidopsis thaliana* beyond few investigated by Campbell et al. (2019) concerning KCS from *Zea mays*, and more recently from *Populus trichocarpa* by Chen et al. (2022).

To date, the most in-depth study investigating evolution events behind KCS great genetic diversity was performed by Guo et al. (2016) on 28 species. This study included three algae, three early land plants and a larger variety of angiosperms covering monocot and dicot families. First, we investigated the evolution of the KCS in order to better understand the KCS distribution in *Arabidopsis thaliana* clades described by Joubès et al. (2008) and monocot-specific groups outlined in Campbell et al., (2019). Second, following this analysis certain KCSs were selected for expression in the yeast system to determine their activity and thus evaluate the conservation of KCS activity across these clades in various species.

1. Evolution of KCS gene family in plants

KCS genes exhibit a significant diversity in plants due to large multigenic families. In their study, Costaglioli et al. (2005) initially surveyed 21 KCS genes in the model organism *Arabidopsis thaliana*. Recently, numerous studies on VLCFA biosynthesis in various agronomic species were published and led to the identification of 30 KCS genes in peanut (*Arachis hypogaea* L., Huai et al., 2020), 33 in barley (*Hordeum vulgare* L., Tong et al., 2021), 25 in *Sorghum bicolor* (Zhang et al., 2022), 30 in pecan (*Carya illinoensis*, Wang et al., 2023), 24 in grapevine (*Vitis vinifera*, Zheng et al., 2023), 22 in *Oryza sativa* (Yang et al., 2023 ; Khan et al., 2023) and 28 in maize (*Zea mays*, Campbell et al., 2019; Xu et al., 2024). Moreover, cotton species *Gossypium hirsutum*, *G. arboreum*, and *G. raimondii* possess 58, 31, and 33 KCS genes, respectively (Xiao et al., 2016), while 58, 33, 33, 50 and 32 KCS genes were reported in *Brassica napus* (4n), *B. rapa*, *B. oleracea*, *B. carinata* (4n) and *B. nigra* (Xue et al., 2020; Khan et al., 2023) respectively. Additionally, 28 KCS genes were found in apple (*Malus × domestica* Borkh., Lian et al., 2020), 31 in Welsh onion (*Allium fistulosum*, Xing et al., 2023), 20 in Yellow horn (*Xanthoceras sorbifolium*, Liu et al., 2023) and 32 in passion fruit (Riwan et al., 2022). Therefore, multiple genome-wide identification studies reported KCS multigenic families of various sizes. KCSs from six citrus

species (Yang et al., 2021), quinoa (*Chenopodium quinoa*, Tariq et al., 2022), *Populus trichocarpa* (Chen et al., 2022) and sunflower (*Helianthus annuus*, Zaib et al., 2022), and *Pseudoroegneria (Nevski) Löve* (Zhai et al., 2024) were also recently studied. This genetic variability among different species clearly highlights a complex evolutionary history of the KCS multigenic family.

Guo et al. (2016) conducted the first thorough investigation of the evolutionary events that led to the great genetic diversity of KCSs. To understand the evolutionary history of the KCS gene family in plant lineages, 28 species covering key systematic positions in plant classification were selected for genome-wide identification of KCS genes and phylogenetic analyses (Figure 1A). These species included the algae *Chlamydomonas reinhardtii* and *Volvox carteri*, early land plants such as fern *Lygodium japonicum* and moss *Physcomitrium patens*, the gymnosperm species *Picea abies*, and a diverse range of angiosperms representing monocotyledonous and dicotyledonous families.

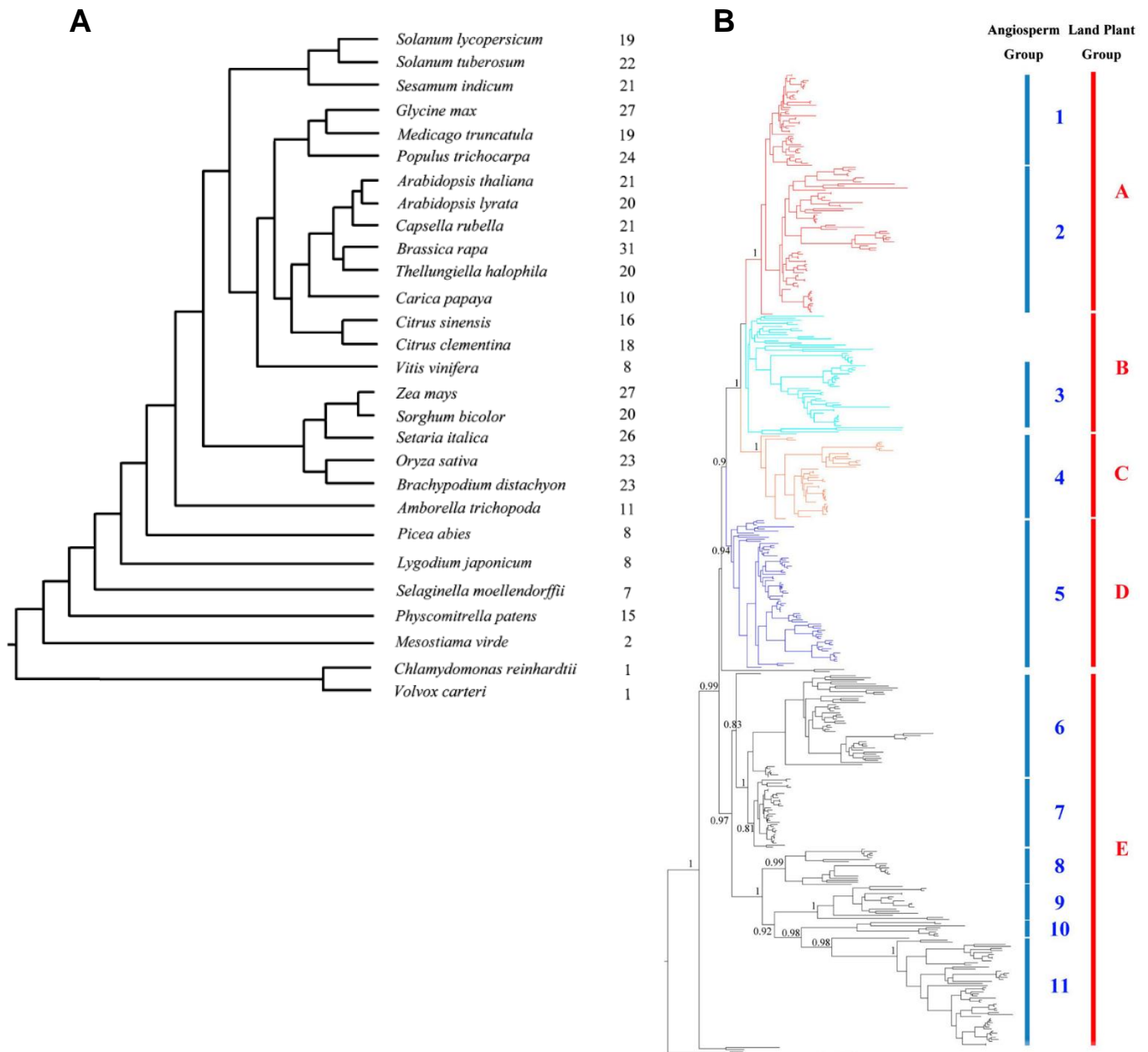


Figure 1. Expansion of plant KCS multigenic families across plant evolution (from Guo et al.,2016). (A)The number of KCS genes identified in each species is indicated on the right of the phylogenetic tree. (B) Five monophyletic groups represented in red emerged among land plants. Eleven monophyletic groups characterize the angiosperms KCS genes, represented in blue.

Genome-wide analysis of KCS genes across different species revealed a global expansion of these genes during plant evolution. The KCS genetic families started with a single gene in *C. reinhardtii* and *V. carteri*, expanded to 7-8 genes in early land plants, or 15 genes in *Physcomitrella patens* which has undergone at least one whole-genome duplication event in its evolutionary history, and a strong expansion was observed in angiosperm species, which on average contain 20 genes (Guo et al., 2016). Guo et al. (2016) described the phylogenetic distribution of KCS genes among land plants in five basic monophyletic groups (Figure 1B), all including early land plants KCS. The distribution suggests a first

duplication event before terrestrial colonization, which led to a fivefold increase in gene number compared to the common ancestor of all land plants. Monocots such as maize, rice and sorghum, were classified based on the eight Arabidopsis KCS subclasses (Campbell et al., 2019), previously labeled as clades α to θ (Joubès et al., 2008). These analyses indicate that every clade defined by the Arabidopsis homologs, except clade η , contains a maize homolog. In addition, three new clades (ι , κ and λ) were identified as monocot-specific subgroups by Campbell et al. (2019). This suggests that new KCS genes may appear after the differentiation of monocots and dicots. Additionally, analysis of synteny showed huge differences in homologous gene pairs between dicots and monocots (Yang et al., 2023; Zheng et al., 2023). However, between grapevine and other plant species, only four VvKCS genes exist in monocots and dicots as related orthologous gene pairs (Zheng et al., 2023), suggesting that these genes were present before dicot and monocots differentiation, and that they may have relatively important and functionally conserved functions.

1.1. Phylogenetic tree

To investigate the KCS phylogenetic relationship between algae, dicot and monocot plants, KCS protein sequences were collected in 14 species, including 3 algae species (13 KCS from *Raphidocelis subcapitata* (annotated RsKCS), 1 from *Chlamydomonas reinhardtii* (CreKCS, Guo et al., 2016), 1 from *Volvox carteri* (VcarKCS, Guo et al., 2016)) and various dicot and monocot species. Monocotyledon species were Foxtail millet, *Setaria italica* (30 SiKCS), *Setaria viridis* (30 SvKCS), *Zea mays* (28 ZmKCS, Xu et al., 2024), *Oryza sativa Japonica* (22 OsKCS, Yang et al., 2023), *Oryza sativa Indica* (32 OsiKCS), *Sorghum bicolor* (25 SbKCS, Zhang et al., 2022), and *Triticum aestivum* (39 TraesKCS/TrKCS), while dicotyledon species were *Arabidopsis thaliana* (21 AtKCS, Joubès et al., 2008), *Solanum lycopersicum* (19 SolycKCS/SoKCS), *Vitis vinifera* (24 VvKCS, Zheng et al., 2023), *Capsella rubella* (21 CarubKCS/CrKCS), and *Brassica napus* (58 BnKCS, Xue et al., 2020).

The phylogenetic tree was constructed based on MUSCLE alignment of 362 amino acid KCS sequences from 14 species, utilizing MEGA11 software and maximum-likelihood method with 500 bootstraps (Figure 2). It revealed that these proteins cluster into 12 subgroups, comprising the 8 Arabidopsis KCS subclasses previously designated as KCS4/9/17-like (α), FAE1-like (β), CER6-like (γ), KCS1-like (δ), KCS2/20-like (ζ), KCS10/FDH-like (ϵ), KCS7/21-like (η), and KCS3/12/19-like (θ) (Joubès et al., 2008) and 3 three novel clades (ι , κ , and λ) identified as monocot-specific by Campbell et al. (2019), as well as an algae-specific subgroup.

Algae

Dicotyledonous plants:

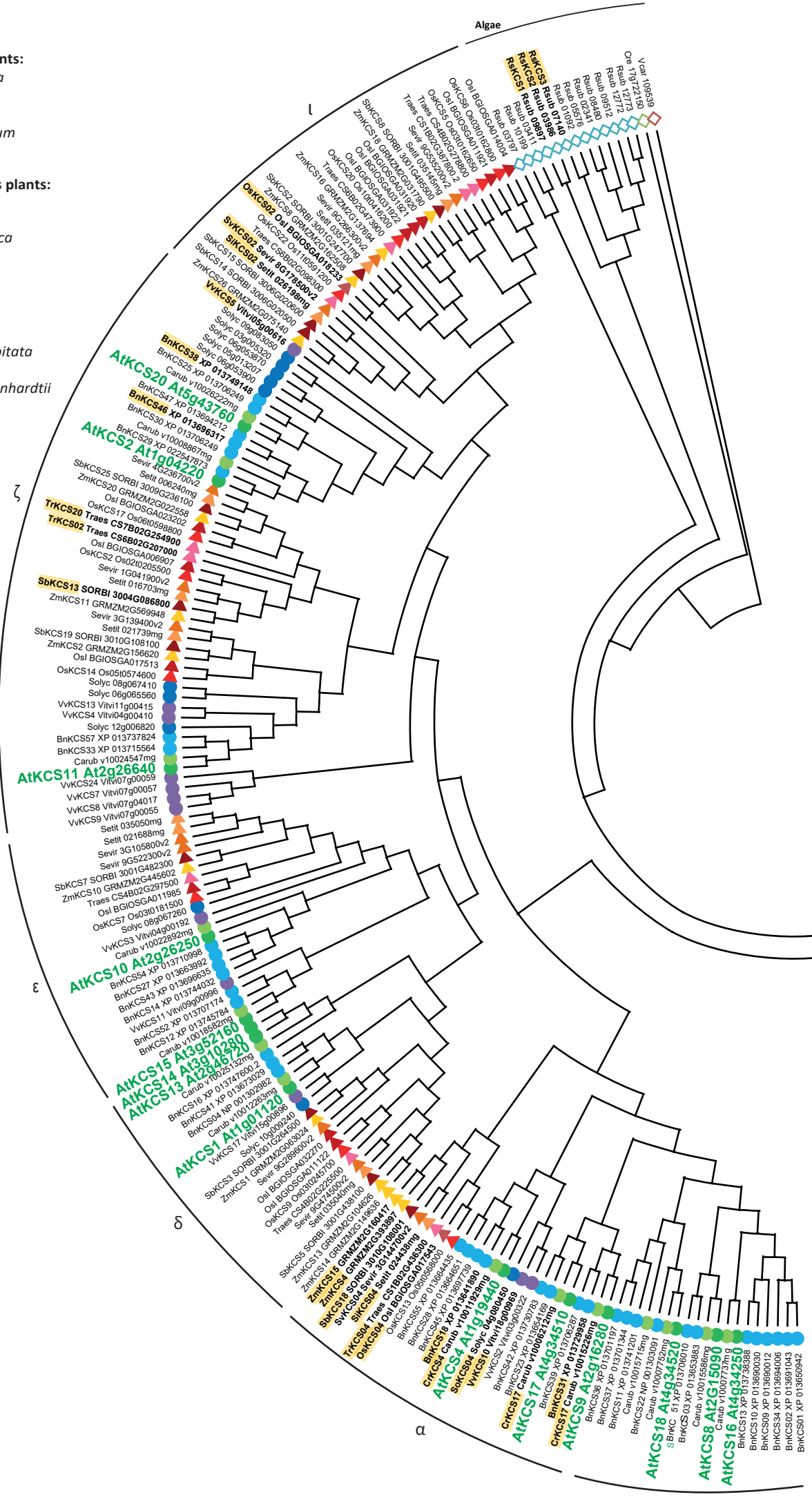
- *Arabidopsis thaliana*
- *Capsella rubella*
- *Brassica napus*
- *Solanum lycopersicum*
- *Vitis vinifera*

Monocotyledonous plants:

- ▼ *Sorghum bicolor*
- ▼ *Oryza sativa Indica*
- ▼ *Oryza sativa Japonica*
- ▼ *Zea mays*
- ▼ *Setaria italica*
- ▼ *Setaria viridis*
- ▼ *Triticum aestivum*

Algae:

- ◇ *Raphidocelis subcapitata*
- ◇ *Volvox carteri*
- ◇ *Chlamydomonas reinhardtii*



β

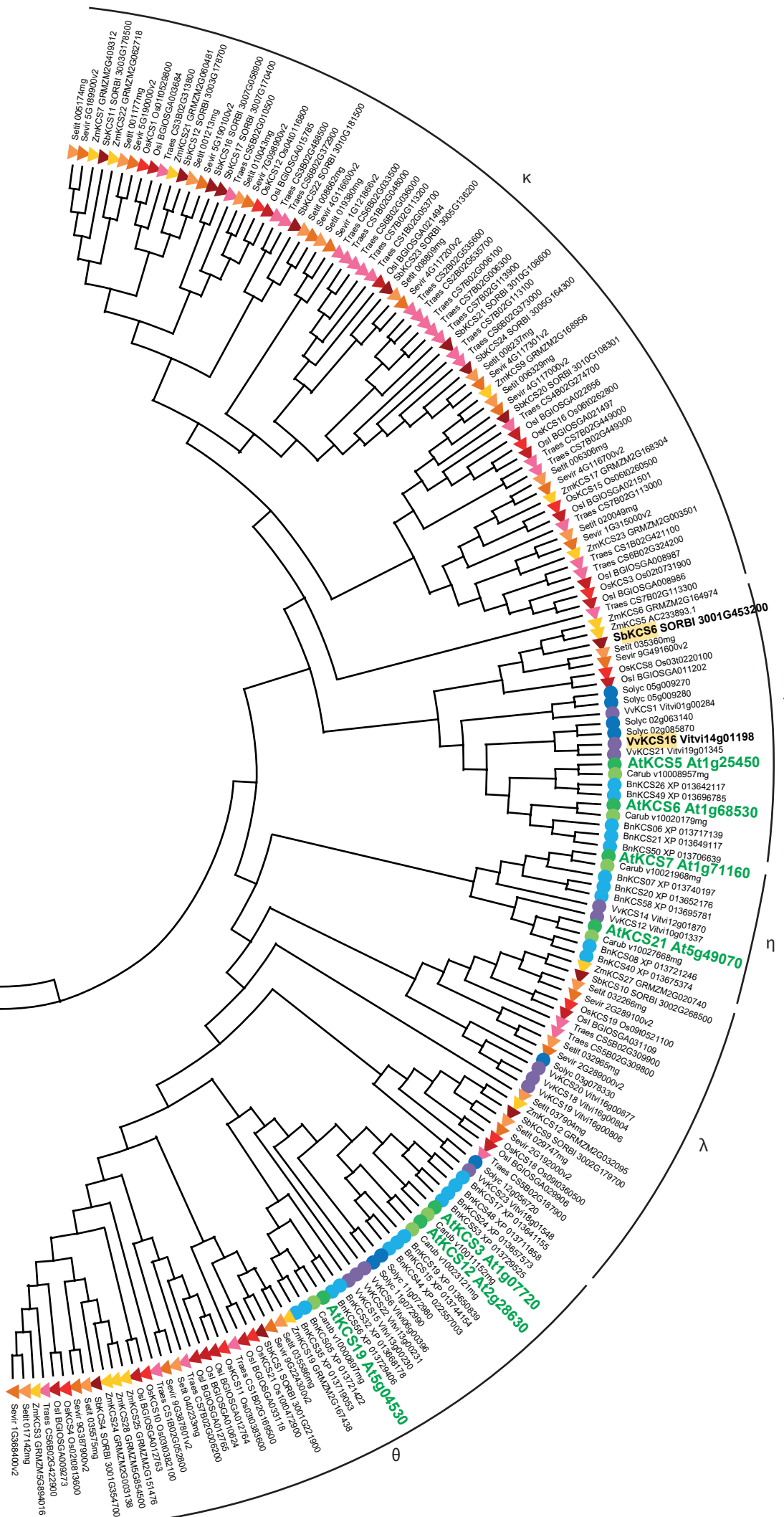


Figure 2. Phylogenetic analysis of KCS proteins using the Maximum Likelihood method with 500 bootstrap. This analysis involved 362 amino acid sequences. There were a total of 1527 positions in the final dataset. Evolutionary analyses were conducted in MEGA11. AtKCS are indicated in bold green letters. Candidates KCSs are indicated in bold.

In our investigation, monocotyledonous plants such as wheat, maize, rice, setaria and sorghum were observed within Arabidopsis KCS subclasses as clades α to θ (Joubès et al., 2008), except for clades η and β , which appear to be dicot-specific subgroups. Specifically, KCS4/9/17-like (α), CER6-like (γ), KCS2/20-like (ζ), KCS10/FDH-like (ϵ), and KCS3/12/19-like (θ) clades contain KCS proteins from both dicot and monocot species, distinctly separated within all subgroups, suggesting the separate evolution of KCS families in monocot and dicot plants since the emergence of monocotyledonous plants (Guo et al., 2016; Yang et al., 2023; Zheng et al., 2023).

The λ group contains a large number of KCS genes, constituting 20% of all analyzed proteins, with 73 sequences. As elucidated by Campbell et al. (2019), κ and ι represent monocot-specific groups, showing a random distribution among the monocot species studied here. However, the λ group which was previously described as a monocot-specific group contains in Figure 2 a few KCS proteins from dicot plants: *Vitis vinifera* and *Solanum lycopersicum*. This result suggests that these orthologous proteins may have existed prior to ancestral divergence, which is consistent with Zheng et al. (2023), as they identified a small number of orthologous gene pairs between *Vitis vinifera* and *Oryza sativa*.

2. Characterization of plant KCS family in a yeast system

2.1. KCS candidates for enzyme activities through plant species

The activity of few plant KCS has been the subject of recent research, in particular by heterologous expression in the yeast *Saccharomyces cerevisiae*. The 21 Arabidopsis KCS genes were cloned and expressed in yeast to characterize their substrate specificity. Among these, 9 AtKCS proteins were identified as active within the yeast system: KCS4, 9, and 17 belonging to the α subgroup, KCS2 and 20 in the ζ group, KCS5 and 6 of the γ subgroup, KCS1 (δ) and KCS18 (ϵ) (Trenkamp et al., 2004; Tresch et al., 2012, Batsale et al., 2023). Several KCS from *Zea mays* (Campbell et al., 2019) and from *Populus trichocarpa* (Chen et al., 2022) were similarly characterized.

To explore KCS activity in different species, we focused on two distinct phylogenetic groups, in which Arabidopsis members were shown to be active in yeast. We hypothesized that within these groups, the catalytic activity of KCS enzymes could be conserved across diverse plant species, in both monocots and dicots, despite the different evolutionary trajectories of these species. Our focus was directed towards the α and ζ groups, due to the considerable species diversity (monocots and dicots) exhibited within these groups. The α group is characterized by robust sequence identity and close substrate specificities, exemplified by AtKCS4, 9, and 17. Contrarily, the ζ group, exemplified by AtKCS2, AtKCS20 and AtKCS11, exhibits more diverse sequences but close elongation specificities. In

order to improve our comprehension of the substrate specificity of the α and ζ KCS groups, we employed BLAST (Uniprot, <https://www.uniprot.org/blast>) searches to identify proteins from 11 different species using Arabidopsis KCS protein sequences as queries, AtKCS4 for clade α and AtKCS20 for clade ζ . Through this method, we aimed to identify potential genes that could confirm whether the enzyme activity remains consistent across various species, including both dicots and monocots, within the same evolutionary branch.

We then selected a total of 28 proteins (represented in bold and highlighted in yellow in the figure 2) for further analysis. Within the green plant lineage, 16 KCS sequences were identified to exhibit close homology to the AtKCS4/9/17 proteins. Specifically, among dicot plant species, these included 3 sequences from *Capsella rubella* (CrKCS4, CrKCS9, CrKCS17), 2 from *Vitis vinifera* (VvKCS10, VvKCS16), 1 from *Solanum lycopersicum* (SoKCS4), and 2 from *Brassica napus* (BnKCS18, BnKCS21). For monocot plant species, they comprised 1 from *Setaria italica* (SiKCS4), 1 from *Setaria viridis* (SvKCS4), 2 from *Zea mays* (ZmKCS4, ZmKCS15 used in Campbell et al., 2019), 2 from *Sorghum bicolor* (SbKCS6, SbKCS18), 1 from *Triticum aestivum* (TrKCS4), and 1 from *Oryza sativa Indica* (OsKCS4). These proteins exhibited identities ranging from 97% to 62% with AtKCS4 and from 90% to 58% with AtKCS17. These identities are always higher with AtKCS4 than with AtKCS17, indicating a closer relationship to AtKCS4 than to AtKCS17. While SbKCS6 and VvKCS16 were initially identified through KCS4 BLAST analysis, their sequences exhibit closer similarity to AtKCS5 and AtKCS6 (76% to 84% identity) compared to the α group (58% to 66% identity), so that are classified within the γ group in Figure 2. Consequently, out of these 16 selected KCS genes, 14 were identified as belonging to the α clade.

Regarding the ζ group, 9 KCS sequences were found within the green plant lineage as closely related to the AtKCS2/20 proteins. Among dicot plants, these included 2 sequences from *Brassica napus* (BnKCS38, BnKCS46) and 1 from *Vitis vinifera* (VvKCS05), while among monocots, they comprised 2 from *Triticum aestivum* (TrKCS2, TrKCS20), 1 from *Sorghum bicolor* (SbKCS13), 1 from *Oryza sativa* (OsKCS02), 1 from *Setaria italica* (SiKCS2), and 1 from *Setaria viridis* (SvKCS2). However, due to the higher number of genes in the ζ group compared to the α group, it was challenging to discern which proteins could share similar activity to AtKCS2/20. In addition, the BLAST analysis allowed us to select KCS sequences associated with the ι group (OsKCS02, SiKCS02, SvKCS02), identified as related to AtKCS2/20 with identities ranging from 65% to 67%.

		clade α			clade ζ		
		AtKCS4 At1g19440	AtKCS9 At2g16280	AtKCS17 At4g34510	AtKCS2 At1g04220	AtKCS20 At5g43760	
Dicotyledon	α	AtKCS04					
		AtKCS09	76%				
		AtKCS17	71%	81%			
		AtKCS02	60%	59%	56%		
		AtKCS20	61%	60%	56%	87%	
		BnKCS18	93%	75%	67%	62%	62%
		BnKCS31	76%	92%	76%	62%	62%
		CrKCS17	73%	80%	90%	61%	62%
		CrKCS4	97%	76%	67%	62%	63%
		CrKCS9	76%	98%	77%	61%	61%
		SoKCS4	83%	77%	68%	60%	62%
		VvKCS10	82%	74%	66%	63%	63%
		BnKCS38	61%	61%	58%	88%	95%
		BnKCS46	60%	60%	55%	92%	86%
		VvKCS05	64%	62%	56%	74%	74%
		γ	VvKCS16	62%	64%	58%	59%
Monocotyledon	γ	SbKCS6	66%	64%	59%	60%	61%
		Osl KCS4	77%	74%	66%	62%	63%
		SbKCS18	76%	73%	66%	62%	63%
		SiKCS4	75%	72%	64%	61%	62%
		SvKCS4	78%	74%	66%	63%	65%
		TrKCS4	75%	72%	63%	60%	61%
		ZmKCS04	78%	74%	66%	62%	64%
		ZmKCS15	77%	74%	66%	62%	64%
		SbKCS13	64%	60%	55%	68%	68%
		TrKCS02	64%	61%	55%	68%	69%
		TrKCS20	64%	61%	56%	71%	73%
	ι	SiKCS2	55%	55%	53%	65%	65%
	SvKCS2	56%	56%	53%	65%	65%	
	Osl KCS2	59%	59%	55%	66%	67%	
Algae		RsKCS2	52%	50%	48%	49%	50%
		RsKCS3	48%	47%	45%	48%	49%
		RsKCS1	51%	50%	48%	49%	49%

Table 1. Percentage identity between protein sequences of AtKCS and KCS candidates from different plant species. Green represent high, red represent low percentage of identity between protein sequences.

Lastly, three *Raphidocelis subcapitata* KCS sequences (RsKCS1/2/3) were included in the selection due to the utilization of this algae in ecotoxicity assays (Ma et al., 2006). These protein sequences exhibited low identities with AtKCS sequences, ranging from 45% to 52%, not allowing to attribute them a putative activity.

2.2. Heterologous expression of KCS in yeast

Acknowledgments: The yeast systems I used to explore the catalytic activities of KCS during my PhD work were engineered by Marie ALONSO, Marguerite BATSALE, Stephanie PASCAL, Didier THORAVALL, Francois DOIGNON, Frederic DOMERGUE and Jérôme JOUBÈS (Batsale et al., 2023).

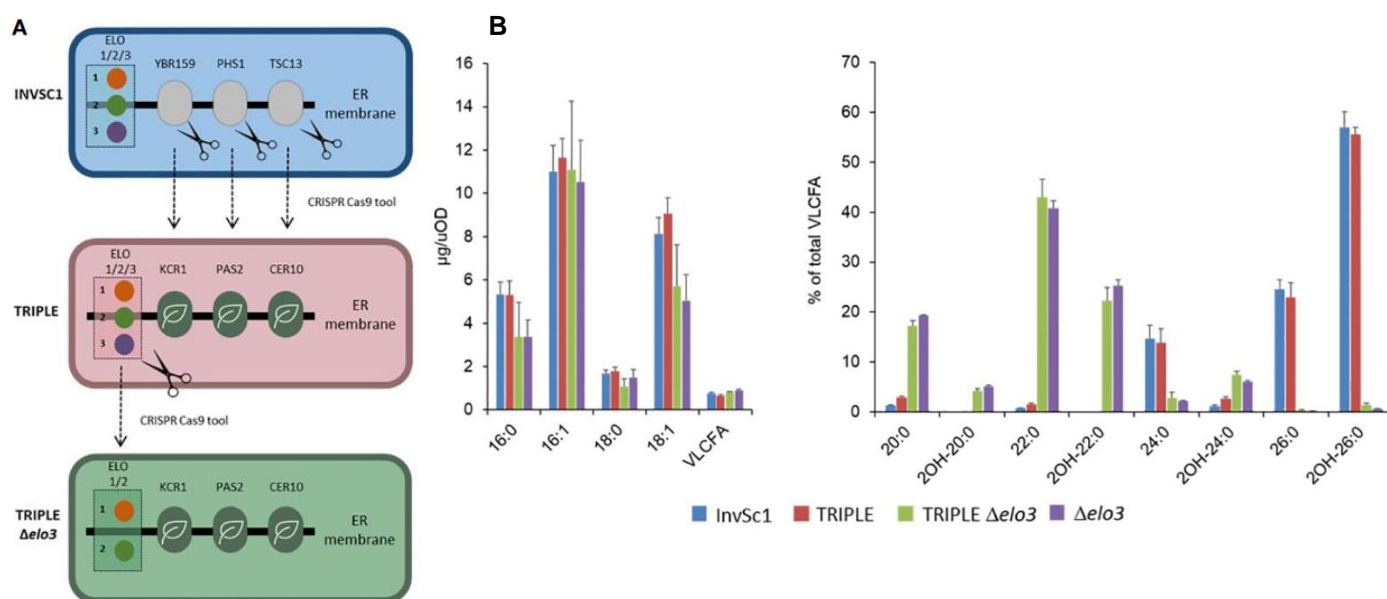


Figure 3. Genetic complementation of yeast elongase by Arabidopsis components (from Batsale et al., 2023). (A) Schematic of the strategy (B) Comparison of the FAMES profile of InvSc1 control strain with the FAMES profiles of the TRIPLE, TRIPLE $\Delta elo3$ and $\Delta elo3$ strains grown for 72 hours. Mean values ($\mu\text{g}/\text{uOD}$ or percentage of total VLCFA) are given with SD ($n = 5$). Each FAME species is designed by carbon chain length and degree of unsaturation

Initially, the CRISPR-Cas9 genome editing tool was used to engineer a yeast strain named TRIPLE. In this yeast strain, the coding sequences for the yeast endogenous Fatty Acid Elongation (FAE) core subunits YBR159, PHS1, and TSC13 were replaced by the corresponding Arabidopsis genes KCR1, PAS2, and CER10 (Figure 3). This genome modification did not impact the fatty acid profile, with the presence of high levels of C16 and C18 long-chain fatty acids, followed by very-long-chain fatty acids (VLCFA) accumulation up to C26.

Subsequently, a second yeast strain was generated by deleting the *ELO3* gene, responsible for the endogenous elongation of C22 to C24 and C26 VLCFA, and named as TRIPLE $\Delta elo3$. In TRIPLE $\Delta elo3$, the microsomal FAE complex was unable to elongate VLCFA beyond C22, leading to the accumulation of C20 and C22 fatty acids (Figure 3). The TRIPLE $\Delta elo3$ fatty acid profile was identical to that of $\Delta elo3$ (Batsale et al., 2023).

These strains were then used to express various KCS genes under the transcriptional control of the constitutive *ADH1* promoter. Alteration of the fatty acid profile was evaluated by direct transmethylation of yeast cells followed by GC-FID analysis.

2.3. Comparative analysis of KCS activity across diverse plant species

The twenty-eight KCS genes from different species (Table1) were cloned in the pVT-LEU vector under the transcriptional control of the constitutive *ADH1* promoter and expressed in the TRIPLE and TRIPLE $\Delta elo3$ yeast strains as described in Batsale et al. (2023). For direct comparison, the Arabidopsis KCS from clade α (AtKCS4/9/17), ζ (AtKCS2/20) and γ (AtKCS5/6) were also expressed.

To focus on the variations in KCS activities within the different groups, we decided to analyse the percentages of total very-long-chain fatty acids (VLCFA): C20, C22, C24, and C26 (figure 4). Among the 28 enzymes tested, 7 KCS (SiKCS4, OsKCS4, BnKCS18, SvKCS2, SiKCS2, BnKCS46 and RsKCS3, all faded in Figure 4) appeared inactive as their expression resulted in VLCFA distribution identical to the both strains TRIPLE and TRIPLE $\Delta elo3$ transformed with the empty vector “ev”. In contrast, 21 were found to be active as they significantly changed the VLCFA distribution in both TRIPLE $\Delta elo3$ or TRIPLE yeast strains. The 28 selected KCS all displayed the putative catalytic triad, except OsKCS04 in which the cysteine residue at the position 236 is replaced by a serine residue, justifying its inactivity in yeast. Furthermore, the 3D protein structure and transmembrane domain number were assessed using AlphaFold website (<https://alphafold.ebi.ac.uk/>), revealing consistent 3D conformation featuring two transmembrane domains, except for RsKCS3, which exhibited only one transmembrane domain (not shown). No construction have been obtained for RsKCS3.

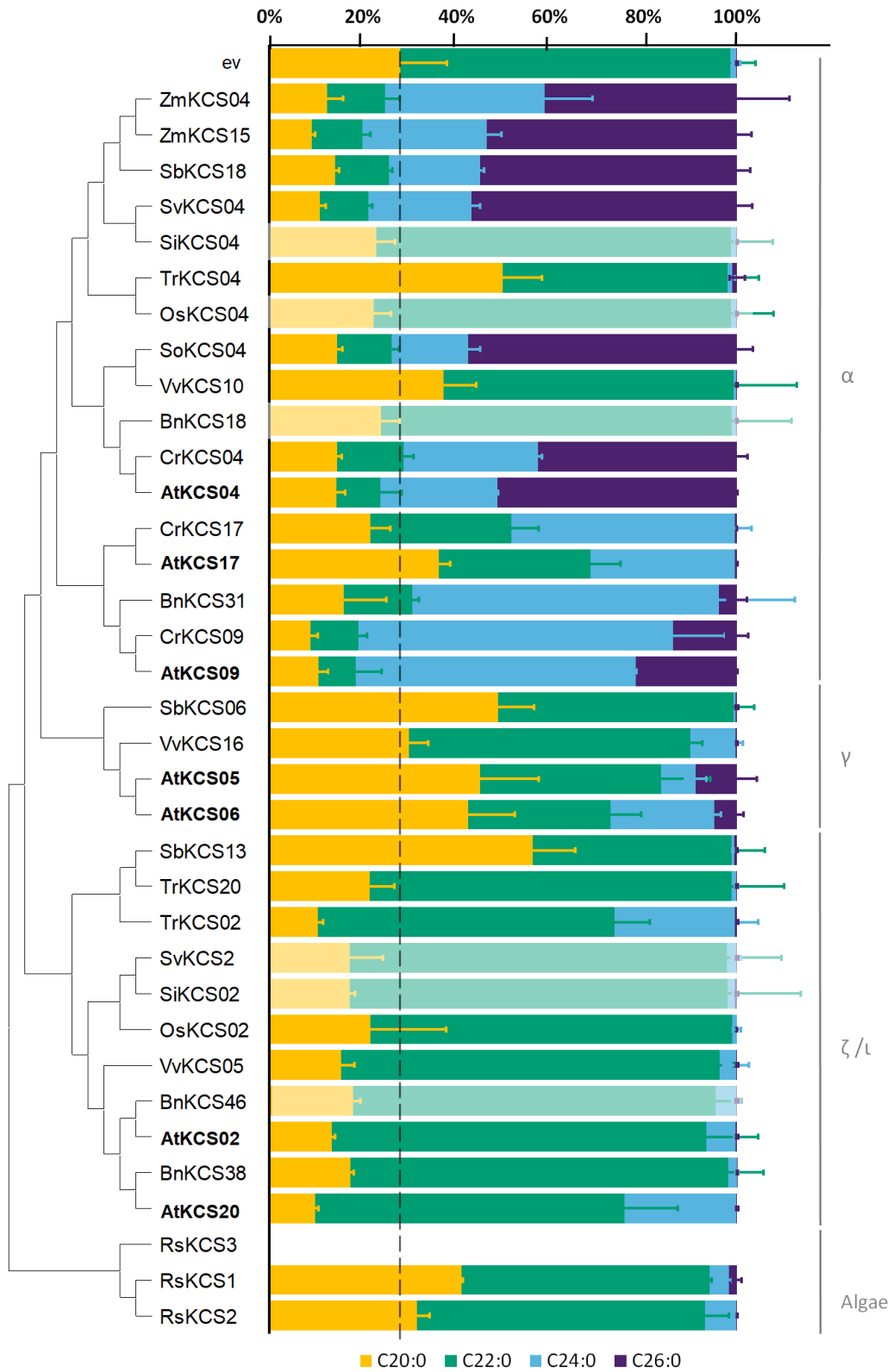


Figure 4. Phylogenetic analysis and FAMES profiles obtained in the strain TRIPLE $\Delta elo3$ expressing a set of KCSs compared to the strain transformed with an empty vector “ev”. Faded bars indicate KCSs that did not demonstrate activity when expressed in yeast. Mean values (percentage of total VLCFA) are given with SD (at least n=4). AtKCS are represented in bold.

RsKCS1 and RsKCS2 from an algae specie, *Raphidocelis subcapitata*, share only approximately 50% identity with AtKCS from α and ζ clades. Even if their VLCFA accumulation profile seems similar to that of AtKCS5 and AtKCS6 in Figure 4, RsKCS are responsible of saturated C20 accumulation in TRIPLE $\Delta elo3$ while AtKCS5/6 elongate C22 into C24 and C26 compounds (Figure 5). The substrate specificity of RsKCS1 and RsKCS2 do not resemble any substrate specificity described in AtKCS.

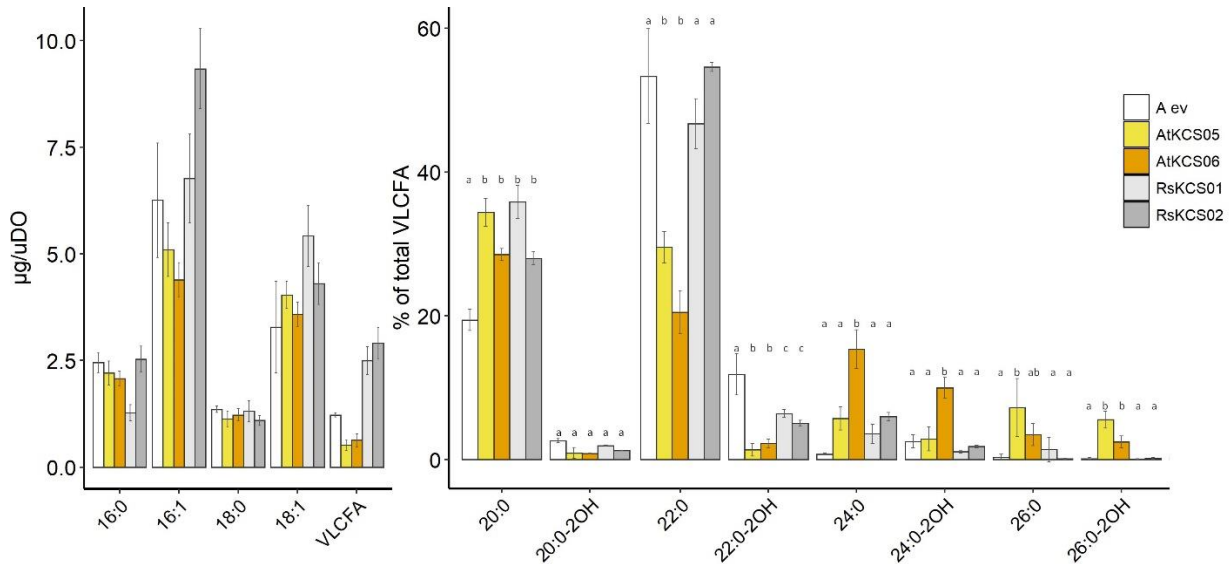


Figure 5. FAMES profiles obtained in the strain TRIPLE $\Delta elo3$ expressing AtKCS05, AtKCS06, RSKC01, RSKCS02 compared to the strain transformed with an empty vector “ev”. Mean values ($\mu\text{g}/\mu\text{DO}$) are given with SD ($n=4$). Different letters indicate statistically significant differences ($P \leq 0.05$) determined with a Tukey post hoc test.

2.3.1. Comparative analysis of clade γ KCS activity

While SbKCS6 and VvKCS16 were initially identified through AtKCS4 BLAST analysis, their sequences exhibit closer similarity to AtKCS5 and AtKCS6 (76% to 84% identity) compared to the α group (58% to 66% identity). In our phylogenetic analysis (Figure 2), SbKCS6 and VvKCS16 in agreement grouped within the γ clade.

In the TRIPLE $\Delta elo3$ strain, the AtKCS5 and AtKCS6 enzymes, which share 88% identity, were responsible for the elongation of C22 into C24 and C26 compounds (Figure 6).

Notably, VvKCS16 displays an activity profile similar to that of AtKCS5 and AtKCS6, characterized by a significant decrease of C22 and increase in C24 (Figure 4, Figure 6), even though VvKCS16 does not accumulate C26 to the same extent as AtKCS5 and AtKCS6. In contrast, SbKCS06 exhibits a markedly different activity profile, despite having 76-78% identity with AtKCS5 and 6, accumulating abundantly C20 VLCFA (Figure 4). More precisely, expression of SbKCS06 results in accumulating C20:1 and C20:0, which is reminiscent of AtKCS1 or AtKCS18 expression in the TRIPLE strain (Figure 7).

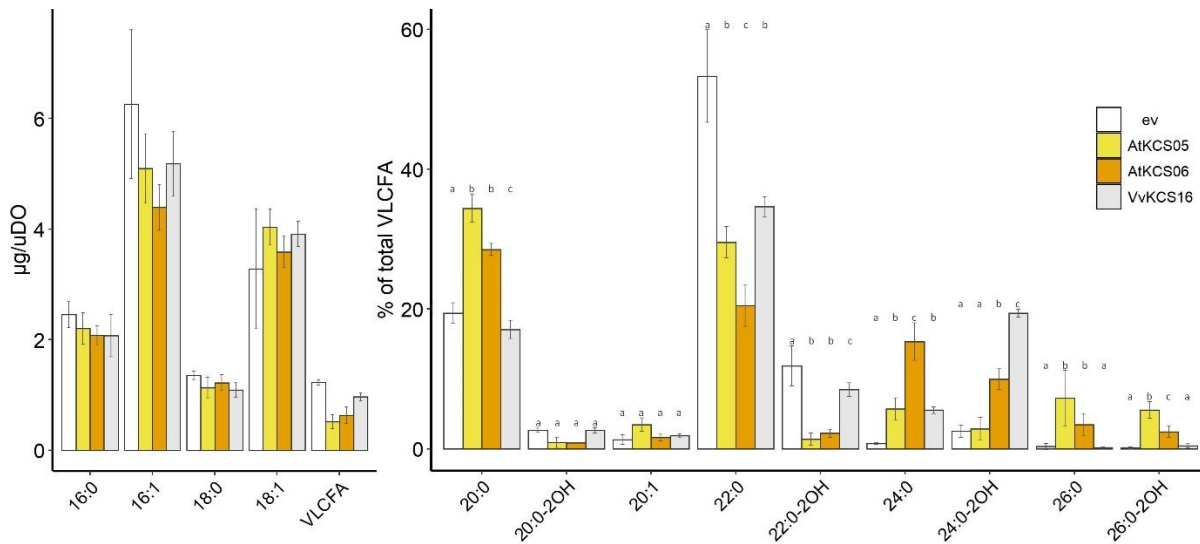


Figure 6. FAMES profiles obtained in the strain TRIPLE $\Delta elo3$ expressing AtKCS5, AtKCS6 and VvKCS16 compared to the strain transformed with an empty vector “ev”. Mean values ($\mu\text{g}/\text{uDO}$) are given with SD ($n=4$).

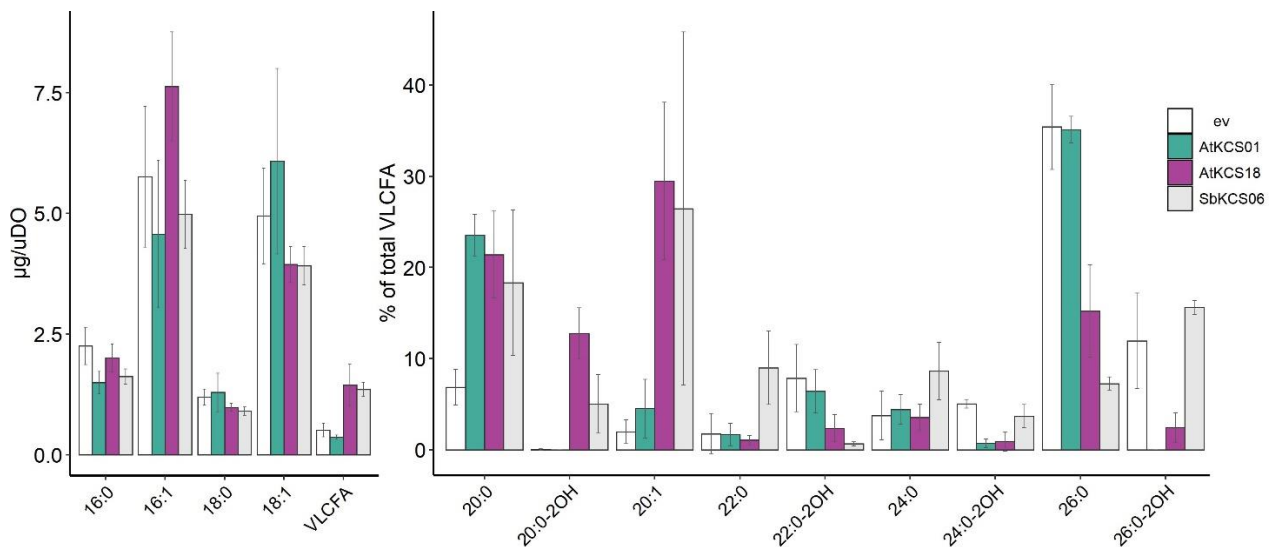


Figure 7. FAMES profiles obtained in the strain TRIPLE expressing AtKCS1, AtKCS18, SbKCS06 compared to the strain transformed with an empty vector “ev”. Mean values ($\mu\text{g}/\text{uDO}$) are given with SD ($n=4$).

The activity of VvKCS16 is therefore similar to those of AtKCS5 and AtKCS6, indicating that enzyme function is partially conserved across evolutionary distances between these plant species. In contrast, this activity does not appear to have been conserved in *Sorghum bicolor* from γ clade suggesting that evolutionary trajectories may have diverged in this case.

2.3.2. Comparative analysis of clade α KCS activity

As described in Batsale et al. (2023), the heterologous expression of AtKCS from the subclass α (KCS4, KCS9 and KCS17) in TRIPLE $\Delta elo3$ strain led to increases in C24 and C26 VLCFAs in different ratio, and increase of C28 in AtKCS4 (Figure 8). KCS9 and KCS17, which share 81% identity, displayed different elongation specificities in the TRIPLE $\Delta elo3$ strain. Although both KCS9 and KCS17 were able to perform the elongation of C22 saturated acyl chains into C24 products, only KCS9 could effectively produce C26 VLCFA. KCS4 shares a relatively high identity with those two KCS, 76% with KCS9 and 71% with KCS17. The expression of KCS4 in the TRIPLE $\Delta elo3$ strain led to even higher amounts of C26 compounds compared to KCS9. Therefore, the three enzymes of the subgroup α appear to share the ability to use C22 saturated acyl chains as initial substrate to elongate them into C24 and C26 VLCFA. However, each enzyme performed those elongation steps with different efficiency.

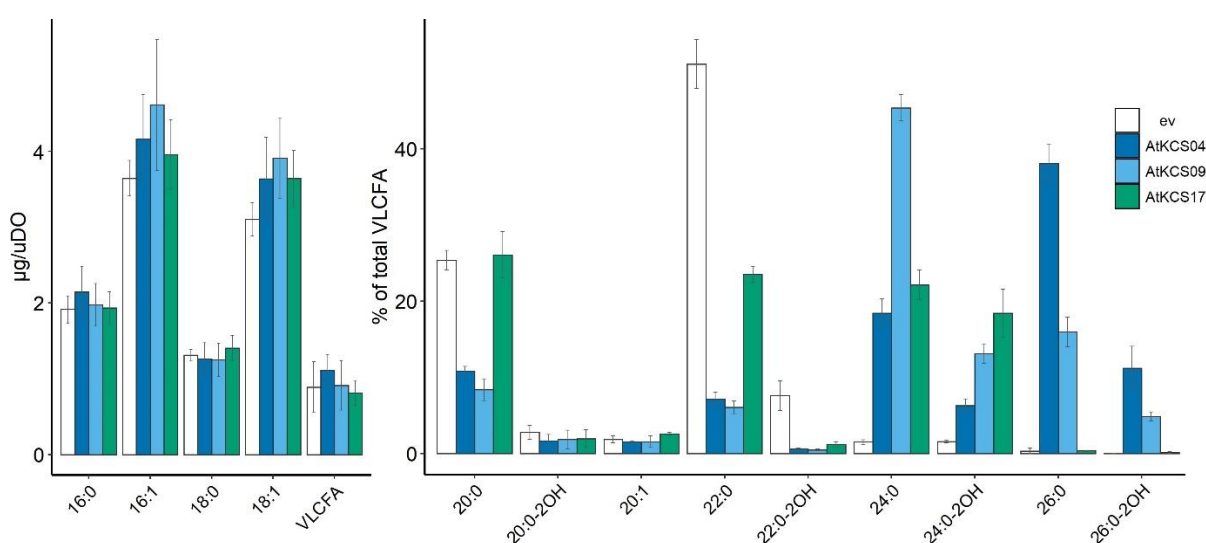


Figure 8. FAMES profiles obtained in the strain TRIPLE $\Delta elo3$ expressing AtKCS4, AtKCS9, AtKCS17 compared to the strain transformed with an empty vector “ev”. Mean values ($\mu\text{g}/\text{uDO}$) are given with SD (n=4).

To compare KCS activities across α subgroups, we expressed the KCSs from various species in yeast and analyzed their percentages of very-long-chain fatty acids (VLCFA) (figure 9). Additionally, two calculations were used to highlight and compare the different KCS activities and specificities. First, the combined proportions of C24 and C26 gives an idea about the catalytic activity of each expressed KCS. Second, the relative substrate specificity of each KCS can be compared by calculating the ratio of C26 compounds produced over C24 compounds. Whereas KCS4 and KCS9 accumulate similar amounts of C24 and C26 products combined together, the C26/C24 ratio of KCS4 is higher than that of KCS9 ratio (2.1 versus 0.4) implying that KCS4 leads to a greater production of C26 acyl-chains when KCS9 enables higher accumulation of C24 compounds upon expression in yeast. KCS17 shows a combined production of C24 and C26 products around two times lower than KCS4 and KCS9. As it accumulates

less >C22 VLCFA products, KCS17 has a lower activity compared to KCS4 and KCS9 (31.3% versus 76.2 and 81.5 % in KCS4 and KCS9, respectively).

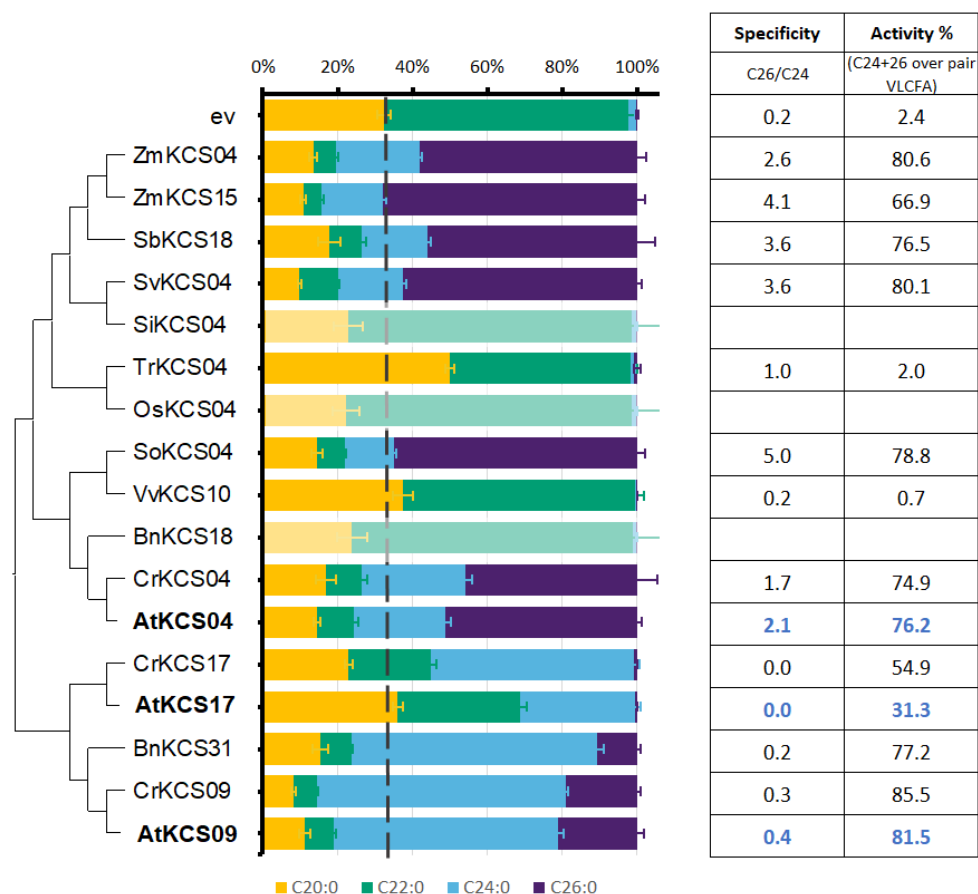


Figure 9. Substrate specificity of KCS from clade α from different species. The barplot represents the relative distribution of quantified VLCFA species from TRIPLE $\Delta elo3$ transformed with the different KCS genes. Mean values (percentage of total VLCFAs) are given with SD (n=4). “ev” stands for the TRIPLE $\Delta elo3$ strain transformed with the empty vector. Right table shows for each construct the combined percentage of C24 and C26 VLCFAs, which is indicative of the level of activity, and the ratio C26/C24, which is indicative of the substrate specificity.

The phylogenetic analysis and expression in yeast revealed that most of the KCS belonging to the α clade were active in yeast, with the exception of SiKCS4, OsKCS4 and BnKCS18 (Figure 4, Figure 9, Figure 10). Therefore, we compare active KCS from many different plant species including *Zea mays* (ZmKCS), *Brassica napus* (BnKCS), *Setaria viridis* (SvKCS), *Capsella rubella* (CrKCS), *Vitis vinifera* (VvKCS), *Sorghum bicolor* (SbKCS), *Solanum lycopersicum* (SoKCS) and *Triticum aestivum* (TrKCS). Sequence homologies ranging from 66% to 98% for ZmKCS4, ZmKCS15, BnKCS31, SvKCS4, CrKCS4/9/17, VvKCS10, SbKCS18, SoKCS4, TrKCS4 with AtKCS from the α group (AtKCS4/9/17) have been demonstrated, with higher identity with AtKCS4 (Table 1). Upon heterologous expression of these KCS in the yeast strain TRIPLE $\Delta elo3$, predominantly KCS4-, KCS9-, and KCS17-like VLCFA profiles were observed.

The KCS4-like VLCFA profile characterized by a significant amount of C26, as evidenced by high C26/C24 ratios (around 3.5) and an C24+C26 VLCFA representing about 75% of the total (Figure 9), is shared among dicots, exemplified by SoKCS4 and CrKCS4, and monocots, represented by ZmKCS4, ZmKCS15, SbKCS18 and SvKCS4 (Figure 10). Similarly, AtKCS9 exhibits a comparable activity profile but with an accumulation of C24 and a value of C26/C24 around 0.2; this KCS9-like VLCFA profile is mirrored by CrKCS9 and BnKCS31. Conversely, expression of CrKCS17 shows no accumulation of C26, indicative of a KCS17-like VLCFA profile. Nevertheless, CrKCS17 seems to accumulate more C24 than AtKCS17, and globally, the fatty acid profiles obtained when expressing these enzymes in yeast are very close to those resulting from Arabidopsis KCS expression (Figure 10).

In contrast, TrKCS04 from wheat, a monocot specie, and VvKCS10 from grape, a dicot, do not exhibit the same activity profile as AtKCS4, 9, and 17 although they share a high degree of identity with AtKCS4 (75-82%). Indeed, expression of these two KCS proteins in the TRIPLE $\Delta elo3$ yeast strain revealed no accumulation of C24 and C26, but instead a significant accumulation of C20 VLCFAs (C20:0, C20:1), which is similar to the profile of AtKCS1 and 18 expressed in the TRIPLE strain (figure 11). A similar profile was obtained with similar SbKCS06 (Figure 11) although it grouped with AtKCS5 and AtKCS6 (clade γ) in our phylogenetic analysis (Figure 2).

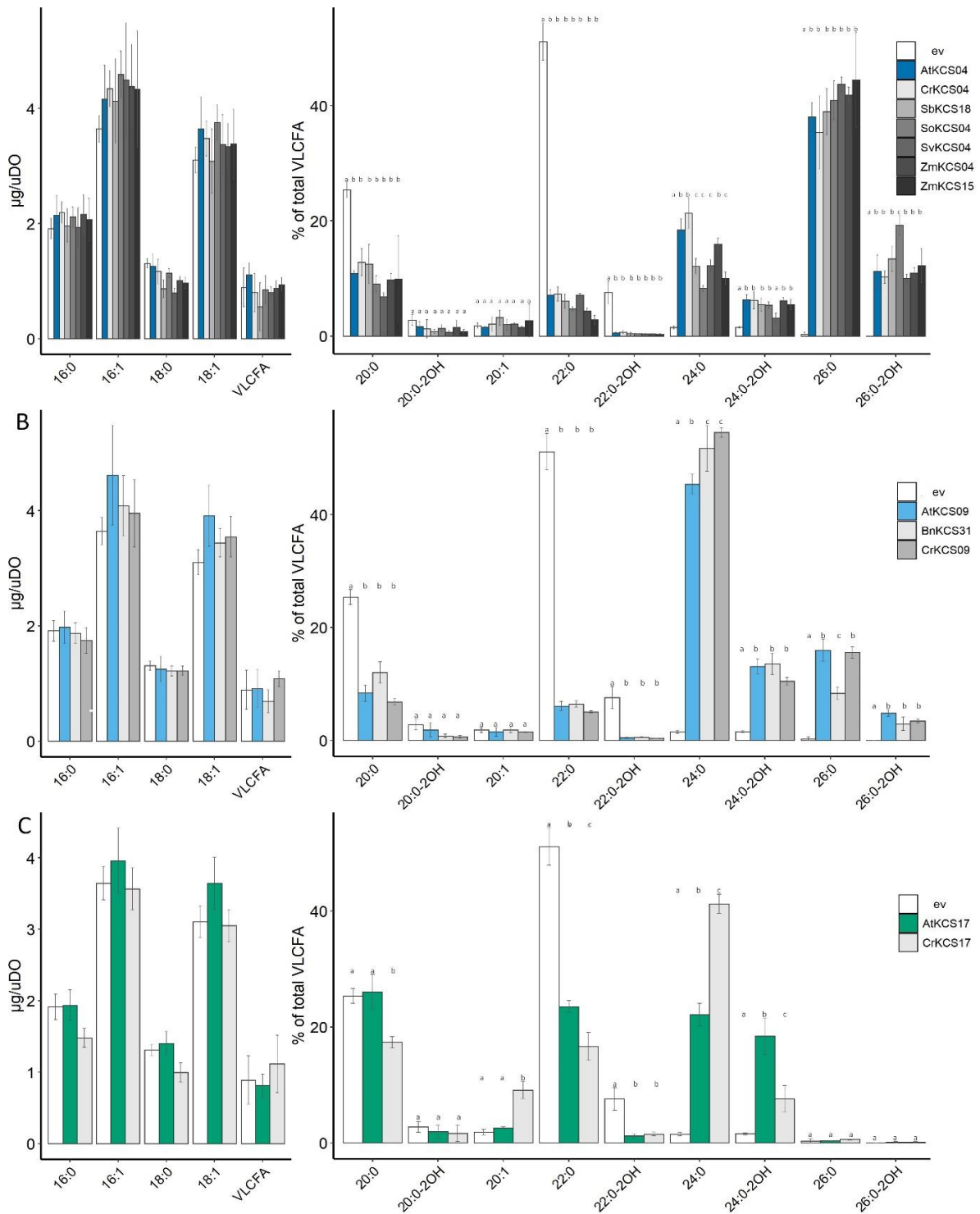


Figure 10. FAMES profiles obtained in the strain TRIPLE $\Delta elo3$ expressing either AtKCS4-like (A), AtKCS9-like (B), AtKCS17-like (C) genes in yeast compared to the strain transformed with an empty vector “ev”. Mean values ($\mu\text{g}/\text{uDO}$) are given with SD ($n=4$). Different letters indicate statistically significant differences ($P \leq 0.05$) determined with a Tukey post hoc test.

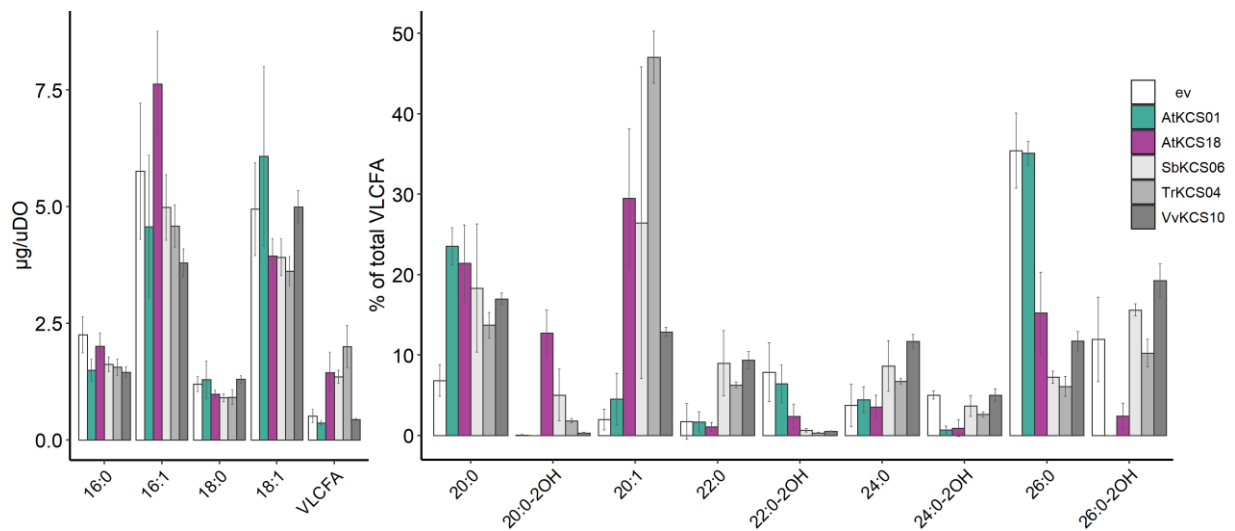


Figure 11. FAMES profiles obtained in the strain TRIPLE expressing AtKCS1, AtKCS18, SbKCS06, TrKCS04, VvKCS10 compared to the strain transformed with an empty vector “ev”. Mean values ($\mu\text{g}/\text{uDO}$) are given with SD ($n=4$).

Altogether these data show that within clade α , 3 KCS were not active in yeast (SiKCS4, OsKCS4 and BnKCS18), two had an activity more related to AtKCS01 and AtKCS18 (TrKCS4 and VvKCS10), but most of the KCS tested (9 in total: ZmKCS4, ZmKCS15, BnKCS31, SvKCS4, CrKCS4/9/17, SbKCS18, SoKCS4) resulted in a VLCFA profile very similar to those of AtKCS4/9/17. The most prevalent activity in the α group was KCS4-like activity, which is observed in both dicot and monocot species. Indeed, related KCS enzymes from *Solanum lycopersicum* and *Capsella rubella* for dicot plants and *Setaria viridis*, *Sorghum bicolor*, or *Zea mays* from monocots, demonstrate similar activity to AtKCS4, suggesting that enzyme function has mainly persisted across evolutionary plant speciation.

2.3.3. Comparative analysis of clade ζ / ι KCS activity

The TRIPLE $\Delta e/o3$ strain exhibited a decrease of C20 and an increase of C22 and C24 saturated acyl chain when AtKCS2 or AtKCS20 (which share 85% identity) were expressed (Figure 13). These results show that these enzymes are responsible for the elongation of C20 into C22 and C22 into C24 compounds. Therefore, the paralogs KCS2 and KCS20 share a common substrate specificity for C20 acyl chains (Batsale et al., 2023). The expression of KCS20 in the TRIPLE $\Delta e/o3$ strain led to even higher amounts of C24 compounds compared to KCS2 (Figure 12).

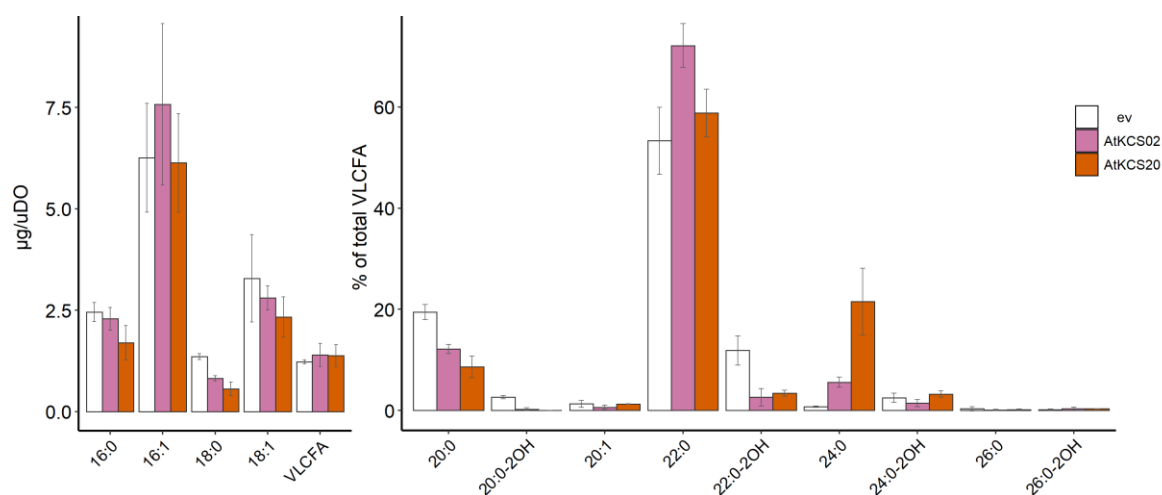


Figure 12. FAMES profiles obtained in the strain TRIPLE $\Delta e/o3$ expressing AtKCS2, AtKCS20 compared to the strain transformed with an empty vector "ev". Mean values ($\mu\text{g/uDO}$) are given with SD (n=4).

A phylogenetic analysis comparing these Arabidopsis KCS with enzymes from other plant species, including *Brassica napus*, *Vitis vinifera*, *Sorghum bicolor*, *Triticum aestivum*, and *Oryza sativa*, revealed sequence homologies ranging from 68% to 95% for BnKCS38, VvKCS5, SbKCS13, TrKCS20, TrKCS2, and OsKCS2 (66%) with AtKCS2 and AtKCS20 (Table 1).

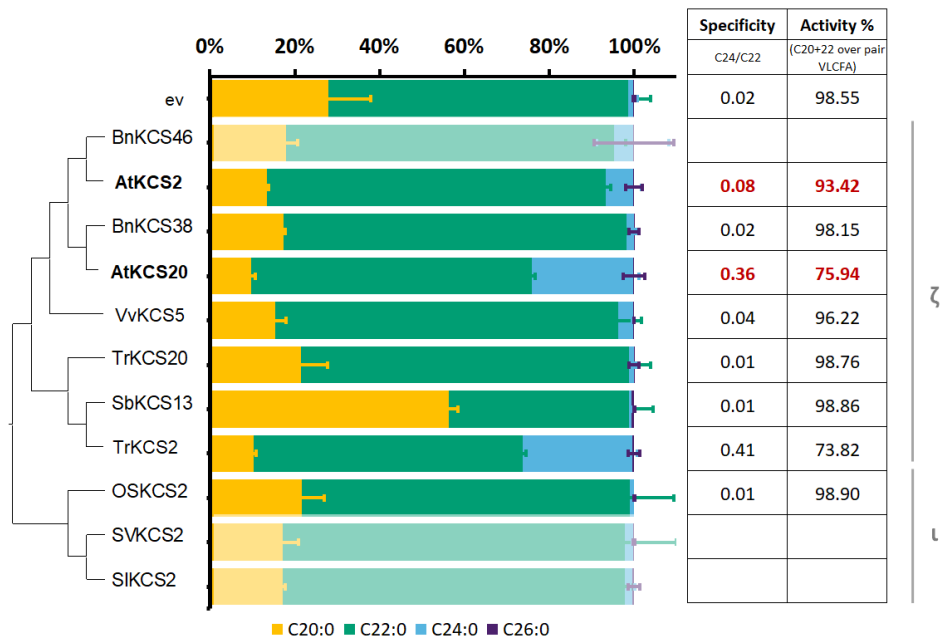


Figure 13. Substrate specificity of KCS from clade ζ / ι from different species. The barplot represents the relative distribution of quantified VLC species from TRIPLE $\Delta elo3$ transformed with the different KCS genes. Mean values (percentage of total VLCFA) are given with SD (n=4). “ev” stands for the TRIPLE $\Delta elo3$ strain transformed with the empty vector pVT-LEU. Right table shows for each construct the combined percentage of C20 and C22 VLCFA, which is indicative of the level of activity, and the ratio C24/C22, which is indicative of the substrate specificity.

The KCS2-like VLCFA profile characterized by a significant amount of C22, as evidenced by high C24/C22 ratios (around 0.05) and an C20+C22 VLCFA representing about 95% of the total, is shared among dicots, exemplified by BnKCS38 and VvKCS15, and monocots, represented by TrKCS20 (Figure 13). Similarly, AtKCS20 exhibits a comparable activity profile but with an accumulation of C24 and a value of C24/C22 around 0.35; this KCS20-like VLCFA profile is mirrored by TrKCS2 (Figure 14). Additionally, in TRIPLE $\Delta elo3$ the expression of OsKCS2 barely impacted the VLCFA distribution (Figure 14).

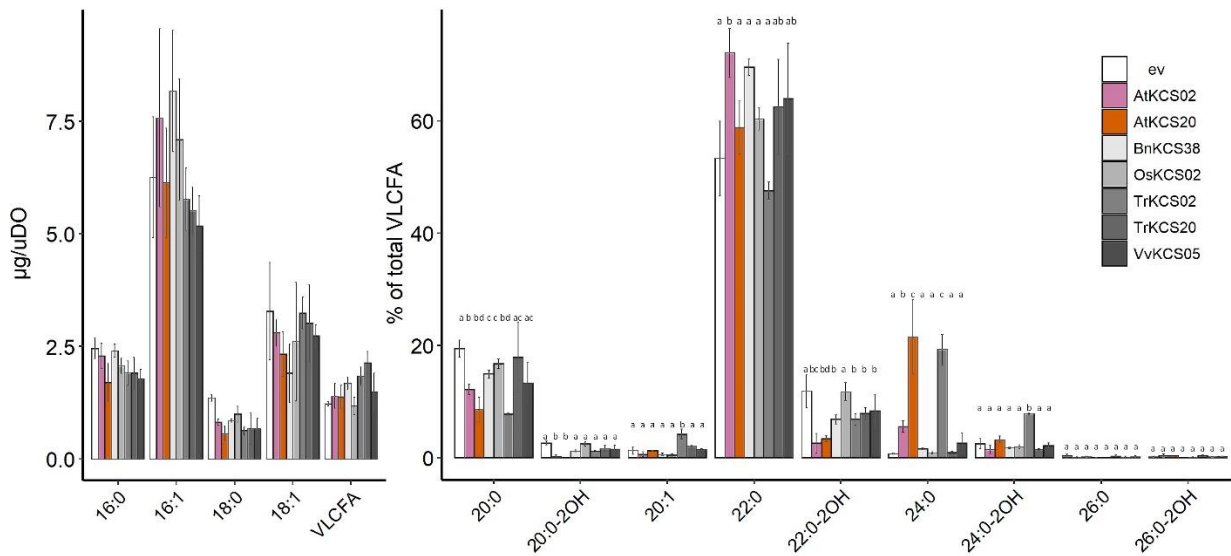


Figure 14. FAMES profiles obtained in the strain TRIPLE Δ elo3 expressing AtKCS2, AtKCS20, BnKCS38, OsKCS02, TrKCS02, TrKCS20, VvKCS05 compared to the strain transformed with an empty vector “ev”. Mean values ($\mu\text{g}/\text{uDO}$) are given with SD ($n=4$). Different letters indicate statistically significant differences ($P < 0.05$) determined with a Tukey post hoc test.

In the TRIPLE yeast strain, SbKCS13 displays a significant accumulation of C20:0 and C20:1, which aligns with the profile of AtKCS18 (Figure 15). Although the activity of OsKCS2 in the TRIPLE Δ elo3 strain was close to the control strain expressing empty vector (Figure 14), it shows a distinct activity in the TRIPLE strain, resulting in accumulation of C20, C22 and a high accumulation of C26:0 (Figure 15).

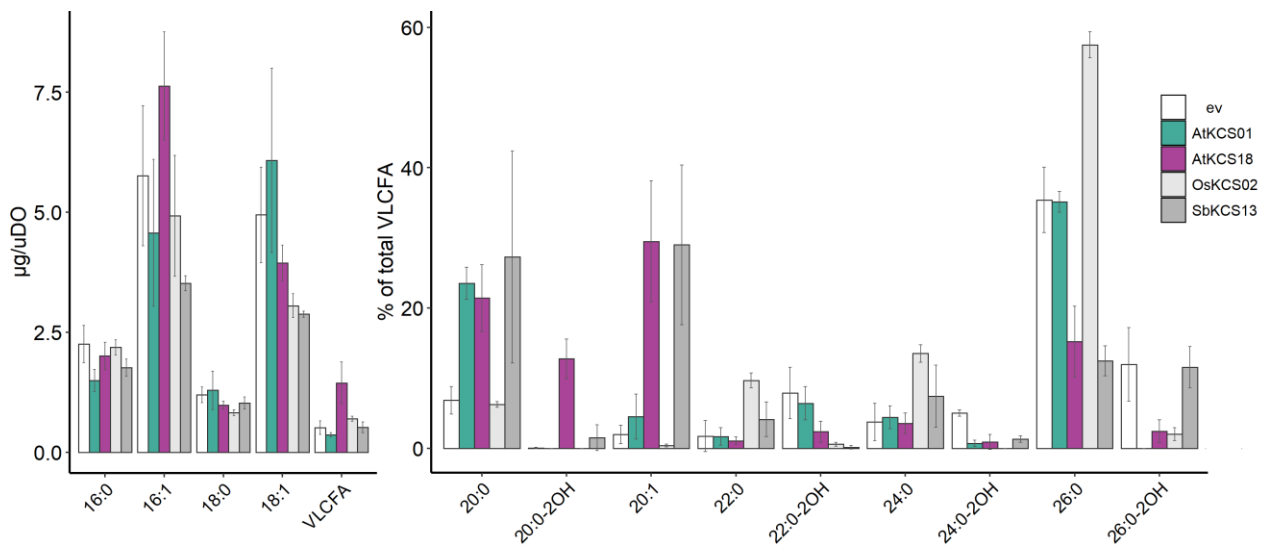


Figure 15. FAMES profiles obtained in the strain TRIPLE expressing AtKCS1, AtKCS18, OsKCS02, SbKCS13 compared to the strain transformed with an empty vector “ev”. Mean values ($\mu\text{g}/\text{uDO}$) are given with SD ($n=4$).

Altogether these results show that within clade ζ/ι, 3 KCS were not active in yeast (SiKCS2, SvKCS2 and BnKCS46). AtKCS2 and AtKCS20 activities were conserved in different species such as *Brassica napus*, *Vitis vinifera* and *Triticum aestivum* (BnKCS38, VvKCS5, TrKCS2 and TrKCS20). SbKCS13 showed an accumulation of C20, similarly to AtKCS18. Our phylogenetic analysis revealed that the monocot-specific ι subgroup shares a common ancestor with clade ζ. We can hypothesize that the activity of AtKCS2 and AtKCS20 has been conserved in monocot, with potential variations in activity among monocot species within the group ι. This perspective emphasizes the significance of further study on the functional roles and potential adaptations of KCS2- and KCS20-like activity, particularly within monocot species, which may offer valuable insights into their evolution.

2.4. Identification of putative specificity-determining residues through multisequence alignments of KCS4-,9-,17-like

Acknowledgments: As part of the Marguerite BATSALE thesis (2022), Florence BORDES, Isabelle ANDRE and Jérémy ESQUE from the Biotechnology Institute, Bio and Chemical Engineering in Toulouse performed in silico 3D modeling of AtKCS4 docked with C26:0 keto-acyl-CoA product.

Since the specific activities in KCS4-, KCS9- and KCS17-like have been demonstrated to be highly conserved across species, we investigate the possibility of identifying key residues involved in substrate specificity via multi-sequence proteins alignment. We used a panel of functionally related KCS enzymes from various plant species. Specifically, we analyzed six KCSs exhibiting AtKCS4-like activity (AtKCS4, CrKCS4, SoKCS4, ZmKCS4, ZMKCS15, SbKCS18, SvKCS4), three KCSs displaying AtKCS9-like activity (AtKCS9, CrKCS9, BnKCS31), and two KCSs displaying AtKCS17-like activity (AtKCS17, CrKCS17). We identified a single residue which is different between KCS4-like, KCS9-like, and KCS17-like proteins. At position 170 of the alignment presented in Figure 17, all KCS4-like have a methionine (M), all KCS9-like have a leucine (L) while all KCS17-like have an isoleucine (I) (yellow frame in Figure 16). Additionally, we observed 12 residues conserved between KCS4-like and KCS9-like proteins but not in KCS17-like proteins (green frames), seven residues conserved between KCS9-like and KCS17-like but absent in KCS4-like proteins (blue frames), and three residues conserved in KCS4-like and KCS17-like but not in KCS9-like proteins (pink frames).

When examining the 3D structure of AtKCS4 proteins with a ligand (3-keto-26:0, the product of 24:0 “elongation” by KCS), the amino acids differing between KCS4-like, KCS9-like, and KCS17-like proteins (represented in red in Figure 17A) appear randomly distributed and distant from the catalytic site, except for three amino acids: P111, V166, and M170 in AtKCS4 (red sticks in Figure 17B), which are positioned in close proximity to the ligand. These residues could therefore potentially modulate local hydrophobic and electrostatic properties, thereby affecting substrate access to the catalytic site. Interestingly, residues at positions 166 and 170 differ between enzymes with KCS4-like activity and those with KCS9/17-like activity. At position 166, the presence of valine (V) in enzymes with KCS4-like activity and leucine (L) in KCS9-,17-like is noted, valine being a smaller and more hydrophobic amino acid than leucine. At position 170, methionine (M) is present in KCS4, leucine (L) in KCS9, and isoleucine (I) in KCS17. These three related amino acids are large and non-polar, but the sulfur group of methionine may increase polarity, hydrophilicity compared with leucine and isoleucine. Based on these observations, it can be inferred that the presence of small amino acids at position 166 and a hydrophobic residue at position 170 may contribute to the accumulation of longer saturated products, as observed in KCS4- and KCS9-like activity (red arrows in Figure 16).

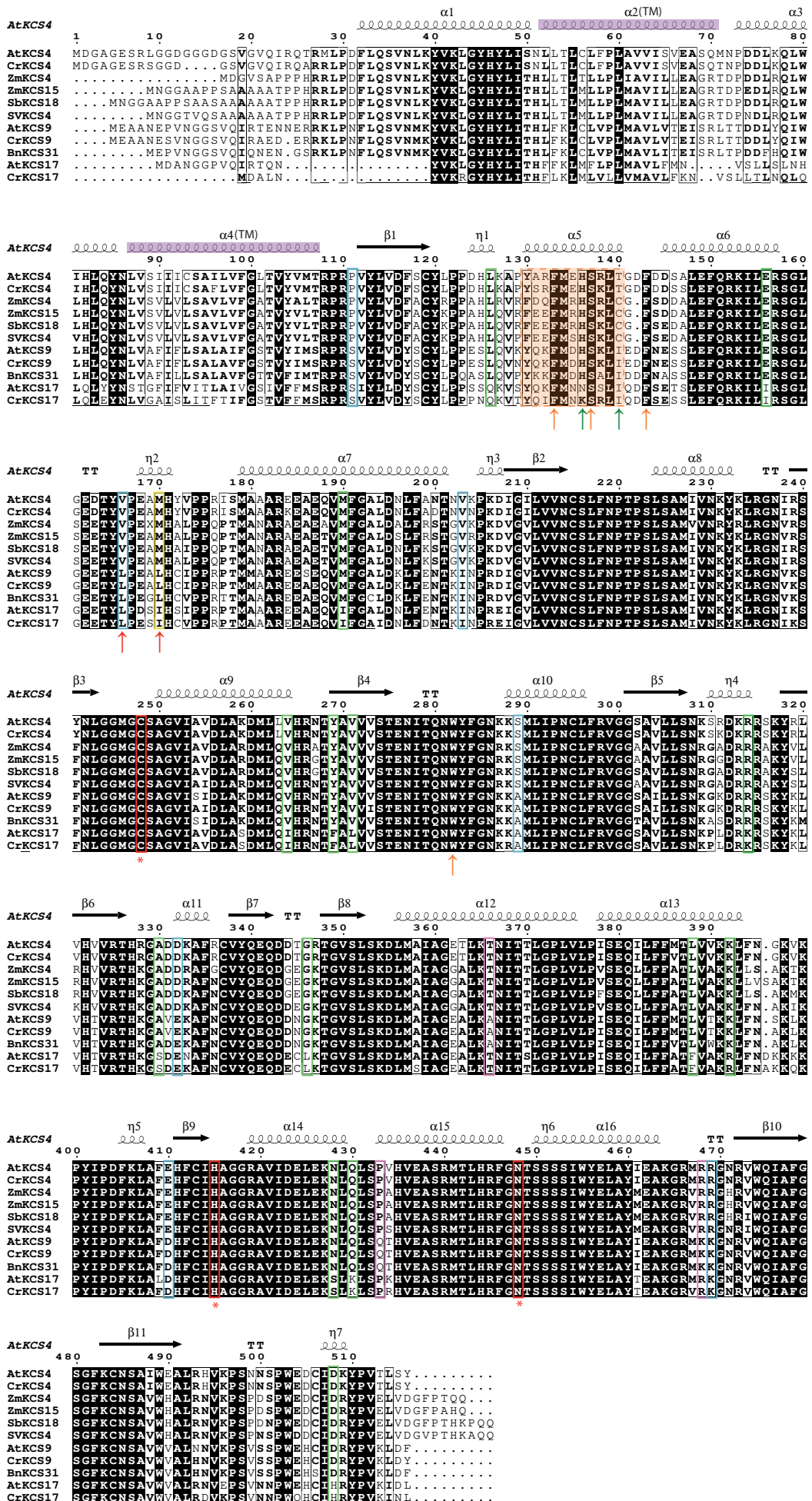


Figure 16. Identification of residues specifically conserved in KCS4-, KCS9- and KCS17-like. Sequence alignments between AtKCS4, AtKCS9, ATKCS17 other plant KCS displaying KCS4-, KCS9- or KCS17-like substrate specificities. Identical residues are included in the shaded box. The two transmembrane domains TMD1 and TMD2 are highlighted in purple. The catalytic triad are framed in red and indicated with *. α -helices and π -helices are displayed as medium and large squiggles, respectively. β -strands are rendered as arrows, strict β -turns as β -turns and strict α -turns as TTT letters according to the nomenclature given by Espritt 3.0. Residues conserved between KCS4-like and KCS9-like proteins but not in KCS17-like proteins (green frames), residues conserved between KCS9-like and KCS17-like but absent in KCS4-like proteins (blue frames), and residues conserved in KCS4-like and KCS17-like but not in KCS9-like proteins (pink frames)

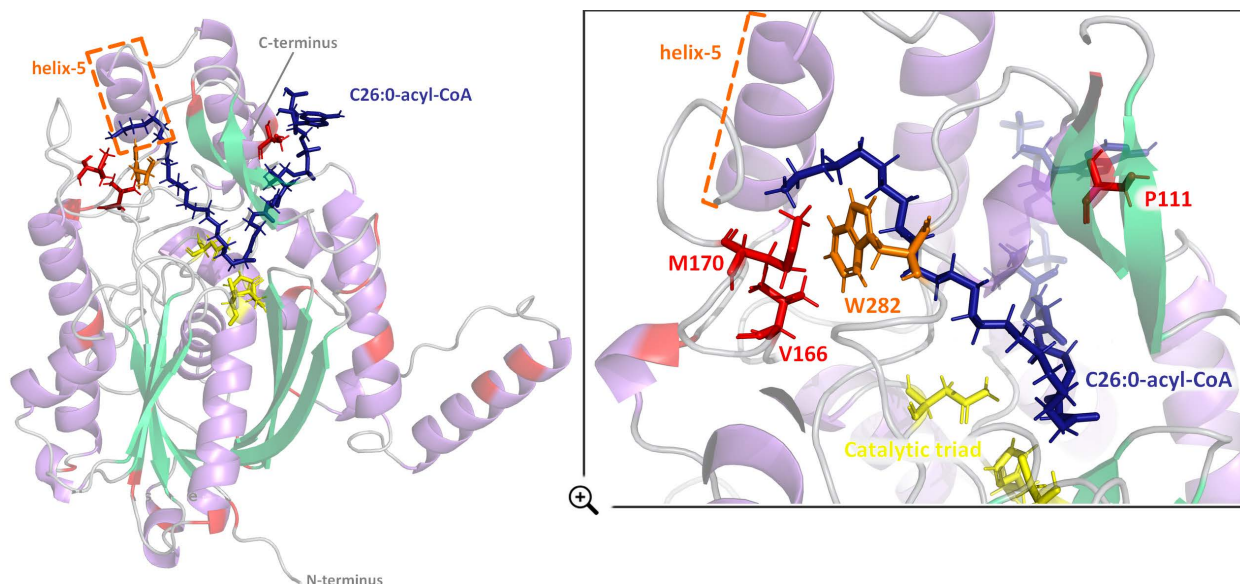


Figure 17. Homology model of the chain A of AtKCS4 docked with C26:0 keto-acyl-product (dark blue) with the catalytic triad shown as yellow sticks and candidate residues identified in Figure 16 are colored in red. Helix-5 is highlighted by an orange dotted line and W282 is represented in orange sticks. Visualization in pyMOL. Red sticks represent 3 residues close to active site.

Very recently, Chen et al. (2022) investigated several KCS candidate isoforms from *Populus trichocarpa* (PtKCS1, PtKCS2 and PtKCS4) sharing different degrees of homology (from 74% to 99%) in order to identify molecular determinants underlying divergent substrate specificities. Both site-directed and domain swap mutants highlighted the essential role of helix-4 in determining PtKCS1, PtKCS2 and PtKCS4 substrate preferences for monounsaturated or saturated VLCFA in yeast. Their results suggest notably that the helix-4 could partially contribute to the recognition of unsaturation motifs in PtKCS1. The corresponding helix in AtKCS4, helix-5, demonstrates a high degree of proximity with its associated ligand (framed in orange, Figure 16, Figure 17). This region of interest exhibits five amino acids that are localized close to the ligand (not shown). Among these residues, F133, S137, and F144 are consistently conserved across all KCSs (orange arrows in Figure 16). At position 136, histidine (H) is observed in KCS4- and KCS9-like enzymes, while asparagine (N) or lysine (K) are present in KCS17-like enzymes, and histidine is more hydrophobic than asparagine or lysine. In addition, in KCS4-like enzymes, threonine (T) and cysteine (C) are found at position 140, while isoleucine (I) is present in KCS9- and KCS17-like enzymes. Importantly, threonine and cysteine are smaller amino acids compared to isoleucine. Based on these observations, it can be inferred that the presence of small amino acids at position 140 and a hydrophobic residue at position 136 may contribute to the accumulation of longer saturated products, as observed in KCS4- and KCS9-like activity (green arrows Figure 16).

Chen et al. (2022) also demonstrated that PtKCS substrate specificity determinants are not restricted to the helix-4. In PtKCS1 and PtKCS4, the length of the substrate specificity-driving amino acid outside the α -helix-4 affects the ability of the enzyme to elongate substrates with longer chain. The

substitution of W277 in PtKCS1 and R283 PtKCS4 by smaller amino acids led to an accumulation of both longer saturated and monounsaturated products. The corresponding residue W282 in AtKCS4 do not vary between KCS from α group (orange arrows in Figure 16, orange sticks in Figure 17).

Structural and sequence comparisons of KCS4-like, KCS9-, KCS17-like activity leads us to highlight potential key residues determining the KCS substrate specificity. We identified four potential residues, H136, T140, V166, M170, that are localized close to the end of the acyl-chain and that could potentially modulate local hydrophobic and electrostatic properties, thereby affecting substrate access to the catalytic site.

3. Conclusion

According to the study of Arabidopsis KCS, it was found that the enzyme activities are well conserved within the phylogenetic groups defined by Joubès et al. (2008) (Batsale et al., 2023). It was expected that this would also apply to KCS from other plant species belonging to these clades. Our analyses highlighted both conserved and divergent activity across KCS enzymes from different species.

Despite the significant number of KCS proteins in clade ζ , the enzymatic activity of AtKCS2 and AtKCS20 has been found to be conserved across various dicot and monocot species, including one KCS from *Brassica napus*, one from *Vitis vinifera* and two from *Triticum aestivum*. However, divergent activity has also been observed for *Oryza sativa* and *Sorghum bicolor* KCSs. The OsKCS02 protein showed an accumulation of C26 accumulation in the TRIPLE strain. Our phylogenetic analysis revealed that the monocot-specific ι subgroup shares a recent common ancestor with the subgroup ζ . Although we did not observe any activity similar to KCS2 and KCS20 in the clade, we can hypothesize that the activity of AtKCS2 and AtKCS20 has been conserved in monocot species within the group ι , with potential variations in activity among these species. This finding highlights the need for further research on the conservation and potential divergence of KCS2- and KCS20-like activity, particularly within monocot species, which may provide valuable insights into their evolution and functional requirements involved in plant lipid metabolism.

The α subgroup has demonstrated the most significant conservation of elongase activity. Within this group, KCS4, 9, and 17 from *Arabidopsis thaliana* have homologous activities in dicot species such as *Capsella rubella* and *Brassica napus*. These enzymes exhibit high sequence proximity to their Arabidopsis homologs and have activities very close to those of AtKCS4, 9, or 17. Additionally, KCS4-like activity, observed in both dicot and monocot species is the most prevalent activity in the α group. KCS enzymes from dicot plants such as *Solanum lycopersicum* and monocot plants including *Setaria*

viridis, *Sorghum bicolor*, or *Zea mays* exhibit similar activity to AtKCS4. This uniformity is attributed to the fact that these KCS enzymes share a more recent common ancestor with KCS4, than with KCS9 or KCS17. Moreover, sequence comparisons of enzymes with KCS4, KCS9-, and KCS17-like activities and structural analysis of AtKCS4 allows us to highlight four potential key residues that determine the specific activity of KCS. We assumed that a modification of these amino acid's combination could change the structural conformation of the protein and affect the access of substrate to the catalytic site, leading to change of activity between KCS4, KCS9- or KCS17-like enzymes. Further investigation through site-directed and domain swap mutants could validate these hypotheses. However, it should be noted that α group KCS enzymes exhibit consistent KCS4-like activity across various plant species, with the exception of KCS from *Vitis vinifera* and *Triticum aestivum*. These KCSs, which display different activities than AtKCS4, 9 or 17, show accumulation of C20, similar to AtKCS18 in the TRIPLE strain. Thus, several KCS have activities that diverge from their respective subgroup, α , ζ or γ . We observed a recurrence of AtKCS18 activity across different clades and species, with two KCS from sorghum (SbKCS13 and SbKCS6), VvKC10 from grapevine and TrKCS4 from wheat that showed an accumulation of C20, and in particular C20:1, which is characteristic of the activity of AtKCS18. Although no monocot or grapevine species are present in the clade β with AtKCS18, over the evolution this elongation activity is present in many plant species belonging to other clades, maybe due to convergent evolution.

**CHAPTER 2 - MECHANISTIC
UNDERSTANDING OF HERBICIDE
MOLECULAR TARGET AND
PLANTS SELECTIVITY *IN VIVO***

Chapter 2 - Mechanistic understanding of herbicide molecular target and plants selectivity *in vivo*

The Herbicide Resistance Action Committee (HRAC) categorizes herbicides into various groups based on their target sites, modes of action, similarities in induced symptoms, or chemical classes. HRAC group K3 and N herbicides, including well-known examples reported in Table 1, were grouped together as HRAC group 15 based on their similar morphological symptoms. HRAC classifies K3 herbicides as inhibitors of cell division or inhibitors of VLCFA synthesis, while N herbicides are described as inhibitors of lipid synthesis. Both K3 and N herbicides inhibit VLCFA biosynthesis in plant and algal cells (Böger et al., 2000).

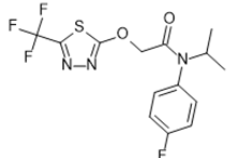
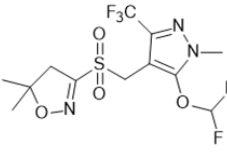
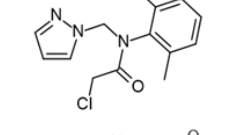
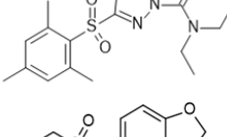
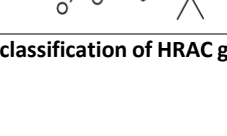
Compound	Structure	Chemical classification	HRAC	Legacy global HRAC
Flufenacet		α -Oxyacetamides	15	K3
Pyroxasulfone		Isoxazolines	15	K3
Metazachlor		α -Chloroacetamides	15	K3
Cafenstrole		Azoly-carboxamides	15	K3
Benfuresate		Benzofurans	15	K3/N

Table 1. Structures and classification of HRAC group 15 herbicides tested as VLCFAE inhibitors in plant elongase-expressing yeast strains.

Recently, the enzymes responsible for VLCFA elongation in *Arabidopsis thaliana* were identified as the targets of these classes of herbicides. The activities of AtKCS enzymes, AtKCS5/CER60, AtKCS6/CER6, AtKCS1, AtKCS2, AtKCS20, and AtKCS18/FAE1, were strongly inhibited by metazachlor, flufenacet, and cafenstrole at different concentrations (Böger et al., 2003; Trenkamp et al., 2004; Tresch et al., 2012), as resumed in Table 2. No significant inhibition of *Arabidopsis* FAE activity in yeast was observed with benfuresate herbicide. *Arabidopsis* plants treated with these herbicides exhibit fusion of the aerial

organs, known as fiddlehead phenotype, which is associated with an inhibition of VLCFA synthesis (Letchelt-Kunze et al., 2003; Trenkamp et al., 2004).

Leaves from maize, barley and cucumber plants treated with metazachlor show a decrease in saturated C20, C22, C24 fatty acid amounts (Matthes et al., 1998). Regarding pyroxasulfone, research conducted by Tanetani et al. (2011b) demonstrated that the activities of AtKCS18/FAE1 and Q6F365, a rice FAE, were inhibited differently by pyroxasulfone. AtKCS18/FAE1 was found to be irreversibly inhibited, while rice FAE was reversibly inhibited by pyroxasulfone. Furthermore, the selectivity of pyroxasulfone inhibition was studied in two monocotyledonous plants, revealing opposite response with wheat appearing as a tolerant crop, while rigid ryegrass weed was susceptible plant (Tanetani et al., 2013a).

Inhibition	Concentration	AtKCS1	AtKCS2	AtKCS5	AtKCS6	AtKCS17	AtKCS18	AtKCS20	References
Flufenacet	100µM	100%	100%	100%			100%	100%	Trenkamp et al., 2004
Pyroxasulfone	10µM						100%		Tanetani et al., 2011b
Metazachlor	100µM	93%	82%	100%	100%	100%	95%	97%	Tresch et al., 2012
	1µM						83%		Böger et al., 2003
Cafenstrole	100µM	100%	100%	100%			100%	100%	Trenkamp et al., 2004
	0.1µM						100%		Böger et al., 2003
Benfuresate	100µM	0%	0%	0%			0%	0%	Trenkamp 2004

Table 2. Herbicides tested as VLCFAE inhibitors in plant elongase-expressing yeast strains from data in the literature. Inhibition as indicated as the percentage inhibition.

Thus, very few studies have investigated whether there is any selectivity in the inhibition of VLCFA synthesis by herbicides between different plants. For instance, it is unclear whether there are differences in the inhibition between plants of agronomic importance and weeds, or between monocotyledonous and dicotyledonous plants. Since, as shown in the first chapter, KCS from a range of plant species, including both monocotyledonous and dicotyledonous plants, were found to be active in the yeast, this heterologous system allowed us to gain a more comprehensive understanding on this subject. First, five herbicides (benfuresate, cafenstrole, flufenacet, metazachlor, pyroxasulfone) from different subgroups of HRAC group 15 were selected for assays of inhibition against FAE expressed in yeast. Second, recently developed herbicides from Bayer were studied to understand their molecular target.

In this project we aimed to identify and validate the inhibitory activity of various herbicides commercially available and under development, to better understand their potential mechanism of specificity.

1. Studies on the mechanism of action of group 15 herbicides

1.1. Influence of K3 herbicides on endogenous VLCFA biosynthesis and yeast growth

First, the influence of herbicide on the endogenous fatty acid composition of untransformed yeast strains was investigated. The five herbicides were applied to the wild-type yeast strain, InvSc1, and the strains we developed, TRIPLE and TRIPLE $\Delta elo3$ (TPE), at a final concentration of 10 μM . The FAMES of the individual samples were extracted and analyzed using GC-MS. Our results indicate that the proportions of VLCFAs in the different strains did not change when herbicides were added (Figure 1), demonstrating that the activities of endogenous yeast ELO elongases were not affected by the herbicides.

Furthermore, the results obtained in TRIPLE and TPE showed that the activities of the Arabidopsis last three enzymes of the FAE complex (KCR, HCD and ECR) are not targets of the different inhibitors used in this assay.

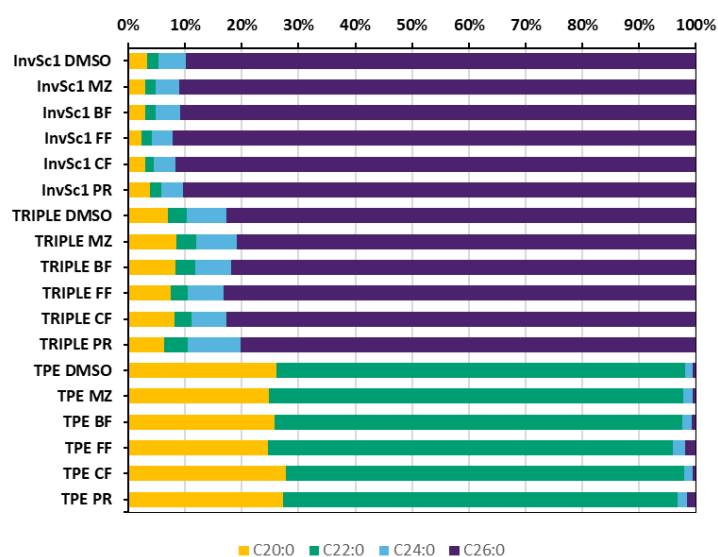


Figure 1. Influence of herbicides on endogenous VLCFA. FAMES profiles of InvSc1, TRIPLE and TRIPLE $\Delta elo3$ (TPE) collections treated with different herbicides (10 μM). Values are the average of five replicates. "DMSO" corresponds to the negative control treatment. MZ : metazachlor, FF : flufenacet, CF : cafenstrole, BF : benfuresate, PR : pyroxasylfone

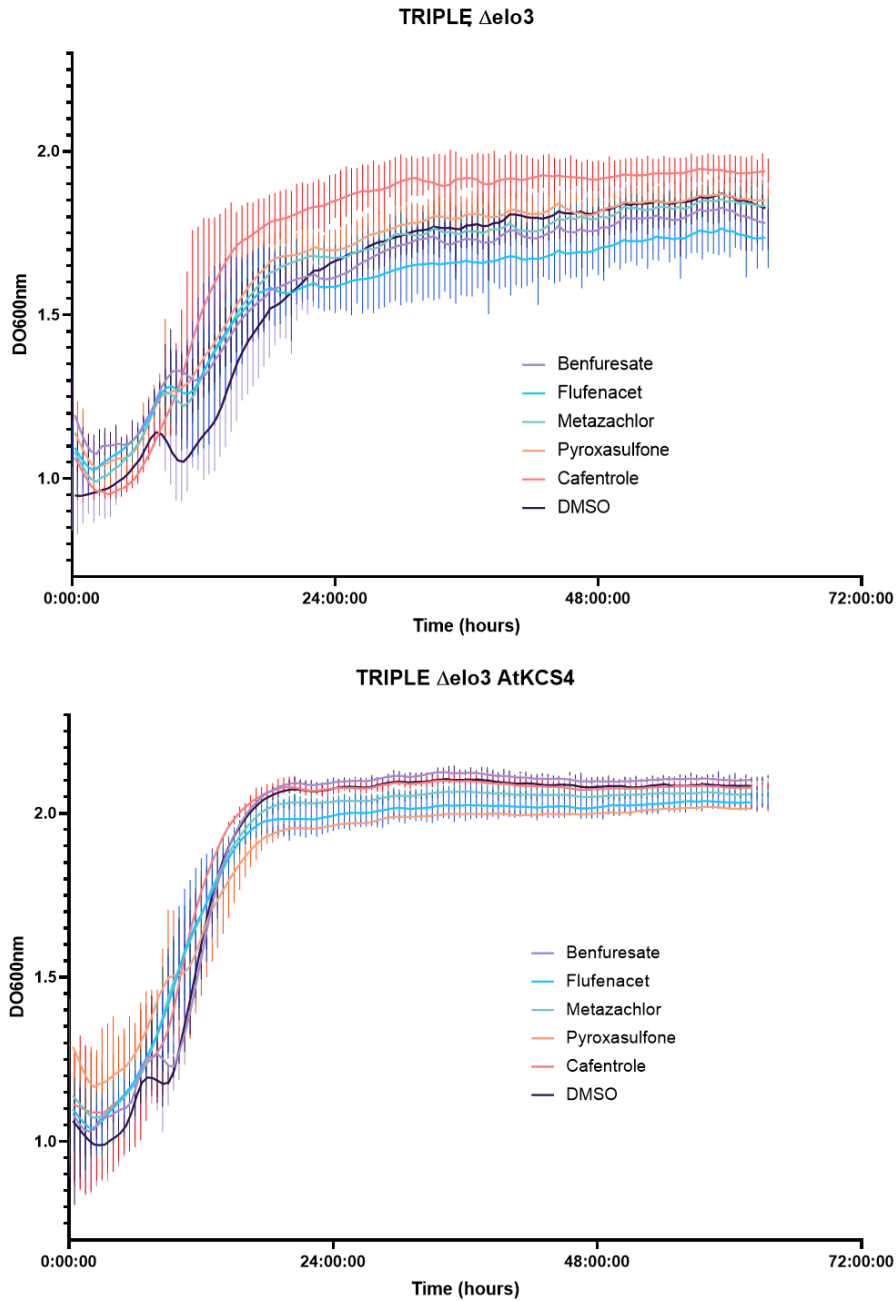


Figure 2. Growth analysis of TRIPLE $\Delta elo3$ and TRIPLE $\Delta elo3$ expressing AtKCS4 strains. Values are the average of 4 samples.

Second, to investigate whether incubation of the yeast cells with the inhibitors has an influence on the growth of the cells, the optical density of the transformed TRIPLE $\Delta elo3$ with empty vector (ev) or AtKCS4 were examined after the addition of inhibitors. The growth of yeast cells was not disturbed or inhibited by the addition of the inhibitors (Figure 2).

1.2. Influence of HRAC group 15 herbicides on elongases expressed in yeast

1.2.1. KCSs from *Arabidopsis thaliana*

To investigate the mode of action of five herbicides from HRAC class 15, benfuresate, flufenacet, cafenstrole, metazachlor, pyroxafulsone, the transgenic *S. cerevisiae* strains expressing different AtKCS and empty vector as control were incubated in their presence. The herbicides were added at final concentrations of 1 μ M and 10 μ M. After 72h of incubation, the FAMES of the individual samples were extracted and analyzed using GC/MS.

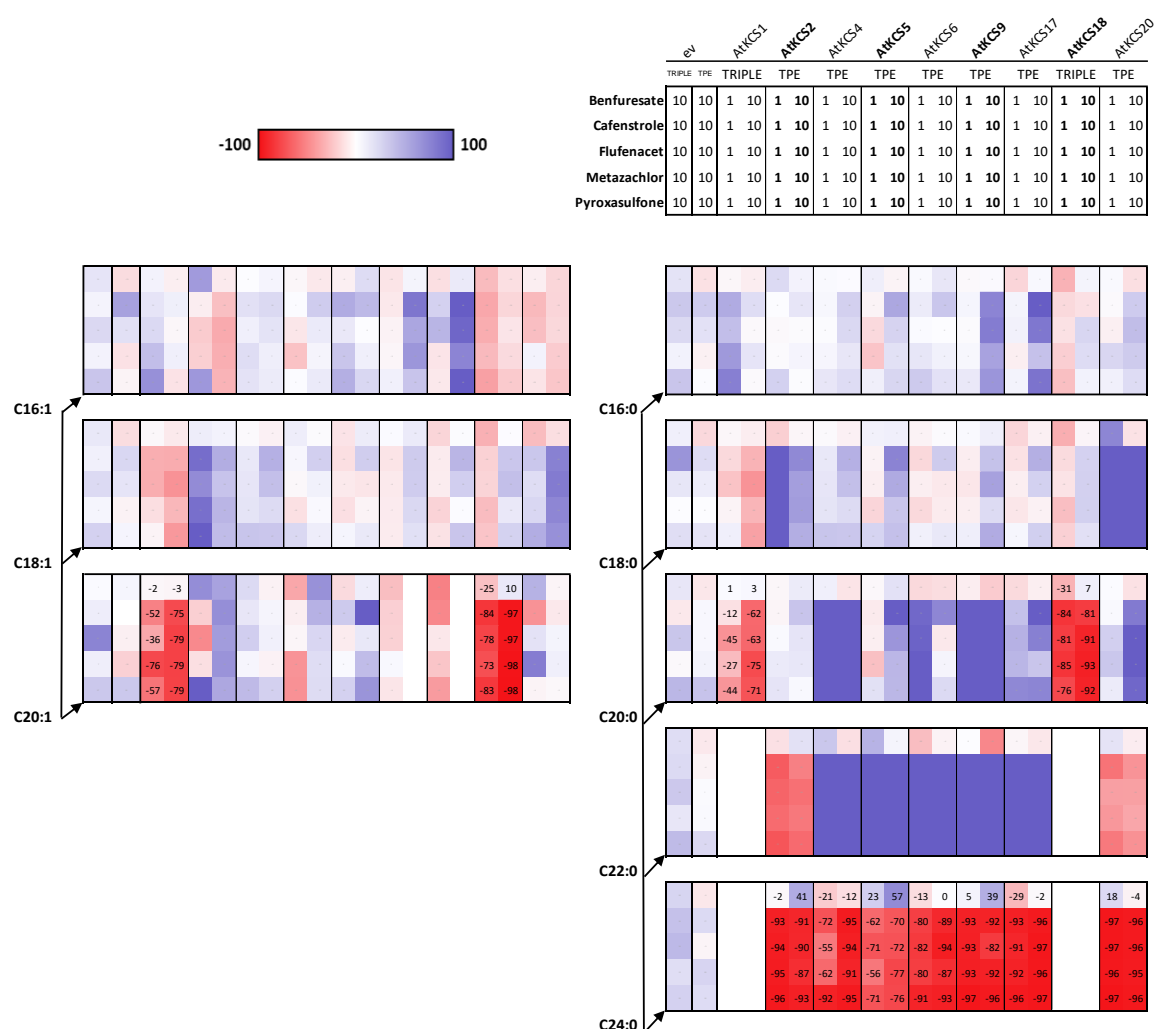


Figure 3. Inhibition of KCS activity by benfuresate, flufenacet, cafenstrole, metazachlor, pyroxasulfone (1 or 10 μ M) demonstrated in *S. cerevisiae* cells which expressed KCS proteins from *Arabidopsis thaliana*. Elongation ratio were calculated as the percentage of detected VLCFA products synthesized by a given KCS in comparison to control treated (DMSO). Genetic backgrounds are annotated as TRIPLE or TPE (TRIPLE Δ elo3). Numerical values used for visualization and respective standard errors are from at least three biological replicates.

Our findings indicate that fatty acids displayed not significant changes when benfuresate was added (Figure 3), demonstrating that this herbicide does not inhibit AtKCS activity tested here, as previously reported by Trenkamp et al (2004). In the case of the other four tested herbicides, decrease of very long-chain fatty acids were observed (bright red, negatives values) (Figure 3).

In yeasts expressing AtKCS4, AtKCS5, AtKCS6, AtKCS9, and AtKCS17 treated with cafenstrole, flufenacet, metazachlor and pyroxasulfone (10 μ M), the accumulation of saturated 24:0 was strongly decreased, around 90%, whereas C22:0 highly accumulated. Fatty acids with less than 20 carbon atoms showed only minor changes, as exemplified in Figure 4 with AtKCS4. These results indicate that the activities of KCSs responsible for the elongation of C22:0 to C24:0 are all inhibited. At 10 μ M concentration of flufenacet, cafenstrole, metazachlor and pyroxasulfone, AtKCS5 expressed yeast exhibits low VLCFA reduction compared to other strains, with inhibition percentages ranging from 56% to 76% for AtKCS5 and 89% to 93% for AtKCS6. A similar low level of inhibition was observed for AtKCS5/CER60 expressed yeast with triallate herbicide (100 μ M) in Trenkamp et al. (2004), therefore AtKCS5 seems less sensitive to inhibitor than the other AtKCS. Regarding AtKCS2 and AtKCS20, which are responsible for the elongation of C20:0 into C22:0 and C24:0, we observed that C20:0 and C22:0 amounts were decreased by the four herbicides, flufenacet, cafenstrole, metazachlor and pyroxasulfone. AtKCS2 and AtKCS20 showed similar percentages of inhibition, approximatively 90%, between treatments with 1 and 10 μ M of herbicides (flufenacet, cafenstrole, metazachlor and pyroxasulfone) (Figure 3).

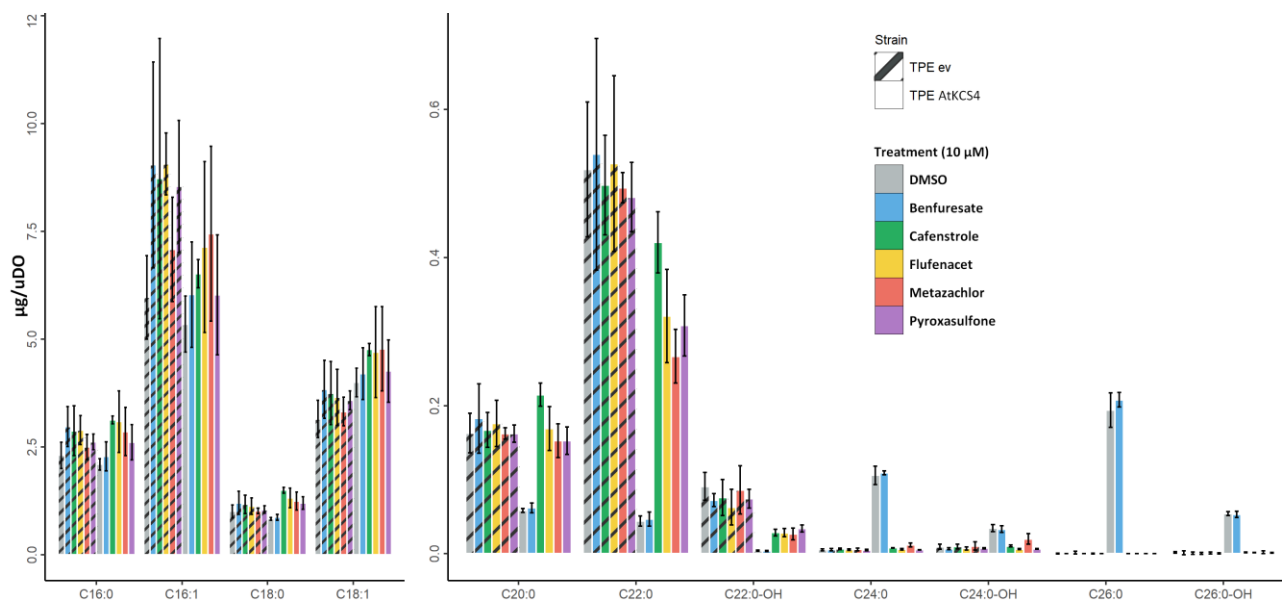


Figure 4. FAMES profiles of the AtKCS4 in TRIPLE Δ elo3 strain treated with different herbicides (10 μ M). Quantification based on the internal standard C17:0 (20 μ g/mL). Values are the average of five replicates. “EV” corresponds to the negative control strain containing the empty vector and “DMSO” corresponds to the negative control treatment.

Finally, the addition of flufenacet, cafenstrole, metazachlor or pyroxasulfone induced a reduction in the saturated and monosaturated C20 amounts in yeasts expressing AtKCS1 and AtKCS18, although AtKCS1 exhibited lower diminution of C20:1 and C20:0 content. As example, the C20:0 amount was reduced by 27% in AtKCS1 and 85% in AtKCS18 with metazachlor, corresponding to the result obtained in Böger et al. (2003) (Table 2). These results indicate that the activity of AtKCS18 is more inhibited than the activity of AtKCS1.

Therefore, we confirmed that the activities of AtKCSs responsible for VLCFA elongation were inhibited by flufenacet, cafenstrole, metazachlor and pyroxasulfone. Few studies have explored the effects of VLCFA synthesis inhibitors on plant species other than *Arabidopsis* (Tanetani et al., 2011b; Chen et al., 2022). Notably, Tanetani et al. (2011b) observed differences in inhibition of AtKCS18/FAE1 and a rice VLCFAE by pyroxasufone, suggesting that this herbicide may have different modes of action. In the next section, we aim to investigate whether these compounds inhibit KCS from different species from the same phylogenetic groups: KCS4/9/17-like (α), CER6-like (γ) or KCS2/20-like (ζ). Using KCSs from algae, dicots and monocots, we aimed to explore the mode of action of the herbicides and investigate the potential selectivity of these compounds.

1.2.2. KCSs from several plant species

To determine the effect of the five herbicides, benfuresate, cafenstrole, flufenacet, metazachlor and pyroxasulfone, on KCSs from different plant species, yeast strains expressing active KCSs were incubated in the presence of inhibitor at concentration of 10 μ M. Elongation ratio were calculated as the percentage of variation of the accumulation of detected VLCFA products synthesized by a given KCS, compared to control treatment (DMSO) and compared to other AtKCS from their respective clade. Our results indicate that the amounts of fatty acids only displayed slight changes with benfuresate, demonstrating that this herbicide does not inhibit any KCS enzyme activities tested here (Table 3, Table 4, Table 5, Table 6), it could inhibit KCS10/FDH.

The amounts of VLCFA synthesized by α clade KCSs (KCS4/9/17-like) are significantly reduced by metazachlor, flufenacet, cafenstrole, and pyroxasulfone, ranging from 70% to 99%, indicating a high level of inhibition. With the exception of two enzymes, where the inhibition is below 60%, all other KCSs were strongly inhibited. SolyKCS4 (*Solanum lycopersicum* KCS) was inhibited at 39% by flufenacet and SbKCS18 (*Sorghum bicolor* KCS) was inhibited at 55% by metazachlor (Table 3).

Gene	Genetic background	VLCFA	% Inhibiton				
			Benfuresate	Cafenstrole	Flufenacet	Metazachlor	Pyroxasulfone
			10 μ M	10 μ M	10 μ M	10 μ M	10 μ M
AtKCS4	TRIPLE Δ elo3	C24:0	-12	-95	-94	-91	-95
SvKCS4	TRIPLE Δ elo3	C24:0	1	-90	-90	-86	-93
ZmKCS4	TRIPLE Δ elo3	C24:0	7	-92	-94	-89	-72
ZmKCS15	TRIPLE Δ elo3	C24:0	-5	-86	-92	-83	-88
CrKCS4	TRIPLE Δ elo3	C24:0	-8	-95	-95	-92	-96
SbKCS18	TRIPLE Δ elo3	C24:0	-26	-89	-91	-55	-93
SoKCS4	TRIPLE Δ elo3	C24:0	-10	-83	-39	-71	-91
AtKCS9	TRIPLE Δ elo3	C24:0	39	-92	-82	-92	-96
BnKCS31	TRIPLE Δ elo3	C24:0	5	-96	-97	-97	-97
CrKCS9	TRIPLE Δ elo3	C24:0	8	-96	-98	-96	-99
AtKCS17	TRIPLE Δ elo3	C24:0	-2	-96	-97	-96	-97
CrKCS17	TRIPLE Δ elo3	C24:0	-1	-98	-98	-97	-98
TrKCS4	TRIPLE Δ elo3	C20:0	-4	-97	-96	-76	-97
VvKCS10	TRIPLE	C20:0	-29	-82	-80	-81	-92

Table 3. Inhibition of KCS activity by benfuresate, flufenacet, cafenstrole, metazachlor, pyroxasulfone (1 or 10 μ M) demonstrated in *S. cerevisiae* cells which expressed KCS proteins from alpha group. Elongation ratio were calculated as percent inhibition of detected VLCFA products synthesized by a given KCS in comparison to control treated (DMSO) *S. cerevisiae* cells. Numerical values used for visualization are calculated from at least three biological replicates.

For the KCSs from the ζ clade (KCS2/20-like), the levels of 24:0 were strongly decreased by metazachlor, flufenacet, cafenstrole, and pyroxasulfone for all tested yeasts expressing KCSs. Therefore, the KCSs from the ζ clade are inhibited by these herbicides, except BnKCS38 which exhibits partial inhibition (Table 4). KCSs from the γ group (AtKCS6-like) were also strongly inhibited by this set of herbicides (Table 5).

Gene	Genetic background	VLCFA	% Inhibiton (μ M)				
			Benfuresate	Cafenstrole	Flufenacet	Metazachlor	Pyroxasulfone
			10 μ M	10 μ M	10 μ M	10 μ M	10 μ M
AtKCS2	TRIPLE Δ elo3	C24:0	41	-91	-90	-87	-93
AtKCS20	TRIPLE Δ elo3	C24:0	-4	-96	-96	-95	-96
TrKCS20	TRIPLE Δ elo3	C24:0	-3	-81	-89	-90	-79
TrKCS02	TRIPLE Δ elo3	C24:0	-14	-97	-98	-98	-98
BnKCS38	TRIPLE Δ elo3	C24:0	-19	-53	-59	-55	-62
ViKCS5	TRIPLE	C24:0	52	-63	-77	-71	-68
OsKCS2	TRIPLE	C24:0	-12	-90	-85	-89	-89

Table 4. Inhibition of KCS activity by benfuresate, flufenacet, cafenstrole, metazachlor, pyroxasulfone (1, 10 μ M) demonstrated in *S. cerevisiae* cells which expressed KCS proteins from ζ group. Elongation ratio were calculated as percent inhibition of detected VLCFA products synthesized by a given KCS in comparison to control treated (DMSO) *S. cerevisiae* cells. Numerical values used for visualization are calculated from at least three biological replicates.

Gene	Genetic background	VLCFA	% Inhibitor (μM)				
			Benfuresate	Cafenstrole	Flufenacet	Metazachlor	Pyroxasulfone
			10 μM	10 μM	10 μM	10 μM	10 μM
AtKCS5	TRIPLE Δelo3	C24:0	57	-70	-72	-56	-76
AtKCS6	TRIPLE Δelo3	C24:0	0	-89	-94	-87	-93
VtKCS16	TRIPLE Δelo3	C24:0	9	-69	-74	-70	-78
SbKCS6	TRIPLE Δelo3	C20:1	7	-97	-97	-81	-97

Table 5. Inhibition of KCS activity by benfuresate, flufenacet, cafenstrole, metazachlor, pyroxasulfone (1 or 10 μM) demonstrated in *S. cerevisiae* cells which expressed KCS proteins from γ clade. Elongation ratio were calculated as percent inhibition of detected VLCFA products synthesized by a given KCS in comparison to control treated (DMSO) *S. cerevisiae* cells. Numerical values used for visualization are calculated from at least three biological replicates.

Gene	Genetic background	VLCFA	% Inhibitor (μM)				
			Benfuresate	Cafenstrole	Flufenacet	Metazachlor	Pyroxasulfone
			10 μM	10 μM	10 μM	10 μM	10 μM
RsKCS1	TRIPLE Δelo3	C24:0	9	-77	-82	-81	-80
RsKCS2	TRIPLE Δelo3	C24:0	12	-98	-98	-84	-98

Table 6. Table 5. Inhibition of KCS activity by benfuresate, flufenacet, cafenstrole, metazachlor, pyroxasulfone (1 or 10 μM) demonstrated in *S. cerevisiae* cells which expressed KCS proteins from algae. Elongation ratio were calculated as percent inhibition of detected VLCFA products synthesized by a given KCS in comparison to control treated (DMSO) *S. cerevisiae* cells. Numerical values used for visualization are calculated from at least three biological replicates.

A decrease in C24:0 content was observed in KCS derived from the algae *Raphidocelis subcapitata*, with inhibition rates of around 80% for RsKCS1 and 95% for RsKCS2 (Table 6).

To conclude, we found that the elongation activity of KCS enzymes, regardless of their plant species origin, is inhibited by the following herbicides: metazachlor, flufenacet, cafenstrole, and pyroxasulfone. While most KCS enzymes are significantly inhibited, some, such as SoKCS4 and SbKCS18, show only partial inhibition by flufenacet and metazachlor, respectively. This result could be due to difference substrate specificity, the C24 to C26 activity should be tested. More precise information regarding the inhibition of FAE activity by herbicides can be obtained by studying the relationship between FAE activity and herbicide concentration.

1.2.3. Concentration dependence of inhibition

We aimed to examine the concentration-dependent inhibition of several elongases using metazachlor. This herbicide was added to transgenic yeast expressing AtKCS4, ZmKCS4 or SvKCS4 at concentrations ranging from 0 to 30 μM . The FAMES of the individual samples were subsequently extracted and analyzed using GC/MS. Based on these analyses, dose-response curves were determined for AtKCS4, ZmKCS4, and SvKCS4 as the percentage of activity relative to the amount of C24:0 as a function of metazachlor concentration. The results indicated that the activity of the enzymes decreased in a dose dependent manner with increasing concentrations of metazachlor (Figure 5). Notably, ZmKCS4 exhibited a slightly higher sensitivity to metazachlor compared to SvKCS4.

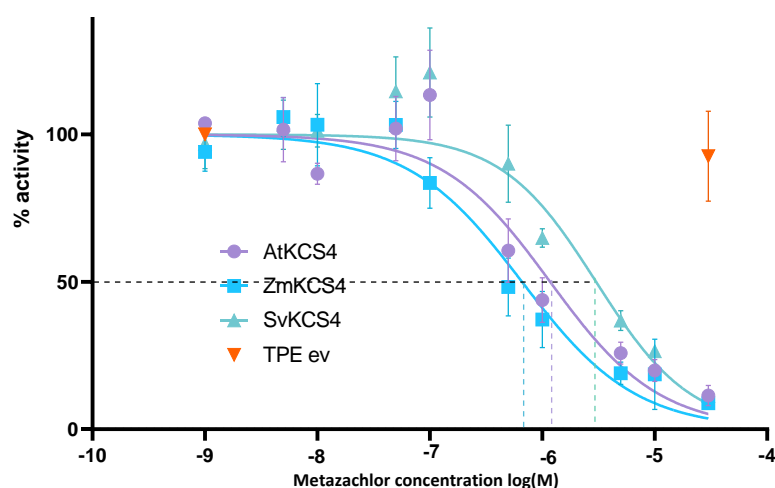


Figure 5. Dose–response curve generated from C24:0 for AtKCS4, ZmKCS4 and SvKCS4 expressed in TRIPLE $\Delta elo3$ with metazachlor treatment and IC50 calculation. The curve is based on the average of three replicates

To reflect to ability of metazachlor to inhibit each KCS, the IC50 (Inhibitory Concentration 50%) value which is the molar concentration required to induce half-maximal inhibition (Olah et Oprea 2007) was calculated for each KCS (Table 7). Regarding the IC50 values obtained from dose-response curves of AtKCS4, ZmKCS4, and SvKCS4 with metazachlor, SvKCS4 exhibited a slightly higher value (3.015 μM), indicating that it is slightly less sensitive to metazachlor compared to AtKCS4 and ZmKCS4, which had IC50 values of 1.176 and 0.66 μM , respectively. However, these differences in IC50 values between the enzymes were relatively small and did not allow for a clear conclusion about the specific target of the inhibitor.

	AtKCS4	ZmKCS4	SvKCS4
IC50 (M)	1.176E-06	6.613E-07	3.015E-06
IC50 (μM)	1.176	0.6613	3.015

Table 7. IC50 values (μM) from inhibition of AtKCS4 ZmKCS4 and SvKCS4 with metazachlor.

In conclusion, none of the inhibitors examined in this study demonstrated differential inhibition specificity regarding the origin of the KCS. Nonetheless, given the growing concern for the impact of plant protection products on the environment and human health, there is an ongoing development of new compounds that should target specifically KCS from weed species.

2. Studies on the mechanism of action new herbicides developed by Bayer SA

2.1. Influence of herbicides on elongases expressed in yeast

To determine the effect of newly developed herbicides, named GIB A, B, C, D and E derived from HRAC group 15 herbicides, on VLCFA biosynthesis compared to the known KCS inhibitor metazachlor, yeast strains expressing AtKCS4, SvKCS4, ZmKCS4 and RskCS2 were incubated in the presence of inhibitors (10 μ M). The FAMES of individual samples were extracted and analyzed using GC/MS to assess C24:0 content (Table 8). The results demonstrated that GIB B and GIB E led to a decrease in C24:0 amount similar to the effects observed with metazachlor for all KCSs studied. With inhibitors GIB A and GIB D, all KCSs were inhibited to the same extent, except for SvKCS4, which only showed 35% and 55% inhibition, respectively. This suggests that SvKCS4 is less sensitive to GIB A and GIB D compared to AtKCS4, ZmKCS4, and RskCS2. Finally, treatment of yeast cultures with the GIB C molecule resulted in low inhibition of the KCS from algae, RskCS2, which was inhibited at 39%, while AtKCS4, SvKCS4, and ZmKCS4 were inhibited by approximately 70%.

Gene	Genetic background	VLCFA	% Inhibitor (μ M)					Metazachlor
			GIB A 10 μ M	GIB B 10 μ M	GIB C 10 μ M	GIB D 10 μ M	GIB E 10 μ M	
AtKCS04	C24		-78	-88	-78	-91	-93	-88
SvKCS04	C24		-35	-90	-65	-55	-81	-80
ZmKCS04	C24		-79	-90	-63	-88	-94	-85
RskCS02	C24		-77	-80	-39	-91	-79	-84

Table 8. Inhibition of KCS activity by 5 herbicides developed by Bayer (GIB A-E) compared to metazachlor (10 μ M) demonstrated in *S. cerevisiae* cells which expressed KCS proteins. Inhibition of fatty acid elongation were calculated as percent inhibition of detected VLCFA products synthesized by a given KCS in comparison to control treated *S. cerevisiae* cells with DMSO. Numerical values used for visualization and respective standard errors from at least three biological replicates.

2.2. Concentration dependence of inhibition

Dose-response curves were determined for AtKCS4, ZmKCS4, and SvKCS4 by measuring their activity relative to the amount of C24:0 in the presence of increasing concentrations of GIB E. The results showed that the activity of the enzymes decreased in a dose-dependent manner with increasing concentrations of metazachlor. SvKCS4 activity decreased at slightly higher concentrations of GIB E compared to AtKCS4 and ZmKCS4 (Figure 6).

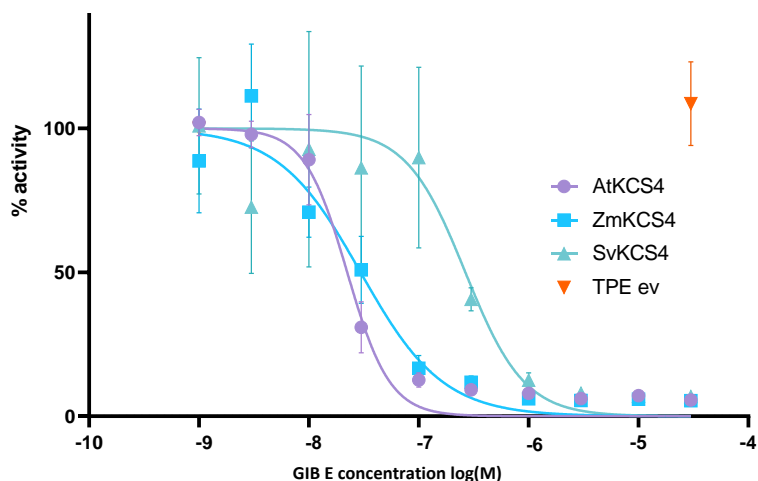


Figure 6. Dose-response curves generated from the sum of C24:0 for AtKCS4, ZmKCS4 and SvKCS4 expressed in TRIPLE $\Delta elo3$ with GIB E treatment. The curve is based on the average of three replicates.

The IC50 values and dose-response curves were determined for AtKCS4, ZmKCS4 and SvKCS4 in the presence of the GIB E compound (Table 9). The IC50 value for SvKCS4 was 10 times higher (0.266 μM), indicating that this enzyme is ten times less sensitive to GIB E compared to AtKCS4 and ZmKCS4, which had IC50 values of 0.02237 and 0.02959 μM , respectively.

E	AtKCS4	ZmKCS4	SvKCS4
IC50 (M)	2.237E-08	2.959E-08	2.66E-07
IC50 (μM)	0.02237	0.02959	0.266

Table 9. IC50 values (μM) from inhibition of AtKCS4, ZmKCS4 and SvKCS4 with GIB E inhibitor.

3. Conclusion

In this section, we investigated the potential inhibition of KCS from various plant species by different herbicides. Benfuresate did not show inhibition of the KCS activities tested in this study, which may be due to a lack of bioactivation or bioavailability in yeast (Trenkamp et al., 2004). Overall, this study demonstrated that the herbicides, metazachlor, flufenacet, cafenstrole and pyroxasulfone, tested at a concentration of 10 μM , did not exhibit selectivity in their mechanism of action, as they did not differentially target KCS from different plant species or with different substrate-specificity. Only two enzymes, SoKCS4 and SbKCS18, showed partial inhibition by flufenacet and metazachlor, respectively. However, by measuring KCS activity as a function of increasing inhibitor concentrations, we were able to provide additional quantitative information about inhibition potency (IC_{50}), which allowed us to compare more precisely the effects of the inhibitors on different enzymes. Only slight differences in inhibition were found between ZmKCS4, SvKCS4, and AtKCS4 with metazachlor, while the newly developed GIB E herbicides inhibited less SvKCS4 than ZmKCS4 and AtKCS4.

Although experiments that produce dose-response curves offer a more accurate assessment of the inhibitory power of a molecule, this type of experiments conducted *in vivo* in yeast expressing KCS requires a large volume of inhibitor due to the volume of culture and does not allow for a large number of conditions to be tested simultaneously. Therefore, to effectively evaluate molecules under development, which are typically synthesized in very small quantities, it is necessary to develop a test with smaller reaction volumes and more precise, such as *in vitro* assays. Moreover, GC-MS analysis of total FAMES alone does not provide a direct indication of enzyme activity or lipid channeling. To gain more precise insights, analysis of the acyl-CoA pool is required.

**CHAPTER 3 - DEVELOPMENT OF A
NON-RADIOLABELED *IN VITRO*
ASSAY FOR EVALUATING KCS
ACTIVITY AND INHIBITION**

Chapter 3 - Development of a non-radiolabeled *in vitro* assay for evaluating KCS activity and inhibition

In contrast to *in vivo* assays, *in vitro* assays provide valuable insights into enzyme kinetics and inhibition. The isolation and characterization of various enzymes with different substrate specificities are essential for precisely characterizing the inhibitory potential of novel molecules. Very-long-chain fatty acids (VLCFAs) are synthesized as acyl-CoAs by the endoplasmic reticulum-localized multiprotein complex known as the fatty acid elongase (FAE) complex. However, elucidating the mechanisms of their reactions is impeded by their membrane-bound nature.

To date, few studies have conducted elongation *in vitro* assays, and they either used microsomal fractions isolated from yeast expressing AtKCSs or tagged KCSs isolated in detergent. In the presence of malonyl-CoA and a diverse array of acyl-CoA substrates in buffer containing co-factors necessary for the reaction, these enzyme assays enabled the direct assessment the elongation activity. Such assays have facilitated the analysis of substrate specificities of KCSs. Being the first FAE gene studied and cloned in yeast, AtKCS18/FAE1 was the first condensation enzyme characterized in an *in vitro* assay. It has been reported that FAE1 KCS exhibits a substrate preference for C16:0-, C16:1-, C18:0-, and C18:1-CoAs, yielding C20:1 acid as the major product and C22:1 as a minor product (Millar and Kunst 1997; Ghanevati and Jaworski 2001; 2002; Blacklock et al., 2002; 2006; Paul et al., 2006). Blacklock et al. (2006) conducted the most extensive study on KCS activities through *in vitro* enzymatic assays *in vitro*, testing nine Arabidopsis KCSs and studying their substrate preferences. Several putative KCSs exhibited activity, KCS1 demonstrated high activity with 16:0-, 16:1-, 18:0-, and 20:0-CoA substrates, while KCS17 exhibited specificity for saturated acyl-CoAs up to C22. KCS11 showed minimal activity with C18:0-CoA. Conversely, KCS3, KCS4, KCS7, KCS13, and KCS19 did not display any activity. Paul et al. (2006) demonstrated that AtKCS2 and AtKCS20 prefer C16:0 and C18:0-CoA while AtKCS9 prefers mostly C22:0-CoA. Furthermore, direct measurement of the KCS product, 3-ketoacyl-CoA, provided precise information about the KCS activity of the FAE complex (Blacklock and Jaworski, 2006; Beaudoin et al., 2002; Ghanevati et Jaworski 2002). Indeed, the elongation cycle is initiated with the condensation of malonyl-CoA with acyl-CoA, forming a 3-ketoacyl-CoA intermediate, which is subsequently reduced by β -ketoacyl-CoA Reductase (KCR) using pyridine nucleotides (NADPH) as reductant. Omitting NADPH from the reaction prevents the reduction of 3-ketoacyl-CoA, leading to its accumulation and allowing to determine the precise activity of KCS enzyme (Blacklock and Jaworski, 2006; Beaudoin et al., 2002; Ghanevati et Jaworski 2002).

In vitro assays were also employed to investigate enzymatic kinetics and inhibition. For example, fenoxasulfone and pyroxasulfone were studied as VLCFAE-inhibiting herbicides in more detail (Tanetani et al., 2011a; 2011b), revealing different inhibition mechanisms by pyroxasulfone between AtKCS18/FAE1 and rice KCS, as well as potential selectivity among plant species. Additionally, enzyme assays are used to assess the inhibitor by calculating the concentration required for 50% inhibition (I50), offering insights into the sensitivity of KCS to various FAE-inhibitors.

However, these *in vitro* assays routinely used radioactive substrates, primarily [¹⁴C]-labeled malonyl-CoA, to quantify radiolabeled acyl-CoA products and determine enzymatic activity. Yet, employing radiolabeled substrates presents challenges such as the need for specialized equipment and waste management, as well as the risk of radiation exposure to laboratory personal. Hence, there is a pressing need to enhance traditional *in vitro* KCS assays by reducing or eliminating the use of radiolabeled substrates.

This section aims to develop enzyme assay for evaluating KCS activity and inhibition without the use of radioactive substrates. Initially, a yeast microsomal preparation was validated for isolating membrane-bound KCS enzymes. Subsequently, an HPLC method was developed to quantify the direct product of the KCS enzyme, the 3-ketoacyl-CoA intermediate. Additionally, assessing the assay activity of KCSs from various species is crucial for understanding their kinetics and substrate preferences. Finally, these *in vitro* assays were employed to investigate the FAE-inhibitor mechanism of action more comprehensively.

1. Validation of yeast microsomes preparation

For precise characterization of both known and putative KCSs using *in vitro* assays, it is essential to isolate the enzyme in an active form. However, elucidating the mechanism of their reactions is hampered by their membrane-bound nature. Several strategies have been employed to achieve this. One approach involved the purification of Histidine-tagged KCS for *in vitro* assays by solubilizing the membrane with a detergent, Triton X-100, and extracting the enzyme using immobilized metal affinity chromatography (Ghanevati and Jaworski 2002; Blacklock and Jaworski 2006). Another method involved the utilization of microsomes, consisting of membranes fragments derived from the endoplasmic reticulum (ER) and Golgi apparatus, containing active condensation enzymes (Beaudoin et al., 2002; Paul et al., 2006; Tanetani et al., 2009; 2011b). Microsomes can be obtained by centrifugation as unbroken cells, nuclei, and mitochondria are pelleting at low speeds (<10,000g) while microsomes pellet at approximately 100,000g.

The choice of yeast microsomal preparation was made for this work, notably because the KCS expressed in yeast in this study were not all tagged, and plant microsomal preparation had already been performed in the laboratory. Yeast microsomal preparation is well-documented in the literature. The preparation process was adapted from three protocols (Table 1). Indeed, Ghanevati and Jaworski (2001) and Paul et al. (2006) utilized yeast microsomes and radioactive substrate to evaluate *in vitro* KCS elongase activities, while Liu et al. (2017) used yeast microsomes for non-radiolabeled *in vitro* assays for recombinant acyltransferases involved in triacylglycerol biosynthesis. The adapted protocol used for this work is illustrated in Figure 1; the yeast pellet was washed twice in TRIS buffer, crushed with glass beads, cells debris were eliminated with low speed centrifugation, and the microsomal pellet was obtained after high-speed centrifugation at 110,000g for 2 hours at 4°C. The pellet was then suspended in 0.5 mL of HEPES storage buffer at pH 7.2 containing 2% glycerol, allowing for slow defrosting on ice to provide optimal protection for elongase activity (Bessoule et al., 1989).

Ghanevati et Jaworski 2001	Paul et al., 2006	Liu et al., 2017
<p>Cells were harvested by centrifugation and washed with 10 ml of ice-cold isolation buffer (80 mM HEPES KOH, pH 7.2, 5 mM EGTA, 5 mM EDTA, 10 mM KCl, 320 mM sucrose, 2 mM dithiothreitol).</p> <p>Cells were pelleted, resuspended in buffer, and broken for three 60 s pulses with a Mini-Beadbeater (Biospec product, Bartlesville, OK) using 0.5 mm glass beads. The supernatant was collected and briefly centrifuged to remove unbroken cells and cellular debris. The clear supernatant was then diluted with IB and the microsomal membrane pellet was recovered after centrifugation at 100 000xg for 60 min. The microsomal membrane pellet was resuspended in ice-cold buffer containing 20% glycerol.</p>	<p>Cells were pelleted at 5000 × g, washed with water, and repelleted. The cell pellets were resuspended in TEGM (0.05 m Tris (7.5), 1 mm EGTA, 1 mm β-mercaptoethanol, 1 mm phenylmethylsulfonyl fluoride, 1x protease inhibitor cocktail) buffer at 1 ml/50 OD cells, and glass beads (0.5-mm diameter) were added to the meniscus. Cells were disrupted by four cycles of vortexing for 1 min followed by cooling on ice for 1 min, and pelleted at 8,000 × g for 10 min. The supernatant was transferred to a fresh tube and spun at 135,000 × g for 30 min. The resulting pellet was resuspended by Dounce homogenization in at least a 10× volume of TEGM buffer and repelleted at 135,000 × g. The final membrane pellet was resuspended in TEGM buffer containing 33% glycerol and stored at -80 °C.</p>	<p>Cells were harvested and washed twice with ice-cold distilled water. The cell pellets were resuspended in cell lysis buffer (containing 5 % glycerol, 20 mM Tris-HCl (pH 8.0), 0.3 M ammonium sulfate, 10 mM MgCl₂, 1 mM EDTA, 1 mM DTT, 1× EDTAfree protease inhibitor cocktail set X (Calbiochem, USA), 1 mM PMSF) and lysed by passing twice through a French pressure cell (Spectronics Instruments, USA). Cell debris was removed from the suspension by centrifugation at 10,000×g for 10 min at 4 °C, and the supernatant was centrifuged further at 100,000×g for 2 h at 4 °C. The resulting microsomal membrane pellets were resuspended in microsomal storage buffer (50 mM Tris-HCl, pH 7.5, 10 % glycerol) to give a protein concentration of 10 µg µL⁻¹ for immediate use or stored at -80 °C.</p>

Table 1. Protocols for yeast microsomes preparation.

To validate the recovery of a KCS enzyme in the yeast microsomal fraction, a Western blot analysis was conducted (Figure 2) with the fractions from different phases of the microsomal preparation, as indicated by the letters in Figure 1. The Western blot was done on the Myc-tagged AtKCS20 yeast microsomal preparation, using a mouse anti-Myc-Tag primary antibody, and a goat anti-mouse IgG secondary antibody.

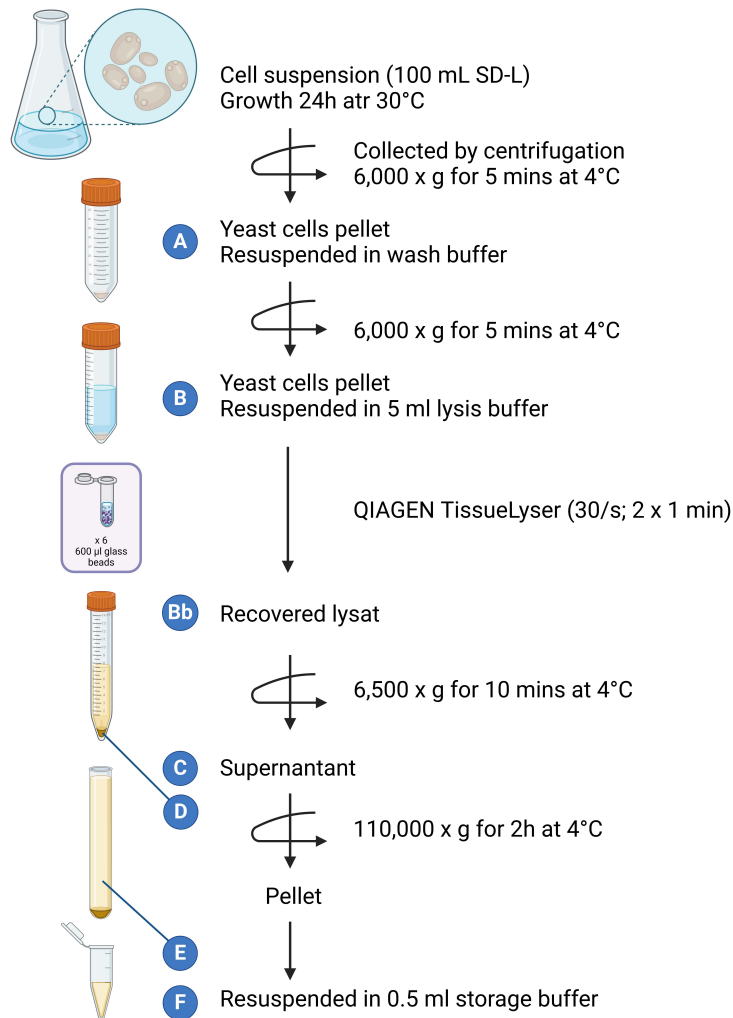


Figure 1. Flow chart for the preparation of microsomes from cultured yeast cells transformed with KCS. Wash buffer : ice-cold 20 mM Tris-HCl distilled water ; Lysis buffer : 20 mM Tris-HCl (pH 7.9), 10 mM MgCl₂, 1 mM EDTA, 5% (vol/vol) glycerol, 1 mM DTT, 0.3 M ammonium sulfate ; Storage buffer : 50 mM HEPES pH 6.8, 1mM DTT, and 2% glycerol. These operations were carried out at 4 °C/on ice. Letters indicate fractions of the microsomal preparation collected for Western blot analysis. Lane A: yeast pellet cells resuspended in wash buffer; Lane B: yeast cells pellet resuspended in lysis buffer; line Bb : recovered lysate from yeast cells crushing; line C : supernatant from recovered lysate low speed centrifugation; D : pellet cells debris from recovered lysate low speed centrifugation; E : supernatant after high speed centrifuge; F: microsomal fraction from high speed centrifuge resuspended pellet

The size of the KCS protein is approximately 56 kDa. As expected, no protein was observed in fractions A, B, C, and E (Figure 2), corresponding respectively to yeast suspended in buffer (wash or lysis), supernatant before and after high-speed centrifugation (Figure 1), although KCS proteins might be present but highly diluted. Nevertheless, small amount of proteins was detected in fraction Bb, which corresponds to the recovered lysate after yeast cell disruption.

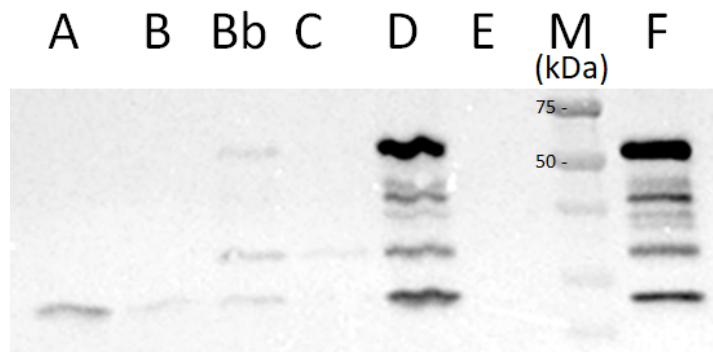


Figure 2 : SDS/PAGE analysis of isolated recombinant Myc-tagged AtKCS20 KCS. Lane A: yeast pellet cells resuspended in wash buffer; Lane B: yeast cells pellet resuspended in lysis buffer; line Bb : recovered lysat from yeast cells crushing; line C : supernatant from recovered lysat low speed centrifugation; D : pellet cells debris from recovered lysat low speed centrifugation; E : supernatant after high speed centrifuge; F; microsomal fraction from high speed centrifuge resuspended pellet

Furthermore, a substantial amount of protein was detected in the cell debris pellet (D), possibly due to inadequate yeast cell disruption, leading to protein precipitation with cellular debris. As expected, a strong signal was nevertheless observed in the final fraction (F) of the preparation, indicating the efficient isolation of AtKCS20-containing microsomal fraction by high-speed centrifugation .

2. Elongase activity assay

In literature, to perform elongase activity, routinely, proteins were added to a final volume reaction between 25 and 200µl in HEPES, TRIS buffer or sodium phosphate buffer at pH 7.2 – pH 7.5 with protein quantities ranging from 5 µg to 400 µg, depending on the source of proteins (Table 2). To monitor the synthesis of the product of the FAE complex *in vitro*, one of the two substrates used, acyl-CoA or malonyl-CoA was radioactive. Co-factors were added to the reaction such as NADPH (0.5 to 1.6 mM) for the functioning of the reductase activities, MgCl₂ (1mM to 20mM) and DTT (1mM) and/or β-mercaptoethanol (10mM) to reduce disulfide bridges, TRITON-X to help protein solubilisation. Ghanevati and Jaworski (2002) indicated that the use of co-factor CoA-SH and ATP had no effect on the condensation activity of the recombinant AtKCS18/FAE1 KCS. Then the reaction mix was incubated at 30°C or 37°C during 10, 30 minutes or 18 hours. Following fatty acids extraction, radioactive elongate product was measured.

	Ghanevati and Jaworski 2001	Ghanevati and Jaworski 2002	Blacklock and Jaworski 2002	Beaudoin et al., 2002	Blacklock and Jaworski, 2006	Paul et al., 2006	Tanetani et al., 2011b
Volume reaction	25µL	25µL	25µL	200 µL	25µL	200 µL	60 µL
protein quantity	5 µg	35 – 70 µg	6 µg (his-tag)	400 µg	6.25 µg (his-tag)	200 µg	10µL ?
Substrat A (acyl coA)	15µM *	20 µM	15µM *	40µM	15µM	40 µM	160µM
Substrat B (Malonyl-CoA)	100µM	18 µM*	100µM	60µM*	20µM*	60µM*	33 µM*
TRIS				50mM pH 7.5		50Mm pH 7.5	
Sodium phosphate		40mM Ph 7.2			10 mM pH 7.2		
Hepes KOH	80 mM pH 7.2		20 mM pH 7.2				
MgCL2	20 mM		20 mM	1 mM		1 mM	
DTT						1 mM	
B-mercaptoethanol				10mM		10 mM	
NADPH	500µM		500µM	1 mM		1 mM	1,6 mM
NADH				1 mM		1 mM	1,6 mM
ATP	1mM						
CoA-SH	10µM		10µM				
Triton-X				150µM	0.05%	150µM	
Incubation	30 min at 30°C	10 min at 30°C	10min at 30°C	0,2, 1, 5 min at 37°C	18h at 30°C	10 min at 37°C	30 - 90 min at 30°C
Stop reaction		0.5 mL of 0.1 M K ₂ HPO ₄ ,0.4M KCl		200 µl of 5M KOH/10% MeOH		200 µl of 5M KOH/10% MeOH	

Table 2. Reagents and parameters used for *in vitro* keto-acyl synthase activity assay. Radioactive substrate is indicated by *.

2.1. GC-FID detection strategy: odd acyl-CoA as substrate

To determine if the yeast microsomal preparation contains active KCS, we used the KCS with the highest activity reported in the literature, AtKCS18 (Blacklock and Jaworski, 2006), which has substrate preference for unsaturated and saturated C16-, C18-, and more lightly C20-CoA (Paul et al., 2006; Blacklock and Jaworski, 2006).

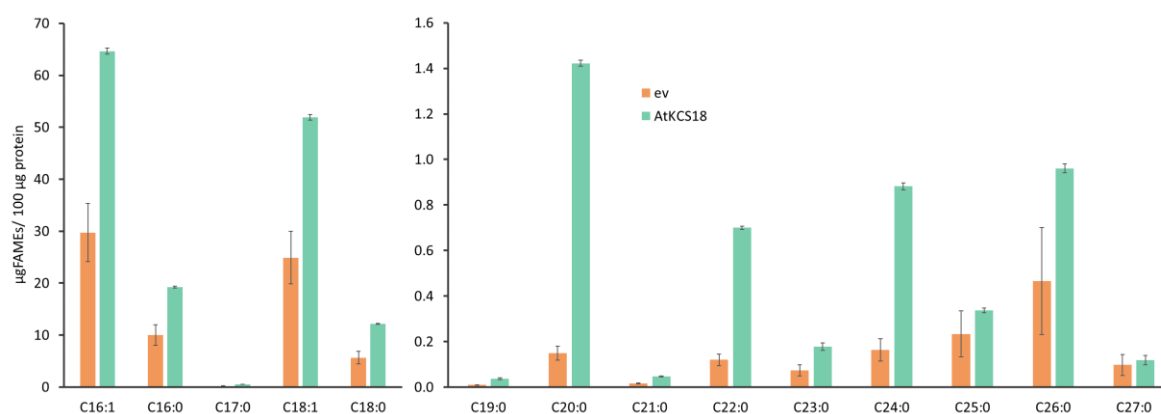


Figure 3. FAMES of microsomes fraction from yeast expressing AtKCS18 and empty vector (ev). Microsomes prepared from yeast expressing putative KCSs as proteins were obtained after high speed centrifuge at 110'000g during 2h at 4°C. The pellet was resuspended in 0.5 mL of HEPES storage buffer at 7.2 pH containing 2% glycerol allowing a slow defrosting on ice. The results are representative of experiments carried out two times.

Microsomes from yeast expressing AtKCS18 and empty vector (ev) were prepared as described in Figure 1. The FAMES of the individual samples were extracted and analyzed using GC/FID. Microsomes from yeast expressing AtKCS18 accumulated LCFA C16:1, C16:0, C18:1, C18:0, and VLCFA C20:0, C22:0 compared to the yeast membrane expressing empty vector (Figure 3). In AtKCS18 microsomes, we noticed low level of odd chain fatty acids, such as C19:0 and C21:0, that can be used for the identification of elongation products. To take advantage of this, we hypothesized that AtKCS18 is capable of adding two carbon atoms to an odd chain CoA, detectable by GC/FID.

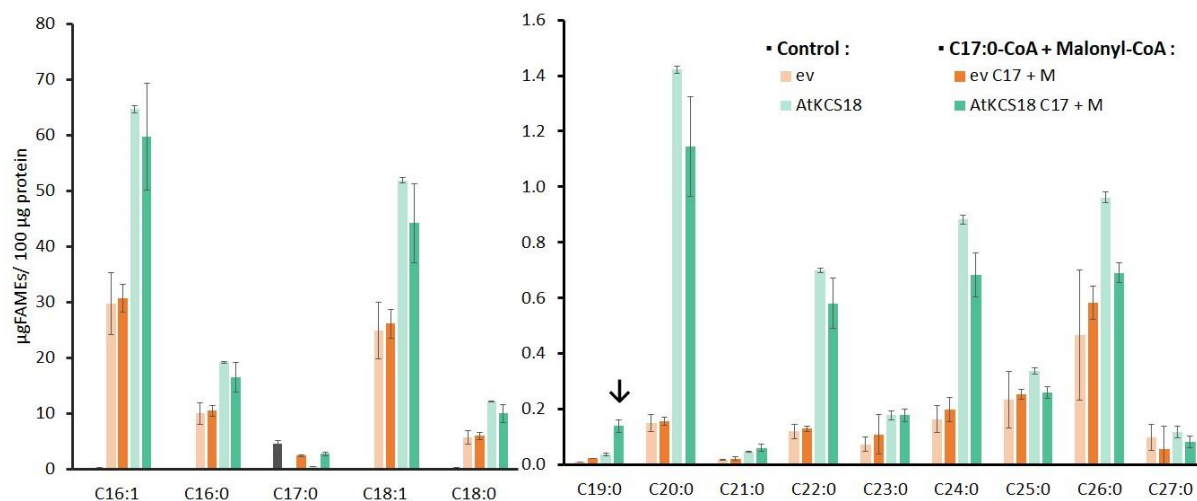


Figure 4. Condensation activity of AtKCS18 microsomes using Malonyl-CoA and C17:0-CoA as substrates (FAMES). 100µM malonyl-CoA (M) and 100µM C17:0-CoA (C17) were incubated with MgCl₂, NAD(P)H, DTT in Hepes Buffer pH 7.2 (mix) at 30°C for 1 hour in the presence (ev or AtKCS 18) or in the absence of microsomal fraction (100 µg). The results are representative of experiments carried out three times.

Hence, to determine whether KCS in the yeast microsomal fraction is functional, an experiment was conducted to assess the elongation of an odd fatty chain. Microsomes were prepared using the method described in Figure 1 and was used in the assay. The assay contained 100 µg of proteins, 50 mM HEPES pH 7.2, 1 mM MgCl₂, 0.5 mM DTT, 1 mM NAD(P)H, and two substrates: 100 mM malonyl-CoA and 0 or 100 mM C17:0 acyl-CoA in a 100 µL reaction volume. The reaction was incubated at 30°C for one hour and stopped by adding 4 mL of methanol with 2.5% sulfuric acid. As show in Figure 4, when C17:0-CoA and malonyl-CoA were used as substrates in 100µM concentration, analysis of microsomes expressing AtKCS18 revealed the presence of C19:0 FAME. No elongation of C17:0-CoA was observed in control microsomes containing the empty vector. These results indicated that the AtKCS18 is able to elongate C17:0-CoA in C19:0-CoA (Figure 4), revealing that the AtKCS18 is active in the microsomes preparation.

In order to optimize microsomes preparation and condensation reaction, several products routinely used in these procedures have been assayed. Indeed, Protease Inhibitor Cocktail (PIC) or PMSF is usually used during yeast or plant protein purification in order to protect the proteins from proteolysis. In addition, bovine serum albumin (BSA) is used to help solubilize fatty acids / acyl-CoA. Our results indicate that the use of PIC and BSA had no effect on the AtKCS18 condensation activity (Figure 5).

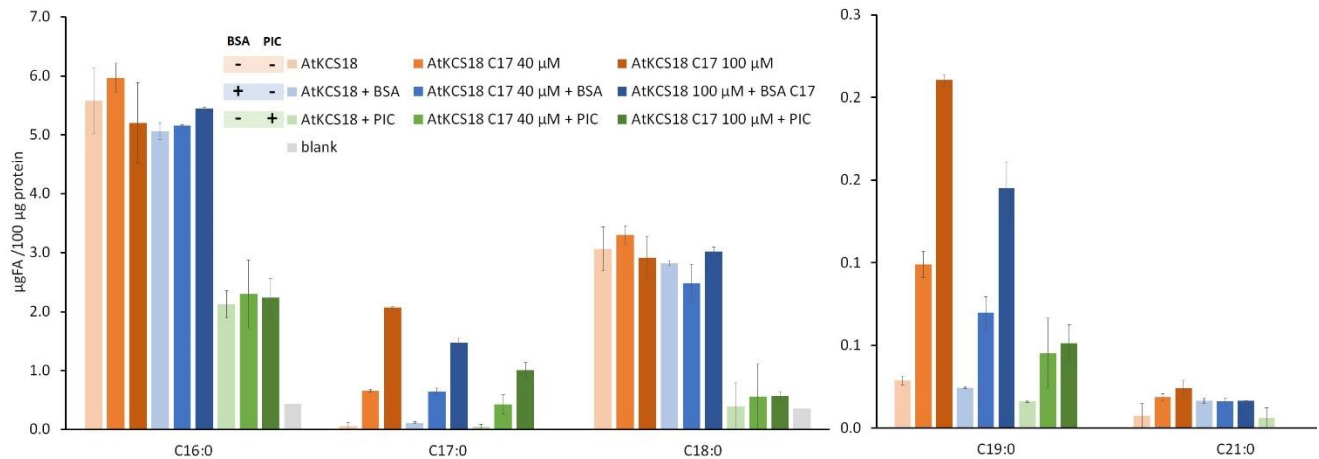


Figure 5. Condensation activity of AtKCS18 microsomes using Malonyl-CoA and C17:0-CoA as substrates (FAMES). AtKCS18 microsomal fraction (100 µg) were incubated with malonyl-CoA and C17:0-CoA (100µM) with MgCl₂, NAD(P)H, DTT in HEPES Buffer pH 7.2 at 30°C for 1 hour. PIC and BSA have been added as indicated in the legend. The results are representative of experiments carried out three times. Blank represent AtKCS18 microsomal fraction in reaction mix without substrates.

Our results demonstrate that the microsomes preparation method employed is effective in generating an active AtKCS18. Specifically, we successfully identified the C19:0 FAME using C17:0-CoA as substrate. We believe that this preparation procedure could therefore be used to measure the activity of other yeast-expressed KCSs.

However, our approach shows certain limitations. As previously mentioned, the FAMES products of AtKCS18 were detectable by GC-FID due to the strong enzymatic activity of AtKCS18, which is similar to that of AtKCS1, as reported in the literature (Blacklock and Jaworski, 2006). For KCSs with lower activity, such as AtKCS20, we were unable to detect the product of odd acyl-chain elongation (not shown). We assume that this is due to a low amount of synthesized product, not detectable in GC-FID as FAMES. Therefore, this strategy cannot be used to assess KCS activity.

2.2. HPLC-MS/MS : acyl-CoA detection

To enhance sensitivity and precision, it is crucial to investigate the elongation product, namely acyl-CoA. Acyl-CoA molecules possess a thioester group, which renders them relatively polar and, as a result, not volatile. This polarity renders them difficult to separate effectively using gas chromatography (GC), while high-performance liquid chromatography coupled with tandem mass spectrometry (HPLC-MS/MS) is a more appropriate method for analyzing acyl-CoA. However, the acyl-CoA variability in term of fatty acyl chain length, saturation levels and functional groups poses a significant challenge in developing comprehensive analytical techniques. Short-chain acyl-CoAs, due to the high polarity of the CoA residue, require acidic mobile phases for improved retention. Conversely, long-chain acyl-CoAs tend to exhibit peak tailing under such conditions because of higher apolarity and so excessive retention, necessitating the use of basic mobile phases to achieve better peak shapes. Furthermore, due to their negatively charged phosphate groups, acyl-CoAs have a propensity to adhere to glassware and stainless steel surfaces, leading to performance degradation after multiple injections. This negative charge need to be neutralize by acidic eluent.

The first objective was the development of an HPLC method to detect acyl-CoA, with the aim of assessing KCS activity. This method must be highly sensitive in order to accurately detect the small amounts of acyl-CoA synthesized through the FAE complex or condensation in *in vitro* reaction.

2.2.1. HPLC method – HPLC-MS/MS

These experiments have been performed on the lipidomic platform of Bordeaux Metabolome, under the supervision of Laetitia FOUILLEN and Pierre VAN DELFT using a high performance liquid chromatography system (1290 Infinity II, Agilent) coupled to a QTRAP 6500 mass spectrometer (Sciex). The chromatographic separation of acyl-CoA was performed on a reverse phase Kinetex C18 5 μm (50 mm x 2.1 mm, 100 \AA , Phenomenex).

To analyze acyl-CoAs, two methods were experimented. First, we assayed acyl-CoA under typical reverse-phase conditions with some modifications. Slightly alkaline pH (pH \geq 8.5) was used for the separation of long-chain acyl-CoAs, along with the implementation of an acidic wash step between injections which can effectively minimize the observed loss of analytes as outlined in Abrankó et al. (2018). Secondly, acyl-CoAs were assayed using a recently developed method described by Li et al. (2021), who proposed a derivatization strategy of acyl-CoAs based on phosphate methylation by trimethylsilyl diazomethane (TMS-DZ) (Figure 6B). This method achieved full coverage (from free CoA to C25:0-CoA) and good peak shape in liquid chromatography. In addition, it solves the analyte loss due to the high affinity of phosphate groups to glass and metallic surfaces, which is beneficial for routine analysis in large-scale lipidomics studies (Li et al., 2021).

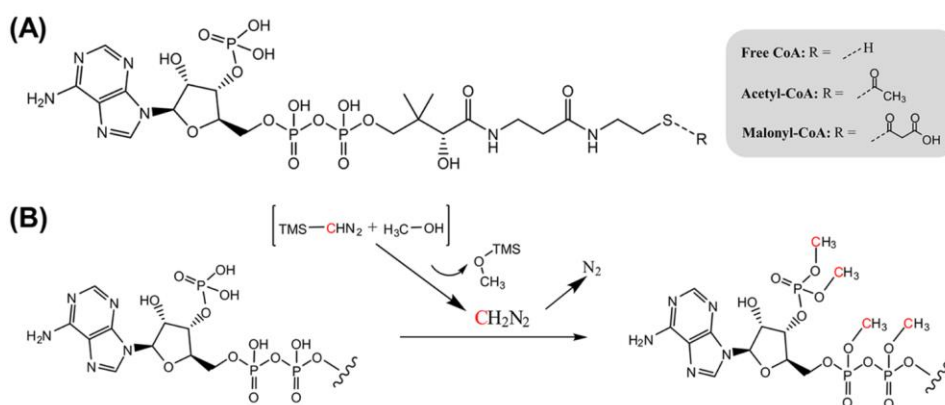


Figure 6. (A) Acyl-CoA structure (B) Phosphate methylation mechanism of acyl-CoAs using trimethylsilyl diazomethane (TMS-DZ) (from Li et al., 2021).

a. MS Detection of Methylated Acyl-CoAs

As shown in Figure 7A, for non-methylated C17:0-CoA, the fatty acyl pantetheine ion (m/z 513.7) was the most abundant fragment ion in ESI+ resulting from a neutral loss of 507 Da (3'-phospho-ADP), accompanied by a protonated 3'-phosphate-AMP product ion (m/z 428) (Figure 7A).

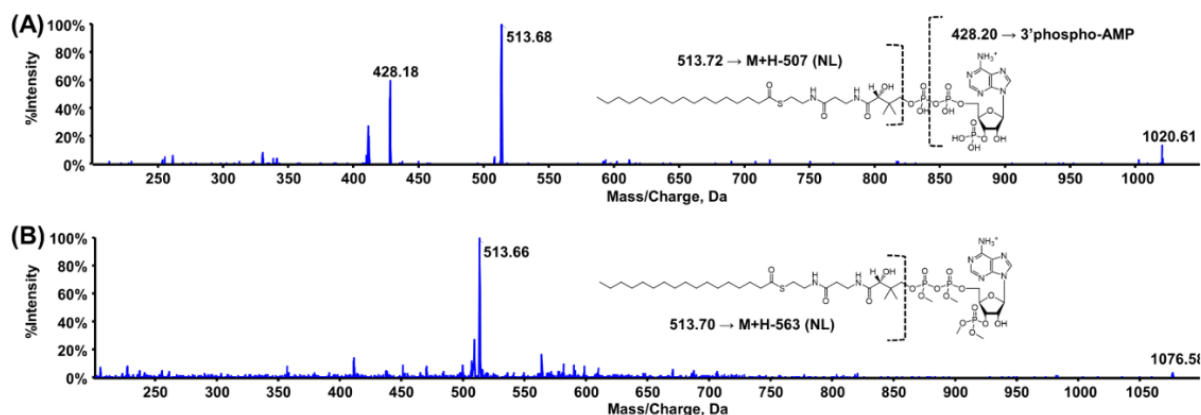


Figure 7. Product ion spectrum (Qtrap) of (A) C17:0-CoA and (B) methylated C17:0-CoA (figure from Li et al., 2021).

As shown in Figure 7B, methylated C17:0-CoA generated only one main fragment in the MS2 level, the same fatty acyl pantetheine ion (m/z 513.7), resulting from a neutral loss of 563 Da (tetra-methylated 3'-phospho-ADP). Methylated C18:0-CoA, C20:0-CoA, C22:0-CoA, and C24:0-CoA have similar fragmentation rules in MS (Figure 8). As described by Li et al. (2021), acyl-CoAs share a similar fragmentation pattern across the whole family after methylation.

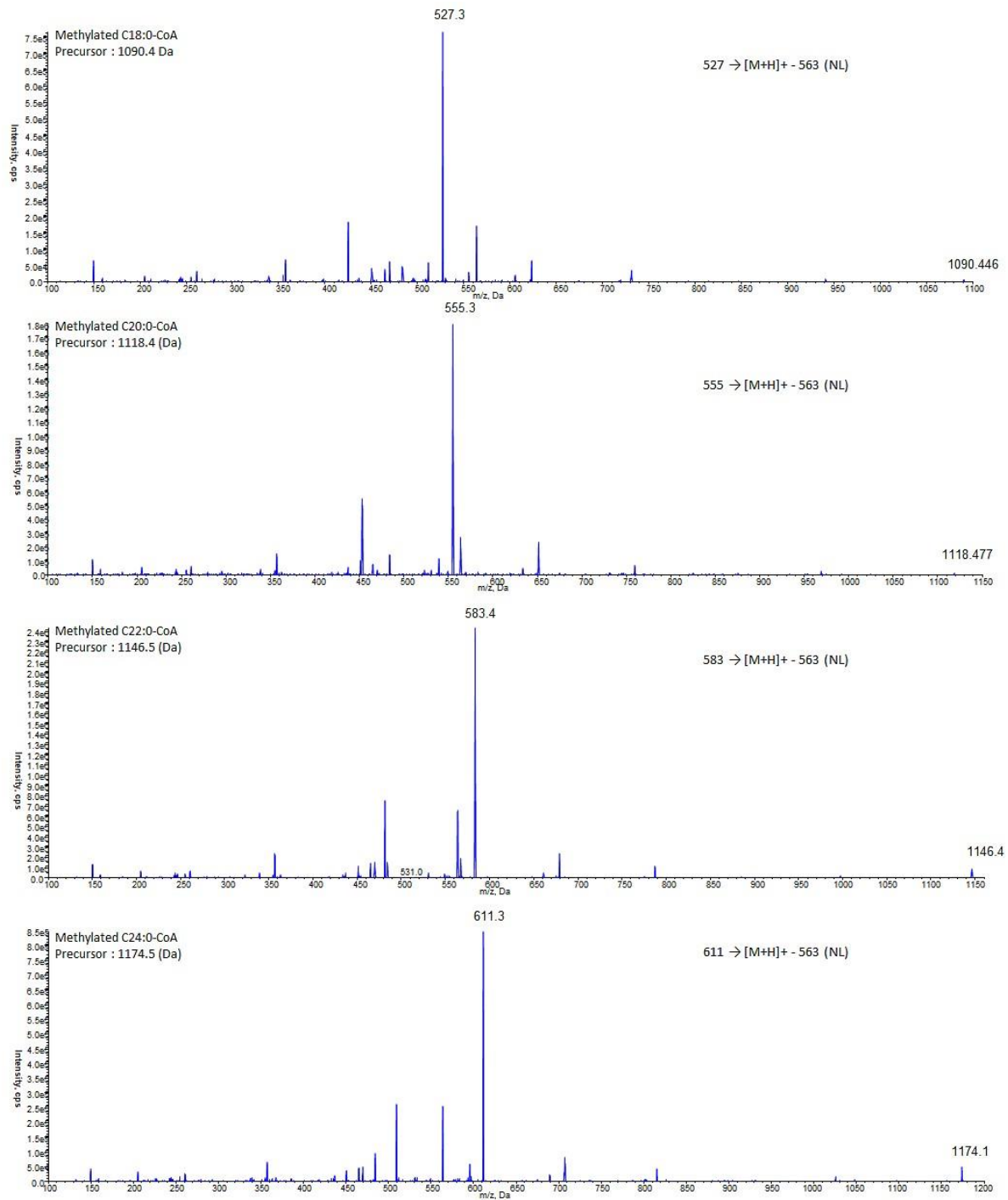


Figure 8. MS/MS spectra of methylated acyl-CoAs obtained in infusion mode.

b. Chromatographic Improvement after derivatization

Non-methylated C16:0-CoA and C24:0-CoA were tested under alkaline condition followed by acidic wash and methylated C16:0-CoA and C24:0-CoA as described in Li et al. (2021) have been compared. As shown in Figure 9A, C16:0-CoA was effectively separated with a good peak shape, while C24:0-CoA could not be efficiently detected.

In contrast, after methylation, acyl-CoAs converted into corresponding neutral molecules were separated within a single analytical run (Figure 9B). Good peak shapes were obtained for C16:0 and C24:0 acyl CoA, and a washing step after multiple injections was no longer required.

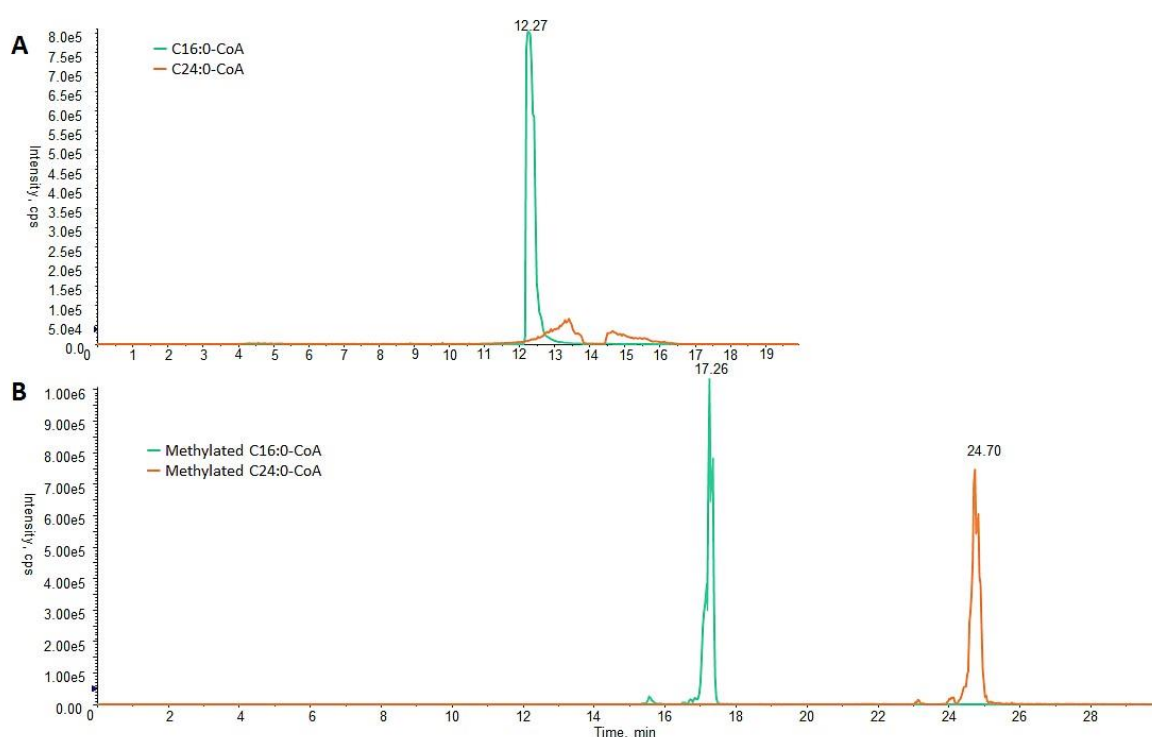


Figure 9. Chromatograms of C16:0-CoA and C24:0-CoA under the conditions of (A) 10 mM ammonium formate in water pH 8.5 + 2% acetonitrile and acetonitrile + 5% 10 mM ammonium formate in water, follow by acidic wash (7 minutes) and equilibration step (6 minutes) (not shown) (B) Chromatogram of derivatized (methylated) 10 mM ammonium formate in water + 2% acetonitrile and acetonitrile + 5% 10 mM ammonium formate in water.

c. Yeast matrix effect on Acyl-CoA

To better understand the impact of the yeast microsome matrix on acyl-CoAs separation and detection, C18:0-CoA, C20:0-CoA, C22:0-CoA, and C24:0-CoA were added to the yeast microsomes and subsequently derivatized as described below. The results indicated that these four acyl-CoAs experienced significant matrix effects, resulting in a loss of 88% to 99% of their peak intensities (Table 3) and poor peak shape compared to when they were analyzed without microsome matrix (Figure 10). Additionally, larger losses of peak intensities were observed for the longer acyl-CoA chains (Table 3). We supposed that the TMS-DZ derivatives other phosphates present in the membranes (Genva et al., 2023) or acyl-CoA are not easily accessible. This problem should be reduced by using sample preparation before derivatization.

TMS	Standards	Yeast matrix + Standards	
	Peak area	Peak area	% matrix effect
CoA18:0-Me	8830000	1026600	-88.37
CoA20:0-Me	12681000	435000	-96.57
CoA22:0-Me	12681000	120000	-99.05
CoA24:0-Me	14400000	52600	-99.63

Table 3. Matrix effect of internal standards based on peak area ratios between pure standards and standards in yeast matrix.

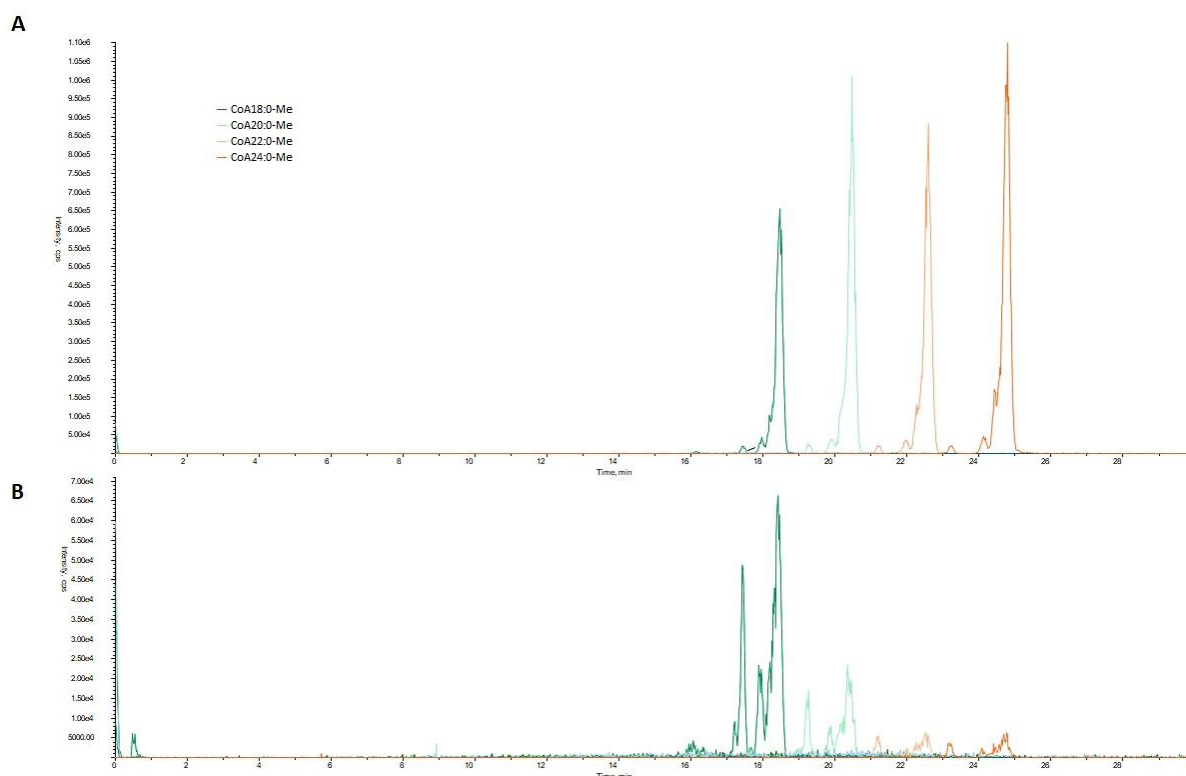


Figure 10. Chromatograms of methylated C18:0-CoA, C20:0-CoA, C22:0-CoA and C24:0-CoA under HPLC condition 10 mM ammonium formate in water + 2% acetonitrile and acetonitrile + 5% 10 mM ammonium formate in water. (A) Standards alone (B) Standards in yeast microsome matrix.

d. Sample preparation before derivatization step

Various sample preparations were evaluated to minimize matrix effects. Initially, the SPE (Solid Phase Extraction) procedure used prior to acyl-CoA derivatization (Li et al., 2021) was assessed. We identified big issues with acyl-CoA methylation and CoAs loss (not show). Subsequently, we attempted two other SPE procedures for acyl-CoA extraction (Yang et al., 2009; Trefely et al., 2022) and a liquid-liquid extraction (LLE) (Haslam et al., 2021), and added a methylation step with TMS-DZ. Extraction recoveries with or without a purification step (SPE or LLE) before derivatization with TMS-DZ were calculated.

Although SPE procedure from Trefley et al. (2022) appeared to result in better peak intensities than the SPE procedure from Yang et al. (2009), methylated acyl-CoA C18:0-CoA, C20:0-CoA, C22:0-CoA, and C24:0-CoA suffered from significant extraction recovery losses ranging from 94% to 99% of peak intensities (table 4), and exhibited poor peak shape (not shown). Additionally, the liquid-liquid extraction (LLE) method described by Haslam et al. (2001;2021), followed by derivatization with TMS-DZ (Li et al., 2021) was assayed for extraction of acyl-CoAs from yeast microsomes. The extraction recovery percentages, ranging from 200% to 2000% (Table 4), may appear counterintuitive, as more acyl-CoA have been extracted in the LLE+TMS-DZ method compared to the TMS-DZ alone method. However, these results may be attributed to analytical interference in the TMS method only, or/and LLE is particularly effective for recovering acyl-CoA in yeast microsomes.

Compound	% extraction recovery		
	SPE (Trefely 2022) + TMS-DZ	SPE (Yang 2009) + TMS-DZ	LLE (Haslam 2021) + TMS-DZ
18CoA-Me	5.6	0.5	265.5
20CoA-Me	3.5	0.3	636.4
22CoA-Me	2.0	0.2	1677.6
24CoA-Me	1.1	0.2	2050.5

Table 4. Extraction recovery of internal standards based on peak area of standards in yeast matrix ratios between TMS-DZ treatment only and three different preparation methods followed by TMS-DZ treatment.

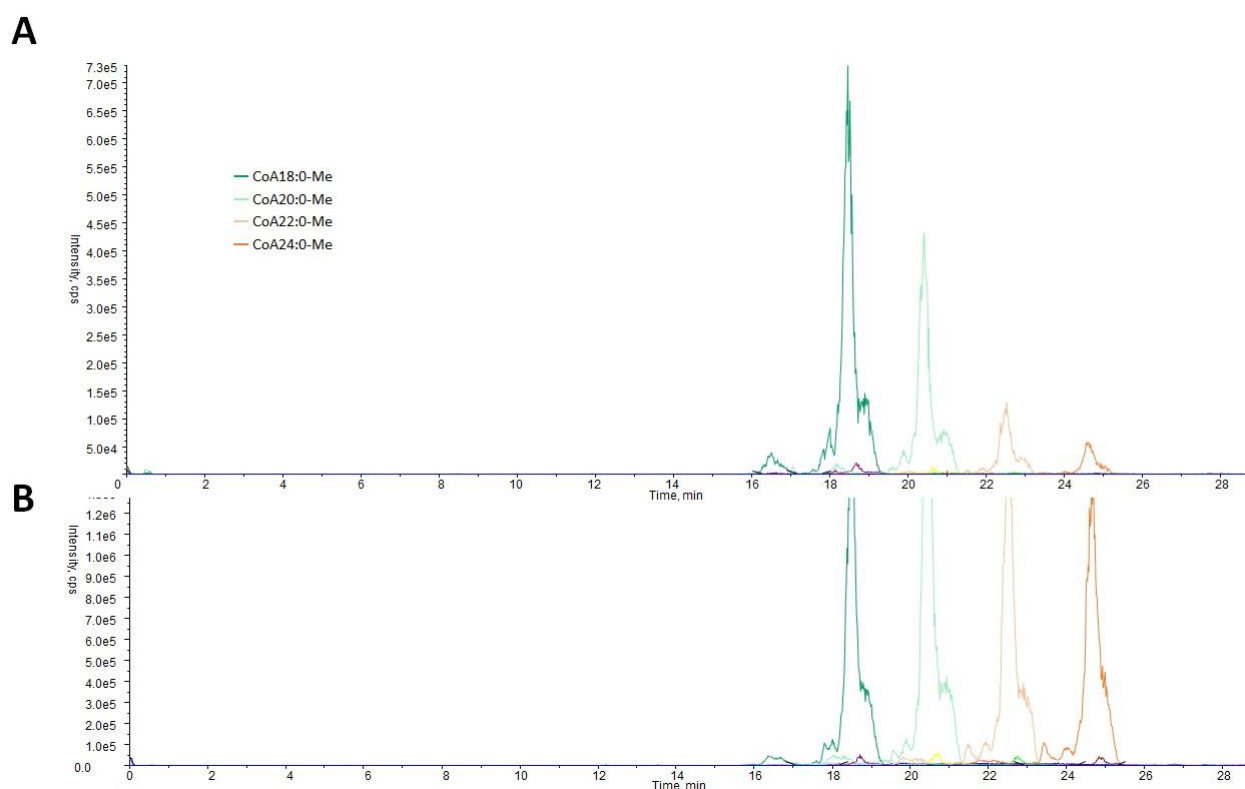


Figure 11. Chromatograms of methylated C18:0-CoA, C20:0-CoA, C22:0-CoA and C24:0-CoA in yeast matrix under HPLC condition 10 mM ammonium formate in water + 2% acetonitrile and acetonitrile + 5% 10 mM ammonium formate in water (A) derivatized with TMS-DZ (B) extracted using LLE (Haslam et al., 2021) before methylation treatment with TMS-DZ (Li et al., 2021).

Lipidomics analysis of acyl-CoAs in biological samples presents challenges due to the diversity of their acyl chains, including different chain length. Indeed, the polarity is proportional to the acyl-CoA chain length, while short-chains are highly polar, long-chain long-chain show apolarity. Furthermore, acyl-CoAs have a propensity to adhere to surfaces due to their negatively charged phosphate groups. To address this complexity, a derivatization strategy for acyl-CoAs (Li et al., 2021) was employed to improve chromatographic performance, resulting in the separation of methylated acyl-CoAs within a single RP-LC run with good peak shapes and minimal sample matrix interference. Notably, this technique eliminates the need for an acidic wash after each injection, thereby reducing analysis time and potential contamination of the LC. However, this method requires a sample preparation step prior to the methylation step due to the strong matrix effect associated with the technique. Therefore, the used of two methods, the liquid-liquid extraction developed by Haslam et al. (2021) followed by derivatization of acyl-CoA performed in Li et al. (2021), seem to recover acyl-CoAs from yeast matrix. Currently, these methods are not sensitive enough to detect elongate product from *in vitro* FAE elongation assays. Therefore, further optimization appears necessary to improve sensitivity and make them suitable for analyzing acyl-CoAs in biological samples such as leaves or *in vivo* yeast.

2.2.2. HPLC method – HPLC-UV-MS/MS

These experiments have been performed on the HPLC-UV-MS/MS of the BAYER laboratory, weed control team, under the supervision of Peter LUEMMEN and Gerlinde USUNOW. Waters Acquity UPLC H-Class UPLC system coupled with a Waters ACQUITY UPLC Tunable UV at 260 nm and Waters MS Xevo TQ-S Micro was used. Separation was performed using chromatographic column Kinetex C18 5 μ m (100 mm x 2.1 mm, 100 Å, Phenomenex)

By combining UV detection with MS/MS, HPLC-UV-MS/MS offers enhanced specificity compared to HPLC-MS/MS alone. UV detection provides initial confirmation of compound presence based on their absorbance characteristics, specifically the eluted acyl-CoA thioesters are detected by UV absorbance at 260 nm. MS–MS offers detailed structural information for precise identification. This combination allows for specific identification of compounds into complex samples.

2.2.2.1. Method validation

a. Linearity and range

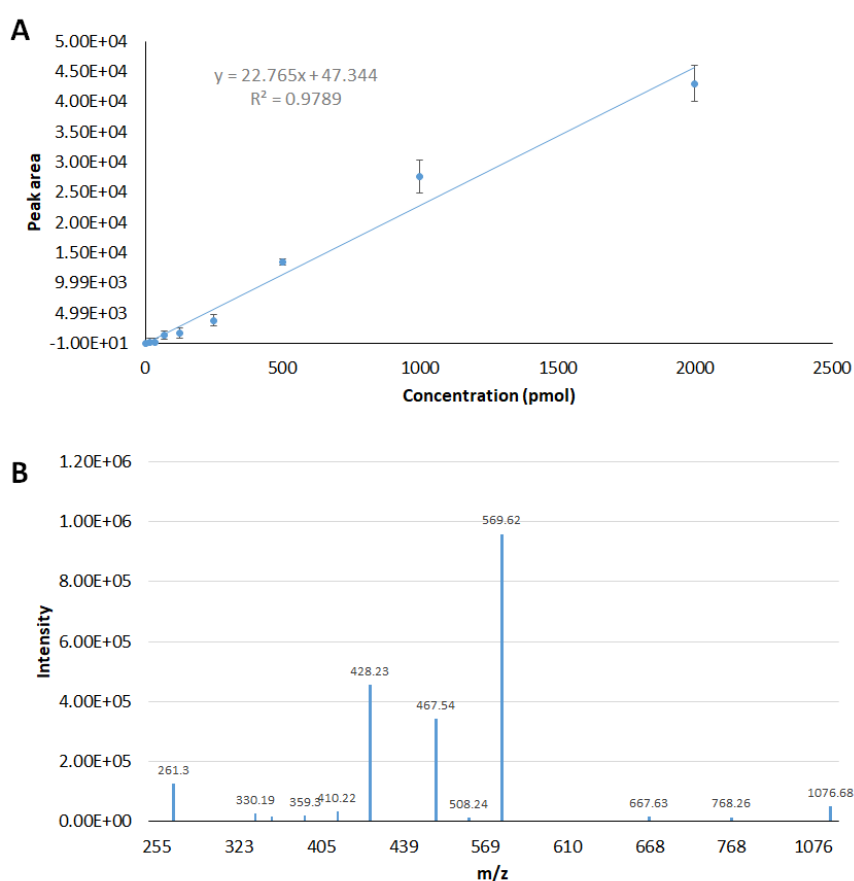


Figure 12. Analyze of 3-keto-C20-CoA (A) Calibration plot of 3-keto-C20-CoA in 1/2 (water/MeOH) (B) Spectrum of 3-keto-C20-CoA with collision energy of 45 eV.

Experiments have utilized established HPLC-UV-MS/MS parameters for the detection and quantification of 3-keto-C20:0-CoA. These parameters were previously employed in prior experiments, and they have proven to be effective for our purposes. It is worth noting that commercial 3-keto-C20:0-CoA is not available, which necessitates its synthesis (BAYER SA). In order to perform relative quantification, a calibration plot for 3-keto-C20:0-CoA and its corresponding spectrum were generated.

Five different concentrations of standard 3-keto-C20:0-CoA solution ranging from 17 to 2000 pmol were analyzed. As shown in Figure 12, the corresponding spectra were generated. The calibration graph was generated using 10 μ l injection loop and the calibration curve was established according to the response (peak area) and the concentration of 3-keto-C20:0-CoA in standard solutions. The results showed a linear relationship. Each standard concentration response was the average of three measurements. The calibration graph (Figure 12) shows a strong positive correlation ($R^2 = 0.98$) between the instrumental signal and the concentration of the 3-keto-C20:0-CoA standards.

b. Sensitivity

Sensitivity of the method was measured in terms of Limit of detection (LOD) and limit of Quantification (LOQ). The LOD and LOQ were determined by measuring the signal to noise ratio from standard low concentration of analyte compared with baseline peak. The LOD and LOQ correspond to the lowest concentration of 3-keto-C20:0-CoA giving a signal/noise (S/N) higher than 3 and 10, respectively. The LOD and LOQ were found to be 0.05 and 0.17 pmol, respectively. The coefficient of determination (R^2) of 0.99 in a linear range from 17,5 to 500 pmol.

c. Stability

3-keto-C20:0-CoA and 3-keto-C22:0-CoA were well extracted in a 1:1 mixture of water and MeOH, whereas longer acyl chains such as 3-keto-C24:0-CoA required a 1:2 mixture of water and MeOH for efficient extraction. Therefore, we utilized a 1:2 mixture of water and MeOH as the resuspension solvent for all subsequent experiments. Additionally, an assay to evaluate the stability of 3-keto-C20-CoA over time was conducted at different temperatures (Figure 13). The results indicated that 3-keto-C20:0-CoA was more stable at temperatures of 4°C or -20°C compared to room temperature. Specifically, no decrease in peak intensity was observed after 6 hours at -20°C, while a decrease in signal was observed after 24 hours at the same temperature. While peak signal decreases rapidly after 6 hours at 4°C, half of the signal was lost after 24h.

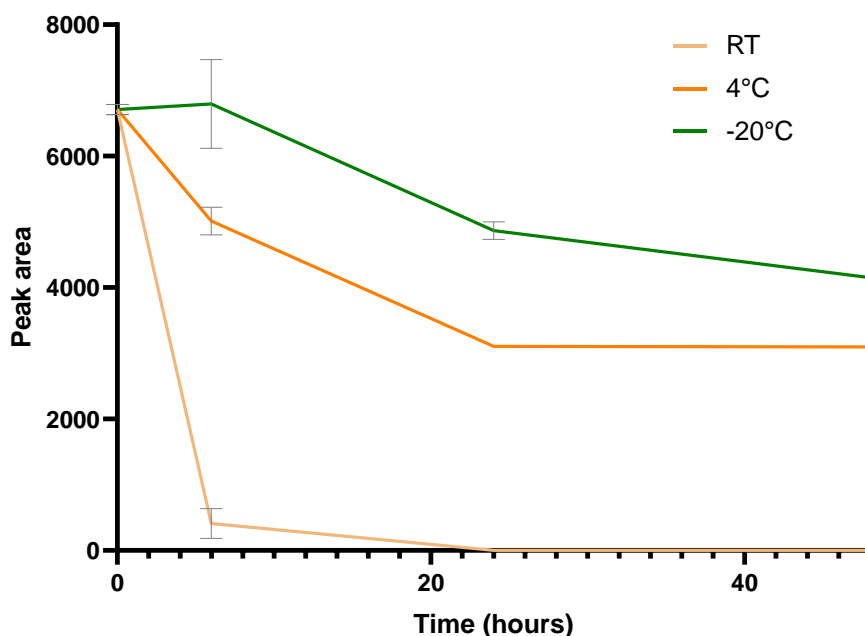


Figure 13. 3-keto-C20:0-CoA in 1:2 (H₂O/MeOH) stability test at room temperature (RT), 4°C and -20°C.

2.2.2.2. Enzyme activity

Yeast microsomes expressing KCSs were used to study the condensation activity of KCS using a diverse range of acyl-CoA substrates. The *in vitro* condensation assay was conducted using malonyl-CoA and commercially available acyl-CoAs. Indeed, the elongation cycle initiates with the condensation of malonyl-CoA with acyl-CoA, resulting in the formation of a 3-ketoacyl-CoA intermediate. This intermediate is reduced by β -ketoacyl-CoA Reductase (KCR), utilizing pyridine nucleotides (NADPH) as a reductant. The absence of NADPH from the reaction prevents the reduction of 3-ketoacyl-CoA, leading to the accumulation of the direct KCS activity product enzyme (Blacklock and Jaworski, 2006; Beaudoin et al., 2002; Ghanevati et al., 2002). However, 3-keto-acyl-CoA, an intermediate in the complex FAE reaction, is not well characterized, likely exists in small quantities and is unstable. Recently, Nie et al. (2021) investigated the binding of 3-keto-C20:0-CoA to mammalian elongation of very long-chain fatty acids elongases (ELOVL1-7), which exhibit the same condensation activity as plant KCS. They proposed a schema outlining EVOVL ping-pong mechanism, we assume that 3-keto-acyl-CoA is produced by a similar reaction using KCS (Haslam and Kunst, 2013) (Figure 14).

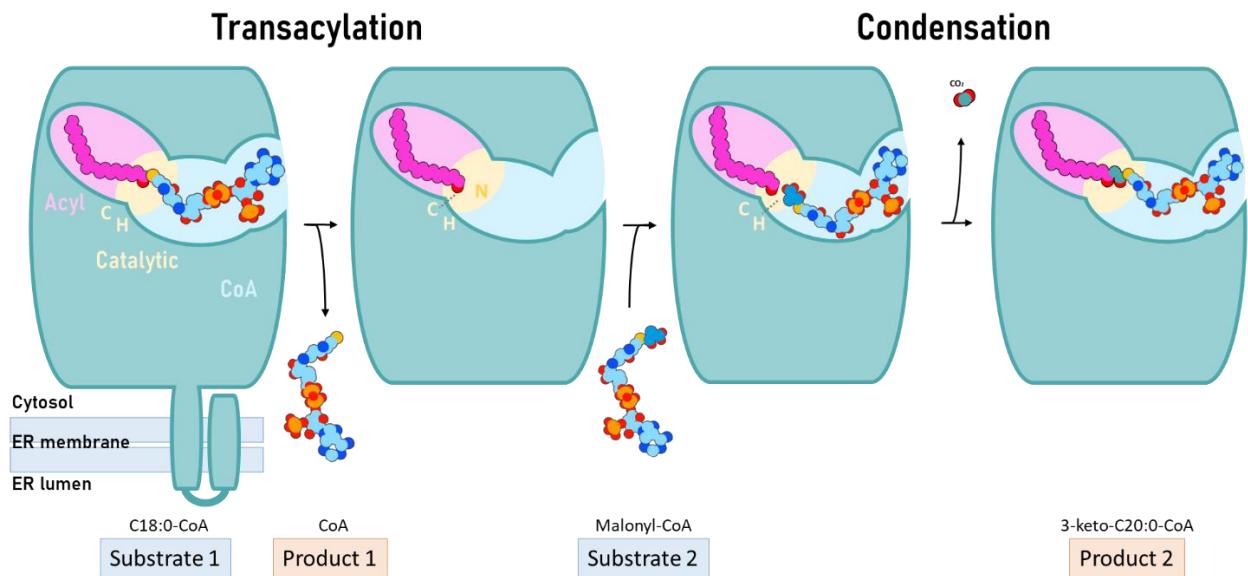


Figure 14. Suggested model of ketoacyl-CoA synthase (KCS) ping-pong catalytic mechanism modified from Haslam and Kunst (2013), and Nie et al. (2021). An acyl group is transferred from acyl-CoA on to a cysteine residue of the KCS. Decarboxylation of the malonyl-CoA driven by the catalytic histidine and asparagine residues, release of a molecule of CO₂, nucleophilic attack of the carbanion intermediate onto the C1 of the thio-acyl intermediate, led to release a β -ketoacyl product.

First, the aim of this study was to determine the best parameters for the *in vitro* KCS activity in terms of time and protein quantity. Routinely, KCS or FAE complex activity are performed for 10 to 30 minutes, and at the end of this time. Yeast proteins from microsomal fractions from 0.01 to 0.4 mg are used in assays (Table 2).

To achieve this, experiments with different reaction times, 0, 15, 30, and 60 minutes of incubation at 30°C, were conducted with three different protein quantities, 20 μ g, 40 μ g, and 60 μ g, from yeast TRIPLE $\Delta elo3$ expressing AtKCS4 (Figure 15). C22:0 acyl-CoA and malonyl-CoA were used as substrates, with a concentration of 100 μ M, as C22:0-CoA was already known to be preferred substrates of AtKCS4. The results of the study showed that 30 minutes was the optimal time for the KCS reaction, as there was more product detected with this time reaction when 40 μ g or 60 μ g of protein were used. However, the product quantity decreased after 30 minutes at 30°C with the 40 μ g or 60 μ g protein quantities, or after 15 minutes with 20 μ g. These results suggested that the 3-keto-acyl-CoA was degraded due to its sensitivity to temperature. **Therefore, for subsequent experiments, a 30-minute reaction time with 40 μ g or 60 μ g of proteins will be used, to ensure a sufficient signal for quantification.**

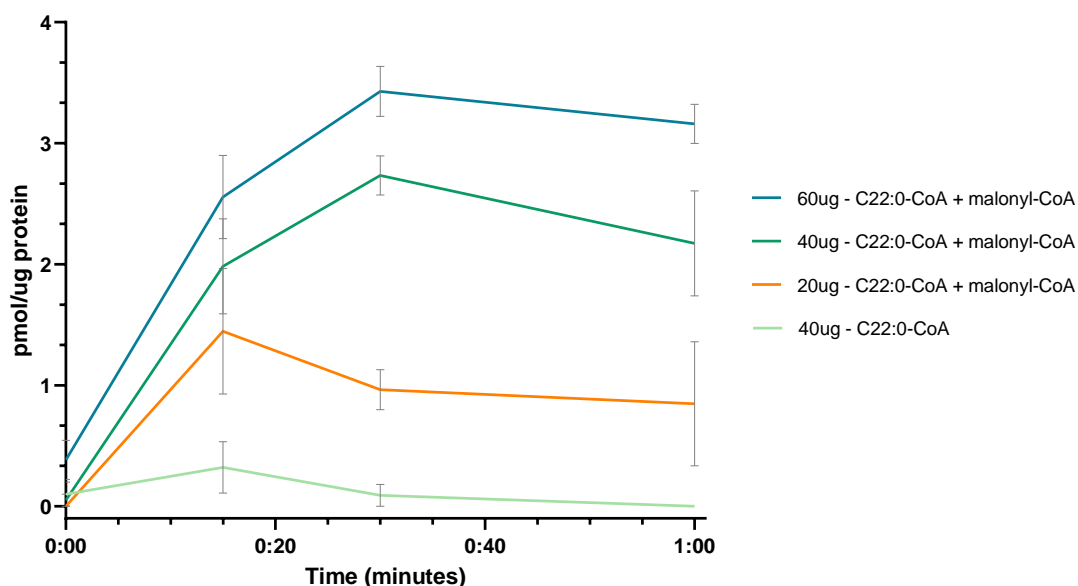


Figure 15. Selection of optimum incubation time and enzyme concentration for AtKCS4 condensation activity. 3-keto-C24-CoA product from the condensation between C22:0-CoA and malonyl-CoA was quantified. Different protein quantities (0, 20, 40, 60 μ g) were incubated with malonyl-CoA (100 μ M) and C22:0-CoA (100 μ M) in NaH_2PO_4 Buffer pH 7.2 at 30°C for 0, 15, 30 or 60 minutes. The activities are representative of experiments carried out three times.

a. Substrate specificity

We characterized the relative substrate specificity of the several KCSs identified as active in yeast in the Chapter 1 with saturated C18 and C22 acyl-CoA substrates. These particular acyl-CoAs were selected for the *in vitro* assay with dual objectives. Using the newly developed non-radiolabeled *in vitro* assay, our aim was to validate the expected activity of AtKCS enzymes, as described in the literature, and the activity of few KCSs from other plant species previously described.

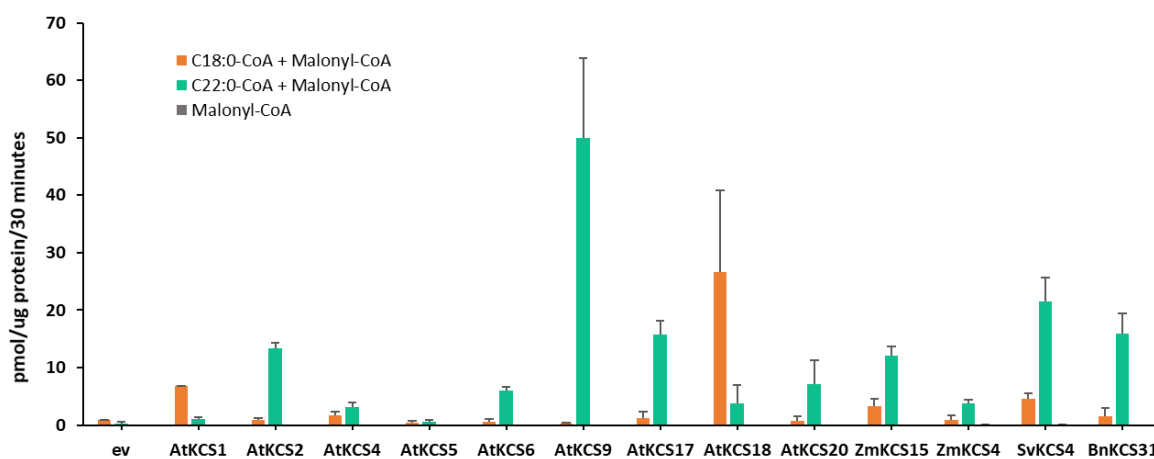


Figure 16. Condensation activity of yeast microsomes expressing different KCS. Microsomal fractions (40 μ g) were incubated with malonyl-CoA (100 μ M) and acyl-CoA (100 μ M) in NaH_2PO_4 Buffer pH 7.2 at 30°C for 30 minutes. The activities are representative of experiments carried out three times.

In this study, we characterized the relative substrate specificity of 12 KCSs, namely AtKCS1, AtKCS2, AtKCS4, AtKCS6, AtKCS9, AtKCS17, AtKCS18, AtKCS20, ZmKCS15, ZmKCS4, SvKCS4, and BnKCS31 (Figure 16). Results indicated that AtKCS18/FAE1 and AtKCS1 exhibit specificity towards acyl-CoAs with 18 carbons, with AtKCS18 displaying particularly high activity. Conversely, AtKCS2, AtKCS4, AtKCS6, AtKCS9, AtKCS17, AtKCS20, ZmKCS15, ZmKCS4, SvKCS4, and BnKCS31 enzymes preferentially utilize C22:0 CoA as substrate.

Furthermore, SvKCS4 demonstrates stronger activity compared to AtKCS4, BnKCS31, and ZmKCS4, as evidenced by the production of 3-keto-C24:0. Interestingly, AtKCS5 did not exhibit activity with either C18:0-CoA or C22:0-CoA, while AtKCS6, which shares related activity, displayed activity with C22:0-CoA.

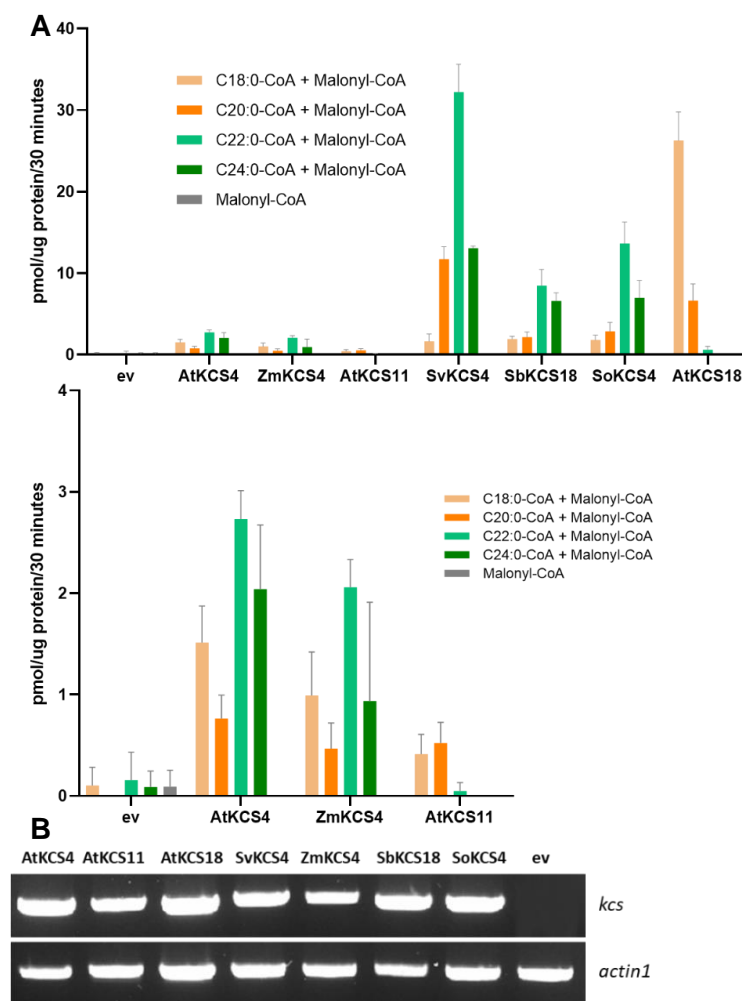


Figure 17. Condensation activity of yeast microsomes expressing different KCS. (A) Microsomal fraction (40 μ g) were incubated with malonyl-CoA (100 μ M) and acyl-CoA (100 μ M) in NaH₂PO₄ Buffer pH 7.2 at 30°C for 30 minutes. The activities are representative of experiments carried out three times. **(B)** Semi-quantitative RT-PCR analysis of steady-state KCS transcripts in INVSC1 TRIPLE Δ *elo3* transformed with the different constructs as indicated. ev corresponds to the strain transformed with the empty vector. The yeast *actin1* gene was used as a constitutively expressed control.

In our investigation, we further characterized the relative substrate specificity of six KCSs, along with AtKCS18/FAE1, utilizing a broader range of saturated acyl-CoA substrates (C18, C20, C22, C24) (Figure 17). Our objective was to confirm similar activity and substrate preferences for five KCSs from various plant species in comparison to AtKCS18/FAE1.

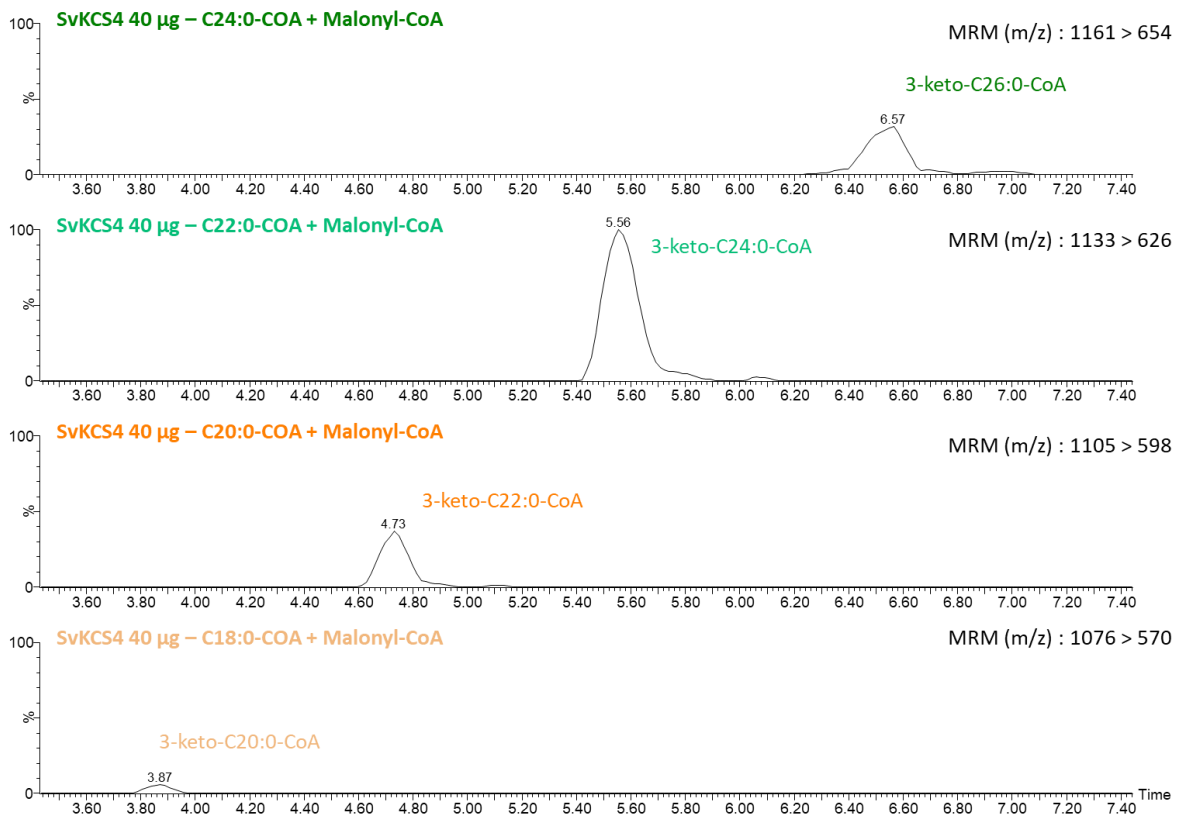


Figure 18. Representative chromatograms of 3-keto-acyl-CoA synthesized from SvKCS4 (yeast microsomes) with different acyl-CoA as substrates. Yeast microsomes expressing SvKCS4 (40 µg) were incubated with malonyl-CoA (100µM) and indicated acyl-CoA (100µM) in NaH₂PO₄ Buffer pH 7.2 at 30°C for 30 minutes.

Notably, AtKCS4 and ZmKCS4 demonstrated low activity and specificity for C22 and C24, even over C18. Conversely, KCSs from *Sorghum bicolor* and *Solanum lycopersicum*, SbKCS18 and SolyKCS4 respectively, exhibited higher activity and a preference for C22 and C24 elongation. Meanwhile, SvKCS4, the KCS from *Setaria viridis*, displayed specificity for C22-CoA elongation, producing ten times more 3-keto-C24-CoA than AtKCS4, suggesting its high activity relative to the others. Representative chromatograms of batch samples are shown in Figure 18 for SvKCS4.

In contrast to this C22 elongation specificity, AtKCS18/FAE1 demonstrates specificity for acyl-CoAs with 18 carbons, exhibiting high activity. Additionally, the chain length specificity of AtKCS11 remains unclear (Batsale et al., 2021), as our assay demonstrated very low activity, this enzyme seems to prefer to use C18- or C20-CoA as substrate.

b. Dose response-curve

To assess the sensitivity of KCSs to inhibitors, SvKCS4, SoKCS4, AtKCS4, and SbKCS18 were subjected to assays in the presence of increasing concentrations of flufenacet up to 100 μ M. Such an inhibition by flufenacet likely could involved the nucleophilic reaction of the SH group of cysteine residue in the KCS active site with flufenacet, as previously proposed for pyroxasulfone and metazachlor in several studies (Böger et al., 2000; Tanetani et al., 2011b).

Additionally, to gain further insights into the mechanism of action of flufenacet, we investigated whether the inhibition exhibited time-dependency by pre-incubating the protein and the inhibitor before initiating the elongase reaction. Previous studies have demonstrated that a 15-minute pre-incubation period is sufficient to inhibit the enzyme (Tanetani et al., 2011b).

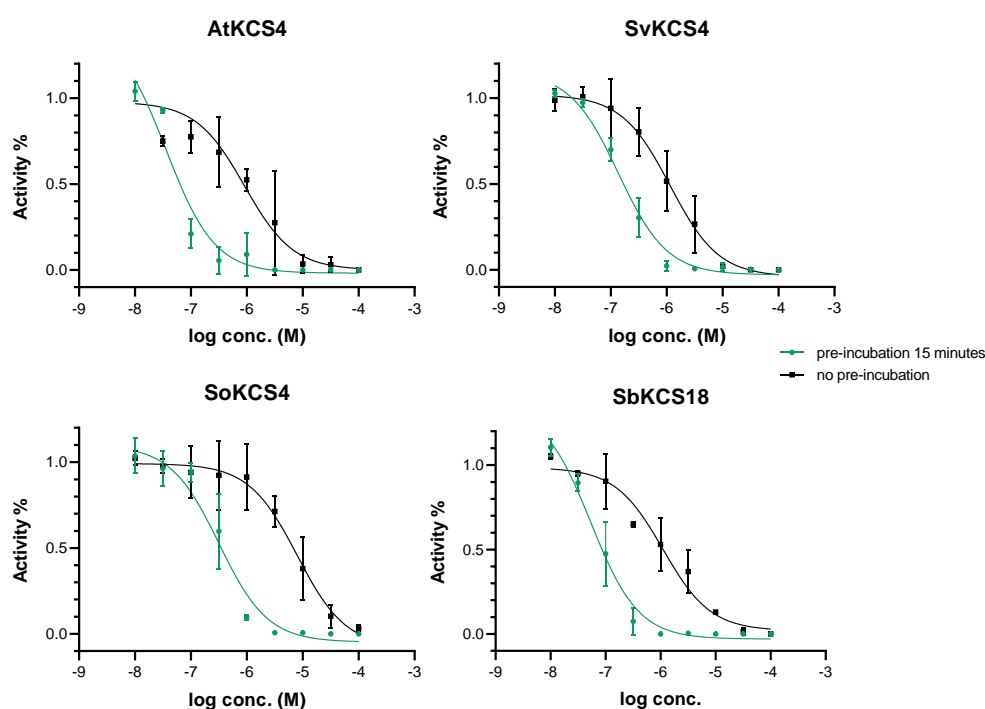


Figure 19. log-inhibitor response curves of KCS in the presence of increasing flufenacet concentration, with (green) or without (black) 15 minutes pre-incubation with yeast microsomes (60 μ g) and flufenacet. The reaction was initiated by adding malonyl-CoA (100 μ M) and acyl-CoA (100 μ M) in NaH_2PO_4 Buffer pH 7.2 at 30 $^\circ$ C for 30 minutes. The activities are representative of experiments carried out two or three times.

The dose-response curves for the four KCSs with flufenacet showed a “pre-incubation” dependent inhibition of FAE activity, as evidenced by distinct dose-response curves between the two conditions: with or without pre-incubation. The inhibition by flufenacet was more pronounced with a 15-minute pre-incubation, suggesting that the inhibition mechanism of the tested KCSs by flufenacet might be irreversible (Figure 19).

	IC50 (µM)	
	Pre-incubation 15 minutes	No pre-incubation
SvKCS4	0.14	1.15
AtKCS4	0.04	0.91
SoKCS4	0.32	7.98
SbKCS18	0.05	1.10

Table 5. IC50 values (µM) from inhibition of SvKCS4, AtKCS4, SoKCS4 and SbKCS18 with flufenacet.

Furthermore, dose response curves exhibited similarity in the absence of pre-incubation, as indicated by the IC50 calculations, suggesting the potency of the inhibitor towards the various KCS. However, SoKCS4 appeared to be less sensitive to the flufenacet compound, with its IC50 value without pre-incubation time (7.98 µM) is higher than that of the other enzymes (approx. 1 µM) (Table 5).

These results suggest that the mechanism of action of flufenacet is consistent across all tested KCSs and does not exhibit selectivity towards plants originating from either monocotyledonous or dicotyledonous species.

3. Conclusion

We have successfully developed a high-throughput, non-radioactive *in vitro* assay aimed at evaluating the activity of KCS enzymes, their substrate specificity and their inhibition by herbicides. Our first step involved improving protocols for yeast microsomes preparation, ensuring active KCS enzymes. Utilizing yeast microsomes expressing KCS from diverse species, we conducted *in vitro* enzyme assays employing an LC-UV-MS/MS method to assess substrate specificity. We were able to validate the expected activity of AtKCS enzymes already described in the literature. This assay was then used to evaluate the inhibition of KCS by herbicides belonging to the HRAC group 15. By employing yeast strains expressing a range of KCS enzymes, we could test the specificity of flufenacet inhibition regarding the origin of KCS. Our results time-dependent inhibition suggesting irreversible inhibition of KCS activity by flufenacet. Furthermore, our findings indicate that flufenacet exhibits non-selective inhibition between KCS from monocot and dicot plants. However, SoKCS4 was less responsive to flufenacet, as evidenced by its lower IC50 value. This finding are in adreement with those presented in chapter 2, which demonstrated that the SoKCS4 expressed in the yeast system *in vivo* was the only one to exhibit partial inhibition of its activity. Furthermore, this enzyme assay allows to identify mode of action following comprehensive physiological profiling and investigation of targeting pathway (Tresch et al., 2013).

In addition, we further investigated the efficient analysis of acyl-CoA using LC-MS/MS. By employing a combination of two methods (1) the liquid-liquid extraction developed by Haslam et al. (2021) and (2) the methylation of CoA group phosphates described by Li et al. (2021), we achieved greater stability of acyl-CoA molecules, resulting in improved peak shape and recovery from the yeast matrix. These methods could be further developed to enable the analysis of acyl-CoA from plant or yeast samples.

DISCUSSION & PERSPECTIVES

Discussion and perspectives

To further investigate VLCFA biosynthesis inhibitors, we employed an integrative biochemical approach that combined the functional characterization of enzymes in heterologous systems and the development of an *in vitro* assay using LC-UV-MS/MS.

Activity of KCS from various plant species

The functional and comparative analysis of the multigenic family members from various plant species, described in Chapter 1, enabled the characterization of the enzymatic activity of 21 KCS enzymes through heterologous expression in yeast.

Our computational study classified KCS homologs in the phylogenetic clades initially defined using *Arabidopsis* KCS homologs (Joubès et al., 2008), and confirmed the existence of three new monocot-specific KCS enzymes clades (clades ι , κ , and λ) (Campbell et al., 2019). We primarily investigated KCS members from clades α and ζ by expressing 28 KCS from different species in an engineered yeast strain and found that 21 were active in this heterologous system. Overall, our results showed that within clade α , the most prevalent measured activity was KCS4-like activity, which was observed with dicot and monocot species KCSs. Related KCS enzymes from *Solanum lycopersicum* and *Capsella rubella* for dicot plants (SoKCS4, CrKCS4) and *Setaria viridis*, *Sorghum bicolor*, and *Zea mays* (SvKCS4, SbKCS18, ZmKCS4, ZmKCS15) for monocots showed activities similar to the activity of AtKCS4, which elongates saturated C22 to C26 fatty acids, suggesting that the enzyme function has largely persisted across evolutionary plant speciation. BnKCS31 and CrKCS9 showed KCS9-like activity, these enzymes elongating saturated C22 to C24 and C26 fatty acids, whereas CrKCS17, which exhibits AtKCS17 activity, catalyzes the elongation of C22:0 to C24:0 fatty acids. Our results indicate that the activities of AtKCS2 and AtKCS20, which are responsible for the elongation of C20 into C22 fatty acids, were conserved across different species, such as *Brassica napus*, *Vitis vinifera* and *Triticum aestivum* (BnKCS38, VvKCS5, TrKCS2, and TrKCS20). OsKCS2 displayed high accumulation of the C26 product in the TRIPLE strain, with which is similar to the profile of AtKCS2 and AtKCS20 when expressed in TRIPLE. Moreover, we observed distinct enzyme substrate preferences with algae-derived KCS (RsKCS1 and RsKCS2) that produced saturated C20 and C22 fatty acids, displaying unique substrate specificities that do not resemble any of AtKCS. Additionally, yeast expressing two KCSs from *Sorghum bicolor* (SbKCS13 and SbKCS6), VvKCS10 from *Vitis vinifera*, and TrKCS4 from *Triticum aestivum* from α or δ clades accumulated C20, particularly C20:1, which is a characteristic of AtKCS18 activity. Although no monocot or grapevine species are present in the clade β with AtKCS18, this elongation activity is

present in many plant species across other clades. It would be interesting to consider how the activities of orthologous KCSs have diversified in other species for future research.

Molecular basis and structure of KCS enzymes

Structural and sequence comparisons of KCS4-, KCS9-, and KCS17-like activities led us to highlight potential key residues that contribute to KCS substrate specificity. We identified four potential residues in the different protein sequences, H136, T140, V166, and M170, located close to the end of the acyl chain located in binding tunnel of the enzyme, that could potentially contribute to the modification of the local hydrophobic and electrostatic properties of the enzyme, thereby affecting substrate access to the catalytic site. Domain-swap and point-mutation experiments could be performed to study the molecular determinants underlying KCS enzyme substrate specificities. Additionally, a greater understanding of the residues responsible for the elongation activity of KCS could lead to the generation of new patterns of substrate preference, or even the introduction of new substrates specificities.

The structural characterization of KCS remains a significant challenge despite extensive research efforts. Obtaining the solved structure of KCS could offer novel insights into its functional mechanisms. Strategies involving the crystallization of KCS enzyme containing substrate and product analogs could facilitate the formation of enzyme-substrate complexes for structural studies. Given that KCSs are membrane-bound proteins, their crystallization poses inherent difficulties. Recent investigations into homo- or hetero-dimer formation highlight another layer of complexity in KCS function (Huang et al., 2022; 2023a; 2023b; Kim et al., 2022), and the impact of these interactions on substrate specificity remains unknown, as exemplified by the modification of AtKCS6 activity by interaction with the CER2-like proteins (Kim et al., 2022). Structural studies could provide valuable insights into the organization of KCS and FAE complexes. As example, co-crystallization of AtKCS6 with AtKCS3 could offer valuable insights into how KCS3 modify the elongation of products generated by AtKCS6 and how KCS3 negatively regulates the plant cuticular waxes synthesis (Huang et al., 2023a).

Differential inhibition of KCS

The heterologous expression of KCS from various plant species in yeast, described in Chapter 1, allowed us to evaluate their inhibition by several herbicides, which have been already identified as inhibitors of VLCFA synthesis targeting AtKCS (Trenkamp et al., 2004; Tresh et al., 2012). In Chapter 2, we examined the potential inhibition of KCS from various plant species by different herbicides *in vivo* in our yeast systems. Benfuresate did not exhibit inhibitory effects on KCS activity, which may be

attributed to the lack of bioactivation in yeast (Trenkamp et al., 2004). Indeed, the bioactivation may take different forms, such as removing protective groups or adding functional groups (Nanbula et al., 2019) and is performed by enzymes. As example, Tanaya et al. (2013b) demonstrated that two derived compounds from thiobencarb, which have one or two extra oxygen atoms, showed more efficient inhibition of VLCFAE in barnyard millet seedling than thiobencarb. We could assume that the enzymes responsible for activation of bensuferaste are not present in yeast.

Overall, our study demonstrated that the herbicides metazachlor, flufenacet, cafenstrole, and pyroxasulfone, did not exhibit selective inhibition, as they did not differentially target KCS from different plant species or with different substrate-specificity. While most KCS enzymes were significantly inhibited, related KCS also showed differential inhibition when treated with K3 herbicides, despite their recent divergence. Two enzymes, SoKCS4 and SbKCS18, showed only partial inhibition by flufenacet and metazachlor, respectively. The determination of IC50 values provide additional quantitative information about the effects of the inhibitors on different enzymes. Only slight differences in inhibition were found between ZmKCS4, SvKCS4, and AtKCS4 with metazachlor, while the newly developed GIB E herbicides inhibited less SvKCS4 than ZmKCS4 and AtKCS4.

Investigate the inhibition mechanism of group 15 herbicides

The development of a high-throughput *in vitro* assay, as described in Chapter 3, allows us to quickly and accurately evaluate the inhibitory potency of herbicides against KCS without using radioactivity. This innovative assay revealed that flufenacet effectively inhibits KCS from both monocot and dicot plants, although the enzyme SvKCS4 exhibited a lower degree of inhibition. The time-dependent nature of this inhibition suggests that flufenacet irreversibly inhibits KCS activity. This irreversible inhibition of VLCFAE is probably due to a nucleophilic reaction between the SH group of a cysteine residue in the enzyme active site and the herbicide metazachlor, as proposed by Böger et al. (2000) and Eckermann et al. (2003). Considering the evolutionary conservation of the cysteine residue in the catalytic site of KCS, it is hypothesized that Group 15 herbicides might not exhibit selective inhibition towards KCSs.

Interestingly, this irreversible inhibition mechanism is not shared by all herbicides. For instance, pyroxasulfone and fenoxasulfone were found to reversibly inhibit a VLCFAE from rice. These results suggest another inhibition mechanism for plant VLCFAEs by isoxazoline-type herbicides. Specifically, pyroxasulfone showed an irreversible inhibition of the VLCFAE activity of recombinant Arabidopsis KCS18/FAE1, whereas the herbicide inhibited the VLCFAE activity of recombinant rice Q6F365 in a reversible manner. This indicates that pyroxasulfone might not react with the SH group of the cysteine

residue in the active center of Q6F365, highlighting a new inhibition mechanism (Tanetani et al., 2011b). This difference is presumed to be due to variations in enzymes conformation or in substrate specificity between KCS18/FAE1 and Q6F365 (Tanetani et al., 2011b; Tanetani, 2012). Chen et al. (2022) found that KCS inhibition could be easily modified by few substitutions, and using a fusion between PtKCS1 and 2, they showed that substrate specificity could be uncoupled from fentrazamide sensitivity. Because KCSs are likely covalently inhibited by K3 herbicides, it is possible that the properties of the active site pocket could change without affecting the terminal end of the VLCFA binding tunnel (Eckermann et al., 2003). Understanding the molecular basis of this inhibition could be useful to develop herbicides that target specific KCSs by analyzing structure-activity relationships. The co-crystallization of KCSs with different K3 herbicides would also help to show the binding site and determine whether they act through covalent inhibition.

Future *in vitro* assays will be crucial to determine whether the differences in inhibition mechanisms, whether reversible or irreversible, are correlated to variations in herbicidal efficacy in plants. Understanding these differences will enhance the ability to design herbicides with optimized effectiveness and species-selectivity.

Limitations

Studies of FAE are compromised by the redundancy of the activity, and the problems of solubilization, and purification of the membrane-associated KCS enzymes. Notably, the production of the Arabidopsis single-KO mutant is not relevant to elongation activity due to KCS redundancy activities. Heterologous expression in yeast has a limitation in that it may not always accurately reflect the activity of KCSs or their inhibition compared to what could be observed *in planta*, due to the absence of certain plant-specific cofactors that are necessary for the activity of KCS enzymes. To study KCS activity *in planta*, transient transformation of *Nicotiana benthamiana* leaves with AtKCS can provide plant co-factors and a closer cell/membrane environment as performed in Batsale et al., 2023.

However, the effects of inhibitors observed *in vitro* or *in vivo* may also vary and not be representative of what can happen *in planta* for several reasons. For example, pyroxasulfone showed less effect on the elongation of C24:0 into C26:0 using maize microsomes than using rice microsomes (Tanetani et al., 2011b), whereas in our study, we did not observe any difference in inhibition with pyroxasulfone between KCS from maize and rice expressed in yeast. This discrepancy could be due to differences in protein conformation between plant species, which may affect the access of the inhibitor to the active

site of the enzyme. Crystallization experiments of KCS proteins with various K3 herbicides could elucidate the binding sites and determine whether inhibition is due to covalent binding and how protein conformation can modulate this inhibition.

We also can hypothesize that the herbicide bioavailability is influenced by the plant species. Indeed, the bioavailability of herbicides, which refers to the ability of the compound to be absorbed by the plant in its active form, remains poorly understood. Nègre et al. (2006) have examined the bioavailability of one herbicide from group 15 herbicides, prosulfocarb. They demonstrated that the type of soil can affect the absorption of this compound by *Lolium multiflorum*. Furthermore, the bioavailability of a molecule is influenced by multiple factors, such as the properties of the soil, the type of soil microorganisms, the molecule itself, or the presence of surfactants (Kanissery et al., 2019).

Additionally, a reduction in flufenacet efficacy due to enhanced glutathione transferase (GST) activity has been described in a few plant species, such as black-grass (*Alopecurus myosuroides* Huds.) populations (Dücker et al., 2020). Flufenacet can also be detoxified by glutathione conjugation, as shown by Dücker et al. (2019).

The necessity of comparing *in vivo* or *in vitro* studies with *in planta* assay cannot be overstated. This is crucial in determining the real impact of herbicides on plants, particularly with regards to selectivity and potency.

Overall, this thesis led to the development of high-throughput *in vitro* assay substrates for evaluating KCS activity and their selective inhibition. To achieve this objective, a collection of yeasts expressing various plant-derived KCS with distinct substrate specificities was produced. This collection serves as a resource for the *in vitro* evaluation of KCS targeted by HRAC group 15 herbicides or newly developed herbicides by Bayer SA.

MATERIALS & METHODS

Materials and Methods

Chemical compounds

Benfuresate, metazachlor, flufenacet compounds were acquired from Sigma-Alrich (Saint-Louis, USA). Pyroxasulfone was obtained from Combi-Blocks and cafenstrole was procured from Atlantic Research Chemicals Ltd. Stock solutions of these compounds at 100 mM were prepared in DMSO.

Phylogenetic analysis of plants FAE enzymes

Protein sequences of the KCS from six monocotyledonous and five dicotyledonous plant species were gathered from UniProt. Monocotyledonous species included *Setaria italica* (Si), *Setaria viridis* (Sv), *Zea mays* (Zm), *Oryza sativa* (Os), *Sorghum bicolor* (Sor), *Triticum aestivum* (Tr). Dicotyledonous species comprised *Arabidopsis thaliana* (At), *Solanum lycopersicum* (Soly), *Vitis vinifera* (Vv), *Capsella rubella* (Bras), and *Brassica napus* (Bn). Additionally, alga species included *Raphidocelis subcapitata*, *Chlamydomonas reinhardtii*, and *Volvox carteri*. Then, MUSCLE alignment of the protein sequences was performed using MEGA11 software, and a neighbor-joining tree with 1000 bootstraps was constructed.

Yeast genetics

Following the CRISPR-Cas9 method described by Batsale et al. (2023), coding sequences of *Arabidopsis* genes *KCR*, *PAS2/HCD*, and *ECR* were introduced into the *Saccharomyces cerevisiae* yeast genome replacing the coding sequences of *IFA38* (YBR159W), *PHS1* (YJL097W), and *Tsc13*(YDL015C), respectively, to create the TRIPLE yeast strain. The TRIPLE strain was further used to generate the TRIPLE $\Delta elo3$ strain by deleting the endogenous *ELO3* gene.

DNA constructs

Non-*Arabidopsis* DNA fragments listed in Table 1 were synthesized by AZENTA and Invitrogen in the destination vectors pU-GW-Kan and pDONR221, respectively, and transferred into pVT-Leu DESTINATION vectors (Karimi et al., 2002; Dittrich-Domergue et al., 2014) using LR clonase (Invitrogen). TRIPLE and TRIPLE $\Delta elo3$ *Saccharomyces cerevisiae* cells were transformed with these constructs using the standard lithium acetate transformation protocol (Gietz et al., 1995) and grown on SD-L solid medium (Synthetic Defined Medium minus leucine). *Saccharomyces cerevisiae* cells were transformed with *Arabidopsis thaliana* constructs as described in Batsale et al. (2023).

Yeast gene expression analysis by RT-PCR

RNA was extracted from *Saccharomyces cerevisiae* using the RNeasy mini kit (Qiagen), and purified RNA was treated with DNase I. First-strand cDNA was synthesized from 1 µg of total RNA using SuperScript Reverse Transcriptase II (Invitrogen) and oligo(dT)₁₈. Semi-quantitative PCR was performed using Q5[®] High-Fidelity DNA Polymerase (New England Biolabs, Evry, France). PCR amplification was performed using the gene-specific primers listed in Table 2.

Heterologous Expression and Inhibition of plant VLCFA Elongases in Yeast

Transformed yeast cells were grown for 72 hours at 30°C in 1mL of SD-L liquid medium with 2% glucose, pelleted, and washed in 1mL of distilled water. Fatty acid composition was analyzed (see Analysis of Fatty Acids) and compared with that of cells transformed with empty pVT-Leu vector. In instances where elongase activity was observed, inhibition was tested in a fresh 1-ml culture by adding K3 or N herbicides to final concentrations of 1mM, 10mM or 100 M at the time of induction. After 72 hours of incubation, cells were processed as described above, and fatty acid composition was compared with that of cells expressing the same elongase grown in the absence of herbicide. Strain growth analyses, were performed using a SPECTROstar Nano microplate reader (BMG LABTECH, Champigny sur Marne, France), maintained at 30 °C, and yeast growth was monitored by measuring OD₆₀₀ every 30 min.

Microsomal fraction preparation (Adapted from Yang et al., 2010 and Liu et al., 2017)

Yeast transformants were first grown in 2 mL of Synthetic Defined medium-Leucine liquid medium with 2% glucose for 24 hours at 30°C. Subsequently, the cells were suspended in 100 mL medium for 24 h at 30 °C aiming for a final OD₆₀₀ of 6 to 10. Yeast cells were harvested (6000 g/5 min/04 °C), washed with ice-cold 20 mM Tris·HCl distilled water (pH 7.9), and centrifuged again (6500 g/10 min/04 °C). The pellets were then resuspended in lysis buffer (20 mM Tris·HCl (pH 7.9), 10 mM MgCl₂, 1 mM EDTA, 5% (vol/vol) glycerol, 1 mM DTT, 0.3 M ammonium sulfate) for disruption with glass beads using a QIAGEN Tissue lyser (frequency: 30/s; 3 × 1 min). The lysat was recovered from glass beads (710-1180 µm), and cell debris were removed from the suspension by centrifugation (6500 g/10 min/04°C). The supernatant was further centrifuged at 110,000 g for 2 hours at 4 °C (Sorval/TH641). The resulting microsomal membrane pellets were suspended in 0.5 mL of storage buffer (50 mM HEPES pH 6.8, 1mM DTT, and 2% glycerol). Protein concentrations were determined using the Bio-Rad protein assay reagent. All these steps were performed at 4 °C/on ice. The microsomal suspensions were stored at -70 °C until the enzyme assay.

Western

Equal amounts of proteins were prepared and denatured using Laemmli buffer, loaded onto a 10% SDS-PAGE and subsequently analyzed by western blot. Detection of AtKCS20-Myc Tag was performed using a mouse anti-Myc-tag antibody at a dilution of 1/5000, followed by incubation with a goat anti-mouse second antibody at a dilution of 1/10000.

Lipid analysis

Analysis of Fatty Acids

Fatty acid methyl esters (FAME) were obtained by transmethylation at 85°C for 2 hours in 1 mL of 0.5 M sulphuric acid in methanol containing 2% (v/v) dimethoxypropane and 20 µg of heptadecanoic acid (C17:0) as an internal standard. After cooling, 1 mL of 2.5% (w/v) NaCl was added, and FAME molecules were extracted in 300 µL of hexane for subsequent analysis using a gas chromatograph (7890A, Agilent, Waldbronn, Germany) equipped with an HP-5MS column (30 m x 0.25 mm x 0.25 mm, Agilent) coupled with mass spectrometry (MS) (5975B insert MSD, Agilent, Waldbronn, Germany). The initial temperature of 50°C was held for 1 min, increased at 25°C.min⁻¹ to 210°C, increased at 10°C.min⁻¹ to 306°C, increased again at 65°C.min⁻¹ to 320°C, and held for 3 min at 320°C, with helium as carrier gas for a total run time of 21 minutes. Data collection and processing were carried out using Agilent MassHunter software. The proportion of each FAME was calculated based on individual and total peak areas of the FAMEs. Quantitative analyses were conducted using an Agilent 7890A gas chromatograph equipped with an Agilent HP-5MS column and flame ionization detector. The same GC program was used, with hydrogen (1.5 mL.min⁻¹) as the carrier gas. Acyl chain quantities were determined relative to the intensity of the peak associated with the quantity of heptadecanoic acid (C17:0).

Elongase activity assays (FID)

Total elongase activity was assessed in a 100 µL volume containing 50 mM HEPES, pH 6.8, 1 mM MgCl₂, 1 mM NADPH, 1mM NADH, 0.5 mM dithiothreitol (DTT), 30 to 60 µM Malonyl-CoA and 0 to 100 µM Acyl-CoA at 30 °C during 1 hour with agitation. The reaction was initiated by the addition of 0.1 mg of microsomal protein from yeast. The reaction is stopped by addition of 4 mL of methanol / 2,5% H₂SO₄ and heating at 85 °C for 2h. Following addition of 2 mL of NaCl 2,5%, FAMES were extracted into 200 µL of hexane. 100 µL of hexane was added, without blown down, 50 µL of hexane was been loaded to quantify FAMES by GC-FID

Acyl-CoA analysis on HPLC-UV-MS/MS

Elongase activity assays

Total elongase activity was measured in a volume of 100 μL containing 10 mM Phosphate sodium (NaH_2PO_4 , Na_2HPO_4) pH 6.8, 10 μM Malonyl-CoA, 10 μM Acyl-CoA, 2% DMSO at 30 $^\circ\text{C}$ during 30 minutes. The reaction was initiated by the addition of 20 to 60 μg of microsomal fraction from yeast expressing KCS gene. The reaction is stopped by addition of 200 μL of methanol, followed by a vortex step of 30 seconds. The samples were centrifuged (13000 g / 2 min), the supernatant was transferred into vials with inserts for LC-MS/MS analysis.

HPLC-UV-MS/MS analysis

The LC-MS/MS analysis was conducted using a Waters Acquity UPLC H-Class UPLC system coupled with a Waters ACQUITY UPLC Tunable UV at 260 nm. Separation was achieved with a Kinetex C18 5 μm chromatographic column (100 mm x 2.1 mm, 100 \AA , Phenomenex) and an ACQUITY UPLC CSH C18 VanGuard precolumn (5 mm x 2.1 mm, 1.7 μm , 130 \AA) (Waters, Milford, MA). The mobile phase A consisted of 10 mM ammonium acetate in water at pH 8.5. The mobile phase B was acetonitrile. Gradient elution (0.0 min, 40% B; 8 min, 95% B; 8.50 min, 95% B; 9 min, 40% B; 12 min, 40% B) was performed at a flow rate of 0.3 mL/min, the injection volume was set at 10 μL and a constant column temperature of 35 $^\circ\text{C}$ was maintained. Acyl-CoA detection was carried out using a Waters Xevo TQ-S micro mass spectrometer operated with ESI probe. Positive electrospray ionization (5500 V) was applied, using nitrogen as desolvation and nebulizing gas. Argon was used as collision gas for fragmentation. Source and desolvation temperatures were set at 150 and 350 $^\circ\text{C}$, respectively. The gas flow to the cone was adjusted at 1 L h^{-1} and the gas desolvation flow at 750 L h^{-1} . Ion transitions, retention times, and compound dependent parameters for all acyl-CoAs are summarized in Table 3. Data was collected and processed by MassLynx 4.1 software.

Acyl-CoA analysis on HPLC-MS/MS

Extraction (adapted from Haslam 2021)

The samples with a volume of 100 μL were washed from lipids with 200 μL of 1:1:0.3 isopropanol/water/petroleum ether. After 2-3 sec vortex to mix, the phases were separated using a low-speed centrifuge (2 g/30 sec) and the upper phase was transferred to waste. This washing step was repeated 3 to 4 times. Subsequently, 5 μL of saturated $(\text{NH}_4)_2\text{SO}_4$ was added to aqueous phase

(containing CoA's). Then, 600 μ l of 2:1 MeOH/CHCl₃ was added, mixed and incubated at room temperature (23°C) for 20 minutes. Following a centrifugation step(17000 g/2mins), the samples were dried under N₂ in an evaporator for approximately 2-3 hours.

Derivatization (adapted from Li et al., 2021)

Dried extracts were reconstituted with 100 μ L of methanol, and 100 μ L of TMS-DM (Trimethylsilyldiazomethane, 2 M in hexane) were added. The solutions were gently mixed. The reaction mixture was incubated for 30 min at room temperature (23°C). Subsequently, 5 μ L of acetic acid was added to stop the reaction, resulting in a visible color change. The samples were dried under N₂ in an evaporator. The dried samples were initially reconstituted with 50 μ L of MeOH. Full recovery of the dried matter was facilitated by a 1-minute sonication. Then, 50 μ L of H₂O was added, followed by 1-minute sonication step. The sample was transferred into vials with inserts for LC-MS/MS analysis.

HPLC-MS/MS analysis

The analysis of methylated and unmethylated acyl-CoA was conducted using a high performance liquid chromatography system (1290 Infinity II, Agilent) coupled to a QTRAP 6500 mass spectrometer (Sciex). The chromatographic separation of acyl-CoA was achieved on a reverse phase Kinetex C18 5 μ m (50 mm x 2.1 mm, 100 Å, Phenomenex). Mobile phase A consisted of water at 10mM ammonium formate and 2% acetonitrile, mobile phase B was acetonitrile with 5% water at 10mM ammonium formate at a flow rate of 0.2 mL/min. A 10 μ L sample was injected and the percentage of solvent B during the gradient elution was as follows : 0-1 min, 50%; 28 min, 100%; 28.1 min, 100%, 29.9 min, 100%; 30 min, 50%. The column temperature was maintained at 35°C. Nitrogen was used for the curtain gas (set to 35), gas 1 (set to 40), and gas 2 (set to 40). Mass spectrometry analysis was performed in the positive ionization mode. Needle voltage was at +5500 V with source heating at 200°C; the dwell time was set to 10 ms. The collision gas was also nitrogen; collision energy (CE) was set between 50 to 58 eV according to the lipid classes (Table 4).

Statistical analysis

The Tukey's post hoc test was conducted using RStudio to determine whether statistically significant effects were observed among the data under different conditions. The reported values represent means \pm standard deviations (SD) of 3 to 5 independent replicates.

Vecteur	pDONR	Gene
pvtLEU (v55)	pDONR221:KCS1-myc(Cter)	At1g01120
pvtLEU (v55)	pDONR221:KCS2-myc(Cter)	At1g04220
pvtLEU (v55)	pDONR221:KCS3-myc(Cter)	At1g07720
pvtLEU (v55)	pDONR221:KCS4-myc(Cter)	At1g19440
pvtLEU (v55)	pDONR221:KCS5-myc(Cter)	At1g25450
pvtLEU (v55)	pDONR221:KCS7-myc(Cter)	At1g71160
pvtLEU (v55)	pDONR221:KCS8-myc(Cter)	At2g15090
pvtLEU (v55)	pDONR221:KCS9-myc(Cter)	At2g16280
pvtLEU (v55)	pDONR221:KCS10-myc(Cter)	At2g26250
pvtLEU (v55)	pDONR221:KCS11-myc(Cter)	At2g26640
pvtLEU (v55)	pDONR221:KCS12-myc(Cter)	At2g28630
pvtLEU (v55)	pDONR221:KCS13-myc(Cter)	At2g46720
pvtLEU (v55)	pDONR221:KCS14-myc(Cter)	At3g10280
pvtLEU (v55)	pDONR221:KCS15-myc(Cter)	At3g52160
pvtLEU (v55)	pDONR221:KCS16-myc(Cter)	At4g34250
pvtLEU (v55)	pDONR221:KCS17-myc(Cter)	At4g34510
pvtLEU (v55)	pDONR221:KCS18-myc(Cter)	At4g34520
pvtLEU (v55)	pDONR221:KCS19-myc(Cter)	At5g04530
pvtLEU (v55)	pDONR221:KCS20-myc(Cter)	At5g43760
pvtLEU (v55)	pDONR221:KCS21-myc(Cter)	At5g49070
pvtLEU(V55)	pDONR221:SvKCS4	SEVIR_3G144700v2
pvtLEU(V55)	pDONR221:SiKCS4	SETIT_024438mg
pvtLEU(V55)	pDONR221:ZmKCS15	GRMZM2G160417
pvtLEU(V55)	pDONR221:ZmKCS4	GRMZM2G393897
pvtLEU(V55)	pDONR221:BnKCS31	BnaA07g03590D
pvtLEU(V55)	pDONR221:BnKCS18	BnaA06g13650D
pvtLEU(V55)	pDONR221:BnKCS38	BnaC05g02350D
pvtLEU(V55)	pDONR221:BnKCS20	BnaA02g22340D
pvtLEU(V55)	pDONR221:SiKCS2	SETIT_026198mg
pvtLEU(V55)	pDONR221:SvKCS2	SEVIR_8G178500v2
pvtLEU(V55)	pDONR221:OsKCS2	BGIOSGA018233
pvtLEU(V55)	pDONR221:OsKCS4	BGIOSGA017543
pvtLEU(V55)	pDONR221:RsKCS1	GBF96892
pvtLEU(V55)	pDONR221:RsKCS2	GBF91682
pvtLEU(V55)	pDONR221:RsKCS3	GBF94153
pvtLEU(V55)	pDONR221:KCS6-myc(Cter)	At1g68530
pvtLEU(V55)	pU-GW-Kan CrKCS17	CARUB_v10006212
pvtLEU(V55)	pU-GW-Kan CrKCS4	CARUB_v10015226
pvtLEU(V55)	pU-GW-Kan CrKCS9	CARUB_v10011929
pvtLEU(V55)	pU-GW-Kan SoKCS4	Solyc04g080450
pvtLEU(V55)	pU-GW-Kan SbKCS6	SORBI_3001G453200
pvtLEU(V55)	pU-GW-Kan SbKCS18	SORBI_3009G236100
pvtLEU(V55)	pU-GW-Kan TrKCS20	TraesCS7B02G254900
pvtLEU(V55)	pU-GW-Kan TrKCS02	TraesCS6B02G207000
pvtLEU(V55)	pU-GW-Kan TrKCS04	TraesCS1B02G436300
pvtLEU(V55)	pU-GW-Kan VvKCS16	Vitvi14g01198
pvtLEU(V55)	pU-GW-Kan VvKCS5	Vitvi05g00616
pvtLEU(V55)	pU-GW-Kan VvKCS10	Vitvi18g00969
pvtLEU(V55)	SorKCS4 in PST	SORBI_3004G086800

Table 1. Genes list

Oligo Name	Sequence (Do not include 5' and 3' mods in the sequence field)
BnKCS46.AS.ATT	TTATCTGGATTGAGAACTGGAAGAAACCAAAGA
BnKCS46.S.ATT	ATGAACGAAAACCATATCCAGTCCGC
BnKCS18.AS.ATT	TTAGTAGGACAAGGTAAGTGGTACTTATCAATG
BnKCS18.S.ATT	ATGGATGGTGCTGATGGTAATGGTTC
BnKCS31.AS.ATT	TTAGAAGTCCAGTTTACTGGGTATCTATCAATAG
BnKCS31.S.ATT	ATGGTGGTTCGGTCAAATCCAAAAC
BnKCS38.AS.ATT	TTAAGAGGAAGTAAGTGGAGTAATTCTTGGAACAG
BnKCS38.S.ATT	ATGACCCAAAATCAAGATCAACCACATAGAC
BsKCS04.AS.ATT	CCCATGGAGAAGAAACAGATGGTTTAAACATTATG
BsKCS04.S.ATT	ATGGAAGCTGCTAATGAATCTGTTAATGGTG
BsKCS09.AS.ATT	CCCATGGAGAATTATTAGATGGTTTAAACATGTCTCA
BsKCS09.S.ATT	ATGGATGGTGCTGGTGAATCTAGATCTG
BsKCS17.AS.ATT	GCCATGGATTATTAACAGATGGTTTAAACATCTCTC
BsKCS17.S.ATT	ATGGACGCTTTAAATTACGTCAAAGAGGTT
OSKCS02.AS.ATT	TTAAGAAGAAGCAGCATCAGCAGTAGC
OSKCS02.S.ATT	ATGAAGTTGTTGTACCATCACGCTATTCTAAC
OSKCS04.AS.ATT	TTATGAGTAGCAAACCGTCAACCAATTCAA
OSKCS04.S.ATT	ATGGTGGTGATGCTGCTGCAG
RsKCS01.AS.ATT	TCATCTTTTCGATGTCGAAACCTTCCC
RsKCS01.S.ATT	ATGTTGAGAGTTGGTCAATTGCATGC
RsKCS02.AS.ATT	TACACTTGAACCCAGAACCGAAACCTAA
RsKCS02.S.ATT	ATGTTGAGAGTCGGTCAATTGTCTGC
SIKCS02.AS.ATT	TTAAGATTGCGCAGCGCGCG
SIKCS02.S.ATT	ATGTCTGCTGCTCAACAAGCTGAA
SIKCS04.AS.ATT	TTATGAGTTGGAACACCGTCAACCAATT
SIKCS04.S.ATT	ATGAACGGTGGTACTGTTCAATCTGC
SoKCS4.AS.ATT	TTCCCATGGACCATCAGGAGATGG
SoKCS4.S.ATT	ATGGTGCTACTGGTACTCAAGTTAATACTGC
SbKCS13.AS.ATT	AATTTTCATCCATCCATGGATTAGTTTCTTTCAGCA
SbKCS13.S.ATT	ATCTAGACAGTTGCCGGATTTTCAACAATCT
SbKCS18.AS.ATT	ATACAATCTTCCCATGGATTATCAGGAGATGG
SbKCS18.S.ATT	ATGAATGGTGGTGCTGCTCCAC
SbKCS6.AS.ATT	TCCCATGGACCATTAGTTGGAGTTTAAATAGATC
SbKCS6.S.ATT	ATGCCAACTGGGGGTGTTTTAGTG
SVKCS02.AS.ATT	ATGTCTGCTGCTCAACAAGCTGAA
SVKCS02.S.ATT	TCAGCTGCAGCAGCAGCG
SVKCS04.AS.ATT	TCATTGTTGAGCTTTGTGTGTTGGAACA
SVKCS04.S.ATT	ATGAACGGTGGTACTGTTCAATCTGC
TrKCS04.AS.ATT	TCAACAGGAAATCTATCAATTTTCATCAGCCC
TrKCS04.S.ATT	ATGGATTCTCCTGCTCCAAATGCTG
TrKCS02.AS.ATT	GGAACATCAACAGGAAAAGTATCAATTCATCCA
TrKCS02.S.ATT	ATGTCTATGGAAGATTCTACTCCACCTGC
TrKCS20.AS.ATT	CAACAGGATATCTATCAATACAATCATCCCATGGA
TrKCS20.S.ATT	ATGAATGGTGGTATTGCTCCACCAC
VvKCS5.AS.ATT	TCCATCCATGGATTTTTTTCTTTAACAGGATCAAT
VvKCS5.S.ATT	ATGGGTGATGAAAAAGAATCTTTGGGTACTTC
VvKCS10.AS.ATT	TGGACCATTTCTAGATGGTTGAACATGTCT
VvKCS10.S.ATT	ATGGATACTGAAATTCCTGGTGGGGG
VvKCS16.AS.ATT	AGCCCATGGACCATCAGTTGGA
VvKCS16.S.ATT	ATGCCGAATTTCTCCTCTGTTAAACT
ZMKCS015.AS.ATT	TCATTGATGTGCTGGAAAACCGTCA
ZMKCS015.S.ATT	ATGGTGGTGCTGCTCCACC
ZMKCS04.AS.ATT	TCACTGTTGAGTTGGAAAACCGTCAA
ZMKCS04.S.ATT	ATGGTGTCTGCTCCACCACC

Table 2. Primers list

Q1 [M+H] ⁺	Q3 [M+H] ⁺	ID	Dwell time (ms)	Cone (V)	CE (V) collision energy
1035	528	CoA18:0	10	5	45
1049	542	CoA18:0-oxo	10	5	45
1063	556	CoA20:0	10	5	45
1077	570	CoA20:0-oxo	10	5	45
1091	584	CoA22:0	10	5	45
1105	598	CoA22:0-oxo	10	5	45
1119	612	CoA24:0	10	5	45
1133	626	CoA24:0-oxo	10	5	45
1148	641	CoA26:0	10	5	45
1161	654	CoA26:0-oxo	10	5	45

Table 3. MS/MS transitions HPLC-UV-MS/MS

Q1 [M+H] ⁺	Q3 [M+H] ⁺	ID	Dwell time (ms)	DP (V) declustering potential	CE (V) collision energy	CXP (V) collision cell exit potential
922.2582506	415.2625052	CoA10:0	10	180	50	13.3
936.2375152	429.2417697	CoA10:0-oxo	10	180	50	13.3
950.2895508	443.2938053	CoA12:0	10	180	50	13.3
964.2688153	457.2730698	CoA12:0-oxo	10	180	50	13.3
978.3208509	471.3251054	CoA14:0	10	180	50	13.3
992.3001155	485.30437	CoA14:0-oxo	10	180	50	13.3
1006.352151	499.3564055	CoA16:0	10	180	50	13.3
1020.331416	513.3356701	CoA16:0-oxo	10	180	50	13.3
1034.383451	527.3877057	CoA18:0	10	180	52	14.3
1048.362716	541.3669702	CoA18:0-oxo	10	180	52	14.3
1062.414751	555.4190058	CoA20:0	10	190	52	15.3
1076.394016	569.3982704	CoA20:0-oxo	10	190	52	15.3
1090.446051	583.4503059	CoA22:0	10	190	53	16
1104.425316	597.4295705	CoA22:0-oxo	10	190	53	16
1118.477352	611.4816061	CoA24:0	10	210	57	17
1132.456616	625.4608706	CoA24:0-oxo	10	210	57	17
1146.508652	639.5129062	CoA26:0	10	220	58	17.5
1160.487916	653.4921707	CoA26:0-oxo	10	220	58	17.5
1174.539952	667.5442063	CoA28:0	10	220	58	17.5
1188.519216	681.5234709	CoA28:0-oxo	10	220	58	17.5
1202.571252	695.5755064	CoA30:0	10	220	58	17.5
1216.550516	709.554771	CoA30:0-oxo	10	220	58	17.5
1230.602552	723.6068066	CoA32:0	10	220	58	17.5
1244.581817	737.5860711	CoA32:0-oxo	10	220	58	17.5
978.321	415.2625052	CoA10:0-Me	10	180	50	13.3
992.300	429.2417697	CoA10:0-oxo-Me	10	180	50	13.3
1006.352	443.2938053	CoA12:0-Me	10	180	50	13.3
1020.331	457.2730698	CoA12:0-oxo-Me	10	180	50	13.3
1034.383	471.3251054	CoA14:0-Me	10	180	50	13.3
1048.363	485.30437	CoA14:0-oxo-Me	10	180	50	13.3
1062.415	499.3564055	CoA16:0-Me	10	180	50	13.3
1076.394	513.3356701	CoA16:0-oxo-Me	10	180	50	13.3
1090.446	527.3877057	CoA18:0-Me	10	180	52	14.3
1104.425	541.3669702	CoA18:0-oxo-Me	10	180	52	14.3
1118.477	555.4190058	CoA20:0-Me	10	190	52	15.3
1132.457	569.3982704	CoA20:0-oxo-Me	10	190	52	15.3
1146.509	583.4503059	CoA22:0-Me	10	190	53	16
1160.488	597.4295705	CoA22:0-oxo-Me	10	190	53	16
1174.540	611.4816061	CoA24:0-Me	10	210	57	17
1188.519	625.4608706	CoA24:0-oxo-Me	10	210	57	17
1202.571	639.5129062	CoA26:0-Me	10	220	58	17.5
1216.551	653.4921707	CoA26:0-oxo-Me	10	220	58	17.5
1230.603	667.5442063	CoA28:0-Me	10	220	58	17.5
1244.582	681.5234709	CoA28:0-oxo-Me	10	220	58	17.5
1258.634	695.5755064	CoA30:0-Me	10	220	58	17.5
1272.613	709.554771	CoA30:0-oxo-Me	10	220	58	17.5
1286.665	723.6068066	CoA32:0-Me	10	220	58	17.5
1300.644	737.5860711	CoA32:0-oxo-Me	10	220	58	17.5

Table 4. MS/MS transitions HPLC-MS/MS

References

- Abrankó, L., Williamson, G., Gardner, S., Kerimi, A., 2018. Comprehensive quantitative analysis of fatty-acyl-Coenzyme A species in biological samples by ultra-high performance liquid chromatography–tandem mass spectrometry harmonizing hydrophilic interaction and reversed phase chromatography. *Journal of Chromatography A* 1534, 111–122. <https://doi.org/10.1016/j.chroma.2017.12.052>
- Abulnaja, K.O., Harwood, J.L., 1991. Thiocarbamate herbicides inhibit fatty acid elongation in a variety of monocotyledons. *Phytochemistry* 30, 1445–1447. [https://doi.org/10.1016/0031-9422\(91\)84182-R](https://doi.org/10.1016/0031-9422(91)84182-R)
- Abulnaja, K.O., Tighe, C.R., Harwood, J.L., 1992. Inhibition of fatty acid elongation provides a basis for the action of the herbicide, ethofumesate, on surface wax formation. *Phytochemistry, The International Journal of Plant Biochemistry* 31, 1155–1159. [https://doi.org/10.1016/0031-9422\(92\)80251-9](https://doi.org/10.1016/0031-9422(92)80251-9)
- Bach, L., Michaelson, L.V., Haslam, R., Bellec, Y., Gissot, L., Marion, J., Costa, M.D., Boutin, J.-P., Miquel, M., Tellier, F., Domergue, F., Markham, J.E., Beaudoin, F., Napier, J.A., Faure, J.-D., 2008. The very-long-chain hydroxy fatty acyl-CoA dehydratase PASTICCINO2 is essential and limiting for plant development. *PNAS* 105, 14727–14731. <https://doi.org/10.1073/pnas.0805089105>
- Banerjee, S., Mazumdar, S., 2012. Electrospray Ionization Mass Spectrometry: A Technique to Access the Information beyond the Molecular Weight of the Analyte. *International journal of analytical chemistry* 2012, 282574. <https://doi.org/10.1155/2012/282574>
- Bao, Z., Wu, Y., Song, R., Gao, Y., Zhang, S., Zhao, K., Wu, T., Zhang, C., Du, F., 2022. The simple strategy to improve pesticide bioavailability and minimize environmental risk by effective and ecofriendly surfactants. *Science of The Total Environment* 851, 158169. <https://doi.org/10.1016/j.scitotenv.2022.158169>
- Batsale, M., Alonso, M., Pascal, S., Thoraval, D., Haslam, R.P., Beaudoin, F., Domergue, F., Joubès, J., 2023. Tackling functional redundancy of Arabidopsis fatty acid elongase complexes. *Front Plant Sci* 14, 1107333. <https://doi.org/10.3389/fpls.2023.1107333>
- Batsale, M., Bahammou, D., Fouillen, L., Mongrand, S., Joubès, J., Domergue, F., 2021. Biosynthesis and Functions of Very-Long-Chain Fatty Acids in the Responses of Plants to Abiotic and Biotic Stresses. *Cells* 10, 1284. <https://doi.org/10.3390/cells10061284>
- Beaudoin, F., Gable, K., Sayanova, O., Dunn, T., Napier, J.A., 2002. A *Saccharomyces cerevisiae* Gene Required for Heterologous Fatty Acid Elongase Activity Encodes a Microsomal β -Keto-reductase *. *Journal of Biological Chemistry* 277, 11481–11488. <https://doi.org/10.1074/jbc.M111441200>
- Bessoule, J.-J., Lessire, R., Cassagne, C., 1989. Partial purification of the Acyl-CoA elongase of *Allium porrum* leaves. *Archives of Biochemistry and Biophysics* 268, 475–484. [https://doi.org/10.1016/0003-9861\(89\)90315-9](https://doi.org/10.1016/0003-9861(89)90315-9)
- Blacklock, B., Jaworski, J., 2006. Substrate specificity of Arabidopsis 3-ketoacyl-CoA synthases. *Biochem Biophys Res Commun* 346, 583–590. <https://doi.org/10.1016/j.bbrc.2006.05.162>
- Blacklock, B.J., Jaworski, J.G., 2002. Studies into factors contributing to substrate specificity of membrane-bound 3-ketoacyl-CoA synthases. *European Journal of Biochemistry* 269, 4789–4798. <https://doi.org/10.1046/j.1432-1033.2002.03176.x>
- Böger, P., 2003. Mode of Action for Chloroacetamides and Functionally Related Compounds. *Journal of Pesticide Science - J PESTIC SCI* 28, 324–329. <https://doi.org/10.1584/jpestics.28.324>
- Böger, P., Matthes, B., Schmalfuß, J., 2000. Towards the primary target of chloroacetamides –new findings pave the way. *Pest Management Science* 56, 497–508. [https://doi.org/10.1002/\(SICI\)1526-4998\(200006\)56:6<497::AID-PS169>3.0.CO;2-W](https://doi.org/10.1002/(SICI)1526-4998(200006)56:6<497::AID-PS169>3.0.CO;2-W)

- Buré, C., Cacas, J.-L., Wang, F., Gaudin, K., Domergue, F., Mongrand, S., Schmitter, J.-M., 2011. Fast screening of highly glycosylated plant sphingolipids by tandem mass spectrometry. *Rapid Commun Mass Spectrom* 25, 3131–3145. <https://doi.org/10.1002/rcm.5206>
- Campbell, A.A., Stenback, K.E., Flyckt, K., Hoang, T., Perera, M.A.D., Nikolau, B.J., 2019. A single-cell platform for reconstituting and characterizing fatty acid elongase component enzymes. *PLOS ONE* 14, e0213620. <https://doi.org/10.1371/journal.pone.0213620>
- Campe, R., Hollenbach, E., Kämmerer, L., Hendriks, J., Höffken, H.W., Kraus, H., Lerchl, J., Mietzner, T., Tresch, S., Witschel, M., Hutzler, J., 2018. A new herbicidal site of action: Cinmethylin binds to acyl-ACP thioesterase and inhibits plant fatty acid biosynthesis. *Pesticide Biochemistry and Physiology* 148, 116–125. <https://doi.org/10.1016/j.pestbp.2018.04.006>
- Carmona-Salazar, L., Cahoon, R.E., Gasca-Pineda, J., González-Solís, A., Vera-Estrella, R., Treviño, V., Cahoon, E.B., Gavilanes-Ruiz, M., 2021. Plasma and vacuolar membrane sphingolipidomes: composition and insights on the role of main molecular species. *Plant Physiology* 186, 624–639. <https://doi.org/10.1093/plphys/kiab064>
- Chai, M., Queralt Castillo, I., Sonntag, A., Wang, S., Zhao, Z., Liu, W., Du, J., Xie, H., Liao, F., Yun, J., Jiang, Q., Sun, J., Molina, I., Wang, Z.-Y., 2021. A seed coat-specific β -ketoacyl-CoA synthase, KCS12, is critical for preserving seed physical dormancy. *Plant Physiol* 186, 1606–1615. <https://doi.org/10.1093/plphys/kiab152>
- Chang, Q., Ji, W., Lu, Q., Xue, J., Hua, R., Wu, X., 2021. Bioavailability and toxicity of imazethapyr in maize plant estimated by four chemical extraction techniques in different soils. *Science of The Total Environment* 801, 149594. <https://doi.org/10.1016/j.scitotenv.2021.149594>
- Chen, J.Y., Mumtaz, A., Gonzales-Vigil, E., 2022. Evolution and molecular basis of substrate specificity in a 3-ketoacyl-CoA synthase gene cluster from *Populus trichocarpa*. *Journal of Biological Chemistry* 102496. <https://doi.org/10.1016/j.jbc.2022.102496>
- Chen, Y.-T.J., 2022. The Evolution and Molecular Basis of Substrate Specificity in 3-Ketoacyl-CoA Synthases from *Populus trichocarpa*.
- Costaglioli, P., Joubès, J., Garcia, C., Stef, M., Arveiler, B., Lessire, R., Garbay, B., 2005. Profiling candidate genes involved in wax biosynthesis in *Arabidopsis thaliana* by microarray analysis. *Biochim Biophys Acta* 1734, 247–258. <https://doi.org/10.1016/j.bbali.2005.04.002>
- James, J., Lim, E., Keller, J., Plooy, I., Ralston, E., Dooner, H.K., 1995. Directed tagging of the *Arabidopsis* FATTY ACID ELONGATION1 (FAE1) gene with the maize transposon activator. *The Plant Cell* 7, 309. <https://doi.org/10.1105/tpc.7.3.309>
- Deal, L.M., Hess, F.D., 1980. An Analysis of the Growth Inhibitory Characteristics of Alachlor and Metolachlor. *Weed Science* 28, 168–175. <https://doi.org/10.1017/S0043174500055041>
- Devaiah, S.P., Roth, M.R., Baughman, E., Li, M., Tamura, P., Jeannotte, R., Welti, R., Wang, X., 2006. Quantitative profiling of polar glycerolipid species from organs of wild-type *Arabidopsis* and a phospholipase Δ alpha1 knockout mutant. *Phytochemistry* 67, 1907–1924. <https://doi.org/10.1016/j.phytochem.2006.06.005>
- Dhillon, N.S., Anderson, J.L., 1972. Morphological, Anatomical and Biochemical Effects of Propachlor on Seedling Growth*. *Weed Research* 12, 182–189. <https://doi.org/10.1111/j.1365-3180.1972.tb01204.x>
- Domergue, F., Vishwanath, S.J., Joubès, J., Ono, J., Lee, J.A., Bourdon, M., Alhattab, R., Lowe, C., Pascal, S., Lessire, R., Rowland, O., 2010. Three *Arabidopsis* Fatty Acyl-Coenzyme A Reductases, FAR1, FAR4, and FAR5, Generate Primary Fatty Alcohols Associated with Suberin Deposition1[C][W][OA]. *Plant Physiol* 153, 1539–1554. <https://doi.org/10.1104/pp.110.158238>

- Dücker, R., Parcharidou, E., Beffa, R., 2020. Flufenacet activity is affected by GST inhibitors in blackgrass (*Alopecurus myosuroides*) populations with reduced flufenacet sensitivity and higher expression levels of GSTs. *Weed Science* 68, 451–459. <https://doi.org/10.1017/wsc.2020.54>
- Dücker, R., Zöllner, P., Parcharidou, E., Ries, S., Lorentz, L., Beffa, R., 2019. Enhanced metabolism causes reduced flufenacet sensitivity in black-grass (*Alopecurus myosuroides* Huds.) field populations. *Pest Management Science* 75, 2996–3004. <https://doi.org/10.1002/ps.5414>
- Eckermann, C., Matthes, B., Nimtz, M., Reiser, V., Lederer, B., Böger, P., Schröder, J., 2003. Covalent binding of chloroacetamide herbicides to the active site cysteine of plant type III polyketide synthases. *Phytochemistry* 64, 1045–1054. [https://doi.org/10.1016/S0031-9422\(03\)00516-8](https://doi.org/10.1016/S0031-9422(03)00516-8)
- Ekler, Z., Stephenson, G.R., 1989. Physiological responses of maize and sorghum to four different safeners for metazachlor. *Weed Res* 29, 181–191. <https://doi.org/10.1111/j.1365-3180.1989.tb00858.x>
- Fedtke, C., 1991. Mode of action studies with mefenacet. *Pesticide Science* 33, 421–426. <https://doi.org/10.1002/ps.2780330404>
- Fehling, E., Mukherjee, K.D., 1991. Acyl-CoA elongase from a higher plant (*Lunaria annua*): metabolic intermediates of very-long-chain acyl-CoA products and substrate specificity. *Biochim Biophys Acta* 1082, 239–246. [https://doi.org/10.1016/0005-2760\(91\)90198-q](https://doi.org/10.1016/0005-2760(91)90198-q)
- Fiebig, A., Mayfield, J.A., Miley, N.L., Chau, S., Fischer, R.L., Preuss, D., 2000. Alterations in CER6, a gene identical to CUT1, differentially affect long-chain lipid content on the surface of pollen and stems. *Plant Cell* 12, 2001–2008. <https://doi.org/10.1105/tpc.12.10.2001>
- Franke, R., Briesen, I., Wojciechowski, T., Faust, A., Yephremov, A., Nawrath, C., Schreiber, L., 2005. Apoplastic polyesters in *Arabidopsis* surface tissues—a typical suberin and a particular cutin. *Phytochemistry* 66, 2643–2658. <https://doi.org/10.1016/j.phytochem.2005.09.027>
- Franke, R., Höfer, R., Briesen, I., Emsermann, M., Efremova, N., Yephremov, A., Schreiber, L., 2009. The DAISY gene from *Arabidopsis* encodes a fatty acid elongase condensing enzyme involved in the biosynthesis of aliphatic suberin in roots and the chalaza-micropyle region of seeds. *The Plant Journal* 57, 80–95. <https://doi.org/10.1111/j.1365-313X.2008.03674.x>
- Genva, M., Fougère, L., Bahammou, D., Mongrand, S., Boutté, Y., Fouillen, L., 2023. A global LC-MS2-based methodology to identify and quantify anionic phospholipids in plant samples. <https://doi.org/10.1101/2023.05.10.539967>
- Ghanevati, M., Jaworski, J.G., 2002. Engineering and mechanistic studies of the *Arabidopsis* FAE1 β -ketoacyl-CoA synthase, FAE1 KCS. *European Journal of Biochemistry* 269, 3531–3539. <https://doi.org/10.1046/j.1432-1033.2002.03039.x>
- Ghanevati, M., Jaworski, J.G., 2001. Active-site residues of a plant membrane-bound fatty acid elongase β -ketoacyl-CoA synthase, FAE1 KCS. *Biochimica et Biophysica Acta (BBA) - Molecular and Cell Biology of Lipids* 1530, 77–85. [https://doi.org/10.1016/S1388-1981\(00\)00168-2](https://doi.org/10.1016/S1388-1981(00)00168-2)
- Gietz, R.D., Schiestl, R.H., Willems, A.R., Woods, R.A., 1995. Studies on the transformation of intact yeast cells by the LiAc/SS-DNA/PEG procedure. *Yeast* 11, 355–360. <https://doi.org/10.1002/yea.320110408>
- González-Mellado, D., Salas, J., Venegas-Calderón, M., Moreno Perez, A., Garcés, R., Martínez Force, E., 2019. Functional characterization and structural modelling of *Helianthus annuus* (sunflower) ketoacyl-CoA synthases and their role in seed oil composition. *Planta* 249, 1–14. <https://doi.org/10.1007/s00425-019-03126-1>
- Götz, T., Böger, P., 2004. The Very-Long-Chain Fatty Acid Synthase Is Inhibited by Chloroacetamides. *Zeitschrift für Naturforschung C* 59, 549–553. <https://doi.org/10.1515/znc-2004-7-818>

- Gray, J.E., Holroyd, G.H., van der Lee, F.M., Bahrami, A.R., Sijmons, P.C., Woodward, F.I., Schuch, W., Hetherington, A.M., 2000. The HIC signalling pathway links CO₂ perception to stomatal development. *Nature* 408, 713–716. <https://doi.org/10.1038/35047071>
- Guan, M., Huang, X., Xiao, Z., Jia, L., Wang, S., Zhu, M., Qiao, C., Wei, L., Xu, X., Liang, Y., Wang, R., Lu, K., Li, J., Qu, C., 2019. Association Mapping Analysis of Fatty Acid Content in Different Ecotypic Rapeseed Using mrMLM. *Front Plant Sci* 9, 1872. <https://doi.org/10.3389/fpls.2018.01872>
- Guo, H.-S., Zhang, Y.-M., Sun, X.-Q., Li, M.-M., Hang, Y.-Y., Xue, J.-Y., 2016. Evolution of the KCS gene family in plants: the history of gene duplication, sub/neofunctionalization and redundancy. *Mol Genet Genomics* 291, 739–752. <https://doi.org/10.1007/s00438-015-1142-3>
- Guo, Y., Mietkiewska, E., Francis, T., Katavic, V., Brost, J.M., Giblin, M., Barton, D.L., Taylor, D.C., 2009. Increase in nervonic acid content in transformed yeast and transgenic plants by introduction of a *Lunaria annua* L. 3-ketoacyl-CoA synthase (KCS) gene. *Plant Mol Biol* 69, 565–575. <https://doi.org/10.1007/s11103-008-9439-9>
- Harwood, J.L., 1996. Recent advances in the biosynthesis of plant fatty acids. *Biochimica et Biophysica Acta (BBA) - Lipids and Lipid Metabolism* 1301, 7–56. [https://doi.org/10.1016/0005-2760\(95\)00242-1](https://doi.org/10.1016/0005-2760(95)00242-1)
- Haslam, R.P., Larson, T.R., 2021. Techniques for the Measurement of Molecular Species of Acyl-CoA in Plants and Microalgae. *Methods Mol Biol* 2295, 203–218. https://doi.org/10.1007/978-1-0716-1362-7_12
- Haslam, T.M., Haslam, R., Thoraval, D., Pascal, S., Delude, C., Domergue, F., Fernández, A.M., Beaudoin, F., Napier, J.A., Kunst, L., Joubès, J., 2015. ECERIFERUM2-LIKE Proteins Have Unique Biochemical and Physiological Functions in Very-Long-Chain Fatty Acid Elongation. *Plant Physiology* 167, 682–692. <https://doi.org/10.1104/pp.114.253195>
- Haslam, T.M., Kunst, L., 2013. Extending the story of very-long-chain fatty acid elongation. *Plant Science* 210, 93–107. <https://doi.org/10.1016/j.plantsci.2013.05.008>
- Haslam, T.M., Mañas-Fernández, A., Zhao, L., Kunst, L., 2012. Arabidopsis ECERIFERUM2 is a component of the fatty acid elongation machinery required for fatty acid extension to exceptional lengths. *Plant Physiol* 160, 1164–1174. <https://doi.org/10.1104/pp.112.201640>
- Hegebarth, D., Buschhaus, C., Joubès, J., Thoraval, D., Bird, D., Jetter, R., 2017. Arabidopsis ketoacyl-CoA synthase 16 (KCS16) forms C36/C38 acyl precursors for leaf trichome and pavement surface wax. *Plant, Cell & Environment* 40, 1761–1776. <https://doi.org/10.1111/pce.12981>
- Huai, D., Xue, X., Li, Y., Wang, P., Li, J., Yan, L., Chen, Y., Wang, X., Liu, N., Kang, Y., Wang, Z., Huang, Y., Jiang, H., Lei, Y., Liao, B., 2020. Genome-Wide Identification of Peanut KCS Genes Reveals That AhKCS1 and AhKCS28 Are Involved in Regulating VLCFA Contents in Seeds. *Frontiers in Plant Science* 11.
- Huang, H., Ayaz, A., Zheng, M., Yang, X., Zaman, W., Zhao, H., Lu, S., 2022. Arabidopsis KCS5 and KCS6 Play Redundant Roles in Wax Synthesis. *International Journal of Molecular Sciences* 24, 4450. <https://doi.org/10.3390/ijms23084450>
- Huang, H., Yang, X., Zheng, M., Chen, Z., Yang, Z., Wu, P., Jenks, M.A., Wang, G., Feng, T., Liu, L., Yang, P., Lü, S., Zhao, H., 2023a. An ancestral role for 3-KETOACYL-COA SYNTHASE3 as a negative regulator of plant cuticular wax synthesis. *The Plant Cell* 35, 2251–2270. <https://doi.org/10.1093/plcell/koad051>
- Huang, H., Yang, X., Zheng, M., Lü, S., Zhao, H., 2023b. Fine-tuning the activities of β -KETOACYL-COA SYNTHASE 3 (KCS3) and KCS12 in Arabidopsis is essential for maintaining cuticle integrity. *Journal of Experimental Botany* erad337. <https://doi.org/10.1093/jxb/erad337>
- Ito, Y., Esnay, N., Fougère, L., Platre, M.P., Cordelières, F., Jaillais, Y., Boutté, Y., 2021. Inhibition of Very Long Chain Fatty Acids Synthesis Mediates PI3P Homeostasis at Endosomal Compartments. *IJMS* 22, 8450. <https://doi.org/10.3390/ijms22168450>

- Jasinski, S., Lécureuil, A., Miquel, M., Loudet, O., Raffaele, S., Froissard, M., Guerche, P., 2012. Natural Variation in Seed Very Long Chain Fatty Acid Content Is Controlled by a New Isoform of KCS18 in *Arabidopsis thaliana*. *PLoS one* 7, e49261. <https://doi.org/10.1371/journal.pone.0049261>
- Jhala, A.J., Singh, M., Shergill, L., Singh, R., Jugulam, M., Riechers, D.E., Ganie, Z.A., Selby, T.P., Werle, R., Norsworthy, J.K., 2023. Very long chain fatty acid-inhibiting herbicides: Current uses, site of action, herbicide-resistant weeds, and future. *Weed Technol* 1–50. <https://doi.org/10.1017/wet.2023.90>
- Jones, A.E., Arias, N.J., Acevedo, A., Reddy, S.T., Divakaruni, A.S., Meriwether, D., 2021. A Single LC-MS/MS Analysis to Quantify CoA Biosynthetic Intermediates and Short-Chain Acyl CoAs. *Metabolites* 11, 468. <https://doi.org/10.3390/metabo11080468>
- Joubès, J., Raffaele, S., Bourdenx, B., Garcia, C., Laroche-Traineau, J., Moreau, P., Domergue, F., Lessire, R., 2008. The VLCFA elongase gene family in *Arabidopsis thaliana*: phylogenetic analysis, 3D modelling and expression profiling. *Plant Mol Biol* 67, 547. <https://doi.org/10.1007/s11103-008-9339-z>
- Kanissery, R., Gairhe, B., McAvoy, C., Sims, G., 2019. Herbicide Bioavailability Determinant Processes in the Soil. *J Bioremediat Biodegrad* 10. <https://doi.org/10.4172/2155-6199.1000458>
- Kasahara, T., Matsumoto, H., Hasegawa, H., Koyama, K., Takeuchi, T., 2019. Characterization of very long chain fatty acid synthesis inhibition by ipfencarbazone. *J Pestic Sci* 44, 20–24. <https://doi.org/10.1584/jpestics.D18-057>
- Kato, S., Tanaka, A., Watanabe, H., Sato, Y., Ikeda, Y., Böger, P., Wakabayashi, K., 2005. Inhibitory Activity of Indanofan and Its Enantiomers on Biosynthesis of Very-Long-Chain Fatty Acids. *Journal of Pesticide Science* 30, 7–10. <https://doi.org/10.1584/jpestics.30.7>
- Khan, U.M., Rana, I.A., Shaheen, N., Raza, Q., Rehman, H.M., Maqbool, R., Khan, I.A., Atif, R.M., 2023. Comparative phylogenomic insights of KCS and ELO gene families in Brassica species indicate their role in seed development and stress responsiveness. *Sci Rep* 13, 3577. <https://doi.org/10.1038/s41598-023-28665-2>
- Kim, J., Jung, J.H., Lee, S.B., Go, Y.S., Kim, H.J., Cahoon, R., Markham, J.E., Cahoon, E.B., Suh, M.C., 2013. *Arabidopsis* 3-Ketoacyl-Coenzyme A Synthase9 Is Involved in the Synthesis of Tetracosanoic Acids as Precursors of Cuticular Waxes, Suberins, Sphingolipids, and Phospholipids1[W]. *Plant Physiol* 162, 567–580. <https://doi.org/10.1104/pp.112.210450>
- Kim, J., Kim, R.J., Lee, S.B., Suh, M.C., 2022. Protein–protein interactions in fatty acid elongase complexes are important for very-long-chain fatty acid synthesis. *Journal of Experimental Botany* 73, 3004–3017. <https://doi.org/10.1093/jxb/erab543>
- Kim, J., Lee, S.B., Suh, M.C., 2021. *Arabidopsis* 3-Ketoacyl-CoA Synthase 4 is Essential for Root and Pollen Tube Growth. *J. Plant Biol.* 64, 155–165. <https://doi.org/10.1007/s12374-020-09288-w>
- Kim, R.J., Han, S., Kim, H.J., Hur, J.H., Suh, M.C., 2023. Tetracosanoic acids produced by 3-ketoacyl-CoA synthase 17 are required for synthesizing seed coat suberin in *Arabidopsis*. *Journal of Experimental Botany* erad381. <https://doi.org/10.1093/jxb/erad381>
- Kunst, L., Taylor, D., Underhill, E.W., 1992. Fatty acid elongation in developing seeds of *Arabidopsis thaliana*. *Plant Physiology and Biochemistry*.
- Larson, T.R., Graham, I.A., 2001. Technical Advance: A novel technique for the sensitive quantification of acyl CoA esters from plant tissues. *The Plant Journal* 25, 115–125. <https://doi.org/10.1111/j.1365-313X.2001.00929.x>
- Lassner, M.W., Levering, C.K., Davies, H.M., Knutzon, D.S., 1995. Lysophosphatidic Acid Acyltransferase from Meadowfoam Mediates Insertion of Erucic Acid at the sn-2 Position of Triacylglycerol in Transgenic Rapeseed Oil. *Plant Physiology* 109, 1389–1394. <https://doi.org/10.1104/pp.109.4.1389>

- Lechelt-Kunze, C., Meissner, R.C., Drewes, M., Tietjen, K., 2003. Flufenacet herbicide treatment phenocopies the fiddlehead mutant in *Arabidopsis thaliana*. *Pest. Manag. Sci.* 59, 847–856. <https://doi.org/10.1002/ps.714>
- Lee, S.-B., Jung, S.-J., Go, Y.-S., Kim, H.-U., Kim, J.-K., Cho, H.-J., Park, O.K., Suh, M.-C., 2009. Two *Arabidopsis* 3-ketoacyl CoA synthase genes, KCS20 and KCS2/DAISY, are functionally redundant in cuticular wax and root suberin biosynthesis, but differentially controlled by osmotic stress. *The Plant Journal* 60, 462–475. <https://doi.org/10.1111/j.1365-313X.2009.03973.x>
- Leprince, A.-S., Savouré, A., 2010. La signalisation lipidique chez les plantes et son rôle dans la transduction des signaux en réponse aux contraintes hydriques. *Biologie Aujourd'hui* 204, 11–19. <https://doi.org/10.1051/jbio/2009045>
- Li, P., Gawaz, M., Chatterjee, M., Lämmerhofer, M., 2021. Targeted Profiling of Short-, Medium-, and Long-Chain Fatty Acyl-Coenzyme As in Biological Samples by Phosphate Methylation Coupled to Liquid Chromatography–Tandem Mass Spectrometry. *Anal. Chem.* 93, 4342–4350. <https://doi.org/10.1021/acs.analchem.1c00664>
- Li, Q., Zhang, S., Berthiaume, J.M., Simons, B., Zhang, G.-F., 2014. Novel approach in LC-MS/MS using MRM to generate a full profile of acyl-CoAs: discovery of acyl-dephospho-CoAs. *J Lipid Res* 55, 592–602. <https://doi.org/10.1194/jlr.D045112>
- Lian, X.-Y., Wang, X., Gao, H.-N., Jiang, H., Mao, K., You, C.-X., Li, Y.-Y., Hao, Y.-J., 2020. Genome wide analysis and functional identification of MdKCS genes in apple. *Plant Physiology and Biochemistry* 151, 299–312. <https://doi.org/10.1016/j.plaphy.2020.03.034>
- Lin, S.-Y., Hsu, W.-H., Lin, C.-C., Chen, C.-J., 2014. Mass spectrometry-based proteomics in Chest Medicine, Gerontology, and Nephrology: subgroups omics for personalized medicine. *BioMedicine* 4, 25. <https://doi.org/10.7603/s40681-014-0025-y>
- Liu, J., Lee, Y.-Y., Mao, X., Li, Y., 2017. A simple and reproducible non-radiolabeled in vitro assay for recombinant acyltransferases involved in triacylglycerol biosynthesis. *J Appl Phycol* 29, 323–333. <https://doi.org/10.1007/s10811-016-0949-6>
- Liu, X., Sadhukhan, S., Sun, S., Wagner, G.R., Hirschey, M.D., Qi, L., Lin, H., Locasale, J.W., 2015. High-Resolution Metabolomics with Acyl-CoA Profiling Reveals Widespread Remodeling in Response to Diet*[S]. *Molecular & Cellular Proteomics* 14, 1489–1500. <https://doi.org/10.1074/mcp.M114.044859>
- Liu, X., Zhao, Z., Yang, Y., Xu, H., Bi, Q., Wang, L., 2023. Genome-Wide Identification and Expression Analysis of the KCS Gene Family in Yellow Horn Reveal Their Putative Function on Abiotic Stress Responses and Wax Accumulation. *Horticulturae* 9, 25. <https://doi.org/10.3390/horticulturae9010025>
- Lolle, S.J., Cheung, A.Y., Sussex, I.M., 1992. Fiddlehead: an *Arabidopsis* mutant constitutively expressing an organ fusion program that involves interactions between epidermal cells. *Dev Biol* 152, 383–392. [https://doi.org/10.1016/0012-1606\(92\)90145-7](https://doi.org/10.1016/0012-1606(92)90145-7)
- Lü, S., Song, T., Kosma, D.K., Parsons, E.P., Rowland, O., Jenks, M.A., 2009. *Arabidopsis* CER8 encodes LONG-CHAIN ACYL-COA SYNTHETASE 1 (LACS1) that has overlapping functions with LACS2 in plant wax and cutin synthesis. *Plant J* 59, 553–564. <https://doi.org/10.1111/j.1365-313X.2009.03892.x>
- Luzarowska, U., Ruß, A.-K., Joubès, J., Batsale, M., Szymański, J., P. Thirumalaikumar, V., Luzarowski, M., Wu, S., Zhu, F., Endres, N., Khedhayir, S., Schumacher, J., Jasinska, W., Xu, K., Correa Cordoba, S.M., Weil, S., Skirycz, A., Fernie, A.R., Li-Beisson, Y., Fusari, C.M., Brotman, Y., 2023. Hello darkness, my old friend: 3-KETOACYL-COENZYME A SYNTHASE4 is a branch point in the regulation of triacylglycerol synthesis in *Arabidopsis thaliana*. *Plant Cell* 35, 1984–2005. <https://doi.org/10.1093/plcell/koad059>
- Lv, B., Wei, K., Hu, K., Tian, T., Zhang, F., Yu, Z., Zhang, D., Su, Y., Sang, Y., Zhang, X., Ding, Z., 2021. MPK14-mediated auxin signaling controls lateral root development via ERF13-regulated very-long-chain fatty acid biosynthesis. *Mol Plant* 14, 285–297. <https://doi.org/10.1016/j.molp.2020.11.011>

- Ma, J., Wang, S., Wang, P., Ma, L., Chen, X., Xu, R., 2006. Toxicity assessment of 40 herbicides to the green alga *Raphidocelis subcapitata*. *Ecotoxicology and Environmental Safety* 63, 456–462. <https://doi.org/10.1016/j.ecoenv.2004.12.001>
- Mancha, M., Stokes, G.B., Stumpf, P.K., 1975. Fat metabolism in higher plants. The determination of acyl-acyl carrier protein and acyl coenzyme A in a complex lipid mixture. *Analytical Biochemistry* 68, 600–608. [https://doi.org/10.1016/0003-2697\(75\)90655-7](https://doi.org/10.1016/0003-2697(75)90655-7)
- Markham, J.E., Li, J., Cahoon, E.B., Jaworski, J.G., 2006. Separation and identification of major plant sphingolipid classes from leaves. *J Biol Chem* 281, 22684–22694. <https://doi.org/10.1074/jbc.M604050200>
- Markham, J.E., Lynch, D.V., Napier, J.A., Dunn, T.M., Cahoon, E.B., 2013. Plant sphingolipids: function follows form. *Curr Opin Plant Biol* 16, 350–357. <https://doi.org/10.1016/j.pbi.2013.02.009>
- Mathieu, M., Zeelen, Jp., Pauptit, R.A., Erdmann, R., Kunau, W.-H., Wierenga, R.K., 1994. The 2.8Å Crystal Structure of peroxisomal 3-ketoacyl-CoA thiolase of *Saccharomyces cerevisiae* : a five-layered $\alpha\beta\alpha$ structure constructed from two core domains of identical topology. *Structure* 2, 797–808. [https://doi.org/10.1016/S0969-2126\(94\)00081-6](https://doi.org/10.1016/S0969-2126(94)00081-6)
- Matthes, B., Böger, P., 2002. Chloroacetamides Affect the Plasma Membrane. *Zeitschrift für Naturforschung C* 57, 843–852. <https://doi.org/10.1515/znc-2002-9-1015>
- Matthes, B., Schmalfuß, J., Böger, P., 1998. Chloroacetamide Mode of Action, II: Inhibition of Very Long Chain Fatty Acid Synthesis in Higher Plants. *Zeitschrift für Naturforschung C* 53, 1004–1011. <https://doi.org/10.1515/znc-1998-11-1211>
- Mietkiewska, E., Giblin, E.M., Wang, S., Barton, D.L., Dirpaul, J., Brost, J.M., Katavic, V., Taylor, D.C., 2004. Seed-Specific Heterologous Expression of a *Nasturtium* FAE Gene in *Arabidopsis* Results in a Dramatic Increase in the Proportion of Erucic Acid. *Plant Physiol* 136, 2665–2675. <https://doi.org/10.1104/pp.104.046839>
- Millar, A.A., Clemens, S., Zachgo, S., Giblin, E.M., Taylor, D.C., Kunst, L., 1999. CUT1, an *Arabidopsis* gene required for cuticular wax biosynthesis and pollen fertility, encodes a very-long-chain fatty acid condensing enzyme. *The Plant Cell* 11, 825. <https://doi.org/10.1105/tpc.11.5.825>
- Millar, A.A., Kunst, L., 1997. Very-long-chain fatty acid biosynthesis is controlled through the expression and specificity of the condensing enzyme. *The Plant Journal* 12, 121–131. <https://doi.org/10.1046/j.1365-313X.1997.12010121.x>
- Morineau, C., Gissot, L., Bellec, Y., Hematy, K., Tellier, F., Renne, C., Haslam, R., Beaudoin, F., Napier, J., Faure, J.-D., 2016. Dual Fatty Acid Elongase Complex Interactions in *Arabidopsis*. *PLoS ONE* 11, e0160631. <https://doi.org/10.1371/journal.pone.0160631>
- Nandula, V., Riechers, D., Ferhatoglu, Y., Barrett, M., Duke, S., Dayan, F., Goldberg-Cavalleri, A., Tétard-Jones, C., Wortley, D., Onkokesung, N., Brazier-Hicks, M., Edwards, R., Gaines, T., Iwakami, S., Jugulam, M., Ma, R., 2019. Herbicide Metabolism: Crop Selectivity, Bioactivation, Weed Resistance, and Regulation. *Weed Science* 67. <https://doi.org/10.1017/wsc.2018.88>
- Nègre, M., Passarella, I., Boursier, C., Mozzetti, C., Gennari, M., 2006. Evaluation of the bioavailability of the herbicide prosulfocarb through adsorption on soils and model soil colloids, and through a simple bioassay. *Pest Manag Sci* 62, 957–964. <https://doi.org/10.1002/ps.1264>
- Neubauer, S., Chu, D.B., Marx, H., Sauer, M., Hann, S., Koellensperger, G., 2015. LC-MS/MS-based analysis of coenzyme A and short-chain acyl-coenzyme A thioesters. *Anal Bioanal Chem* 407, 6681–6688. <https://doi.org/10.1007/s00216-015-8825-9>
- Nie, L., Pascoa, T., Pike, A., Bushell, S., Quigley, A., Ruda, G.F., Chu, A., Cole, V., Speedman, D., Moreira, T., Shrestha, L., Mukhopadhyay, S., Burgess-Brown, N., Love, J., Brennan, P., Carpenter, E., 2021. The structural basis of fatty

acid elongation by the ELOVL elongases. *Nature Structural & Molecular Biology* 28, 1–9. <https://doi.org/10.1038/s41594-021-00605-6>

Nobusawa T., Umeda M., 2012. Very-long-chain fatty acids have an essential role in plastid division by controlling Z-ring formation in *Arabidopsis thaliana*. *Genes to Cells* 17, 709–719. <https://doi.org/10.1111/j.1365-2443.2012.01619.x>

Ohlrogge, J., Browse, J., 1995. Lipid biosynthesis. *The Plant Cell* 7, 957–970. <https://doi.org/10.1105/tpc.7.7.957>

Paul, S., Gable, K., Beaudoin, F., Cahoon, E., Jaworski, J., Napier, J.A., Dunn, T.M., 2006. Members of the Arabidopsis FAE1-like 3-Ketoacyl-CoA Synthase Gene Family Substitute for the Elop Proteins of *Saccharomyces cerevisiae* *. *Journal of Biological Chemistry* 281, 9018–9029. <https://doi.org/10.1074/jbc.M507723200>

Perera, M.A.D.N., Choi, S.-Y., Wurtele, E.S., Nikolau, B.J., 2009. Quantitative analysis of short-chain acyl-coenzymeAs in plant tissues by LC–MS–MS electrospray ionization method. *Journal of Chromatography B* 877, 482–488. <https://doi.org/10.1016/j.jchromb.2008.12.053>

Pollard, M., Beisson, F., Li, Y., Ohlrogge, J.B., 2008. Building lipid barriers: biosynthesis of cutin and suberin. *Trends Plant Sci* 13, 236–246. <https://doi.org/10.1016/j.tplants.2008.03.003>

Pruitt, R.E., Vielle-Calzada, J.-P., Ploense, S.E., Grossniklaus, U., Lolle, S.J., 2000. FIDDLEHEAD, a gene required to suppress epidermal cell interactions in Arabidopsis, encodes a putative lipid biosynthetic enzyme. *Proceedings of the National Academy of Sciences* 97, 1311–1316. <https://doi.org/10.1073/pnas.97.3.1311>

Pulsifer, I.P., Kluge, S., Rowland, O., 2012. Arabidopsis LONG-CHAIN ACYL-COA SYNTHETASE 1 (LACS1), LACS2, and LACS3 facilitate fatty acid uptake in yeast. *Plant Physiology and Biochemistry* 51, 31–39. <https://doi.org/10.1016/j.plaphy.2011.10.003>

Purves, R.W., Ambrose, S.J., Clark, S.M., Stout, J.M., Page, J.E., 2015. Separation of isomeric short-chain acyl-CoAs in plant matrices using ultra-performance liquid chromatography coupled with tandem mass spectrometry. *Journal of Chromatography B* 980, 1–7. <https://doi.org/10.1016/j.jchromb.2014.12.007>

Qin, Y.-M., Hu, C.-Y., Pang, Y., Kastaniotis, A.J., Hiltunen, J.K., Zhu, Y.-X., 2007. Saturated Very-Long-Chain Fatty Acids Promote Cotton Fiber and Arabidopsis Cell Elongation by Activating Ethylene Biosynthesis. *The Plant Cell* 19, 3692–3704. <https://doi.org/10.1105/tpc.107.054437>

Qiu, X., Janson, C.A., Konstantinidis, A.K., Nwagwu, S., Silverman, C., Smith, W.W., Khandekar, S., Lonsdale, J., Abdel-Meguid, S.S., 1999. Crystal Structure of β -Ketoacyl-Acyl Carrier Protein Synthase III: A KEY CONDENSING ENZYME IN BACTERIAL FATTY ACID BIOSYNTHESIS *. *Journal of Biological Chemistry* 274, 36465–36471. <https://doi.org/10.1074/jbc.274.51.36465>

Qiu, X., Janson, C.A., Smith, W.W., Head, M., Lonsdale, J., Konstantinidis, A.K., 2001. Refined structures of beta-ketoacyl-acyl carrier protein synthase III. *J Mol Biol* 307, 341–356. <https://doi.org/10.1006/jmbi.2000.4457>

Razeq, F.M., Kosma, D.K., Rowland, O., Molina, I., 2014. Extracellular lipids of *Camelina sativa*: Characterization of chloroform-extractable waxes from aerial and subterranean surfaces. *Phytochemistry* 106, 188–196. <https://doi.org/10.1016/j.phytochem.2014.06.018>

Rivera, L.G., Bartlett, M.G., 2018. Chromatographic methods for the determination of acyl-CoAs. *Anal. Methods* 10, 5252–5264. <https://doi.org/10.1039/C8AY01472H>

Rizwan, H.M., Shaozhong, F., Li, X., Bilal Arshad, M., Yousef, A.F., Chenglong, Y., Shi, M., Jaber, M.Y.M., Anwar, M., Hu, S.-Y., Yang, Q., Sun, K., Ahmed, M.A.A., Min, Z., Oelmüller, R., Zhimin, L., Chen, F., 2022. Genome-Wide Identification and Expression Profiling of KCS Gene Family in Passion Fruit (*Passiflora edulis*) Under Fusarium kyushuense and Drought Stress Conditions. *Frontiers in Plant Science* 13.

- Roudier, F., Gissot, L., Beaudoin, F., Haslam, R., Michaelson, L., Marion, J., Molino, D., Lima, A., Bach, L., Morin, H., Tellier, F., Palauqui, J.-C., Bellec, Y., Renne, C., Miquel, M., Dacosta, M., Vignard, J., Rochat, C., Markham, J.E., MOREAU, P., Napier, J., Faure, J.-D., 2010. Very-long-chain fatty acids are involved in polar auxin transport and developmental patterning in Arabidopsis. *The Plant cell* 22, 364–75. <https://doi.org/10.1105/tpc.109.071209>
- Rui, C., Chen, X., Xu, N., Wang, J., Zhang, H., Li, S., Huang, H., Fan, Y., Zhang, Y., Lu, X., Wang, D., Gao, W., Ye, W., 2022. Identification and Structure Analysis of KCS Family Genes Suggest Their Repending to Regulate Fiber Development in Long-Staple Cotton Under Salt-Alkaline Stress. *Front Genet* 13, 812449. <https://doi.org/10.3389/fgene.2022.812449>
- Sayanova, O., Haslam, R., Guschina, I., Lloyd, D., Christie, W., Harwood, J., Napier, J., 2007. A Bifunctional $\Delta 12, \Delta 15$ -Desaturase from *Acanthamoeba castellanii* Directs the Synthesis of Highly Unusual n-1 Series Unsaturated Fatty Acids. *The Journal of biological chemistry* 281, 36533–41. <https://doi.org/10.1074/jbc.M605158200>
- Schmalfuß, J., Matthes, B., Mayer, P., Boger, P., 1998. Chloroacetamide Mode of Action, I: Inhibition of Very Long Chain Fatty Acid Synthesis in *Scenedesmus acutus*. *Zeitschrift für Naturforschung C* 53, 995–1003. <https://doi.org/10.1515/znc-1998-11-1210>
- Schmalfuß, J., Matthes, B., Knuth, K., Böger, P., 2000. Inhibition of Acyl-CoA Elongation by Chloroacetamide Herbicides in Microsomes from Leek Seedlings. *Pesticide Biochemistry and Physiology* 67, 25–35. <https://doi.org/10.1006/pest.2000.2473>
- Serrano, M., Coluccia, F., Torres, M., L'Haridon, F., Métraux, J.-P., 2014. The cuticle and plant defense to pathogens. *Front Plant Sci* 5, 274. <https://doi.org/10.3389/fpls.2014.00274>
- Snyder, N.W., Tomblin, G., Worth, A.J., Parry, R.C., Silvers, J.A., Gillespie, K.P., Basu, S.S., Millen, J., Goldfarb, D.S., Blair, I.A., 2015. Production of stable isotope-labeled acyl-coenzyme A thioesters by yeast stable isotope labeling by essential nutrients in cell culture. *Anal Biochem* 474, 59–65. <https://doi.org/10.1016/j.ab.2014.12.014>
- Suhaimi, N., Maeda, Y., Yoshino, T., Tanaka, T., 2022. Effects of fatty acid synthase-inhibitors on polyunsaturated fatty acid production in marine diatom *Fistulifera solaris* JPCC DA0580. *Journal of Bioscience and Bioengineering* 133, 340–346. <https://doi.org/10.1016/j.jbiosc.2021.12.014>
- Sun, D., Cree, M.G., Wolfe, R.R., 2006. Quantification of the concentration and ^{13}C tracer enrichment of long-chain fatty acyl-coenzyme A in muscle by liquid chromatography/mass spectrometry. *Analytical Biochemistry* 349, 87–95. <https://doi.org/10.1016/j.ab.2005.10.006>
- Sun, X., Pang, H., Li, M., Peng, B., Guo, H., Yan, Q., Hang, Y., 2013. Evolutionary Pattern of the FAE1 Gene in Brassicaceae and Its Correlation with the Erucic Acid Trait. *PLOS ONE* 8, e83535. <https://doi.org/10.1371/journal.pone.0083535>
- Tanaya, Y., 2013. Department of Biofunctional Science Doctor of Agriculture Dissertation Graduate School of Life and Environmental Sciences Study on action mechanism and selectivity of isoxazoline herbicides.
- Tanetani, Y., 2012. Action mechanism of isoxazoline-type herbicides. *Journal of Pesticide Science* 37, 261–262. <https://doi.org/10.1584/jpestics.J12-05>
- Tanetani, Y., Fujioka, T., Horita, J., Kaku, K., Shimizu, T., 2011a. Action mechanism of a novel herbicide, fenoxasulfone. *J. Pestic. Sci.* 36, 357–362. <https://doi.org/10.1584/jpestics.G10-97>
- Tanetani, Y., Fujioka, T., Kaku, K., Shimizu, T., 2011b. Studies on the inhibition of plant very-long-chain fatty acid elongase by a novel herbicide, pyroxasulfone [WWW Document]. undefined. URL /paper/Studies-on-the-inhibition-of-plant-very-long-chain-Tanetani-Fujioka/e5840a4e0729e7bcc0de283d9abbea4a8c5fb3cb (accessed 3.17.21).

- Tanetani, Y., Ikeda, M., Kaku, K., Shimizu, T., Matsumoto, H., 2013a. Role of metabolism in the selectivity of a herbicide, pyroxasulfone, between wheat and rigid ryegrass seedlings. *Journal of Pesticide Science* 38, 152–156. <https://doi.org/10.1584/jpestics.D13-014>
- Tanetani, Y., Kaku, K., Ikeda, M., Shimizu, T., 2013b. Action mechanism of a herbicide, thiobencarb. *J. Pestic. Sci.* 38, 39–43. <https://doi.org/10.1584/jpestics.D12-047>
- Tanetani, Y., Kaku, K., Kawai, K., Fujioka, T., Shimizu, T., 2009. Action mechanism of a novel herbicide, pyroxasulfone. *Pesticide Biochemistry and Physiology* 95, 47–55. <https://doi.org/10.1016/j.pestbp.2009.06.003>
- Tariq, F., Zhao, S., Ahmad, N., Wang, P., Shao, Q., Ma, C., Yang, X., 2022. Overexpression of β -Ketoacyl CoA Synthase 2B.1 from *Chenopodium quinoa* Promotes Suberin Monomers' Production and Salt Tolerance in *Arabidopsis thaliana*. *International Journal of Molecular Sciences* 23, 13204. <https://doi.org/10.3390/ijms232113204>
- Todd, J., Post-Beittenmiller, D., Jaworski, J.G., 1999. KCS1 encodes a fatty acid elongase 3-ketoacyl-CoA synthase affecting wax biosynthesis in *Arabidopsis thaliana*. *The Plant Journal* 17, 119–130. <https://doi.org/10.1046/j.1365-313X.1999.00352.x>
- Tong, T., Fang, Y., Zhang, Z., Zheng, J., Zhang, Xian, Li, J., Niu, C., Xue, D., Zhang, Xiaoqin, 2021. Genome-wide identification and expression pattern analysis of the KCS gene family in barley. *Plant Growth Regul* 93, 89–103. <https://doi.org/10.1007/s10725-020-00668-3>
- Tonon, T., Harvey, D., Li, Y., Larson, T., Graham, I., 2005. Identification of a Long-Chain Polyunsaturated Fatty Acid Acyl-Coenzyme A Synthetase from the Diatom *Thalassiosira pseudonana*. *Plant physiology* 138, 402–8. <https://doi.org/10.1104/pp.104.054528>
- Trefely, S., Huber, K., Liu, J., Noji, M., Stransky, S., Singh, J., Doan, M.T., Lovell, C.D., von Krusenstiern, E., Jiang, H., Bostwick, A., Pepper, H.L., Izzo, L., Zhao, S., Xu, J.P., Bedi, K.C., Rame, J.E., Bogner-Strauss, J.G., Mesaros, C., Sidoli, S., Wellen, K.E., Snyder, N.W., 2022. Quantitative subcellular acyl-CoA analysis reveals distinct nuclear metabolism and isoleucine-dependent histone propionylation. *Molecular Cell, Focus on technology* 82, 447-462.e6. <https://doi.org/10.1016/j.molcel.2021.11.006>
- Trenkamp, S., Martin, W., Tietjen, K., 2004. Specific and differential inhibition of very-long-chain fatty acid elongases from *Arabidopsis thaliana* by different herbicides. *Proc Natl Acad Sci U S A* 101, 11903–11908. <https://doi.org/10.1073/pnas.0404600101>
- Tresch, S., 2013. Strategies and future trends to identify the mode of action of phytotoxic compounds. *Plant Science* 212, 60–71. <https://doi.org/10.1016/j.plantsci.2013.08.005>
- Tresch, S., Heilmann, M., Christiansen, N., Looser, R., Grossmann, K., 2012. Inhibition of saturated very-long-chain fatty acid biosynthesis by mefluidide and perfluidone, selective inhibitors of 3-ketoacyl-CoA synthases. *Phytochemistry* 76, 162–171. <https://doi.org/10.1016/j.phytochem.2011.12.023>
- Vercampt, H., Koleva, L., Vassilev, A., Horemans, N., Biermans, G., Vangronsveld, J., Cuypers, A., 2016. The functional role of the photosynthetic apparatus in the recovery of *Brassica napus* plants from pre-emergent metazachlor exposure. *Journal of Plant Physiology* 196–197, 99–105. <https://doi.org/10.1016/j.jplph.2016.04.001>
- Voisin, D., Nawrath, C., Kurdyukov, S., Franke, R.B., Reina-Pinto, J.J., Efremova, N., Will, I., Schreiber, L., Yephremov, A., 2009. Dissection of the Complex Phenotype in Cuticular Mutants of *Arabidopsis* Reveals a Role of SERRATE as a Mediator. *PLOS Genetics* 5, e1000703. <https://doi.org/10.1371/journal.pgen.1000703>
- Wang, H., He, T., Huang, C., Wang, K., Shi, D., Si, X., Xu, Y., Lyu, S., Huang, J., Li, Y., 2023. Genome-wide identification of KCS gene family in *Carya illinoensis* and their roles under abiotic stress conditions. *Scientia Horticulturae* 321, 112343. <https://doi.org/10.1016/j.scienta.2023.112343>
- Wattelet-Boyer, V., Brocard, L., Jonsson, K., Esnay, N., Joubès, J., Domergue, F., Mongrand, S., Raikhel, N., Bhalerao, R.P., Moreau, P., Boutté, Y., 2016. Enrichment of hydroxylated C24- and C26-acyl-chain sphingolipids mediates

PIN2 apical sorting at trans-Golgi network subdomains. *Nat Commun* 7, 12788. <https://doi.org/10.1038/ncomms12788>

Woldegiorgis, G., Spennetta, T., Corkey, B.E., Williamson, J.R., Shrago, E., 1985. Extraction of tissue long-chain acyl-CoA esters and measurement by reverse-phase high-performance liquid chromatography. *Analytical Biochemistry* 150, 8–12. [https://doi.org/10.1016/0003-2697\(85\)90434-8](https://doi.org/10.1016/0003-2697(85)90434-8)

Xiao, G.-H., Wang, K., Huang, G., Zhu, Y.-X., 2016. Genome-scale analysis of the cotton KCS gene family revealed a binary mode of action for gibberellin A regulated fiber growth. *Journal of Integrative Plant Biology* 58, 577–589. <https://doi.org/10.1111/jipb.12429>

Xing, J., Zhu, M., Xu, H., Liu, H., Wang, Y., 2023. Genome-wide characterization of the role of the KCS gene family in *Allium fistulosum* L. as regulators of abiotic stress responses. *Scientia Horticulturae* 322, 112407. <https://doi.org/10.1016/j.scienta.2023.112407>

Xu, L., Hao, J., Lv, M., Liu, P., Ge, Q., Zhang, S., Yang, J., Niu, H., Wang, Y., Xue, Y., Lu, X., Tang, J., Zheng, J., Gou, M., 2024. A genome-wide association study identifies genes associated with cuticular wax metabolism in maize. *Plant Physiology* kiae007. <https://doi.org/10.1093/plphys/kiae007>

Xue, D., Zhang, X., Lu, X., Chen, G., Chen, Z.-H., 2017. Molecular and Evolutionary Mechanisms of Cuticular Wax for Plant Drought Tolerance. *Front Plant Sci* 8, 621. <https://doi.org/10.3389/fpls.2017.00621>

Xue, Y., Jiang, J., Yang, X., Jiang, H., Du, Y., Liu, X., Xie, R., Chai, Y., 2020. Genome-wide mining and comparative analysis of fatty acid elongase gene family in *Brassica napus* and its progenitors. *Gene* 747, 144674. <https://doi.org/10.1016/j.gene.2020.144674>

Yang, H., Mei, W., Wan, H., Xu, R., Cheng, Y., 2021. Comprehensive analysis of KCS gene family in Citrinae reveals the involvement of CskCS2 and CskCS11 in fruit cuticular wax synthesis at ripening. *Plant Sci* 310, 110972. <https://doi.org/10.1016/j.plantsci.2021.110972>

Yang, L., Fang, J., Wang, J., Hui, S., Zhou, L., Xu, B., Chen, Yujuan, Zhang, Y., Lai, C., Jiao, G., Sheng, Z., Wei, X., Shao, G., Xie, L., Wang, L., Chen, Ying, Zhao, F., Hu, S., Hu, P., Tang, S., 2023. Genome-wide identification and expression analysis of 3-ketoacyl-CoA synthase gene family in rice (*Oryza sativa* L.) under cadmium stress. *Frontiers in Plant Science* 14.

Yang, S., Sadilek, M., Synovec, R.E., Lidstrom, M.E., 2009. Liquid chromatography - tandem quadrupole mass spectrometry and comprehensive two-dimensional gas chromatography - time-of-flight mass spectrometry measurement of targeted metabolites of *Methylobacterium extorquens* AM1 grown on two different carbon sources. *J Chromatogr A* 1216, 3280–3289. <https://doi.org/10.1016/j.chroma.2009.02.030>

Yang, W., Pollard, M., Li-Beisson, Y., Beisson, F., Feig, M., Ohlrogge, J., 2010. A distinct type of glycerol-3-phosphate acyltransferase with sn-2 preference and phosphatase activity producing 2-monoacylglycerol. *Proceedings of the National Academy of Sciences* 107, 12040–12045. <https://doi.org/10.1073/pnas.0914149107>

Yang, X., Guschina, I.A., Hurst, S., Wood, S., Langford, M., Hawkes, T., Harwood, J.L., 2010. The action of herbicides on fatty acid biosynthesis and elongation in barley and cucumber. *Pest Management Science* 66, 794–800. <https://doi.org/10.1002/ps.1944>

Yang, X., Ma, Y., Li, N., Cai, H., Bartlett, M.G., 2017. Development of a Novel Method for the Determination of Acyl-CoA Compounds by Liquid Chromatography Mass Spectrometry to Probe the Metabolism of Fatty Acids. *Anal Chem* 89, 813–821. <https://doi.org/10.1021/acs.analchem.6b03623>

Yephremov, A., Wisman, E., Huijser, P., Huijser, C., Wellesen, K., Saedler, H., 1999. Characterization of the FIDDLEHEAD gene of *Arabidopsis* reveals a link between adhesion response and cell differentiation in the epidermis. *Plant Cell* 11, 2187–2201.

- Zaib, P., Shaheen, T., Hamyat, M., Mahmood-ur-Rahman, 2022. COMPARATIVE GENOMICS AND EXPRESSION ANALYSIS OF KCS GENES UNDER DROUGHT STRESS IN SUNFLOWER (*HELIANTHUS ANNUUS* L.). *THE JAPS* 32. <https://doi.org/10.36899/JAPS.2022.5.0545>
- Zhai, X., Wu, D., Chen, C., Yang, X., Cheng, S., Sha, L., Deng, S., Cheng, Y., Fan, X., Kang, H., Wang, Y., Liu, D., Zhou, Y., Zhang, H., 2024. A chromosome level genome assembly of *Pseudoroegneria Libanotica* reveals a key Kcs gene involves in the cuticular wax elongation for drought resistance. *BMC Genomics* 25, 253. <https://doi.org/10.1186/s12864-024-10140-5>
- Zhang, A., Xu, J., Xu, X., Wu, J., Li, P., Wang, B., Fang, H., 2022. Genome-wide identification and characterization of the KCS gene family in sorghum (*Sorghum bicolor* (L.) Moench). *PeerJ* 10, e14156. <https://doi.org/10.7717/peerj.14156>
- Zhao, H., Kosma, D.K., Lü, S., 2021. Functional Role of Long-Chain Acyl-CoA Synthetases in Plant Development and Stress Responses. *Front Plant Sci* 12, 640996. <https://doi.org/10.3389/fpls.2021.640996>
- Zheng, H., Liang, Y., Hong, B., Xu, Y., Ren, M., Wang, Y., Huang, L., Yang, L., Tao, J., 2023. Genome-Scale Analysis of the Grapevine KCS Genes Reveals Its Potential Role in Male Sterility. *IJMS* 24, 6510. <https://doi.org/10.3390/ijms24076510>
- Zhukov, A., Popov, V., 2022. Synthesis of C20–38 Fatty Acids in Plant Tissues. *International Journal of Molecular Sciences* 23, 4731. <https://doi.org/10.3390/ijms23094731>